TKTL1 plays a critical role in ameliorating intracellular oxidative stress under hyperglycemic conditions

by

Sulandy Reuter

Dissertation presented for the degree of Master of Science (Physiological Sciences)

in the Faculty of Natural Science at Stellenbosch University

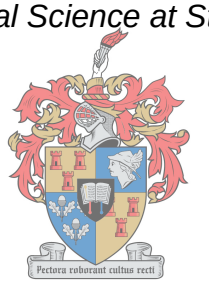

Supervisor: Prof. M. Faadiel Essop

Co-supervisor: Dr. Danzil E. Joseph

March 2018

Declaration

By submitting this thesis electronically, I declare that the entirety of the work contained therein is my own, original work, that I am the sole author thereof (save to the extent explicitly otherwise stated), that reproduction and publication thereof by Stellenbosch University will not infringe any third party rights and that I have not previously in its entirety or in part submitted it for obtaining any qualification.

March 2018

Abstract

Diabetes is a growing, global concern, reaching a prevalence far beyond the projected statistics. Hyperglycemia is a common denominator of type 1 and type 2 diabetes mellitus that if left untreated, results in detrimental outcomes, e.g. oxidative damage. The pentose phosphate pathway (glucose-6-phosphate dehydrogenase [G6PD] and transketolase [TKT] as rate-limiting enzymes) offers an alternate "safer" route for excess metabolic fuels, while also replenishing anti-oxidant defenses and thus potentially offers value as a novel therapeutic target. As TKT-like 1 (TKTL1), a relatively novel member of the transketolase family, has been overlooked in this regard, we employed a TKTL1-knock-out (KO) mouse model as a targeted approach to evaluating TKTL1 function. Multiple low doses of streptozotocin (STZ) (40 mg/kg, intraperitoneal injections on five consecutive days) were used to induce hyperglycemia, a pathophysiologic state known to culminate in oxidative stress and damaging outcomes. Hyperglycemia incidence was 40% and 90% in wild-type (WT) and TKTL1-KO STZ-injected male groups, respectively, while only the TKTL1-KO STZ group displayed significantly higher blood glucose levels compared to the WT control ($p<0.001$) and the TKTL1-KO control group ($p<0.001$). The male TKTL1-KO STZ-treated group displayed larger relative liver weights ($p<0.001$) and kidney weights ($p<0.05$), respectively, compared to both WT and TKTL1-KO controls. Gastrocnemii weight of the TKTL1-KO STZ-treated group was lower than that of the WT control group ($p<0.01$). There was a significant, negative correlation between liver G6PD activity and blood glucose levels (Spearman's correlation coefficient [r]=-0.37, p=0.03) while this correlation was not observed in cardiac tissue. In the latter, both TKTL1-KO groups displayed ~50% diminished transketolase activity compared to the WT control ($p<0.001$). No significant differences were noted in any of the oxidative stress and damage assessments of blood, heart, or liver samples. However, several adaptations were revealed in hepatic anti-oxidant defenses: STZ-treated TKTL1-KO mice displayed increased catalase activity ($p<0.05$), with catalase activity showing a significant, positive correlation with blood glucose ($r=0.39$, $p=0.02$); ferric reducing anti-oxidant power (FRAP) concentrations as well as the

reduced glutathione (GSH):to oxidized glutathione (GSSG) ratio were, significantly decreased in STZ-treated TKTL1-KO group ($p<0.05$) while both of these measurements were negatively correlation with blood glucose levels ($r=0.45$, $p<0.01$ for FRAP, $r=-0.36$, $p=0.03$ for GSH:GSSG ratio). Our data reveal that TKTL1 may play an anti-oxidant role in the liver to protect against hyperglycemia and to maintain overall glucose homeostasis. Thus our study demonstrates novel insights into TKTL1 function and shows that it remains a feasible therapeutic target for the treatment of diabetes.

Uittreksel

Diabetes is ‘n wêreldwye bekommernis waarvan die geprojekteerde voorkoms by verre onderskat is. ‘n Algemene kenmerk van tipe 1 sowel as tipe 2 diabetes mellitus is hiperglukemie wat lei tot skadelike uitkomste soos oksidatiewe skade. Die pentose-fosfaat padweg (PPP) (glukose-6-fosfaat dehidrogenase [G6PD] en transketolase [TKT] as tempo-aangewende ensieme) bied ‘n alternatiewe, "veiliger" weg vir oorskot metaboliese brandstof terwyl dit ook antioksidante aanvul, dus is die PPP ‘n potensiële teiken vir behandeling. Siende dat ‘n ensiem soortgelyk aan TKT, TKTL1, se potensiaal in hierdie area van navorsing nog nie ontgin is nie het ons ‘n TKTL1-uitslaan (KO) muismodel gebruik as ‘n geteikende benadering om die funksie van TKTL1 te evalueer. Lae dosise van streptozotosien (STZ) (40 mg/kg daagliks op vyf agtereenvolgende dae) was gebruik om hiperglukemie, ‘n patologie geassosieer met oksidatiewe stress en skadelike uitkomstes, te bewerkstellig. Hiperglukemie voorkoms in die manlike STZ-behandelde groepe was 40% in wilde-tipe (WT) en 90% in die TKTL1-KO, waar slegs die TKTL1-KO groep wat STZ behandeling ontvang het, beduidend hoër bloedglukosevlakke getoon het in vergelyking met die WT kontrole groep ($p<0.001$). Die manlike TKTL1-KO STZ-behandelde groep se lewer- ($p<0.001$) en nier gewig ($p<0.05$) was verhoog in vergelyking met beide die WT en die TKTL1-KO kontroles. Inteenstelling hiermee, was die gastrocnemi spiere van die TKTL1-KO groep se gewig kleiner as dié van die WT kontrole groep ($p<0.01$). ‘n Beduidende, negatiewe korrelasie is opgemerk tussen lewer G6PD aktiwiteit en bloedglukosevlakke (Spearman se korrelasie koëffisiënt [r] =-0.37, p=0.03), wat nie in die hart van toepassing was nie. In hartweefsel het beide TKTL1-KO groepe ‘n ~50% verlaging getoon in TKT aktiwiteit in vergelyking met die WT kontrole ($p<0.001$). Geen beduidende veranderige in oksidatiewe stres en –skade asseseerings is gevind in bloed, hartweefsel of lewerweefsel nie. Hierinteen is verskeie aanpassings in die antioksidatiewe verdedigings meganismes opgelet. STZ-behandelde TKTL1-KO muise het verhoogde katalase aktiwiteit getoon (p,0.05) terwyl ‘n positiewe korrelasie ook opgemerk is tussen katalase aktiwiteit en bloedglukose vlakke (r=0.39, p=0.02); yster-reduserende antioksidant

mag (FRAP) asook die fraksie van gereduseerde glutathione (GSH):geoksideerde glutathione (GSSG) was albei beduidend verlaagin die STZ-behandelde TKTL1-KO groep ($p<0.05$) terwyl beide van hierdie merkers ‘n negatiewe korrelasie met bloedglukosevlakke getoon het ($r=0.45$, $p<0.01$ vir FRAP, $r=-0.36$, $p=0.03$ vir GSH:GSSG fraksie). Ons data onthul ‘n antioksidatiewe rol vir hierdie ensiem in die lewer wat beskerm teen hiperglukemie en selfs kan byrae tot algehele glukose homeostase. Dus lewer ons studie nuwe insigte in die funksie van TKTL1 wat steeds ‘n moontlike teiken is vir die behandeling van diabetes.

Acknowledgements

I would like to express my sincere gratitude to my supervisor and mentor, Professor M. Faadiel Essop, without which this project and my postgraduate career would not have been possible. I have learned so much from you the past two years both professionally and personally. You have the amazing ability to see the best in any situation no matter how awful it may seem. You inspire each person in CMRG to become the finest researcher and person they are capable of being.

To Danzil Joseph, my co-supervisor, your guidance throughout my time in CMRG is absolutely invaluable. Your advice "control the controllables" which you so often gave, will stick with me forever. Thank you for your support throughout the past two years and especially for entertaining my random ideas about this project and helping me to sort through it all.

Gaurang and Tanya, you made me feel at home in my visits to the Postdoc room and provided critical insights when I needed those most. Gaurang, thanks for the coffee breaks and chats about TKTL1 and my project.To the rest of CMRG, I would like to thank all of you for your support and advice throughout this degree, your input is greatly appreciated.

Daleen you're incredible! Your support and friendship during my time at the department kept me on track, while the mini-road trips to see "Sequel" and "Impi" kept me sane. Yigael, thanks for participating in the most random conversations and being my driving-buddy. The laughs with you have been priceless and much needed at times! Gustav, dankie dat jy geluister het as ek uit motivering uit gehardloop het en dat jy altyd in NARGA was al was dit net om te weet ek werk nie alleen nie. André, dankie dat jy kon sien presies wanneer koffiebreek benodig het en vir die "hoe gan dit met die skryf?" juis op die dae wat ek nie meer wou nie end it my gemotiveer het om aan te gaan.

Aan my familie, baie dankie vir al die ondersteuning beide deur my studie loopbaan. Ek waardeer elke opoffering wat julle met graagte so deurgaan net sodat ek my studies kon voltooi. Dankie vir die laat aande wat Mamma spandeer het om my werk te proeflees. Aan die Joubert gesin, julle is 'n absolute seën in my lewe. Julle bystand die afgelope paar jaar was onbeskryflik en ek waardeer dit ongelooflik baie.

Table of Contents

List of Tables

List of Figures

List of Abbreviations

A

AAPH	2,2'Azobis(2-methylpropionamidine)-dihydrochloride
Acetyl-CoA	Acetyl coenzyme A
ADA	American diabetes association
ADP	Adenosine diphosphate
AGE	Advanced glycation end-products
ANOVA	Analysis of variance
ATP	Adenosine triphosphate

B

β-NAD	β-Nicotinamide adenine dinucleotide
b.p.	Base pairs

C

Ca^{2+}	Calcium
$CaCl_2$	Calcium chloride
CDs	Conjugated dienes
CoQ	Coenzyme Q
C-terminal	Carboxy-terminal
CytC	Cytochrome C

D

DETAPAC	diethylenetriamine-pentaacetic acid
df	Dilution factor
dH_2O	Distilled water
DTNB	5,5'-Dithiobis(2-nitrobenzoic acid)

E

e^-	Electrons
EDTA	Ethylenediaminetetraacetic acid
Em	Emission
eNOS	Endothelial nitric oxide synthase
ETC	Electron transport chain
Ex	Excitation

F

F6P	Fructose 6-phosphate
$FADH_2$	Flavin adenine dinucleotide
$FeCl_3$	Iron(III)chloride
FGP	Fating plasma glucose
FRAP	Ferric reducing anti-oxidant power

G

G3P	Glyceraldehyde 3-phosphate
G6P	Glucose 6-phosphate
G6PD	Glucose 6-phosphate dehydrogenase
GAPDH	Glyceraldehyde 3-phosphate dehydrogenase
6-HD	6-hydroxydopamine
GLUT	Glucose transporter
GSH	Reduced glutathione
GSSG	Oxidized glutathione

H

H&E	Hematoxylin and Eosin
H^+	Protons
H_2O	Water
HbA1c	Glycated hemoglobin

HBP	Hexosamine biosynthetic pathway
HEPES	4-(2-hydroxyethyl)-1-piperazineethanesulphonic acid
HIF-1α	Hypoxia-inducible factor 1 α
HRP	Horseradish peroxidase

I

IFG	Impaired fasting glucose
IgG	Immunoglobulin G
IGT	Impaired glucose tolerance

J

K

KCl	Potassium chloride
KO	Knock-out

L

M

M2VP	1-methyl-2-vinyl-pyridinium trifluoromethane sulphate
$MgCl_2$	Magnesium chloride
$MgSO_4 \cdot H_2O$	Magnesium sulphate heptahydrate
Mn-SOD	Manganese-dependent superoxide dismutase
MPA	Metaphosphoric acid
MPA	Malondialdehyde
mPTP	Mitochondrial permeability transition pore

N

NaCL	Sodium chloride
NADH	Nicotinamide adenine dinucleotide
$NADP^+$	Oxidized nicotinamideadenine dinucleotide phosphate
NADPH	Nicotinamide adenine dinucleotide phosphate

NADPt	Total NADP
NC	Negative control
NF-κB	Nuclear factor kappa-light-chain-enhancer of activated B cells
NIDDM	Non-insulin-dependent diabetes mellitus
NO	Nitric oxide
NOGPs	Non-oxidative glucose pathways
NOX	Nicotinamide adenine dinucleotide phosphate oxidase
N-terminal	Amine terminal

O

$O^{\cdot -}_2$	Superoxide radical
O_2	Oxygen
OGTT	Oral glucose tolerance test
$OH^{\cdot -}$	Hydroxyl radical
$ONOO^-$	Peroxynitrite
ORAC	Oxygen radical absorbance capacity

P

PARP	Poly-adenosine diphosphate-ribose polymerase
P_i	Inorganic phosphate
PI3K/Akt	Phosphatidylinositol 3-kinase/ Protein kinase B
PKC	Protein kinase C
PP	Pyrophosphate
PPP	Pentose phosphate pathway
Pyr	Pyrimidine

Q

R

R5P	Ribose 5-phosphate

RAGE	Receptor for advanced glycation end-products
RLU	Relative light units
Ru5P	Ribulose 5-phosphate

S

SANS	South African National Standards
SEM	Standard error of the mean
SOD	Superoxide dismutase
SOD	Superoxide dismutase
SSA	Statistics South Africa
STZ	Streptozotocin

T

T-cells	Thymus cells
T1DM	Type 1 diabetes mellitus
T2DM	Type 2 diabetes mellitus
TBA	Thiobutyric acid
TBARS	Thiobutyric acid reactive substances
TBARS	Thiobutyric acid reactive substances
TCA	Tricarboxylic acid
TDP	Thiamine diphosphate
TKT	Transketolase
TKTL1	Transketolase-like 1
TKTL1-KO	Transketolase-like 1 knock-out
TKTL2	Transketolase-like 2
TPP	Thiamine pyrophosphate
TPTZ	2,4,6-Tris(2-pyridyl)-5-triazine
Tris	Trisaminomethane

Tris-HCl	Trisaminomethane hydrochloric acid

U

UDP-GlcNAc	Uridine-*N*-acetyl glucosamine
UV	Ultraviolet

V

vs.	Versus

W

WHO	World health organization
WT	Wild type

X

X5P	Xylulose 5-phosphate

Y

Z

Units and other

%	Percent
~	Approximately
<	Smaller than
>	Larger than
Δ	Change increment
≥	Larger than or equal to
°C	Degrees Celsius
A	Absorbance
AUC	Area under curve
cm	Centimeter
dl	Deciliter

g	Gram
g	Relative centrifuge force
h	Hour
kg	Kilogram
L	Liter
M	Molar
mg	Milligram
min	Minute
mm	Millimeter
mmol	Millimole
mU	milliunit
nm	Nanometer
s	Second
TE	Trolox equivalent
U	Unit
V	Volt
v/v	volume per volume
β	Beta
ε	Extinction coefficient
κ	Kappa

Chapter 1: Introduction

1.1 Diabetes mellitus

Diabetes mellitus describes a group of metabolic conditions of manifold etiologies of genetic and environmental origin (World Health Organization [WHO], 2006). The most noticeable characteristics of diabetes include hyperglycemia and dysfunctional insulin secretion and/or action. The latter results in disturbed carbohydrate, protein and lipid metabolism.

1.1.1 Critical numbers of this international crisis

Diabetes is a growing concern worldwide as it is currently one of the major causes of mortality and disability (Murray *et alet al*., 2013). The mortality rate attributed to diabetes mellitus in 2015 was 1.59 million – making it the sixth leading cause of death globally (WHO, 2017). Furthermore, a large percentage of diabetic individuals commonly remain undiagnosed (Bailey *et alet al*., 2016). Therefore, it is likely that the reported deaths attributed to diabetes are rather conservative and do not mirror the true danger of this disease.

At the turn of the century, an estimated 171 million individuals worldwide suffered from diabetes (Wild *et al*., 2004). This number was expected to rise to 366 million by 2030; however, by 2008 it had already risen to 347 million (Shisana *et al*., 2013). In 2016, an estimated 422 million of overall, global morbidity was attributed to diabetes (WHO, 2016). These statistics illustrate the epidemic proportions to which this disease has escalated in the past two decades.

1.1.2 Diabetes in South Africa

When focusing on South Africa, there is a paucity of epidemiological studies that rely on biomarkers to determine the prevalence of diabetes (Shisana *et al*., 2013). However, current data show that diabetes contributes ~6% to the morbidity in South Africa (WHO, 2016).

A report compiled from the General Household Survey in 2011 indicated that 4.7% of the population were diagnosed with some form of diabetes (Statistics South Africa [SSA], 2013), while the The South African National Health and Nutrition Examination Survey [SANHANES-

1] reported a 10% prevalence of diabetes (glycated hemoglobin [HbA1c] > 6.5%, blood glucose > 7 mM) in the same population (Shisana *et al*., 2013). One major drawback of the data acquired from the General Household Survey report is that it relied solely on questionnaires and did not consider undiagnosed cases as there were no diagnostic tests involved. In the SANHANES-1 report the data consisted of a self-reported, previously diagnosed section as well as diagnostic testing of collected blood samples.

1.1.3 Diabetes, closer to home – Western Cape

In 2011, 6.8% of the Western Cape population was reportedly diagnosed with diabetes with the majority (98.4%) receiving treatment (SSA, 2013). Furthermore, a prevalence and management study in the region reported that among 12,496 individuals partaking in the study, 9.4% suffered from diabetes (non-fasting blood glucose ≥ 11.1 mmol/L) (Bailey *et al*., 2016). Of these patients, 12.7% were previously undiagnosed and 59.4% of the self-reported diagnosed patients were not receiving treatment for this disease. These data suggest that the impact of diabetes is significantly undervalued. A report released by SSA confirmed diabetes as the leading underlying cause of mortality in 2015, with 7.2% of deaths in the Western Cape ascribed to this disease (SSA, 2017). Taken together these statistics indicate a somber future.

1.2 Type 1 vs type 2 diabetes

Diabetes is broadly classified into two subsets – type 1 and type 2 (WHO, 2006). Type 1 diabetes mellitus (T1DM) accounts for ~10% of diabetic cases and is generally considered an autoimmune disorder (Gillespie, 2006; Jouvion *et al*., 2006). T1DM is broadly characterized by insulin deficiency and the need for insulin therapy from a relatively early stage. By contrast, type 2 diabetes mellitus (T2DM) is a metabolic disorder with insulin resistance the key feature (WHO, 1999). A common characteristic of both diabetes types is hyperglycemia, with varied pathophysiological consequences (discussed in more detail below, refer Table 1.2.1 for comparative assessment of T1DM and T2DM).

Table 1.2.1 **Comparison between T1DM and T2DM**

Diabetes Mellitus	T1DM	T2DM
Diagnostic criteria	FPG: ≥ 7.0 mM **or** HbA1c: ≥ 6.5% **or** 2-h plasma glucose*: ≥ 11.1 mM Autoantibodies, autoantigens, decreased C-peptide.	FPG: ≥ 7.0 mM **or** HbA1c: ≥ 6.5% **or** 2-h plasma glucose*: ≥ 11.1 mM
Bio-markers	Classic: Hyperglycemia, ketonemia/ ketonuria, ↓ insulin and C-peptide levels, reduced β-cell mass. Autoantibodies: glutamic acid decarboxylase, insulin and/ or islet cells. Antigens: human leukocyte antigen-related	Classic: Hyperglycemia, hyperinsulinemia, hyperlipidemia. ↑ Inflammatory markers ↓ Anti-inflammatory markers
Physical symptoms	Classic: Polydipsia, polyuria, polyphagia, blurry vision, fatigue, and weight loss.	Commonly asymptomatic.
Complications	Retinopathy, neuropathy, cardiovascular disease, hypoglycemia.	Retinopathy, micro- and macrovascular complications, lower-limb ulcers, myocardial infarction.
Etiology and risk factors	Genetic: predisposition to the auto-immune destruction of pancreatic β-cells. Environmental: infection, insulin resistance, obesity, toxins (streptozotocin [STZ], alloxan, vacor), vitamin D deficit. Idiopathic: no known etiology.	Obesity (especially visceral), age, sedentary lifestyle, hypertension, dyslipidemia, ethnicity.
Treatment strategies	Dependent on insulin for survival.	Weight reduction, increased physical activity, pharmacological treatments (metformin, intermediate-acting insulin, gliclazide).

* Venous plasma glucose 2 hours after ingestion of 75 g oral glucose load. FPG: Fasting plasma glucose, HbA1c: glycated hemoglobin, STZ: streptozotocin. Diagnostic criteria compiled from WHO and American Diabetes Association (ADA) criteria.

The etiology of both T1DM and T2DM is multifaceted and is thought to include genetic predisposition as well as environmental stimuli (reviewed in Scheen, 2004). For T2DM the pathophysiology is predominantly associated with obesity, insulin resistance and hyperglycemia. These are interrelated and converge on the chronic availability of energy substrates, i.e. hyperglycemia and increased circulating free fatty acids and triglycerides (reviewed in Nolan *et al*., 2011). As the spotlight of this study is on hyperglycemia this will be the focus from now onwards.

1.3 Hyperglycemia

Hyperglycemia leads to robust uptake of glucose into insulin-independent tissues (Jagdale *et al*., 2016). It also triggers biochemical and electrophysiological perturbations that contribute to contractile dysfunction (Mapanga *et al.,* 2014). For example, exposure to chronic hyperglycemia is often associated with increased incidence of acute myocardial infarction, macrovascular damage (e.g. stroke), diabetic cardiomyopathy and eventually heart failure, which together form the major causes of death in patients with diabetes (reviewed in Mapanga and Essop, 2016).

Diabetes-related hyperglycemia also contributes to microvascular damage such as retinopathy and nephropathy which are relatively common occurrences in diabetic patients (Stratton *et al*., 2000; reviewed in Singleton *et al*., 2003). Here lower limb amputations strongly correlate with vascular complications and diabetes (Hämäläinen *et al*., 1999; Kurowski *et al*., 2015). The kidneys and the liver which play vital roles in metabolism and detoxification - are also vulnerable to the effects of hyperglycemia (refer Section 1.3.5). Furthermore, pancreatic β-cells are particularly susceptible to hyperglycemic damage which can induce islet formation to compensate for increased apoptosis in these regions (Bonner-Weir *et al*., 1989). The eventual failure of this adaptation is thought to underlie progression to overt hyperglycemia and diabetes (discussed below). By contrast, the liver is predisposed to mitochondrial dysfunction prompted by hyperglycemia. This has been shown in a variety of cell culture and

animal models that utilized a range of diabetes-inducing agents such as alloxan and streptozotocin (STZ), as well as in human studies (reviewed in Dey and Swaminathan, 2010).

The literature reviewed indicate the intricate nature of hyperglycemia as it affects numerous organs in a distinct fashion. Before we consider the mechanisms at play in hyperglycemia-induced damage, it is important to first examine the onset of hyperglycemia.

1.3.1 The progression of hyperglycemia

The concentration of glucose in the blood is determined by two critical factors, the rate of glucose entering the bloodstream and its rate of clearance from circulation (Dinneen, 1997). When homeostasis of either of such processes is disturbed then hyperglycemia ensues. Hyperglycemia in the context of diabetes management is commonly divided into a number of pathological stages (Table 1.3.1) – normoglycemia (non-diabetic), impaired fasting glucose (IFG) and impaired glucose tolerance (IGT, pre-diabetes), and hyperglycemia (diabetes) (Seino *et al*., 2010). Before considering the derangement of glucose homeostasis, the maintenance of glucose homeostasis in normoglycemic individuals will be discussed.

Table 1.3.1 **Criteria for the diagnosis of pre-diabetes and diabetes**

Diabetic status	Nondiabetic (Normoglycemic)	Prediabetic		Diabetic
		Impaired fasting glucose (IFG)	Impaired glucose tolerance (IGT)	
Fasting plasma glucose	<6.1 mmol/L	Between 6.1 and 6.9 mmol/L	<7.0 mmol/L	≥7.0 mmol/L
Non-fasting blood glucose	~5.1 mmol/L			≥11.1 mmol/L
Oral glucose tolerance test	<7.8 mmol/L	<7.8 mmol/L	≥7.8 and <11.1 mmol/L	≥11.1 mmol/L
HbA1c				≥6.5%

1.3.1.1 Normal glucose homeostasis

Under fasting conditions, blood glucose concentrations are maintained at roughly 5 mmol/L and this occurs by glucose transporter (GLUT)-2 that is expressed in the liver (Unger, 1991). The liver produces glucose via glycogenolysis and gluconeogenesis where glucose is secreted into the bloodstream to prevent hypoglycemia (reviewed in Dinneen, 1997). This intricate balance is sustained by two antagonistic hormones: insulin and glucagon (Unger and Orci, 1981). In the fasting state, glucagon (secreted by pancreatic α-cells) primes the liver to secrete glucose which is subsequently used by the brain and other tissues as a fuel substrate (reviewed in Unger, 1991).

Upon the ingestion of a carbohydrate-containing meal, glucose from the gastrointestinal tract enters the bloodstream. This action triggers GLUT-2 receptors on pancreatic β-cells which respond with insulin secretion in two phases (Ceriello and Motz, 2004; reviewed in Unger, 1991). The first phase is a pronounced, acute entry of insulin into the bloodstream triggering GLUT-4 translocation to the plasma membrane on insulin-sensitive tissues (muscle and adipose tissue) via the phosphatidylinositol 3-kinase (PI3K)/Protein kinase B (Akt) pathway (Bergman *et al*., 1981, reviewed in Leahy, 2005; Sano *et al*., 2003). Here, glucose enters the tissue at a rate matching its entry into circulation thereby allowing the return to normoglycemia (Maruyama *et al*., 1984). Concurrently, insulin impedes glucagon secretion from pancreatic α-cells thereby suppressing hepatic glucose release and promoting its uptake. In this phase, glycogenesis and protein synthesis are stimulated, lipolysis attenuated, and energy levels maintained by glucose breakdown (reviewed in Baumgard *et al*., 2016; reviewed in Dinneen, 1997). The second phase of insulin secretion is a slow-release response which persists until normoglycemia is restored (reviewed in Leahy, 2005).

The dysregulation of glucose homeostasis is commonly verified with the testing of glucose tolerance. This is accomplished by monitoring glucose levels for two hours after the delivery of an oral or intravenous glucose bolus (Figure 1.3.1.1.1) (reviewed in Leahy, 2005; Scheen,

2004; Seino *et al*., 2010). This is commonly referred to as an oral glucose tolerance test (OGTT).

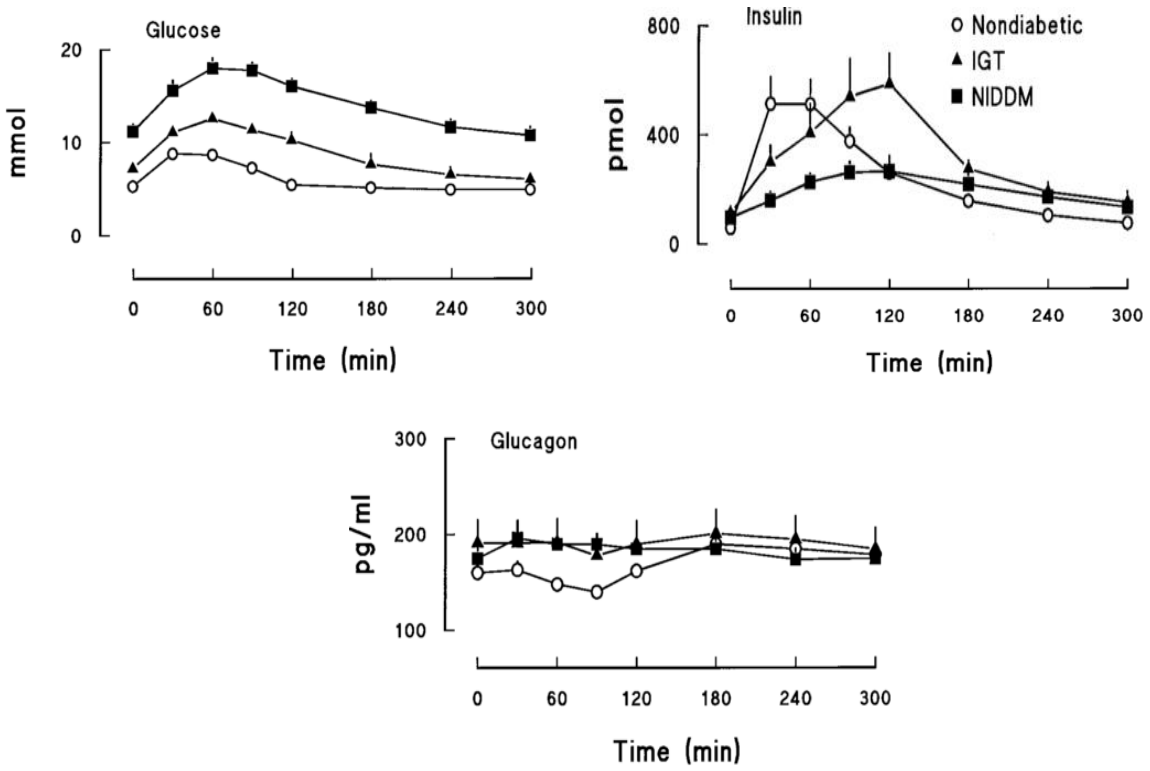

Figure 1.3.1.1.1 **Humoral response of nondiabetic, impaired glucose tolerance (IGT) and non-insulin-dependent diabetes subjects (NIDDM or T2DM).** In individuals with progressive hyperglycemic impairment, glucose concentration, as well as hormones such as insulin and glucagon, provide crucial information on the extent of the impairment. With the advancement of the dysfunction, glucose concentrations increase dramatically and remain relatively high. In parallel, the insulin response is delayed (IGT) or diminished (NIDDM), whereas glucagon levels remain relatively high (Butler and Rizza., 1991; reviewed in Dinneen, 1997).

1.3.1.2 Impaired glucose metabolism

In individuals with IGT, the first-phase insulin response is deferred (Figure 1.3.1.1.1). This is accompanied by periods of intermittent postprandial hyperglycemia as the rate of glucose clearance is attenuated (Butler and Rizza., 1991). Various mechanisms are proposed to explain the delayed responsiveness to postprandial hyperglycemia, including impaired insulin secretion (Seltzer *et al*., 1967; reviewed In Dinneen, 1997).

Decreased insulin and GLUT-2 mRNA levels are routinely found with IGT (Polonsky *et al*., 1996). This translates to attenuated pancreatic β-cell function as insulin output per cell is diminished. To compensate for β-cell dysfunction, islet hyperplasia arises allowing for increased total insulin secretion – hyperinsulinemia (Polonsky *et al*., 1996). Although insulin secretion is defective in IGT, disrupted insulin action is thought to be the major contributor to postprandial hyperglycemia (Basu *et al*., 1997; reviewed in Dinneen *et al*., 1997). This suggests that insulin resistance precedes IGT and may therefore be one of the initial pathophysiological mechanisms by which it occurs.

Insulin resistance of insulin-dependent tissues, especially muscle with GLUT-1 and GLUT-4 transporters, has been investigated as a possible cause of IGT (Ebeling *et al*., 1998; Henriksen and Dokken, 2006). The hypothesis is that glucose taken up by GLUT-1 and GLUT-4 has different fates. Here glucose transported via GLUT-1 (insulin-independent) is phosphorylated by hexokinase I and is available for further metabolism by various pathways, while glucose taken up via the predominant glucose transporter – GLUT-4 (insulin-dependent) – is phosphorylated by hexokinase II and primarily metabolized by glycogenolysis and glycolysis (Ebeling *et al*., 1998). When systemic glucose levels rise, glucose uptake via GLUT-1 is augmented and excess intracellular glucose can enter the hexosamine biosynthetic pathway (HBP). This attenuates insulin-dependent GLUT-4 translocation to the plasma membrane and therefore less glucose is taken up by this transporter, i.e. insulin resistance (reviewed in Petersen and Shulman, 2006).

Hyperinsulinemia has also been implicated in insulin resistance, especially in pancreatic β-cells where the infusion of insulin led to alterations in GLUT-2 expression patterns and impaired signaling and function (Chen *et al*., 1990). Furthermore, it rendered pancreatic β-cells increasingly unresponsive to the excess glucose in the bloodstream (Johnson *et al*., 1990). A 25-year follow-up study of normoglycemic individuals with a predisposition to developing T2DM was crucial in delineating the mechanisms behind the transition from IGT to diabetes (Martin *et al*., 1992). Here individuals who underwent the transition to diabetes

showed signs of a compensatory insulin response which declined gradually before the onset of diabetes (Martin *et al*., 1992). This was attributed to pancreatic β-cell decompensation, accompanied by increased superfluous hepatic glucose production and resulting in IFG (Efendić *et al*., 1985; Lillioja *et al*., 1993). A significant theme from the follow-up study was that insulin sensitivity and insulin-dependent glucose clearance inversely correlated with the risk of T2DM development. This was substantiated by insulin resistance strongly correlating with the progression of IGT and IFG to overt hyperglycemia (diabetes) (Knowler *et al*., 1990).

1.3.1.3 Overt hyperglycemia

The fasting state of T2DM is characterized by decreased glucose uptake in insulin-dependent tissues as well as increased hepatic glucose production which maintains chronic fasting hyperglycemia (reviewed in Unger, 1991). In the postprandial state, there is an influx of glucose from dietary substrates, causing extensive hyperglycemia (Figure 1.3.1.1.1). Unlike the normal response, pancreatic β-cells of diabetic persons are insensitive to increased blood glucose levels (delayed first phase response). This results in insufficient insulin secretion which in turn leads to decreased GLUT-4 translocation and attenuated glucose uptake (blunted first phase response) (reviewed in Polonsky *et al*., 1996). This signifies the decompensation of pancreatic β-cells as they can no longer maintain insulin levels high enough to overcome hyperglycemia (reviewed in Polonsky *et al*., 1996). Additional mechanisms of pancreatic β-cell dysfunction include reduced insulin gene expression due to deoxyribonucleic acid (DNA) damage and apoptosis of such cells (Pick *et al*., 1998; Piro *et al*., 2002; Shimabukuro *et al*., 1998). Both mechanisms occur as a result of "glucolipotoxicity", i.e. excessive amounts of intracellular glucose and fatty acids which trigger oxidative stress (Zhou and Grill, 1994; Sako and Grill, 1990; Piro *et al*., 2002). Moreover, glucagon inhibition by insulin is diminished and hepatic glucose production continues in the postprandial state (Efendíc *et al*., 1985; Lillioja *et al*., 1993). These compounding effects contribute to chronic hyperglycemia, with circulating glucose levels not returning to the normal, homeostatic range.

The effect of chronic hyperglycemia on various mechanisms of oxidative stress and anti-oxidant will now be discussed in more detail.

1.3.2 Hyperglycemia and oxidative stress

Various hypotheses have been proposed to explain the link between hyperglycemia and the development of diabetic complications. Some of these include the activation of protein kinase C (PKC), activation of the polyol pathway, increased formation of advanced glycation end-products (AGEs), pseudohypoxia and oxidative stress (reviewed in Thornalley *et al*., 2001). In line with the focus of this project, we will focus on oxidative stress as a key mechanism responsible for hyperglycemia-induced damage.

1.3.2.1 Mitochondrial superoxide

Mitochondria are the powerhouses of the cell and play an essential role in maintaining intracellular energy homeostasis (Figure 1.3.2.1.1). However, under hyperglycemic conditions excess intracellular glucose availability causes mitochondrial energy production to become dysfunctional. This can be compared to a machine that becomes overheated and cannot function properly leading to damaging outcomes. Du and colleagues (2000) first proposed that hyperglycemia-related damaging effects are primarily mediated by excess mitochondrial reactive oxygen species (ROS), and specifically superoxide ($O^{\cdot -}_2$) production.

Under normal conditions glucose enters glycolysis where it is metabolized to pyruvate in the cytosolic compartment. Pyruvate subsequently enters the tricarboxylic acid (TCA) cycle in the mitochondrion to generate e^- donors, i.e. nicotinamide adenine dinucleotide (NADH) and flavin adenine dinucleotide ($FADH_2$). Such donors transfer electrons (e^-) to complex I and II, respectively, while (in parallel) protons (H^+) are transported to the impermeable mitochondrial intermembrane space (Figure 1.3.2.1.1). The e^- are next shuttled by coenzyme Q (CoQ) to complex III, where cytochrome C (CytC) shuttles it to complex IV. Here the e^- are transferred to oxygen (O_2) to form water (H_2O). Adenosine triphosphate (ATP) synthase subsequently utilizes the H^+-gradient to convert adenosine diphosphate (ADP) and an inorganic phosphate (P_i) to ATP (reviewed in Brownlee *et al*., 2005).

With excessive glucose availability a surplus of NADH and $FADH_2$ are supplied to the electron transport chain (ETC) (Figure 1.3.2.1.1). Here it causes a progressive increase in mitochondrial membrane potential (above the physiological threshold) as H^+ is continually pumped into the intermembrane space. When this occurs the e^- transfer to complex III is hindered and trapped on CoQ. The latter subsequently donates a single e^- to O_2, forming $O^{\cdot-}_2$, a volatile form of ROS.

Increased $O^{\cdot-}_2$ levels can trigger DNA strand breaks which subsequently stimulates poly-ADP-ribose polymerase (PARP) as a reparative mechanism (Du *et al*., 2003). As a secondary effect to PARP activation, glyceraldehyde-3-phosphate dehydrogenase (GAPDH) activity is repressed by poly(ADP-ribosyl)ation (Du *et al*., 2003). This enzyme is crucial in glycolysis and its inactivity leads to a build-up of glycolysis intermediates that can be channeled into other metabolic pathways – non-oxidative glucose pathways (NOGPs – discussed in Section 1.3.2.2 below) – with detrimental consequences (Brownlee *et al*., 2005). This sequence of events has been termed the "unifying hypothesis of hyperglycemic damage" and forms the premise of NOGP activation. Moreover, as hypothesized by Ebeling and colleagues (1998), glucose taken up by GLUT-1 can also be channeled through the NOGPs further exacerbating this cycle of activation. Although mitochondrial $O^{\cdot-}_2$ forms the basis of this hypothesis (backed by robust experimental evidence), additional sources and mechanisms of intracellular ROS production cannot be ruled out. For example, subsequent studies have lent credence to a more complex and interrelated set of mechanisms that may facilitate this (Joseph *et al*., 2014; reviewed in Schaffer *et al*., 2012; Serpillon *et al*., 2009). In line with this, we next discuss additional sources of ROS production, the variety of ROS and intracellular anti-oxidant systems that are all targeted by hyperglycemia-mediated derangements.

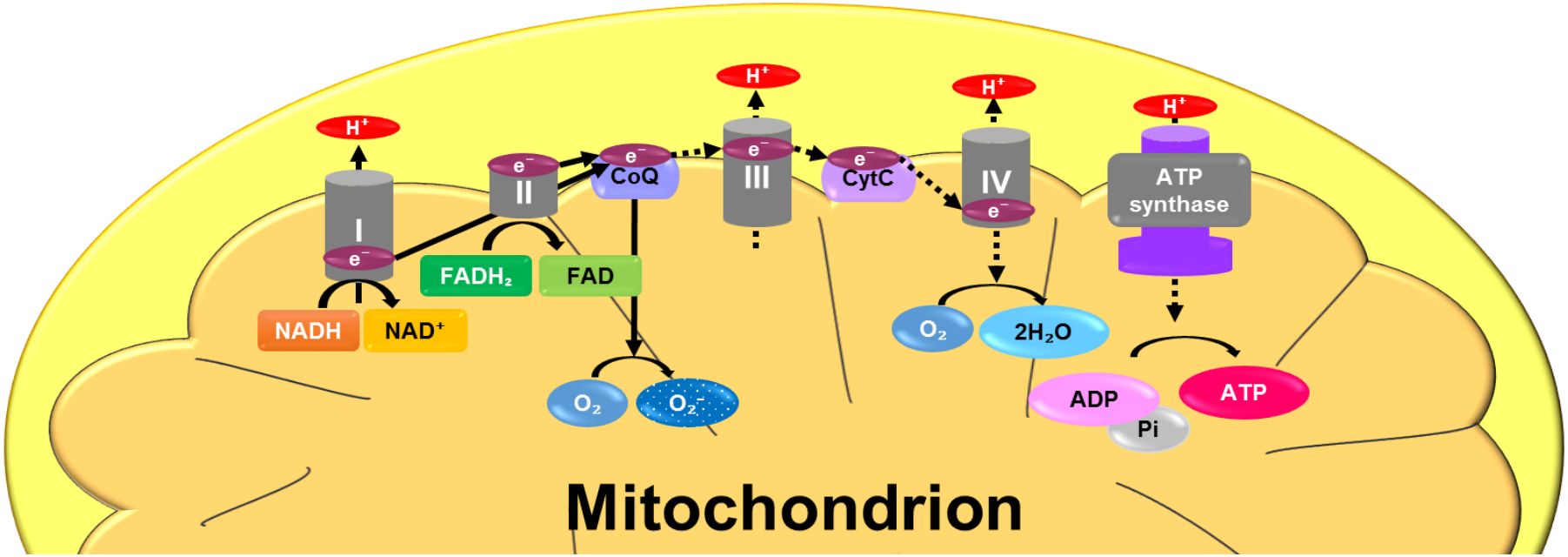

Figure 1.3.2.1.1 **The ETC under physiological and hyperglycemic conditions. Physiological conditions:** NADH and $FADH_2$ donate their e^- to the ETC which transports it from complexes I to IV where it is subsequently used to reduce oxygen to water. In parallel, H^+ is pumped into the impermeable mitochondrial intermembrane space. ATP synthase provides an outlet for the H^+ to re-enter the inner membrane and subsequently combine ADP and P_i to yield ATP. **Hyperglycemic conditions:** excessive glucose breakdown leads to an increase in reducing equivalents, i.e. NADH and $FADH_2$. Matching e^- donation, H^+ accumulate in the intramembrane space and reaches an inoperable threshold. As a result, e^- cannot be escorted to complex III and therefore the transport protein CoQ donates excess e^- to oxygen to form $O^{\cdot-}_2$ – an extremely volatile oxidizer. Adapted from Brownlee, 2005.

1.3.2.2 Nicotinamide adenine dinucleotide phosphate (NADPH) oxidase (NOX)

While mitochondria are proposed to be the main supplier of intracellular ROS, various types of NOX are also implicated in the formation of oxidative species under hyperglycemic conditions (Syed *et al*., 2011). NADPH oxidase catalyzes the reduction of O_2 to $O^{\cdot-}_2$ by simultaneously oxidizing NADPH to $NADP^+$ (Pircher *et al*., 2016). For this reason it is proposed to function as an oxygen sensor that participates in intracellular signaling. However, when hyperglycemia ensues this role is obscured by excessive ROS production (Syed *et al*., 2011).

How does NOX activation contribute to detrimental outcomes? Syed and colleagues (2011) proposed a possible mechanism where NOX initiates mitochondrial dysfunction and apoptosis in pancreatic β–cells by upregulating ROS to such an extent that it triggers c-Jun N-terminal kinases activation (a pathway activated by stress). The pancreatic β-cells subsequently undergo apoptosis and decompensation when a critical impairment is reached. This proposed mechanism has since been partly corroborated by the same group which showed that ROS generation and downstream mitochondrial damage is indeed mediated by NOX (Kumar *et al*., 2015). NADPH oxidase activity also plays a role in mediating hyperglycemic damage in the heart (Balteau *et al*., 2011; Zhang *et al*., 2006; Santos *et al*., 2011). For example, our laboratory found that acute hyperglycemia stimulated the production of a small amount of mitochondrial ROS in rat heart cells that resulted in downstream effects such as NOX activation (Joseph *et al*., 2014). The initial mitochondrial "trigger" ROS is thought to stimulate a downstream cascade of more NOX-dependent ROS production that culminates in reduced insulin action in these cells.

1.3.2.3 Other sources and species of ROS

Various other sources also promote ROS formation under hyperglycemic conditions, including xanthine oxidase, glucose autoxidation, peroxynitrite ($ONOO^-$), uncoupled endothelial nitric oxide synthase (eNOS) and cytochrome p450. Hypoxanthine is converted to xanthine and subsequently to uric acid with xanthine oxidase acting as the catalytic enzyme (reviewed in Singh *et al*., 2009). A by-product of this reaction is $O^{\cdot-}_2$ which is subsequently converted to

hydrogen peroxide (H_2O_2) and hydroxyl radicals ($OH^{\cdot}$) (reviewed in Szkudelski, 2001). There is an increase in xanthine oxidase activity in diabetic persons and a parallel increase in radicals that oxidize molecules they encounter (Desco *et al*., 2002). With hyperglycemia there is also a concomitant increase in $O^{\cdot-}_2$ and nitric oxide (NO) (Cosentino *et al*., 1997) and the reaction of these two molecules form $ONOO^-$, an extremely reactive oxidizing agent that can cause significant cellular damage (reviewed in Ceriello *et al*., 2002). Peroxynitrite can also uncouple eNOS which causes a further increase in $O^{\cdot-}_2$ (reviewed in Kayama *et al*., 2015; Satoh *et al*., 2005). Such ROS described are considered dangerous due to their volatile nature and "reactive" oxidizing agents that can interact with DNA, lipids and, proteins to thereby modify their functional and structural characteristics. Such macromolecules are then unable to perform their physiological function and are considered hazardous to their immediate cellular environment.

In summary, various cellular mechanisms contribute to ROS formation which can lead to ROS-induced damage and modifications of macromolecules. This causes an impairment of their respective physiological functioning and thereby leading to organelle and cellular dysfunction. However, under physiological conditions the oxidative balance can be restored as cells possess inherent anti-oxidant mechanisms that help neutralize oxidative species and thereby serve in a protective capacity against oxidative stress.

1.3.3 Intracellular anti-oxidant mechanisms

Cells possess various anti-oxidant mechanisms that safeguard against oxidative damage due to excessive ROS production (Figure 1.3.3.1). Here superoxide dismutase (SOD), catalase and glutathione are a few of the anti-oxidant systems that cells have available in their defense arsenal. Superoxide dismutase converts $O^{\cdot-}_2$ (an extremely reactive oxidant) to H_2O_2, a lesser reactive species which is subsequently metabolized by catalase to H_2O and O_2. Glutathione peroxidase is also able to sequester H_2O_2 by employing reduced glutathione (GSH) as e^- donor to produce H_2O and oxidized glutathione (GSSG). The latter is recycled by glutathione

reductase - a NADPH- dependent enzyme- to replenish GSH levels (reviewed in Münzel *et al*., 2017).

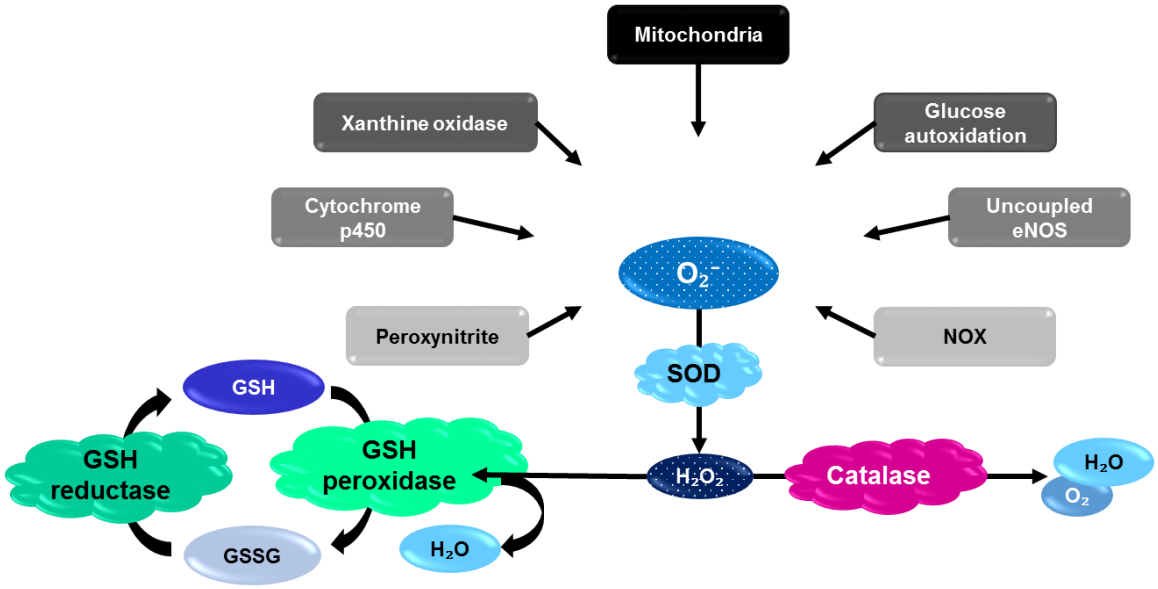

Figure 1.3.3.1 **Intracellular anti-oxidant systems that guard against oxidative stress.** Various sources contribute to ROS formation. Superoxide is an oxygen radical that is extremely unstable. Several anti-oxidant mechanisms serve as protective measures against $O^{\cdot-}_2$. For example, SOD is able to dismutate O_2^- to H_2O_2, which is a less reactive oxidizer. H_2O_2 can subsequently be converted to H_2O and O_2 by catalase or it can enter the glutathione recycling pathway. Here glutathione peroxidase catalyzes the conversion of GSH and H_2O_2 to GSSG and H_2O, whereafter glutathione reductase uses NADPH to reduce GSSG to GSH.

Under pathophysiological circumstances such as diabetes, endogenous anti-oxidant systems often fail as they cannot compensate for cumulative ROS. When this occurs the homeostatic redox balance is disrupted and oxidative-mediated stress occurs - mechanisms discussed below. It is necessary to point out here that reactive oxygen and –nitrogen species have a physiological role and that impaired functioning occurs as a result of hyperglycemic conditions.

1.3.4 Hyperglycemia and ROS enhances flux through metabolic circuits

As discussed, hyperglycemia triggers mitochondrial $O^{\cdot-}_2$-production that results in PARP activation and the accumulation of upstream glucose metabolites (reviewed in Brownlee, 2005 and refer Section 1.3.2.1 above). Accumulated glucose intermediates such as glyceraldehyde-

3-phosphate (G3P) can activate the AGE pathway and the PKC pathway, while glucose and fructose 6-phosphate (F6P) are shunted into the polyol pathway and the HBP, respectively (Figure 1.3.4.1) (reviewed in Brownlee, 2005; reviewed in Zhang, 2014). Each of these pathways can in their own way contribute to ROS and oxidative stress, either via the production of oxidative species or by consuming anti-oxidants.

1.3.4.1 Advanced Glycation End-products

Glycation is the irreversible, enzyme-independent modification of proteins and lipids as it reacts with aldose sugars, which result in the formation of AGEs (Schmidt *et al*., 1994; Natalizio *et al*., 2001). The sources of AGEs are plenty, as multiple pathways are responsible for its formation and also for some pathway intermediates (reviewed in Forbes *et al*., 2005). Here pathways include the Wolff pathway where glucose self-oxidizes, the Namiki pathway where Schiff bases are formed, and the Hodge pathway which produces Amadori products (reviewed in Baynes and Thorpe, 1999; reviewed in Mapanga and Essop, 2016). All these pathways converge to form reactive dicarbonyls that are well-known AGE intermediates (reviewed in Mapanga and Essop 2016).

Advanced glycation end products contribute to ROS formation in three main ways. Firstly, the process by which AGE are formed generates free radicals (Yim *et al*., 2001). Secondly, the interaction of AGEs and their receptors (RAGE) can activate pathways such as nuclear factor kappa-light-chain-enhancer of activated B cells (NF-*κ*B) that are also involved in ROS formation (Schmidt *et al*., 1994). Lastly, their modification of molecules – specifically anti-oxidants – can result in dysfunction (Kawamura *et al*., 1992; Morgan *et al*., 2002).

1.3.4.2 Polyol pathway

About 3% of glucose-6-phosphate (G6P) enters the polyol pathway under physiological conditions (Morrison *et al*., 1970). However, under hyperglycemic conditions this figure increases by more than tenfold (González *et al*., 1984). The conversion of glucose to sorbitol is catalyzed by aldose reductase where NADPH (enzyme cofactor) is oxidized to $NADP^+$ (González *et al*., 1984). The regeneration of NADPH consumes GSH, the most abundant

natural anti-oxidant (Shakeel, 2015). Thus increased polyol pathway flux indirectly depletes GSH which in turn leads to increased intracellular ROS levels.

1.3.4.3 Protein kinase C

Protein kinase C belongs to a family of protein kinases involved in various signaling pathways (Newton, 2003). No less than eleven PKC isoforms are known to date and these are categorized into classical-, new-, and atypical PKCs according to their structure and dependence on calcium (Ca^{2+}) (reviewed in Koya and King, 1998). Hyperglycemia causes the activation of some conventional PKC isoforms (i.e. β, δ, and α) via the induction of diacylglycerol (Inoguchi *et al*., 2000). Subsequently, PKC forms ROS via the upregulation of NOX which in turn stimulates $O^{\cdot-}_2$ production (refer Section 1.3.2.1 and 1.3.2.2).

1.3.4.4 Hexosamine biosynthetic pathway

Under physiological conditions, the HBP functions as a nutrient sensing pathway (especially glucose) and produces uridine diphosphate-*N*-acetyl glucosamine (UDP-GlcNAc) (Rajapakse *et al*., 2008). Further processing of UDP-GlcNAc results in the transfer of *O*-linked β-*N*-acetylglucosamine moieties to side chains of target proteins or lipids (reviewed in Hardiville and Hart, 2014). Hyperglycemia induces increased flux through this pathway due to increased availability of substrates and this has also been linked to ROS formation as well as diabetes-related complications such as insulin resistance, pancreatic β-cell dysfunction and cardiac-specific damage (reviewed in Garson *et al*., 2014; Rajapakse *et al*., 2008).

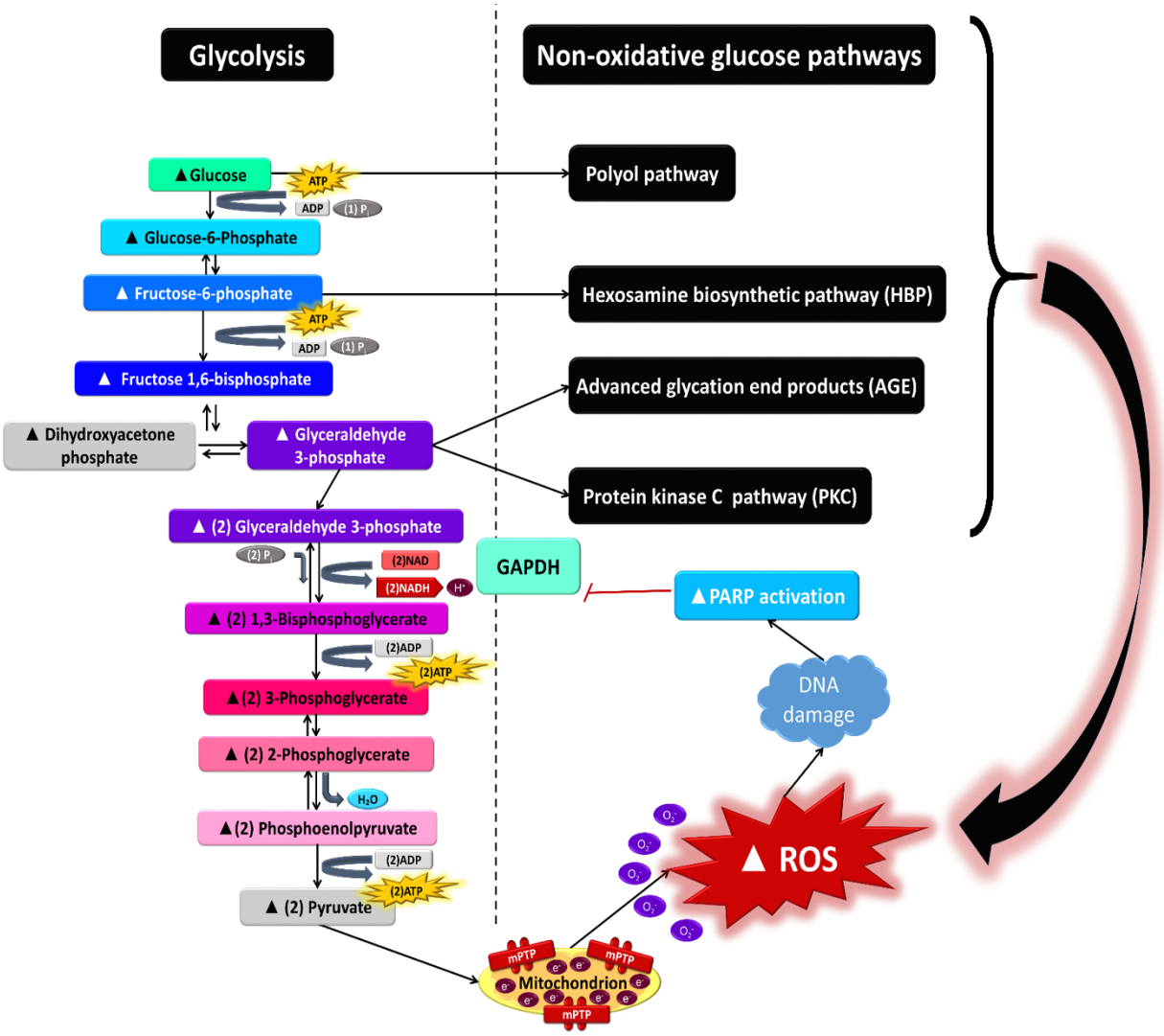

Figure 1.3.4.1 **Glycolytic metabolites enter NOGPs.** Hyperglycemia leads to increased intracellular glucose availability. The most common pathway for glucose breakdown is via anaerobic glycolysis. With increased glycolysis, there is a concomitant upsurge in mitochondrial ROS which leads to DNA damage. PARP is activated to repair DNA damage, but this inhibits the glycolytic enzyme GAPDH. Non-oxidative glucose pathway flux is enhanced to help clear the build-up of intracellular glucose metabolites. However, hyperactivation of NOGPs leads to increased ROS production with damaging outcomes. This forms a vicious cycle of ROS-induced-ROS where excessive ROS can further activate the NOGPs.

Hyperglycemia-mediated ROS can lead to glucose toxicity or "glucotoxicity" as it can lead to several downstream effects including cell death (Giacco and Brownlee, 2010). Glucotoxicity can also be facilitated by other cellular stresses that include endoplasmic reticulum stress and mitochondrial stress, and cross-talk between such systems (Mooradian, 2016).

As described previously (refer Sections 1.3.2 to 1.3.3), it is evident that oxidative stress plays a mechanistic role in hyperglycemia-induced damage. Oxidative stress can also exacerbate hyperglycemia-mediated effects by contributing to diabetes-related complications such as insulin resistance, glucotoxicity, and pancreatic β-cell dysfunction. Moreover, various positive feedback cycles exist such as ROS-inducing-ROS, where mitochondrial $O^{\cdot-}_2$ can lead to the activation of metabolic circuits (NOGPs) that themselves increase ROS generation. NADPH oxidase also generates $O^{\cdot-}_2$ that can further fuel NOGP activation. As such mechanisms are interlinked, this complicates the advance of therapeutic options to alleviate and salvage hyperglycemia-induced organ and cellular damage. In the next section, we will discuss the effect of hyperglycemia and hyperglycemia-induced oxidative damage on particular organs of interest to this study.

1.3.5 Effect of hyperglycemia and downstream oxidative stress on the heart, liver, and circulation

Hyperglycemia affects many tissues, but the extent to which damage is caused is often tissue- or even cell-specific. It is with this rationale in mind that we next discuss the effects of hyperglycemia and hyperglycemia-induced oxidative stress on specific organs of interest to this study.

1.3.5.1 Effect of hyperglycemia and downstream oxidative stress on the heart

When the heart is subjected to chronic hyperglycemia, metabolic perturbations are often encountered. Here oxidative stress is induced by all the previously described mechanisms – increased mitochondrial $O^{\cdot-}_2$ production, surplus flux via NOGPs, as well as NOX hyperactivity and decreased anti-oxidant defense capacity. Extensive ROS accumulation can impact on the mitochondrial ETC, causing hyperpolarization of the inner mitochondrial membrane as

discussed (reviewed in Brownlee, 2005). This can trigger mitochondrial permeability transition pore (mPTP) opening (attempting to equilibrate membrane ionic imbalances), leading to the accumulation of intracellular Ca^{2+} (Baines, 2009).

Cardiomyocytes are especially vulnerable to mitochondrial dysfunction and subsequent Ca^{2+} dysregulation as they are particularly rich in mitochondrial content to match energy demands to sustainably perform its ATP-intensive function (Page and McCallister, 1973). Moreover, Ca^{2+} is highly regulated by the sarcoplasmic reticulum and governs cardiomyocyte contraction (reviewed in Stammers *et al*., 2015). Altered Ca^{2+} homeostasis can impede cardiac functionality and induce maladaptive cardiac remodeling as it is centrally involved in signaling pathways (reviewed in Berridge *et al*., 2000; reviewed in Berridge *et al*., 2003).

Besides damaging DNA, oxidative species are also known to react with macromolecules such as lipids and protein. For example, cardiolipin is a mitochondrial membrane constituent that is often a casualty of increased intracellular ROS levels (reviewed in Circu and Aw, 2010). Due to the large mitochondrial capacity of cardiac tissues, cardiolipin oxidation renders the heart especially vulnerable to oxidative damage and subsequent cell death via apoptosis. Similarly, a disproportionate amount of ROS can initiate protein unfolding, carbonylation, and oxidation that can prompt apoptosis (reviewed in Berlett and Stadtman, 1997; reviewed in Suzuki *et al*., 2011).

Hyperglycemia-induced oxidative stress can also initiate myocardial insulin resistance via the induction of mitochondrial dysfunction and NOGP activation. Data from our laboratory demonstrate that NOGP stimulation elicits impaired GLUT-4 translocation in rat heart cells (Joseph *et al*., 2014). Moreover, our laboratory also found that acute hyperglycemia resulted in hyperglycemia-mediated oxidative stress and NOGP activation that subsequently diminished the contractile function of *ex vivo* perfused hearts (Mapanga *et al*., 2014). Collectively these data show that the heart is susceptible to oxidative stress within the context of hyperglycemia.

1.3.5.2 Effects of hyperglycemia-induced oxidative stress on the liver

The liver plays a central role in metabolism as it acts as an energy-substrate "manufacturer and distributor" for the rest of the body. As a result of this crucial role, the liver is exposed to continual oxidative stress and therefore needs an arsenal of anti-oxidant capacity. The latter is linked to fuel substrate availability, e.g. diabetic individuals can display increased blood glucose concentrations due to greater hepatic glucose uptake (Efendíc *et al*., 1985). Together with amplified glycogenolysis and gluconeogenesis it increases hepatic glucose production that contributes to systemically elevated glucose levels (Magnusson *et al*., 1992). The metabolism of the liver is thus increased, leading to greater ROS generation.

Hepatocyte mitochondria are strongly implicated in this process within the diabetic context. Such effects seem to be due to hyperglycemia *per se* as similar results were found for both T1DM and T2DM. Thus mitochondrial dysfunction and particularly diminished oxidative and phosphorylative activities, increased oxidative stress and a depleted anti-oxidant defenses are significant hyperglycemia-mediated outcomes in liver cells (reviewed in Dey and Swaminathan, 2010).

The most prevalent mechanisms that contribute to excessive hyperglycemia-induced hepatic ROS are lipid peroxidation and protein carbonylation (Jang *et al*., 2000; Lukivskaya *et al*., 2007). Lipid peroxidation, as measured by thiobutyric acid reactive substances (TBARS), can lead to inflammation and further damage (Dias *et al*., 2005). With increased ROS, there is a parallel decrease in anti-oxidant systems, particularly GSH and the mitochondria-specific form of SOD – manganese (Mn)-SOD (Jang *et al*., 2000).

It is interesting to note that the mitigation of hyperglycemia-induced oxidative stress (protein carbonylation) partially rescued mitochondrial function irrespective of mitochondrial enzyme activity (Lukivskaya *et al*., 2007). It is still unclear whether mitochondrial dysfunction is a cause or result of oxidative stress; however, it is more likely that it is one of the various mechanisms that contribute to ROS formation and hepatocyte dysfunction.

1.3.5.3 Effects of hyperglycemia-induced oxidative stress in circulation

Unlike biopsies of the heart and liver, blood samples are relatively easy to obtain as it can be collected with minimal invasiveness. This has allowed researchers the ability to assess the oxidative status of individuals with diabetes. Here data show that individuals who suffer from T1DM display advanced levels of lipid peroxidation (TBARS) as measured in plasma and erythrocytes (Matteucci and Giampietro, 2000). Moreover, non-diabetic siblings of such individuals also exhibited significantly more lipid peroxidation compared to controls. However, anti-oxidant defenses (GSH) were only diminished in the diabetic cohort.

Erythrocytes and other blood constituents are susceptible to modifications that alter their characteristics and functions (Olszewska *et al*., 2012; Wautier *et al*., 1994). For example, erythrocytes from diabetic patients are often glycated and this is used as one of the diagnostic markers of this metabolic disease (Table 2). The glycation of erythrocytes allows for interaction with RAGE and subsequently induce oxidative stress in other targets such as endothelial cells (Wautier *et al*., 1994). This in turn increases the risk of developing atherosclerosis and cardiovascular diseases.

To summarize, hyperglycemia induces ROS formation which (if not neutralized effectively) causes oxidative stress and subsequent damage. Moreover, increased ROS levels can enhance NOGP activation that in turn leads to more ROS formation and NOGP-induced damage. The focus will now shift to a NOGP of high relevance for the current study, i.e. the pentose phosphate pathway (PPP).

1.4 Pentose Phosphate pathway

The PPP provides an alternate path for glucose intermediates and serves two other important functions, namely NADPH production (reducing equivalent used for anabolic reactions and replenishment of GSH) and the generation of ribose-5-phosphate (R5P) (used for nucleotide biosynthesis).

The PPP consists of two parts, the oxidative and the non-oxidative branches (Figure 1.4.1) (Horecker, 1964; Srivastava and Hübscher, 1966). In the oxidative branch G6P undergoes three irreversible reactions of which glucose-6-phosphate dehydrogenase (G6PD) catalyzes the rate-limiting step. These reactions yield NADPH, a reducing equivalent for lipid biosynthesis as well as anti-oxidant defense, and ribulose-5-phosphate (Ru5P) (reviewed in Patra and Hay, 2014). Subsequently, Ru5P enters the reversible non-oxidative branch where it can be converted to R5P or xylulose-5-phosphate (X5P, glycolytic intermediates) (reviewed in Riganti *et al*., 2012). The flux-controlling enzymes of the non-oxidative phase, transketolases (TKTs) are able to recycle such pentose phosphate products back into PPP or into glycolysis (Berthon *et al*., 1992; Gumaa *et al*., 1969; Schenk *et al*., 1998; Srivastava and Hübscher, 1966).

The glycolytic pathway consists of two phases: an "investment phase" that consumes ATP, and the "payoff phase" that produces ATP (Figure 1.4.1). Glyceraldehyde-3-phosphate is one of the products that is recycled into glycolysis and enters this pathway at the beginning of the payoff phase. This means that G6P can enter the PPP and enhance anti-oxidant defenses, produce substrates for nucleotide synthesis and be used as a substrate for ATP production. Moreover, F6P can be reversibly converted back to G6P and can re-enter the PPP and thereby facilitate more NADPH formation.

Of note, some of the initial work on the PPP was conducted on human erythrocytes (Strömme and Eldjarn, 1962; Szeinberg and Marks, 1961). Here it was established that hemolytic anemia correlated with deficient GSH due to insufficient PPP activity that renders the erythrocytes vulnerable to oxidation (reviewed in Patra and Hay, 2014). This highlighted the significant role of the PPP in redox homeostasis as the replenishment of GSH relies solely on NADPH – a by-product of the PPP (Mayes, 1993). As the PPP and glycolysis are interlinked, it stands to reason that hyperglycemia will have a tremendous effect on the PPP.

.

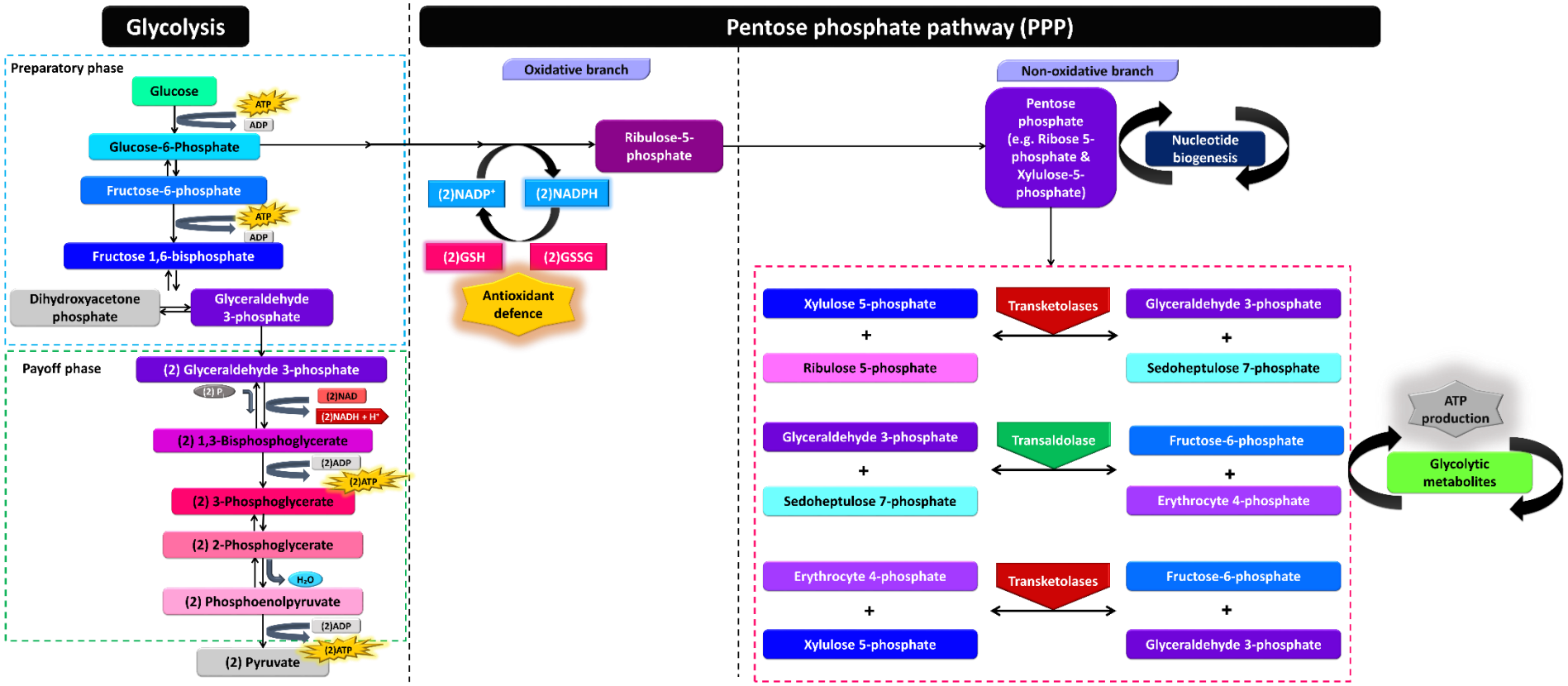

Figure 1.4.1 **Pentose phosphate pathway**. Glucose-6-phosphate passes through the oxidative phase of the PPP where it is converted to Ru5P and pentose phosphates (X5P and R5P). The latter can exit the PPP to enter nucleotide biosynthesis or continue through the PPP – the non-oxidative branch. Here transketolase enzymes (TKT, TKTL1, TKTL2) governs two reversible reactions namely, the conversion of X5P and Ru5P to G3P and sedoheptulose 7-phosphate, and erythrocyte 4-phosphate and X5P to F6P and G3P, respectively. Transaldolase catalyzes the formation of F6P and erythrocyte 4-phosphate from the products of the first transketolase-catalyzed reaction. NADPH: Nicotinamide adenine dinucleotide phosphate, GSH: reduced glutathione, GSSG: oxidized glutathione, TKT: transketolase, TKTL1: TKT-like 1, TKTL2: TKT-like 2, ATP: Adenosine triphosphate. Adapted from Joseph, 2014 and Schenck *et al*., 1998.

1.4.1 Effect of hyperglycemia on the PPP

What happens to the PPP in response to hyperglycemia/diabetes? Here data have been somewhat controversial as evidence for an increase and a decrease in activity has been reported (Gamaa *et al*., 1969; Leroux *et al*., 1975; Novello *et al*., 1969). It should be noted that the response of the PPP seems to be tissue-specific which may help explain such disparate findings. Considering the harmful effects of hyperglycemia (refer Sections 1.3.3 and 1.3.4), it stands to reason that enhanced PPP flux should allow for replenishment of intracellular anti-oxidant defenses, promote nucleotide and lipid biosynthesis and also provide metabolic substrates for ATP generation. Moreover, it is a generally accepted notion that favoring PPP flux shunts glycolytic intermediates away from damaging NOGPs and thereby providing additional beneficial effects (Du *et al*., 2008; Joseph *et al*., 2014; Katare *et al*., 2010).

1.4.2 Enhancing flux via the PPP and benefits

Pentose phosphate pathway activation can be achieved by supplementation with derivatives of vitamin B1, thiamine or benfotiamine [BFT], with the latter displaying superior bioavailability compared to the former (reviewed in Garson *et al*., 2014). Benfotiamine is a lipid-soluble derivative proposed to elicit various health-promoting effects as it acts as an anti-oxidant, anti-inflammatory and cardio-protective agent (Shoeb and Ramana, 2012; Katare *et al*., 2010; Schmid *et al*., 2008). Both thiamine and BFT enhance PPP flux as they act as cofactors for TKT thereby increasing its activity (Joseph and Essop, 2014).

Studies employing BFT found that PPP induction can prevent NOGP activation, including the HBP, advanced glycation, and PKC activation and thereby alleviated diabetic retinopathy (Hammes *et al*., 2003). BFT supplementation also diminished NF-κB activation (a key regulator of inflammation) and protected against the onset of diabetic nephropathy (Babaei-Jadidi *et al*., 2003). It also protects against micro- and macrovascular impairment, most likely through the inhibition of AGEs (Stirban *et al*., 2006). In cardiac progenitor cells of diabetic patients the clearance of AGEs and other oxidative species is upregulated by BFT, leading to

increased cell survival (Katare *et al*., 2013). Notably, thiamine and its beneficial effects arise from the activation of the non-oxidative branch of the PPP which is governed by TKT (Joseph and Essop, 2014). In view of the protective effects of TKT *per se*, and as it forms the basis of this study, we next discuss this enzyme family in more depth.

1.5 The transketolases

Transketolases are enzymes that catalyze the reversible transfer of ketol groups from a ketose to an aldose with thiamine and divalent cations as cofactors (Abedinia *et al*., 1992; Berthon *et al*., 1992; Clark and Williams, 1971; Meloche, 1964; Nikkola *et al*., 1994; Traviesa, 1974). The TKT family include TKT and two TKT-like genes (TKTL1 and TKTL2) that play an integral part in several facets of metabolism including possibly contributing to total TKT (tTKT) activity (Coy *et al*., 2005). The reason for this is that TKTs (and to a lesser extent transaldolases) are the flux-controlling enzymes of the non-oxidative branch of the PPP (Berthon *et al*., 1992; Schenk *et al*., 1998).

1.5.1 Transketolase structure

Around four decades after its discovery, both the purification and the partial sequencing of human TKT were completed (Abedinia *et al*., 1992). Here it was shown that this roughly 70 kDa homodimer displays a relatively high sequence similarity to associated enzymes in other species such as *Hansenula polymorpha* and *Rhodobacter sphaeroides*. Each of the identical subunits possesses three domains namely an amine (N)-terminal pyrophosphate (PP)-domain, a pyrimidine-binding (Pyr) domain, and a carboxy (C)-terminal domain (Lindqvist *et al*., 1992). Both the PP-domain and the Pyr domain are involved in dimerization and cofactor binding, while the function of the C-terminal domain remains to be determined (Schneider *et al*., 1998). The complete structural resolution of human TKT was achieved during 2010 (Figure 1.5.1.1) (Mitschke *et al.*, 2010). This allowed for the sequence alignment of TKT among several different species that included microorganisms, plants, and animals and revealed several interesting findings.

First, the three-dimensional structure of human TKT is conserved among species. It consists of two homodimers which rely on thiamine diphosphate (TDP) and Ca^{2+} to perform its function (Mitschke *et al*., 2010). Second, the researchers noted that the substrate channel of mammalian TKT is more tapered compared to other TKTs, which provides an explanation why the substrate range of mammalian TKT is limited compared to that of lower organisms. Lastly, although there are multiple point mutations, the overall function of the enzyme seems to be well conserved. This suggests that TKT provides an evolutionary advantage which seems to have become more specialized over time. Although the substrates of TKT differ among species, mammalian TKT catalyzes reactions of only four substrates as shown in Figure 1.5.1.2 (modified from Schenck *et al*., 1998).

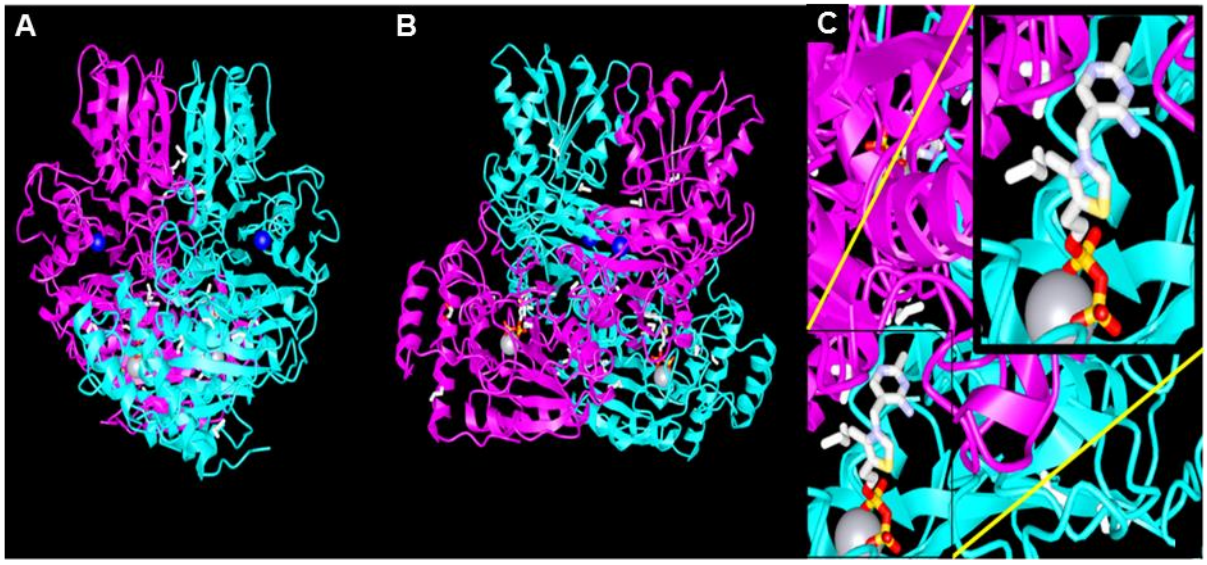

Figure 1.5.1.1 **Structure of human transketolase**. A: 3-dimensional (3D) model of human transketolase holodimer with TDP and Ca^{2+} cofactors. B: Rotated 3D model of human TKT. C: Thiamine bound to TKT. Cyan & magenta: TKT subunits, blue spheres: Na^{+}, grey spheres: Ca^{2+}.Image created with iCn3D: The Structure Of Human Transketolase (PDB ID 3MOS).

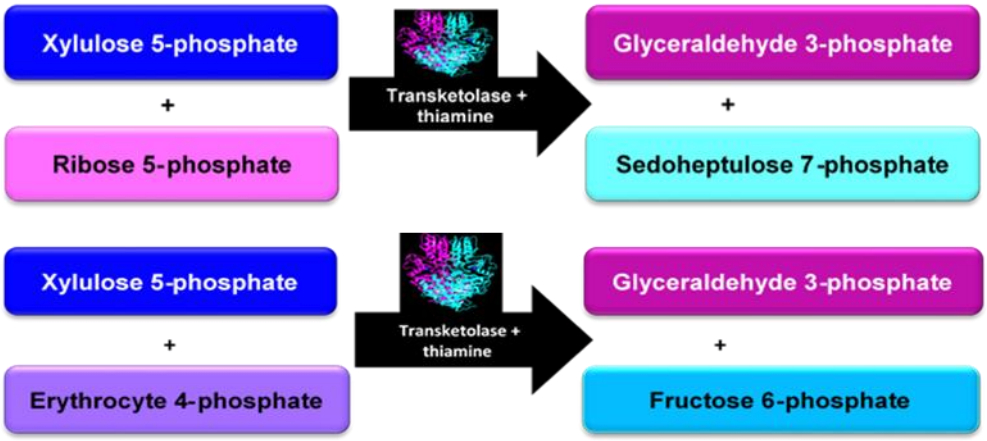

Figure 1.5.1.2 **Reactions catalyzed by human transketolase** (modified from Schenck *et al*., 1998).

1.5.1.1 Interaction of transketolase with its cofactor – thiamine diphosphate

Like all other thiamine-dependent enzymes, the binding site for thiamine diphosphate lies in a deep crevice at the interface of the dimer (Muller *et al*., 1993). Here TDP enters the binding site to form a TKT-TDP intermediate. Thereafter, TDP causes several conformational changes in the enzyme. This allows the PP domain of one subunit to attach to the diphosphate group, while the Pyr domain of the other subunit fastens the aminopyrimidine ring (Schneider *et al*., 1998). Thus TKT is activated only when TDP binds to and causes conformational changes in the apoenzyme, thereby completing the catalytically active holodimer.

1.5.1.2 Transketolase activity

The evidence concerning the evolutionary conservation of TKT is plentiful (Burrai *et al*., 2017; Schenk *et al*., 1998; reviewed in Zhao and Zhong, 2009). This supports the notion that TKT activity is fundamental in the maintenance and expansion of life. The earliest mention of TKT activity dates to the 1950s (reviewed in Kochetov and Solovjeva, 2014) and it gained further interest when decreased TKT activity was implicated in various pathologies, including Beriberi and Wernicke-Korsakoff encephalopathy (Gibson *et al*., 1988; Leigh *et al*., 1981; McCandless *et al*., 1968; Saito *et al*., 1987; Sheu *et al*., 1988; Traviesa, 1974; Wang *et al*., 1997). It was in

the undertaking to determine the mechanism behind such pathologies that the biological function of this enzyme was eventually elucidated.

Decreased TKT activity due to a deficiency of thiamine and/or magnesium was initially investigated for a causal role in several neurological disorders – most prominently Wernicke-Korsakoff encephalopathy and Alzheimer's disease (Gibson *et al*., 1988; Leigh *et al*., 1981; Sheu *et al*., 1988; Traviesa *et al*., 1974; Wang *et al*., 1997). More relevant to the context of the current study, decreased TKT activity was also linked to metabolic disturbances such as diabetes and related complications (Saito *et al*., 1987). This suggests that there is a minimum required level of TKT activity that, if not sustained, can lead to neurological and/or metabolic disorders (McCandless *et al*., 1968). As diabetes is a fundamental part of this study, the focus will shift to what is known about TKT in this particular context.

1.5.1.3 Transketolase in diabetes

Various studies employed an established STZ-induced diabetes model to gain further insights into this question (Furman, 2015; Katare *et al*., 2010; Mapanga *et al*., 2014). For example, decreased thiamine concentrations and TKT expression/activity could be ameliorated by BFT or thiamine treatment of STZ-treated rats (Babaei-Jadida *et al*., 2003). Such treatment also prevented nephropathy which the authors attributed to the induction of TKT expression that presumably decreases flux through several NOGPs. Thus hyperglycemia-mediated damaging effects (discussed earlier) can be ameliorated by increasing TKT activity through the intake of thiamine. In support, others showed that BFT oral supplementation lowered diabetes-related complications (Du *et al*., 2008; Hammes *et al*., 2003). These studies concluded that such protection was achieved via the increase of TKT activity, thereby favoring PPP flux versus the other more harmful NOGPs.

Such evidence is also corroborated by studies recently performed in our research group using an *in vitro* model of hyperglycemia (Figure 1.5.1.3.1) (Joseph, 2014). Here rat heart cells subjected to simulated hyperglycemia showed increased NOGP activation which could be reversed with BFT treatment. Likewise, another study that employed the rodent STZ-induced

diabetes model demonstrated that BFT treatment alleviated oxidative stress and decreased diabetes-induced damage (Wu and Ren, 2006).

Although not concluded by the authors, the results show that there is an increase in the GSH:GSSG ratio which indicates that the protective effect may be directly or indirectly attributable to PPP activation. Others showed that the use of BFT as TKT activator prevented STZ-induced vascular endothelial dysfunction and nephropathy by diminishing pathological changes in glomeruli and reducing oxidative stress (Balakumar *et al*., 2009). However, the protective effects of TKT activation are not only limited to the clinical context of nephropathy.

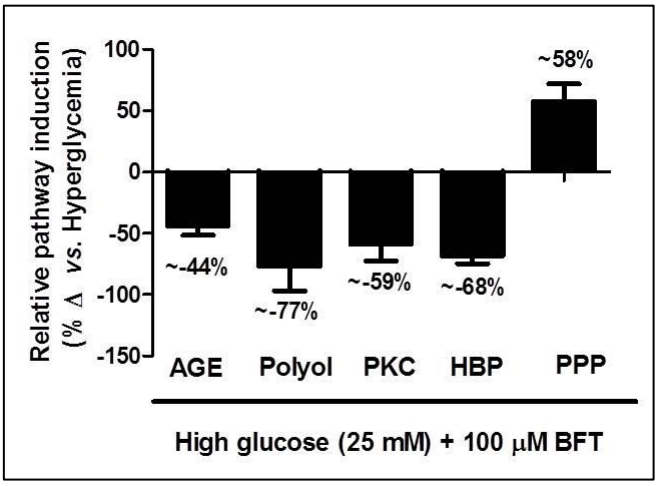

Figure 1.5.1.3.1 **BFT reverses hyperglycemia-induced NOGP activation.** In this *in vitro* model (rat heart cells) of simulated hyperglycemia (25 mM glucose for 24h), BFT (100 µM) reverses NOGP activity while concurrently activating the PPP. (Joseph, 2014).

For example, BFT treatment improved post-ischemic recovery in STZ-diabetic mice by favoring survival pathways (Gadau *et al*., 2006), while others found it also ameliorated diabetes-induced cardiac dysfunction (Ceylan-Isik *et al*., 2006). The inhibition of TKT activity by oxythiamine (a thiamine derivative and irreversible inhibitor of TKT) can induce apoptosis and also inhibit cell proliferation by reducing nucleotide and NADPH availability (Burrai *et al*., 2017). Notably, studies from our laboratory concluded that BFT induces activation of TKT *per se,* as G6PD activity remained unaltered (Figure 1.5.1.3.2) upon BFT treatment (Joseph *et al*., 2014).

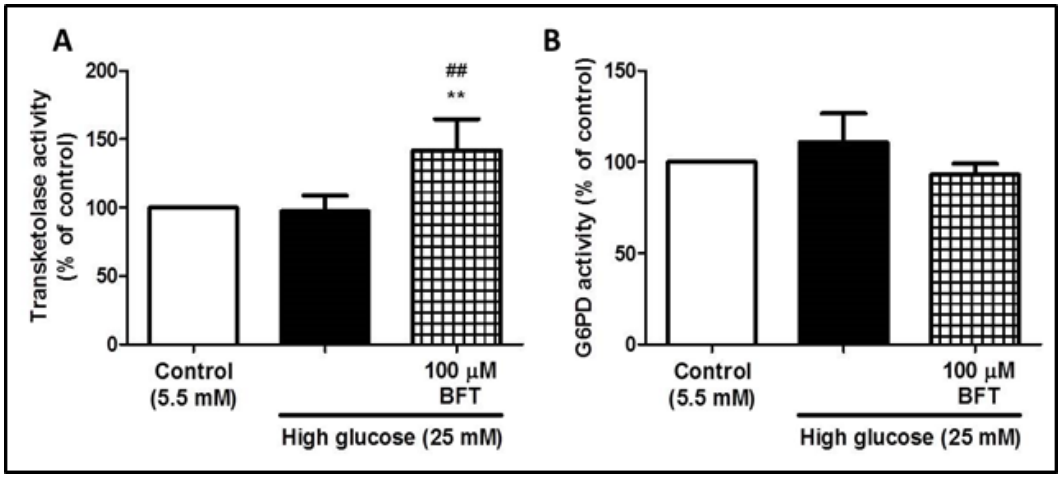

Figure 1.5.1.3.2 **BFT activates PPP in an *in vitro* model of hyperglycemia.** Treatment with BFT (100 µM) induces PPP flux by increasing transketolase activity rather than affecting G6PD activity (Joseph *et al*., 2014).

Data from our research group also demonstrate that TKT expression is unaffected in pre-diabetic and diabetic subjects but that this is not the case for TKTL1 which shows a stepwise increase in its expression (Figure 1.5.1.3.3). In light of this intriguing finding, our group has focused its efforts on understanding the role of TKTL1 within the diabetic context. This MSc study forms part of this broader initiative and the available literature concerning TKTL1 will next be reviewed.

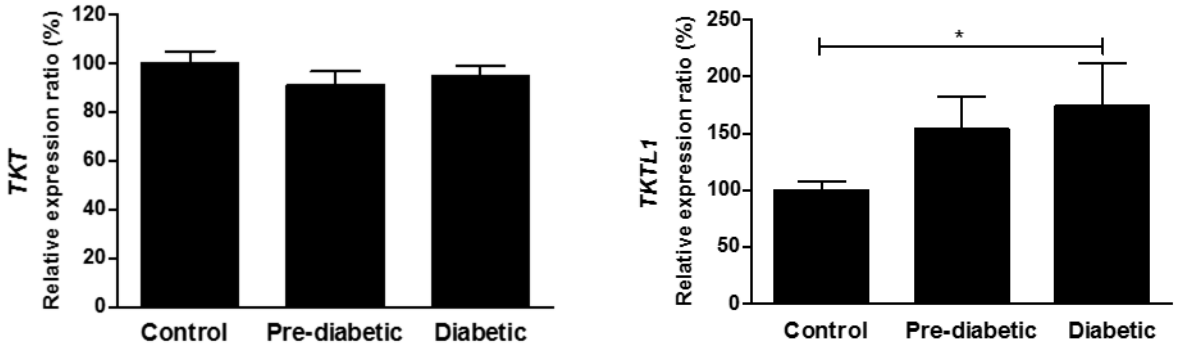

Figure 1.5.1.3.3 **Expression patterns of transketolase and TKTL1 in leukocytes of control, pre-diabetic, and diabetic patients.** Expression normalized to β-actin (Coomer and Essop, unpublished data).

1.5.2 Transketolase-like 1 (TKTL1)

1.5.2.1 TKTL1 Structure and activity

Initially named TKT related-gene, TKTL1 was first discovered in 1996 (Coy *et al*., 1996). Here different tissue isotypes were identified and the authors suggested that this points to tissue-specific functions. Some key differences between transketolase and TKTL1 include a deletion of 47 amino acids that is assumed to interfere with the active site and a 38 amino acid deletion that contains residues involved in cofactor binding (Schneider *et al*., 2012). However, it was proposed that this enzyme might act as a regulator of TKT activity irrespective of differences compared to TKT (Coy *et al*., 2005). A haploinsufficiency model of TKT in mice prompted the question whether or not TKTL1 itself possesses TKT activity (Xu *et al*., 2002). This is because TKTL1 exhibited no compensation for TKT loss which was as much as 50% in the testes – where TKTL1 is generally overexpressed. Almost a decade after its discovery, further research into this enzyme revealed that it may not only possess the expected TKT activity but it was also hypothesized to catalyze a unique one-substrate reaction (Coy *et al*., 2005). This together with its specific localization (nuclear and cytosolic) indicates that the function of TKTL1 is likely multifactorial. Moreover, a striking association between TKTL1 expression and aerobic glycolysis (Warburg effect) was revealed. Thus began the strong association between TKTL1 and cancer (refer Section 1.5.2.2).

There are several articles that explored the nature of TKTL1 activity, with some stating that it has no function due to the 38 amino acid deletion, while others claim that it does indeed contribute to TKT activity. Here an important consideration is that insights regarding TKT activity up to that point were based on the assumption that it involved only one enzyme (Coy *et al*., 2005). Various studies (refer to Table 2 below) using siRNA to inhibit TKTL1 expression revealed that TKTL1 plays a critical role in total TKT activity (Zhang *et al*., 2007; Hu *et al*., 2007; Chen *et al*., 2009). This may either occur directly or indirectly (regulatory) as total TKT activity was significantly attenuated in such studies.

By contrast, other studies reported contradictory findings by frequently inferring that TKTL1 does *not* possess any TKT activity due to the aforementioned 38 amino acid deletion (Maslova *et al*., 2012; Meshalkina *et al*., 2013; Mitschke *et al*., 2010; Schneider *et al*., 2012). The comparison of TKTL1 with *Saccharomyces cerevisiae* TKT and human TKT showed that TKTL1 contains multiple mutations and/or that are critical for cofactor binding and invariant among other TKTs (Mitschke *et al*., 2010). Thus the authors concluded that TKTL1 is most likely incapable of TKT activity. Moreover, a computational model of TKTL1 in which the researchers assessed primary-, secondary-, tertiary-, and quaternary structures supported the work of Mitschke and co-workers (Maslova *et al*., 2012). Here it was concluded that TKTL1 is most likely to be unable to bind to thiamine and therefore not catalytically active. These researchers also noted that an alternative mechanism of cofactor binding, however unlikely, cannot be excluded. A mutant variant of TKT that accommodated the 38 amino acid deletion present in TKTL1 was also used to demonstrate that TKTL1 is devoid of TKT activity (Meshalkina *et al*., 2013). Of note, such studies based their conclusions on the inability of TKTL1 to bind to its cofactor.

A recent study from our group employed homology modeling and structural analysis of the human TKT family combined with a thiamine cofactor to further investigate this contentious matter (Deshpande *et al*., submitted). Here it was demonstrated that TKTL1 binding to its cofactor is indeed plausible (Figure 1.5.2.1.1).

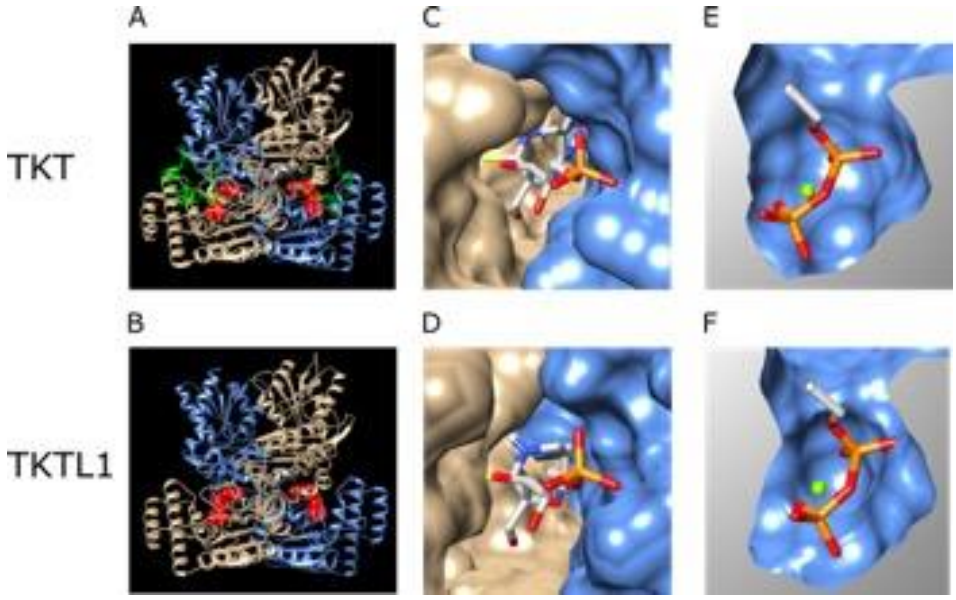

Figure 1.5.2.1.1 **Homology of TKTL1 based on the transketolase co-crystal structure with thiamine diphosphate-D-xylulose-5-phosphate adduct.** A) Ribbon representation of the homodimer (tan and blue sub-units) of TKT with the TDP-X5P adduct ligand shown as red spheres. The η1, α4 and η2 helices (green), as well as H77 and H110 (yellow) (absent in TKTL1), are shown. (B) Homology model of TKTL1 shown as a homodimer (tan and blue sub-units) and fitted to the coordinates of TKT to show the location of the substrate adduct, indicated by the red spheres. (C) The ligand present in the substrate cleft that is formed between the surfaces of the two units in the TKT homodimer is shown. (D) A similar substrate cleft is visible between the two units of the homodimer in the homology model of TKTL1. (E) A di-phosphate binding cavity is visible on the surface within the substrate cleft of each monomer in the TKT homodimer. (F) A di-phosphate binding cavity is also visible within the substrate cleft of the TKTL1 homology model. (Deshpande *et al*., submitted).

This structural model of TKTL1 in conjunction with two recent publications from different laboratories that employed radio-labeling experiments now provide useful insights into the intricate workings of TKTL1. Here Diaz-Moralli and colleagues (2016) demonstrated that TKTL1 catalyzes TKT reactions in the non-oxidative branch of the PPP and thus contributes to total TKT activity. Moreover, a unique role for TKTL1 in fatty acid metabolism was revealed, with lipid synthesis proposed to occur due to a TKTL1-catalyzed one-substrate (X5P) reaction with G3P and acetyl coenzyme A (acetyl-CoA) as products. The latter can be used for the biosynthesis of lipids. Similarly, others provided evidence of significant TKTL1 flux in Chinese

hamster ovary cells that were previously shown to possess increased total TKT activity (Ahn *et al*., 2016). They also presented supporting evidence for the one-substrate reaction with G3P and a two-carbon molecule (most likely acetyl-CoA) generated as products. To put these studies into context, two independent studies provided evidence that TKTL1 does indeed possess TKT activity and that it can also catalyze a unique one-substrate reaction. These two factors may help explain the notorious advantage that TKTL1 is proposed to offer various cancers.

1.5.2.2 TKTL1 in cancer

As the literature on TKTL1 is predominated by its role in cancer (refer Tables 1.5.2.2.1 and 1.5.2.2.2), it is necessary to consider contemporary thoughts on the matter. The Warburg effect explains the altered metabolism by cancer cells where there is a robust upregulation of aerobic glycolysis (reviewed Liberti and Locasale, 2016). Here TKT mediates the upregulation of non-oxidative glucose metabolism and has therefore been implicated in the development and migration of cancer (Figure 1.5.2.2.1) (Chao *et al*., 2016; Rais *et al*., 1999; Upadhyay *et al*., 2013). However, expression of TKTL1 (but not TKT or TKTL2) is elevated in various types of cancers (reviewed in Sun *et al.*, 2010). This suggests that TKTL1 could play an integral role in the governing processes of cancer cells and may offer some insights on the function of this enzyme. Table 1.5.2.1.1 (below) summarizes some of the literature on the manipulation of TKTL1 in various cancer cell lines. Taken together, these findings suggests that TKTL1, 1) either directly or indirectly, contributes to total TKT activity, 2) assists in the survival and proliferation of cancer cells, and 3) may be a key regulator in the metabolic changes, such as increased glucose consumption and the Warburg effect, that are common characteristics of cancer cells.

Table 1.5.2.2.1 **Summary of studies manipulating TKTL1 expression in cancer cell lines and main findings**

TKTL1 manipulation	Cell line tested	Main findings	References
siRNA	HepG2 (human liver cancer)	▼ TKT activity ▼ Proliferation	Zhang *et al*., 2007
siRNA	LoVo (human colon cancer)	▼ TKT activity, ▼ Proliferation.	Hu *et al*., 2007
siRNA & shRNA	HCT116 (human colon carcinoma)	▼ Glucose consumption ▼ Lactate production ▼ Proliferation ▲ Sensitivity to ROS	Xu *et al*., 2009
siRNA	HeLa (human cervix adenocarcinoma)	▼ TKT activity ▼ Proliferation ▲ Apoptosis	Chen *et al*., 2009
siRNA	Human esophageal squamous cell carcinoma	▼ Proliferation ▼ Invasion ▼ Migration ▲ Apoptosis	Li *et al*., 2015
siRNA	Melanoma cell lines	▼ Proliferation ▼ Invasiveness ▼ Glucose consumption ▼ Lactate production	Jayachandran *et al*., 2016

The augmented expression of TKTL1 in various cancers is well documented (reviewed in Furuta *et al*., 2010; reviewed in Riganti *et al*., 2012). It is also proposed that TKTL1 could serve as a prognostic marker for cancer as its expression correlates with tumor metastasis and poor patient outcome (Langbein *et al*., 2006; Schwaab *et al*., 2011; Ahopelto *et al*., 2016). Table 1.5.2.2.2 objectively summarizes literature on the potential role for TKTL1 as a prognostic marker in various cancers and highlights the major findings of these studies.

Table 1.5.2.2.2 **Summary of studies investigating TKTL1 expression and influence in cancer**

TKTL1	Type of cancer	Advantages/ major findings	Reference
▲TKTL1 mRNA expression	Colon adenocarcinoma & urothelial carcinoma	▲TKTL1, but not TKT or TKTL2 in cancer. ▲TKTL1 correlates with ▲ invasiveness of tumors and poor prognosis.	Langbein *et al*., 2006
▲TKTL1 IHC staining (JFC12T10 mAB)	Breast cancer	A positive correlation between ▲TKTL1 and ▲Her2/neu (growth-promoting protein). No significant correlation between ▲TKTL1 and poor prognosis.	Földi *et al*., 2007
▲TKTL1 IHC staining (JFC12T10 mAB)	Ovarian carcinoma	▲TKTL1 correlates with ▲ tumor progression, poor prognosis.	Krockenberger *et al*., 2007
▲TKTL1 IHC staining (JFC12T10 mAB)	Uterine and cervical cancer	▲TKTL1 and ▲phosphorylated-Akt with the histopathological grade of various cancers.	Kohrenhagen *et al*., 2008
RT-qPCR and JFC12T10 mAB (WB)	6 different malignant cell lines	No evidence of relevant TKTL1 expression in malignant cell lines at mRNA level. The JFC12T10 antibody is questionable as it yields multiple bands.	Mayer *et al*., 2010
▲TKTL1 (RT-qPCR)	Rectal cancer	▲TKTL1 correlates with poor prognosis.	Schwaab *et al*., 2011
IHC staining (JFC12T10 mAB)	Lung cancer	Expression of TKTL1 is not related overall survival, disease-free survival or any other variables in tumor staging system.	Fritz *et al*., 2012
▼TKTL1 (RT-qPCR)	Chronic myeloid leukemia	▼Expression of TKTL1 as the disease progresses.	Philipp *et al*., 2014

Table 1.5.2.2.2 (continued) **Summary of studies investigating TKTL1 expression and influence in cancer**

TKTL1	Type of cancer	Advantages/ major findings	Reference
▲TKTL1 IHC staining (JFC12T10 mAB)	Muscle-invasive bladder cancer	The PPP and TKTL1 play a key role in tumorigenesis of MIBC. ▲ TKTL1 in a subgroup of patients. No significant correlation between ▲TKTL1 and poor prognosis.	Semilia *et al*., 2015
Detection with: RT-qPCR, (WB and IHC) with 3 ABs	17 human malign and benign cell lines	▲ TKTL1 expression in only two cell lines. No significant correlation between ▲TKTL1 and ▲ lactate or ▲ chemoresistance.	Kämmerer *et al*., 2015
▲RT-qPCR TKTL1 JFC12T10 mAB	Metastatic melanoma	▲TKTL1 in melanoma tumors. ▲ TKTL1 correlates with ▲ invasiveness	Jayachandran *et al*., 2016
▲ TKTL1 IHC, WB, RT-qPCR	Colorectal cancer	A significant correlation between ▲TKTL1 and poor prognosis.	Ahopelto *et al*., 2016

mRNA: messenger ribonucleic acid; IHC: immunohistochemistry, mAB: monoclonal antibody, ABs: antibodies RT-qPCR: reverse transcription -quantitative polymerase chain reaction, WB: Western blot.

The rationale behind TKTL1 as a potential prognostic marker is that it is upregulated in various cancer types that have a poor prognosis. It is already known that cancer cells have dysregulated metabolic pathways that allow them to proliferate and grow faster than healthy cells. In this regard, the upregulation of TKTL1 might be one of the adaptations that is advantagous to cancerous cells. It is critical to understand how TKTL1 may be upregulated in cancer cells in order to assess whether the increased expression of this enzyme is directly involved and contributes to the changes in metabolism of cancer cells or if it is an independent factor that occurs simultaneously. It is for this reason that the focus now shifts to the regulation of TKTL1 and its putative role in cancer.

Ras mutation is a common manifestation in cancer which leads to attenuated Ras-mitogen-activated protein kinase (MAPK) signaling (reviewed in Bos, 1989; reviewed in Furuta *et al*., 2010). This in turn decreases DNA methylation, causing gene promoters (e.g. TKTL1) to become hypomethylated (Deng *et al*., 1998). TKTL1 promoter hypomethylation leads to increased transcription and a corresponding enhancement of enzymatic activity (Sun *et al*., 2010). TKTL1 activity upregulation also shows a strong association with augmented aerobic glycolysis, i.e. GLUT-1 facilitated glucose uptake and hypoxia-inducible factor (HIF)-1α stabilization (reviewed in Kumar *et al*., 2017; Sun *et al*., 2010). Together such factors create an acidic microenvironment that facilitates tumorigenesis (Figure 1.5.2.2.1) (Langbein *et al*., 2006; Sun *et al*., 2010).

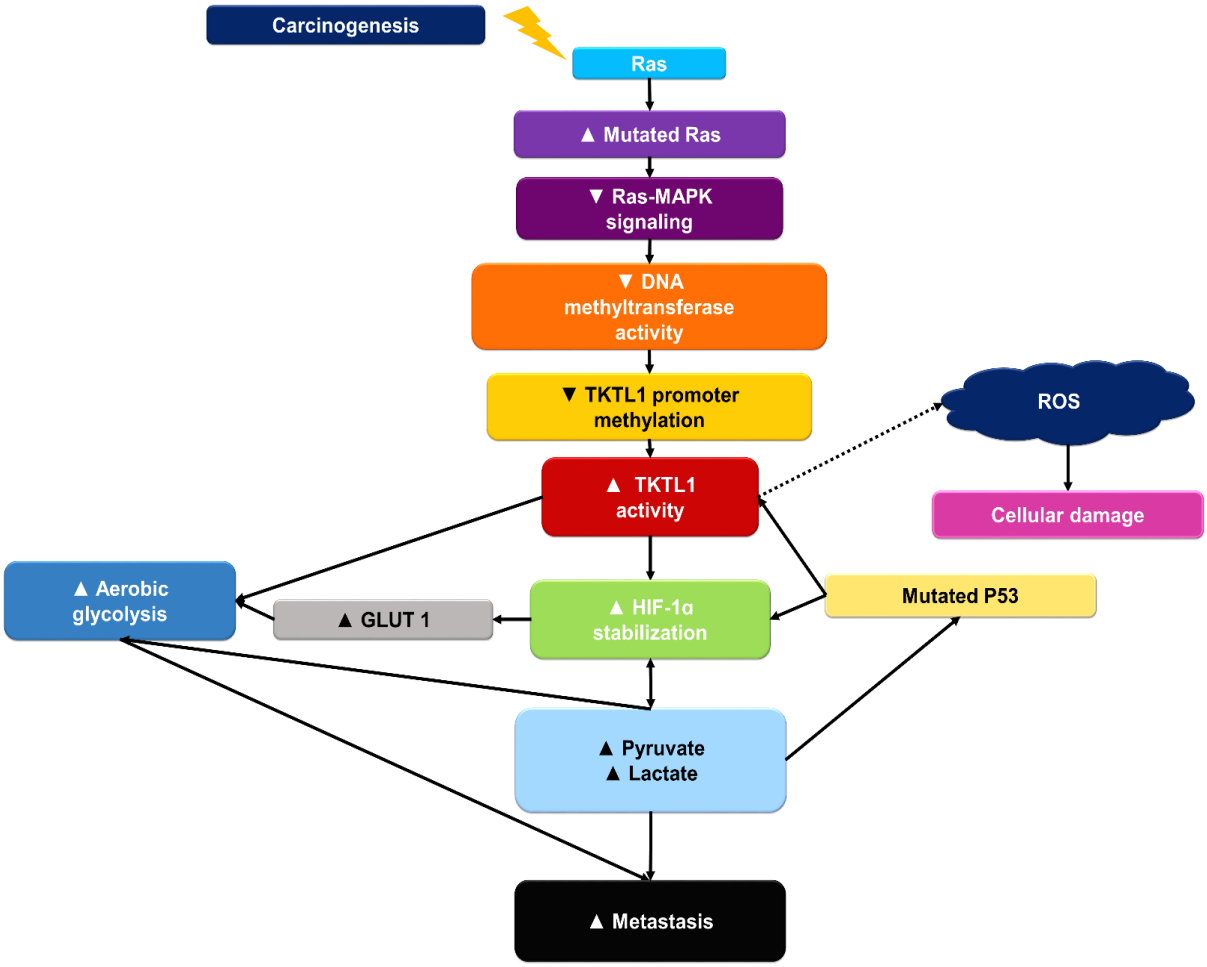

Figure 1.5.2.2.1 **A role for TKTL1 in cancer.**

1.5.2.2.1 Advantages that TKTL1 offer in the cancer context

Although the utilization of anaerobic glycolysis as opposed to oxidative phosphorylation may seem illogical due to its inefficient energy production, the exploitation of TKTL1 provides various benefits to cancer cells. As cancer cells have accelerated proliferative rates they need large amounts of energy and nucleotides to ensure rapid proliferation. Thus the one-substrate reaction catalyzed by TKTL1 creates the perfect opportunity to satisfy such needs:

- Augmented metastasis facilitated by induction of acidified environment that enables proliferation, angiogenesis, matrix breakdown and aerobic glycolysis.
- Acetyl-CoA (lipogenesis) and R5P (nucleotide biogenesis) that expedite tumorigenesis (Diaz-Moralli *et al*., 2016).
- Rapid, mitochondria-independent generation of ATP.
- Protection against oxidative damage via the provision of NADPH – a key regulator of redox homeostasis (Xu *et al*., 2009).

1.5.2.3 TKTL1 in diabetes

This brings us back to our research group's focus, i.e. the role of the PPP and TKTL1 within the diabetic context. As discussed, data from our laboratory demonstrated that TKTL1 expression, but not that of TKT, was higher in diabetic and prediabetic individuals. A logical explanation for this finding is that it occurs to help dispose of (via the PPP) the relatively high amounts of available glucose. This likely serves multiple purposes as the PPP serves as a shunt for excess glucose, produces glycolytic intermediates and also enhances antioxidant defenses, thereby collectively dissipating hyperglycemia and resultant damage (reviewed in Mapanga and Essop, 2016). Moreover, PPP upregulation can provide cardio-protection by attenuating glucose flux via other damaging NOGPs (discussed in Section 1.4).

Previous work established that both total TKT activity and thiamine levels are decreased with diabetes (clinical and animal data) (Saito *et al.*, 1987; Joseph and Essop, 2014). Moreover, there is a causal relationship between decreased vitamin B1-derivative and TKT activity, as treatment with thiamine and BFT (both biologically active forms of vitamin B1) successfully

increased TKT activity. Taken together these results provide evidence that TKTL1 may be a significant contributor to TKT activity and reiterates its dependence on thiamine. There is also evidence that TKTL1 can elicit protective effects against oxidative stress which is present in high levels in cancer cells (Xu *et al.*, 2009). The authors concluded that this was most likely due to its role as partial flux controlling enzyme of the PPP which produces NADPH necessary for restoring anti-oxidant defenses.

1.6 Problem statement and hypothesis

Considering the data presented above it is likely that TKTL1 contributes to total TKT activity. Apart from the conventional TKT activity, TKTL1 may possess a unique type of TKT activity where it catalyzes a one-substrate reaction. The combined data from our research group suggest that TKTL1 *per se* is step-wise upregulated with the progression of diabetes and that an increase in PPP – specifically TKT activity - may be a compensatory mechanism which offers protection against hyperglycemia-induced damage. However, the extent of the protection and the downstream mechanisms that mediate this protection remains unknown. Thus, we hypothesize that:

TKTL1 plays a critical role in ameliorating intracellular oxidative stress under hyperglycemic conditions.

1.7 Aim and objectives

1.7.1 Aim

For this project, we aimed to evaluate the putative defensive role of TKTL1 in a mouse model of hyperglycemia and to elucidate mechanisms underlying this process.

1.7.2 Objectives

- Establish an STZ-mouse model to induce hyperglycemia in wild type (WT) and TKTL1-knock-out (KO) mice.
- Assess the oxidative status of highly metabolic tissues (liver, heart) as well as in circulation.

- Evaluate downstream effects of hyperglycemia in the aforementioned tissues.
- Evaluate the putative protective action of TKTL1 against hyperglycemia-mediated oxidative stress and downstream effects thereof.
- Assess the contribution of TKTL1 to total transketolase activity.

Chapter 2: Materials and Methods

2.1 Animals and ethics statement:

For this study we aimed to elucidate the possible role of transketolase-like 1 (TKTL1) in oxidative stress and downstream damage in the setting of STZ-induced hyperglycemia. We employed a TKTL1-knock-out (TKTL1-KO) mouse model to provide a holistic approach for extricating the role of TKTL1. The C57BL/6-TKTL1-KO breeders (female mice) were kindly provided by Dr. Johannes Coy (Tavergenix GmbH, Pfungstadt, Germany) and housed and bred with wild type (WT) C57BL/6 male mice. Offspring were crossbred to produce TKTL1-KO and WT littermates that were used in this study. A reversed 12h/12h day/night cycle was employed and animals had *ad libitum* access to food (standard rodent chow) and water. All breeding and animal procedures were carried out in the Animal Facility of the Faculty of Health Sciences, Stellenbosch University, Tygerberg, South Africa.

Animals were treated in agreement with the accepted standards for the use of animals in research and teaching as reflected in the South African National Standards (SANS) 10386: 2008. This study was performed with the approval of the Animal Ethics Committees of Stellenbosch University, Stellenbosch, South Africa (Ethics # SU-ACUD16-00052, refer appendix A).

2.2 Genotyping analysis:

Genotyping analysis was performed to identify WT and TKTL1 littermates using the KAPA Hotstart Fast mouse tail genotyping kit (Sigma-Aldrich, St. Louis, MO). Here, genomic DNA was extracted from tail cuts using the DNA extraction protocol according to the manufacturer's instructions. Briefly, 2 mm sections of tail samples were added to 100 µl DNA extraction master mix (10X KAPA Express Extract Buffer and 1 U/µl KAPA Express Extract Enzyme diluted in PCR-grade water). Samples were then incubated at 75°C for 10 min followed by 95°C for 5 min using a thermocycler. Stock DNA was transferred to fresh PCR tubes and diluted 10X with 10 mM Tris-HCl (pH 8). The diluted DNA samples were used for genotyping PCR analysis

with the following primer pair: 5'-ATGGCTCATGTTTCTGCTGC-3' (forward primer – intron 3) and 5'-CTTGCCTTGCTTCTGTAAGG-3' (reverse primer – intron 7) (Bentz *et al*. 2011). Here, 1 µl of DNA was added to 24 µl PCR reaction master mix containing (final concentration): 1X KAPA 2G Fast Genotyping Mix, 0.5 µM forward primer and 0.5 µM reverse primer diluted in PCR-grade water. The PCR cycling protocol was set up as described in Table 2.2.1. PCR reaction products were subjected to 1% agarose gel electrophoresis at 120 V for 45 min. Gels were visualized using the Bio-Rad Chemidoc MP gel imaging system (Bio-Rad, Hercules, CA). With electrophoresis, TKTL1-KO resulted in a distinctive band of 338 base pairs (bp), while WT animals did not display any bands (Bentz *et al*. 2011).

Table 2.2.1 **PCR cycling protocol**

Step	Temperature (°C)	Time	Cycles
Initial denaturation	95	3 min	X1
Denaturation	95	15 s	X35
Annealing	60	15 s	X35
Extension	72	15 s	X35
Final extension	72	1 min	X1

2.3 Experimental design:

TKTL1-KO and WT mice, aged 10-12 weeks, were randomly assigned to receive either vehicle (0.1 M sodium citrate buffer, pH 4.5 – control groups) or STZ (40 mg/kg STZ freshly prepared in 0.1 M sodium citrate buffer, pH 4.5 – STZ groups) at n=10 males per group and n=5 females per group (refer Figure 2.3.1 A and B). Here mice were administered a single intra-peritoneal (i.p.) injection daily, for 5 consecutive days (Furman, 2015). The multiple low dose STZ protocol has previously been described and employed as it achieves hyperglycemia with minimized mortality. Control groups were injected with an equal volume of citrate buffer (according to animal weight). The welfare of all study animals was monitored and recorded daily. Blood glucose (tail prick, measurement with a GlucoPlus blood glucose monitoring

system) and body weight were recorded weekly until the following criteria were met: 1) statistically significant higher non-fasting blood glucose levels in STZ injected groups vs. controls, 2) mean, non-fasting blood glucose levels ≥ 200 mg/dL (11.1 mmol/L), 3) ≥ 90% of animals in STZ treated group display glucose levels ≥ 11.1 mmol/L on two consecutive reading days (Wu and Huan, 2008; Furman, 2015). While all three criteria were satisfied in the KO STZ-treated group, only criterion 2 was met in the WT STZ-treated group regardless of a three weeks grace period in which blood glucose levels as well as hyperglycemia incidence of the WT STZ-treated group plateaued (data discussed in the Results section below). As all three criteeria were met seven weeks after the injections, mice were terminated and organs (blood, heart, and liver) harvested for further analyses. This study forms part of a larger project and all animal handling and procedures were performed by Dr. Danzil Joseph and Ms. Natasha Driescher under the guidance and supervision of Mr. Noel Markgraaff (animal technician) and Dr. Sven Parsons (veterinarian) at the Animal Facility of the Faculty of Medicine and Health Sciences, Stellenbosch University, Tygerberg. The tissue analysis was performed in a blinded fashion. Here, each animal was assigned a unique experimental number that was randomized using Microsoft Excel (done by another researcher). The identity of the animals (genotype and treatment group) was hereby "hidden" and analysis performed on samples with only the experimental number known.

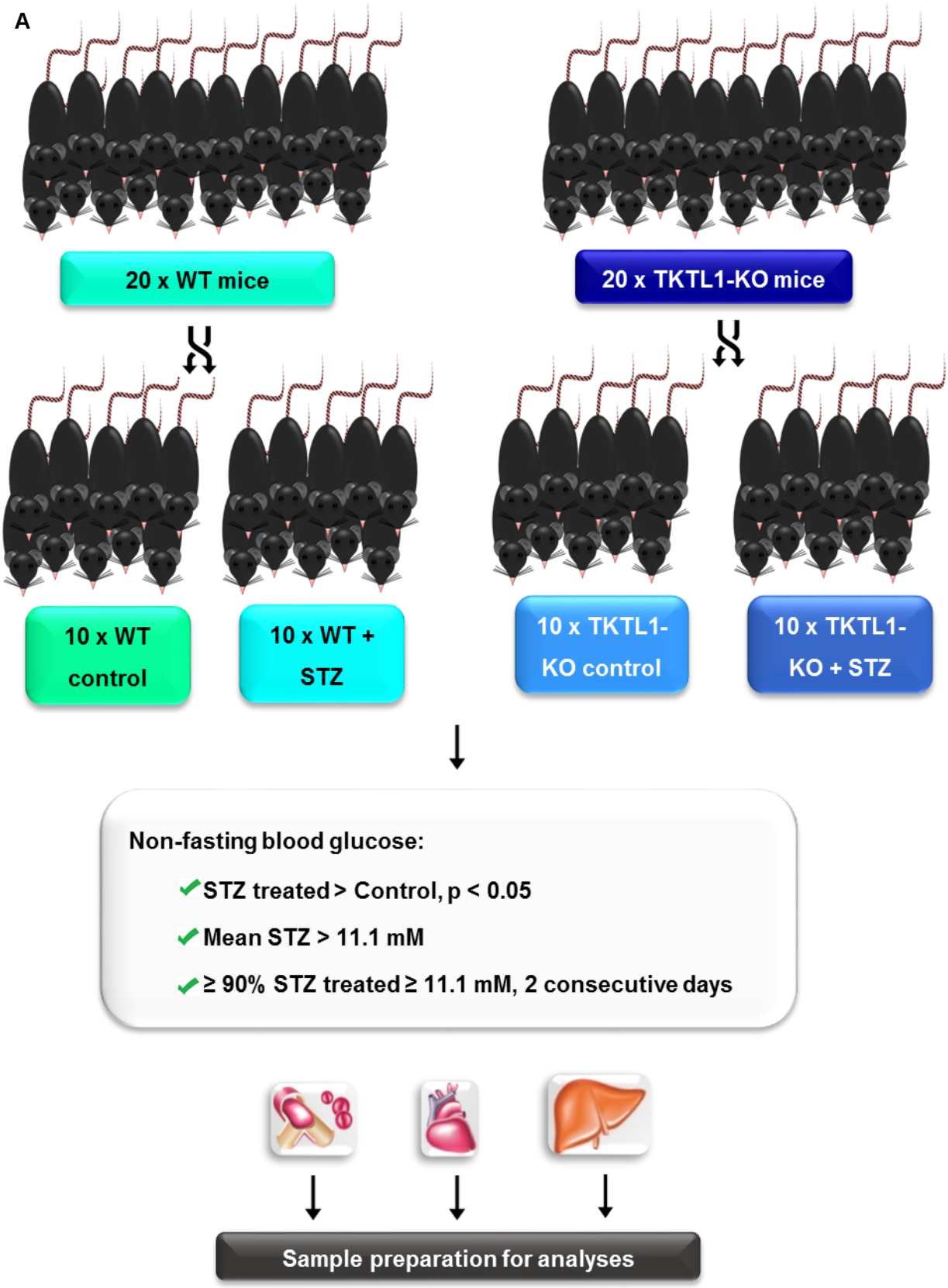

Figure 2.3.1 A: (males). **Illustration of the animal model and experimental design used to ascertain the role of TKTL1.**

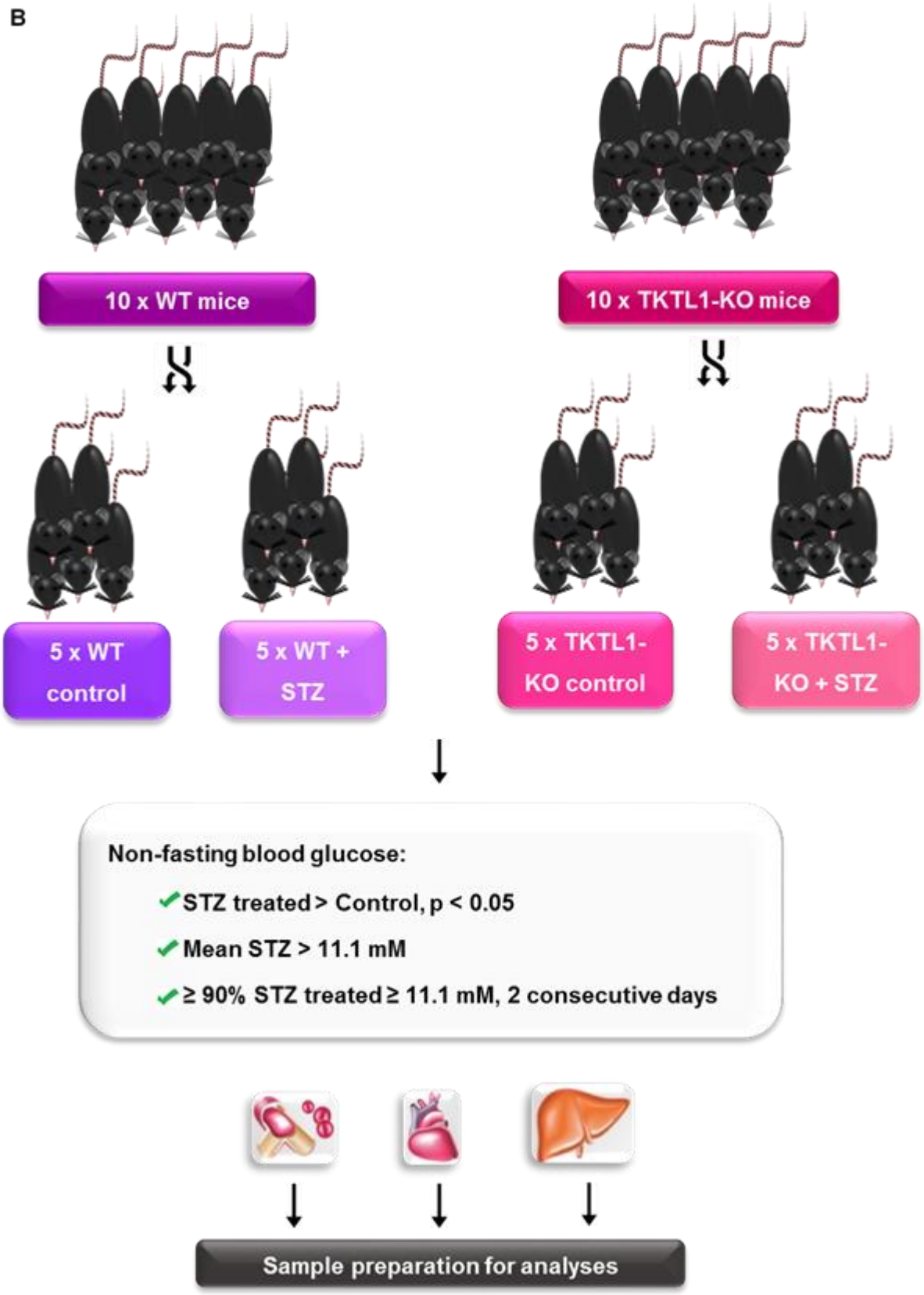

Figure 2.3.1 B: (females). **Illustration of the animal model and experimental design used to ascertain the role of TKTL1.**

2.4 Sample preparation for oxidative stress and activity assay analyses:

2.4.1 Blood samples

On the day of termination, blood samples were collected in serum tubes via cardiac puncture. A 25 µl aliquot of whole blood was added to a microfuge tube followed by addition of 2.5 µl 1-methyl-2-vinyl-pyridinium trifluoromethane sulfonate (M2VP, an anti-oxidant) (Sigma-Aldrich, St. Louis, MO). After 5 s of vortexing, the samples were stored at -80°C until GSSG assay was performed. The remaining blood was centrifuged at ~5000 x *g* for 10 min at 4°C and the serum subsequently divided into 25 µl aliquots that were stored at -80°C until further analyses.

2.4.2 Tissue samples

Upon tissue extraction, tissue sections were frozen at -80 °C. At the time of tissue preparation, two sections of tissue of each heart- and liver sample were weighed off. Roughly 30 mg was required for GSSG analysis and 100 mg for the rest of the oxidative stress analyses. Samples were then placed into ice-cold 1X phosphate buffered saline (PBS) containing 1X cOmplete™ Protease Inhibitor Cocktail (Sigma-Aldrich, St. Louis, MO). The buffer of the GSSG samples contained 10 mM M2VP (Sigma-Aldrich, St. Louis, MO) in order to prevent further oxidation of GSH. Tissue was homogenized on ice using a Polytron PT 2100 homogenizer (Kinematica, Luzern, CH). The homogenates were subsequently centrifuged (Labnet, Edison, NJ) at ~16000 x *g* for 10 min at 4°C and the supernatant was divided into several ~100 µl aliquots that were stored at -80°C until further analysis.

2.5 Assessment of the pentose phosphate pathway (PPP)

2.5.1 Glucose-6-phosphate dehydrogenase (G6PD) activity assay

G6PD activity (the first and rate-limiting enzyme of the PPP) was monitored using a commercially obtained fluorimetric assay kit (Abcam, Cambridge, MA). This assay is based on the conversion of $NADP^+$ by G6PD to yield NADPH. The latter triggers an NADPH sensor which fluoresces red and can be monitored at 590 nm.

Heart and liver samples (refer Section 2.4.2) were subjected to protein concentration determination using the Pierce™ BCA Protein Assay Kit (Thermo Fisher Scientific, Waltham, MA). Twenty-five µl of either blank, serial dilutions of G6PD, or the actual sample were added (in duplicate) to appropriate wells of a black-walled, clear, flat bottom 96 well plate. This was followed by the addition of 25 µl of assay mixture (enzyme probe and $NADP^+$ in assay buffer) after which fluorescence intensity was kinetically monitored at 590 nm using a Fluoroskan Ascent™ Microplate Fluorometer (Thermo Fisher Scientific, Waltham, MA) at 1 min intervals until the $NADP^+$ conversion rate stabilized.

After a standard curve was plotted and the equation determined, G6PD activity was calculated as follows:

$$G6PD\ activity = \frac{(Corrected\ slope)}{[protein\ ]} \times df$$

Where: df = dilution factors required for the samples to fit the standard curve.

2.5.2 NADP+/ NADPH assay

A commercially available $NADP^+$/ NADPH colorimetric assay (Abcam, Cambridge, MA) was employed to establish the respective concentrations of $NADP^+$ and NADPH as well as estimate the $NADP^+$: NADPH ratio in the heart and liver samples. At the time of the assay, an aliquot (refer to Section 2.2.2) of each sample was thawed, after which NADPH extraction buffer was added to dilute the samples. For heart samples, a 1:2 dilution sufficed, while liver samples required a 1:5 dilution. These samples contained the total NADPH ($NADP^+$ and NADPH) and each was divided into two aliquots – one used to determine total NADPH and the other heated at 60°C for 30 min to decompose $NADP^+$ in the samples.

A serial dilution was used to generate a standard curve. Twenty-five µl of each blank, standard or sample was added to a clear 96-well plate in duplicate. The reaction mixture (50 µl), containing $NADP^+$ cycling buffer and $NADP^+$ cycling enzyme mix, was pipetted into each well. This was followed by an incubation period of 5 min at room temperature during which time the

conversion of $NADP^+$ to NADPH occurred. Hereafter, 5 µl of NADPH developer was added and optical density monitored at 450 nm for four 20 min intervals, using a Multiskan™ Spectrum Microplate Reader (Thermo Fisher Scientific, Waltham, MA), until the absorbance stabilized.

The standard curve was plotted and the equation thereof determined. This allowed for the extrapolation of [NADPH] and total NADPH [NADPt] according to the following:

$$[NADPt] = \frac{Corrected\ absorbance - (y - intercept)}{\frac{slope}{[protein]}}$$

$$[NADPH] = \frac{Corrected\ absorbance - (y - intercept)}{\frac{slope}{[protein]}} - [NADPt]$$

$$[NADPH] = [NADPt] - [NADP^+]$$

$$NADP^+ : NADPH = \frac{NADPt - NADPH}{NADPH}$$

With this assay some problems were encountered as the boiling step, which decomposed the $NADP^+$ in the samples, led to the formation of fat drplets due to the high fat content of the liver samples. Unfortunetely, due to time constraints as well as the great expense of the kit used, we were unable to optimize this technique further. In future, I would recommend that samples be centrifuged at ~16000 x *g* for 30 min and the middle layer transferred to a new tube while taking special care not to disrupt the top lipid layer.

2.5.3 Transketolase activity assay

Transketolase activity, the main flux regulating enzyme of the PPP, was determined using an amended protocol from Diaz-Moralli and colleagues (2011). All (analytical grade) reagents used were purchased from Sigma Aldrich (St. Louis, MO). Twenty µl of each sample (heart and liver) was added in triplicate to 50 µl of assay buffer (50 mM Tris-HCl buffer pH 7.6, 5 mM $MgCl_2$, 0.1 mM thiamine pyrophosphate [TPP], 0.2 mM β-NAD, 0.2 U/ ml α-glycerophosphate dehydrogenase-triosephosphate isomerase) to appropriate wells of a Greiner UV-Star®96-well

plate (Sigma-Aldrich, St. Louis, MO). This was followed by the incubation of the foil-covered plate at 25°C for 10 min before the addition of the reaction solution (25 µl) that contained 15 mM D-ribose-5-phosphate and 7.24 mM D-xylulose-5-phosphate. Subsequently, the absorbance was monitored at 340 nm for 10 min using an EZ Read 400 Microplate Reader (Biochrom, Cambridge, UK).

Transketolase activity was calculated as follows:

$$Units\ per\ ml\ of\ enzyme = \frac{(\Delta A_{340\ nm}/\min test - \Delta\frac{A_{340\ nm}}{(\min blank)(0.3)(df)})}{(6.22)(0.01)}$$

The values were presented as:

$$Units\ per\ mg\ protein = \frac{units\ /\ ml\ enzyme}{mg\ protein\ /\ ml\ enzyme}$$

(Δ-change increment; A-absorbance; df-dilution factor; ml-millilitre; mg-milligram)

Technical difficulties were experienced with the liver samples as negative values were obtained. The optimization of this in-house assay could not be performed as 1) time was a limiting factor as the reagents arrived late and not all at once, 2) some of the reagents were enough for only one set of activity assays, 3) the reagents were very expensive, and 4) there was too little sample left to prepare a complete set to try and optimize the assay.

2.6 Determining the oxidative status of the serum and tissue

Mr. Fanie Rautenbach from the Oxidative Stress Research Centre, Cape Peninsula University of Technology (Bellville, Western Cape) kindly provided the reagents, protocols, workspace and guidance to assess oxidative stress (all except NADPH oxidase assay) and anti-oxidant mechanisms.

2.6.1 Indications of oxidative damage

2.6.1.1 NADPH oxidase (NOX) activity

We employed a modified protocol previously used in our laboratory derived from a NOX activity assay performed by Abid and colleagues (2007) (Joseph *et al*., 2014). The NOX complex generates electrons that can cause oxidative damage if there is higher activity. In this assay, the electrons generated by the NOX complex react with lucigenin, causing it to emit light that can be detected with a luminometer.

For sample preparation refer to Section 2.4.2. Protein concentrations were determined using a Direct Detect™ instrument (Bio-Rad, Hercules, CA). Ten µl of the blank or sample (heart and liver) was added in triplicate. This was followed by the addition of 50 µl of assay buffer, containing 250 mM HEPES buffer (pH 7.4), 120 mM NaCl, 5.9 mM KCl, 1.2 mM $MgSO_4 \cdot 7H_2O$, 1.75 mM $CaCl_2 \cdot 2H_2O$, 11 mM glucose, 0.5 mM EDTA, 100 µM NADH and 5 µM lucigenin. Luminescence was measured using a Glomax-96 luminometer (Promega, Madison, WI). NOX activity was expressed as relative light units (RLU)/ mg protein.

2.6.1.2 Conjugated dienes (CDs)

This assay estimates the levels of CDs in tissue and acts as a marker of early damage attributed to free radicals. For serum and tissue sample preparation, please refer to Sections 2.4.1 and 2.4.2. Briefly, 90 µl of chloroform: methanol (2:1) solution was added to 20 µl (serum) or 45 µl (tissue) samples followed by a 10 s vortex step and 5 min centrifugation at 10000 x *g* at 4°C. Uncapped microfuge tubes were then left overnight at 4°C to allow for the evaporation of the solution. On the day of the assay, the residue was dissolved in 500 µl of cyclohexane followed by a 10 s vortex step. Next, 150 µl of each blank (cyclohexane) or sample was aliquoted in triplicate into the appropriate wells. The absorbance was read at 232 nm using a Fluoroskan Ascent™ Microplate Fluorometer (Thermo Fisher Scientific, Waltham, MA).

The concentration of CDs are expressed as mol/g and are calculated as follows:

$$[CDs] = \frac{(A_{Sample} - A_{Blank})}{\varepsilon} \times \frac{weight}{exctracion\ volume} \times df$$

Where A= absorbance, ε = extinction coefficient (29500 L/mol/cm), df = dilution factor.

2.6.1.3 Thiobutyric acid reactive substances (TBARS)

Similar to the CDs assay above, the TBARS assay detects lipid peroxidation (specifically malondialdehyde [MDA]) that arises due to the actions of free radicals. However; this step occurs much further in the oxidative pathway and is therefore indicative of advanced damage. In this assay, an MDA:TBA complex is formed when heated to 90°C that can be monitored at 535 nm.

All chemicals (analytical grade) used were obtained from Sigma-Aldrich (St. Louis, MO). Briefly, 45 µl of 0.2 M orthophosphoric acid and 5.6 µl of cold 4 mM ethanol were added to 45 µl of liver lysates. This was followed by a 10 s vortex step and the addition of 5.6 µl TBA reagent and again followed by a 10 s vortex step. Subsequently, samples were heated to 90°C for 45 min before being cooled for 2 min on ice. The samples were thereafter allowed to stabilize until it reached room temperature before 450 µl of n-butanol and 45 µl of saturated NaCl were added. After a 10 s vortex step, samples were centrifuged at 4°C for 2 min at ~ 6000 x *g*. For heart samples (25 µl), the same ratios of the sample:reagents were used. Three hundred µl of blank (butanol) and each sample (top butanol layer) was then added in triplicate to appropriate wells of a 96-well clear plate after which the absorbance was monitored at 535 nm using a Multiskan™ Spectrum Microplate Reader (Thermo Fisher Scientific, Waltham, MA). The same rations were used for heart samples (25 µl).

The concentration of TBARS was expressed as µmol/g and was calculated as follows:

$$[TBARS] = \frac{Corrected\ absorbance}{\varepsilon} \times \frac{weight}{exctracion\ volume} \times df$$

Where ε = extinction coefficient (156000 l/mol/cm), df = dilution factor.

2.6.2 Anti-oxidant mechanisms:

2.6.2.1 Superoxide dismutase (SOD) activity assay

This enzyme is responsible for the conversion of detrimental $O_2^{-}\cdot$ to a lesser reactive H_2O_2. In this assay, SOD is able to neutralize the auto-oxidation of ROS-inducer (6-hydroxydopamine (6-HD) that otherwise reacts with diethylenetriamine-pentaacetic acid (DETAPAC) to form a pink/orange colored complex that can be monitored with a microplate reader at 490 nm.

Twelve µl of each sample (heart and liver) was added to wells (in triplicate) of a 96-well plate. Subsequently, 15 µl 6-HD (Sigma-Aldrich, St. Louis, MO) was added to each well. Following the addition of 170 µl DETAPAC (Sigma-Aldrich, St. Louis, MO), SOD activity was colorimetrically monitored at 490 nm in 30 s intervals for a total of 5 min using a Multiskan™ Spectrum Microplate Reader (Thermo Fisher Scientific, Waltham, MA). A commercially available Pierce™ BCA Protein Assay Kit (Thermo Scientific, Waltham, MA) was utilized for the determination of the protein content of the samples, allowing for the expression of SOD activity as U/mg protein.

SOD activity was calculated as follows:

$$Activity = \frac{Corrected\ slope - (y - intercept)}{[protein]}$$

2.6.2.2 Catalase

Although H_2O_2 is less reactive than superoxide radicals, it is still able to trigger damaging effects. Catalase is able to convert hydrogen peroxide to water and oxygen thereby neutralizing its detrimental effects. The catalase assay is based on the rate of H_2O_2 conversion from which we are able to infer catalase activity.

Ten µl of each blank or sample (heart and liver) was added in triplicate to the appropriate wells followed by the addition of 170 µl catalase assay buffer (50 mM K_3PO_4, pH 7.0). Immediately after 75 µl H_2O_2 supplementation, the absorbance was read at 240 nm at 30 s intervals for a

total of 5 min using a Multiskan™ Spectrum Microplate Reader (Thermo Fisher Scientific, Waltham, MA).

Catalase activity, expressed as µmol/min/mg, was calculated as follows:

$$Activity = \frac{\frac{Corrected\ slope}{\varepsilon}}{[protein]} \times df$$

Where ε = extinction coefficient (0.00394 mmol/L/cm), [protein] = protein concentration, df = applicable dilution factors.

2.6.2.3 Ferric reducing anti-oxidant power (FRAP)

FRAP refers to the reducing power of anti-oxidants that function via the single electron transfer mechanism. Vitamin C serves as the standard for this assay which is based on the ability of the sample to neutralize the reactivity of Fe^{3+} by reducing it to Fe^{2+} thereby allowing for the formation of a Fe^{2+}: 2,4,6-Tris(2-pyridyl)-s-triazine (TPTZ) complex that is blue in color and can be detected at 593 nm.

Five µl of each sample (blood, heart, and liver) was added to a clear 96-well plate in triplicate. This was followed by the addition of 300 µl of FRAP reagent (20 mM $FeCl_3$, 10 mM TPTZ, 300 mM acetate buffer (pH 3.6) in dH_2O). Plates were covered and allowed to incubate at room temperature for 30 min before the absorbance was read at 593 nm using a Multiskan™ Spectrum Microplate Reader (Thermo Fisher Scientific, Waltham, MA).

The concentration of FRAP was expressed as µM and calculated as follows:

$$[FRAP] = \frac{corrected\ absorbance - (y - intercept)}{slope} \times \frac{extraction\ volume}{weight} \times df$$

Where df = dilution factor required to fit sample on the standard curve.

2.6.2.4 Oxygen radical absorbance capacity (ORAC)

This assay measures intracellular anti-oxidant capacity through the hydrogen atom transfer (HAT) mechanism that neutralizes radicals. The principle of this assay is based on a peroxyl

radical 2,2'-Azobis(2-methylpropionamidine) dihydrochloride (AAPH) reacting with fluorescein (representing proteins and/or lipids) that has an $Ex_{458\ nm}/Em_{530\ nm}$. Anti-oxidants that function via the hydrogen atom transfer mechanism are able to partially inhibit this reaction, thereby, decreasing the emission of light from fluorescein at 530 nm.

A standard curve was prepared using a 0.5 mM Trolox (synthetic vitamin E) stock solution. Twelve µl of each blank, standard, internal control* or sample (blood, heart or liver) was added (in triplicate) to a black 96-well plate. This was followed by the addition of 138 µl of fluorescein (Sigma-Aldrich, St. Louis, MO). Immediately prior to reading, 50 µl of AAPH (Sigma-Aldrich, St. Louis, MO) was added to each well. Light emission was monitored for 2 hours at 1 min intervals using a Fluoroskan Ascent™ Microplate Fluorometer (Thermo Fisher Scientific, Waltham, MA).

*Internal control used to standardize readings as assay was performed on multiple days.

ORAC was expressed as Trolox equivalent (TE)/ dl and calculated using a regression equation between Trolox concentration (Y) and the net area under the fluorescence decay curve (AUC) (X) (µM):

$$(\mathrm{Y} = \mathrm{a} + \mathrm{bX} + \mathrm{cX2})$$

$$AUC = (0.5 + f2/f1 + f3/f1 + f4f1 + \ldots + fi/f1)\, x\, CT$$

Where f1 = initial fluorescence reading at cycle 1, fi = fluorescence reading at cycle i, and CT = cycle time in min.

2.6.2.5 Glutathione levels

The ratio of GSH: GSSG is commonly used as an indication of tissue oxidative status. In this assay, GSH in the sample converts 5,5′-Dithiobis(2-nitrobenzoic acid) (DTNB) to its reduced form (yellow color) and can be monitored at 412 nm. A standard curve is essential as it is used to extrapolate the concentrations of both GSH and GSSG in the samples.

For the determination of GSH concentration in blood, heart and liver samples (refer Section 2.2.1 and 2.2.2 for preparation), 175 µl of 5% metaphosphoric acid (MPA) was added to 25 µl of the sample followed by a 10 s vortex step. Samples were then centrifuged at 10000 x *g* for 5 min at 4°C. Ten µl of the supernatant was thereafter added to 600 µl of Buffer A (500 mM $NaPO_4$ and 1 mM EDTA). Fifty µl of blank, standard or sample was added in triplicate to a 96-well clear plate. Subsequently, 50 µl of DNTB and 50 µl of glutathione reductase was added. Thereafter, NADPH (50 µl) was added followed by the monitoring of absorbance at 412 nm with a Multiskan™ Spectrum Microplate Reader (Thermo Fisher Scientific, Waltham, MA).

The proteins of GSSG samples (as prepared in Sections 2.4.1 and 2.4.2) were precipitated by adding 72.5 µl of 5% MPA to 25 µl of the sample followed by a 10 s vortex step and centrifugation at 10000 x *g* for 5 min at 4 °C. Subsequently, 25 µl of supernatant was mixed with 350 µl of Buffer A and the same procedure was then followed (as described) to determine the GSH concentration.

GSH and GSSG concentrations were expressed as µmol/g and calculated as follow:

$$[GSH] = \frac{corrected\ absorbance - (y - intercept)}{slope} \times \frac{exctration\ volume}{weight} \times df$$

$$[GSSG] = \frac{corrected\ absorbance - (y - intercept)}{slope} \times \frac{exctration\ volume}{weight} \times df\ \times 2^{*}$$

Where GSH = reduced glutathione, GSSG = oxidized glutathione, df = dilution factors

*Structurally GSH = 2 x GSSG with a disulfide bond connecting the two molecules.

2.7 Histological analysis

2.7.1 Sample preparation for histological analysis

Upon harvesting, heart samples (n=2) and liver samples (n=4) of each group samples were stored in formaldehyde solution (Sigma-Aldrich, St. Louis, MO) until further processing. An automated tissue processor was used to fix (paraformaldehyde), dehydrate (increasing concentrations of ethanol), clear (xylene) and embed (paraffin) tissue samples. Prior to

sectioning, samples were re-embedded with paraffin wax. Serial sections of tissue samples were obtained using a Leica RM2125 RT (Leica, Wetzlar, DE) microtome. These were then rehydrated and fixed on a microscope slide until staining ensued.

2.7.2 Hematoxylin and eosin (H&E) staining

Sections were stained using a Leica ST4020 (Leica, Wetzlar, DE) automated stainer in the following sequence: xylene, xylene, 100% ethanol, 95% ethanol, 70% ethanol, H_2O, Hematoxylin, warm H_2O, Scott's water, H_2O, Eosin, H_2O, 95% ethanol and 100% ethanol, with sections immersed in each solution for 2 min. After air-drying, sections were sealed with Mounting Medium (Sigma-Aldrich, St. Louis, MO) and coverslips. Dr. Carol Chase, a retired histologist kindly assisted in the initial analysis of ultrastructure (H&E) and possible changes thereof. Images were taken using a Nikon DS-Fi2 camera fitted to a Nikon eclipse e400 microscope (Minato, TYO, Japan). Five random regions of interest were taken at 20X magnification as well as a whole section image at 4X magnification.

2.7.3 Sirius red stain: identifying possible fibrosis

Deparaffinized sections were stained with Picro-Sirius red for one hour prior to two 2 min immersions in (0.5% v/v) acetic acid solution. Subsequently, sections were subjected to two changes of 100% ethanol followed by a clearing step with xylene. Slides were allowed to air-dry after which they were mounted with Mounting medium (Sigma-Aldrich, St. Louis, MO) and a coverslip. Microscopic analysis was done using a Nikon Eclipse E400 and images (five random fields of view [20X] and whole section image [4X]) were obtained with a Nikon DS-Fi2 camera (Minato, TYO, Japan). Collagen content and/or fibrosis was quantified using ImageJ combined with a color thresholding algorithm developed by G. Landini (Hadi *et al*., 2011).

$$\%\, fibrosis = \frac{area\ of\ fibrosis}{total\ area + area\ of\ fibrosis}$$

2.8 Western Blot analysis: apoptotic cell death

Roughly 100 mg of each heart and liver sample was weighed off and submerged in 1 ml of ice cold radioimmunoprecipitation assay buffer (RIPA) containing 1X cOmplete™ Protease Inhibitor Cocktail (Sigma-Aldrich, St. Louis, MO), 1 mM sodium orthovanadate, 1 mM sodium fluoride , and 1 mM phenylmethylsulfonyl fluoride (PMSF). Thereafter, samples were cut into small pieces using sharp scissors, taking care to sterilize the instruments between samples as to prevent contamination of the samples. Samples were then homogenized on ice using a Polytron PT 2100 homogenizer (Kinematica, Luzern, CH). Subsequently, homogenates were centrifuged (Labnet, Edison, NJ) at ~16000 x *g* for 10 min at 4°C and the supernatants were stored at -80°C until further preparation.

In the second preparation phase, samples were thawed on ice. Five microliter of each sample was added to a clean tube which served as the loading control. Protein concentration was determined using a Direct Detect™ instrument (Bio-Rad, Hercules, CA) and was used to determine the amount of each sample, 2X Laemmli buffer (containing 2-β-mercaptoethanol) and RIPA buffer to be added to each sample tube to be loaded onto the gel.

Heart and liver samples were subjected to Western Blotting analysis routinely performed in our laboratory using 15% sodium dodecyl sulfate-polyacrylamide gel electrophoresis hand-cast gels (Joseph *et al*., 2014; Joseph and Essop, 2014; Mapanga *et al*., 2014). These gels were transferred onto polyvinyldene fluoride membranes (Bio-Rad, Hercules, CA) using a Trans-Blot® Turbo™ Transfer system (Bio-Rad, Hercules, CA) that were subsequently blocked with 5% fat-free milk in 1% Tris-buffered saline-0.1% Tween (TBS-T). Membranes were subsequently incubated with a 1:1000 Caspase-3 (Cas-3) (8G10) Rabbit mAB (Cell Signaling Technology, Danvers, MA) antibody made up in the blocking solution overnight at 4°C followed by a 1 hour incubation with 1:10000 anti-rabbit IgG HRP-linked antibody (Cell Signaling Technology, Danvers, MA) in 5% fat free milk - 1% TBS-T at room temperature. Total protein was visualized with UV light using a ChemiDoc™ MP System (Bio-Rad, Hercules, CA), while the protein of interest was detected using enhanced chemiluminescence (Bio-Rad, Hercules,

CA). Western blots were analysed using the “Total lane protein” method of Image Lab™ Software to determine the relative concentration of the protein of interest as a percentage of the loading control.

Troubleshooting of Western blots:

The first set of Western blots contained streaks believed to be due to the high fat content. The quality of the blots were improved by using the same preparation used for the oxidative status tests and activity assays (refer Section 2.4.2) as well as increasing the centrifuge time and speed. Samples were centrifuged at ~16000 x g for 30 min at 4°C and the supernatant aliquoted into a new tube. These samples were stored at -80°C until further preparation as described above.

2.9 Statistical Analysis

Statistical analyses were performed using STATISTICA 13.2.92.1. Normality was tested by means of a Normal Probability Plot which takes into account Kolmogorov–Smirnov, Lilliefors, and Shapiro-Wilk values. Subsequently, Levene’s test for homogeneity of variances was calculated. Data that were not normally distributed, was transformed using the BoxCox transformation. Statistical significance between groups was determined with either a Two-way analysis of variance (ANOVA) or Three-way ANOVA, depending on the independent variables. This was followed by a Fisher’s least significant difference post-hoc test for normally distributed data or by a Games-Howell post hoc test for transformed data. Spearman’s correlation coefficient was used to determine whether or not correlations existed between experimental values and blood glucose levels. P-values were considered statistically significant if $p<0.05$. GraphPad PRISM version 5.0 was used to present statistical data.

Chapter 3: Results

For this project we aimed to 1) establish an STZ-mouse model to induce hyperglycemia in wild type (WT) and TKTL1-knock-out (KO) mice, 2) assess the oxidative status of highly metabolic tissues (liver, heart) as well as in circulation, 3) evaluate downstream effects of hyperglycemia in the aforementioned tissues, 4) Evaluate the putative protective action of TKTL1 against hyperglycemia-mediated oxidative stress and downstream effects thereof, and 5) assess the contribution of TKTL1 to total transketolase activity. We employed a TKTL1-KO mouse model as a targeted approach to evaluating TKTL1 function. Briefly, animals received injections of either citrate buffer or low doses (40 mg/kg) of STZ on five consecutive days (Furman, 2015). Treatment with STZ destroys insulin-producing pancreatic β-cells and therefore leads to hyperglycemia, a pathophysiologic state known to culminate in oxidative stress and damaging outcomes (refer Chapter 1).

3.1 Genotyping of WT and TKTL1-KO mice to be used in this study

We initially identified WT and TKTL1-KO mice by genotyping PCR analysis of genomic DNA extracted from tail tissue, with the aim to breed greater numbers for subsequent experiments (Bentz *et al*. 2011). The deletion of exon 4 to exon 7 results in a shortened gene fragment of ~338 bp. Our genotyping PCR results (analyzed by agarose gel electrophoresis) shows a distinct band at ~338 bp in TKTL1-KO mouse tail tissues, whereas the WT animals displayed no bands (refer Figure 3.1.1). Mice were subsequently divided into WT or TKTL1-KO groups according to the PCR results and then subjected to STZ treatment.

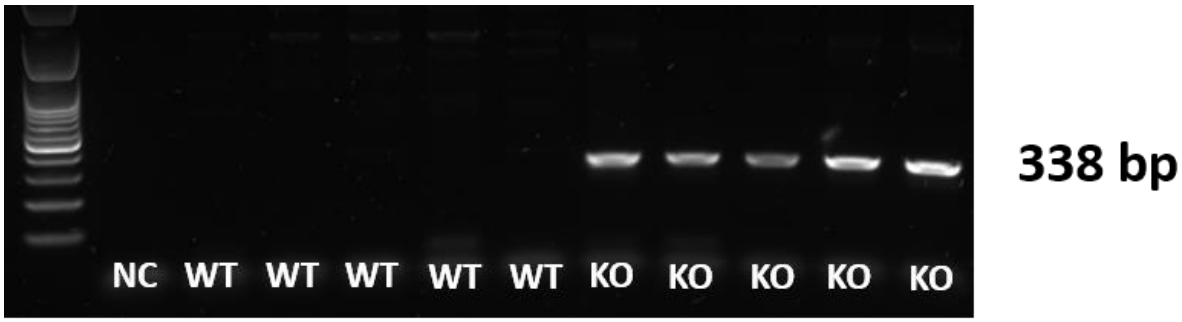

Figure 3.1.1 **Genotyping PCR analysis of WT and TKTL1-KO mice.** WT: wild type, KO: knock-out, NC: negative control.

3.2 Differential development of STZ-induced hyperglycemia

We employed a GlucoPlus™ glucometer to measure non-fasting blood glucose levels from tail-veins weekly until the following criteria for hyperglycemia were met: 1) statistically significant non-fasting blood glucose levels in STZ injected groups vs. controls, 2) mean, non-fasting blood glucose levels ≥200 mg/dl (11.1 mmol/L), 3) ≥90% hyperglycemia incidence (i.e. the percentage of animals in STZ treated groups displaying non-fasting blood glucose levels ≥11.1 mmol/L on two consecutive reading days) (Wu and Huan, 2008; Furman, 2015; Lazar *et al*., 1968). Female mice in both WT and TKTL1-KO groups showed resistance to STZ-induced hyperglycemia, as none of the groups displayed non-fasting blood glucose ≥11.1 mmol/L (refer Figure 3.2.1 A). Our results indicate that the male TKTL1-KO STZ group displayed higher blood glucose levels compared to both the WT control group ($p<0.001$) and the TKTL1-KO control group ($p<0.001$) at termination (i.e. 7 weeks after completion of the STZ injection protocol) (refer Figure 3.2.1 B). The WT group treated with STZ did not exhibit a significantly higher blood glucose compared to the WT control group. As only 40% of the WT STZ-treated males reached hyperglycemia, we clustered these mice as responders (blood glucose ≥ 11.1 mmol/L, refer Figure 3.2.1 C) and non-responders (blood glucose < 11.1 mmol/L, refer Figure 3.2.1 D). Data was then re-analyzed separately in order to determine whether the non-responder group affected the results. However, blood glucose levels for this group was not significantly higher ($p=0.08$) than the WT control group (criterion 1). The mean non-fasting blood glucose was, however, concealed by the non-responding mice. Here non-responders showed a mean blood glucose level of 9.08 ± 0.34 mmol/L compared to 14.67 ± 1.71 mmol/L for the responders.

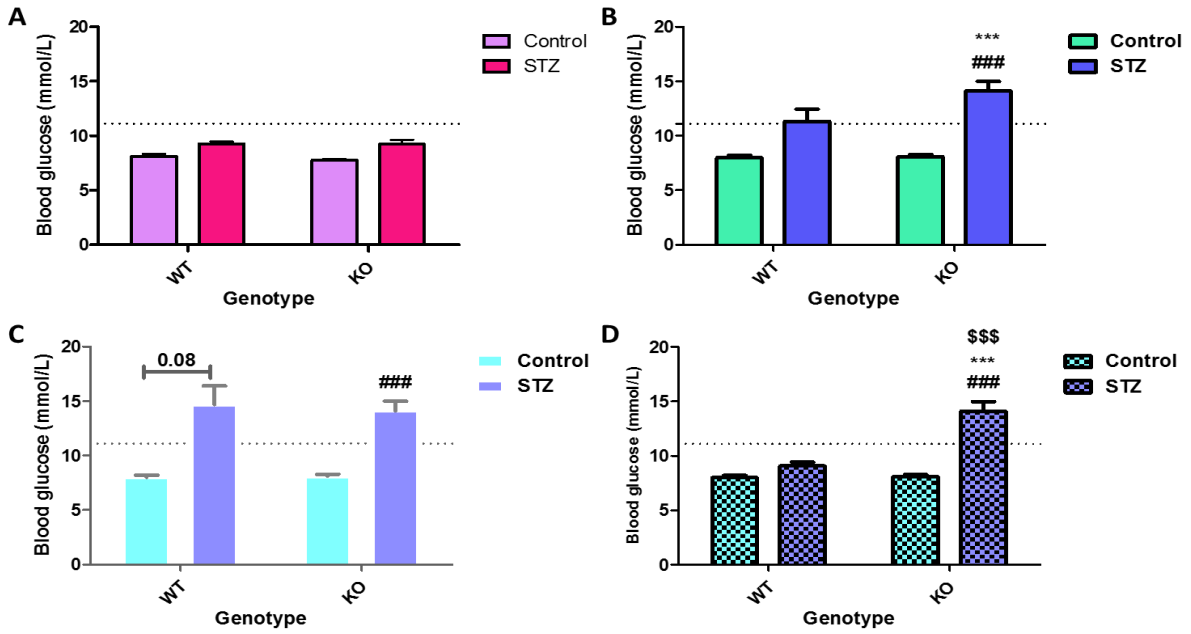

Figure 3.2.1 **Non-fasting blood glucose levels of female (A) and male mice: B (combined data), C (responding, WT-STZ), D (non-responding, WT-STZ) mice at termination (7 weeks post-STZ protocol)**. Data presented as mean ± SEM, n=5 (females), n=10 (males), WT STZ-responders n=4, WT STZ non-responders n=6, ***p<0.001 vs. WT control, ###p<0.001 vs. TKTL1-KO control, $$$p<0.001 vs. WT STZ. The dotted line indicates the 11.1 mmol/L cut-off value (criterion 2).

Hyperglycemia incidence (percentage of mice displaying non-fasting blood glucose ≥11.1 mmol/L) was 30% and 45% in WT and TKTL1-KO STZ-injected male groups, respectively, one week after the STZ injection protocol ended (refer Figure 3.2.2). This increased to 40% and 54% in the respective groups by weeks 2 to 3. The TKTL1-KO animals displayed a sharp increase in hyperglycemia incidence (to 81.8%) from week 4 and reached 90% (criterion 3) after 7 weeks, while that of the WT animals remained at a plateau (40%) throughout. Although both STZ-treated groups displayed a mean non-fasting blood glucose concentration of ≥11.1 mmol/L (criterion 2) after 7 weeks, this was achieved earlier and to a greater extent in the TKTL1-KO group. These levels ranged from 9.64 ± 0.69 mmol/L (week 1) to 11.34 ± 1.12 mmol/L (week 7) in WT mice, and from 10.76 ± 0.71 mmol/L (week 1) to 14.5 ± 0.89 mmol/L (week 7) in the TKTL1-KO group (refer Figure 3.2.3).

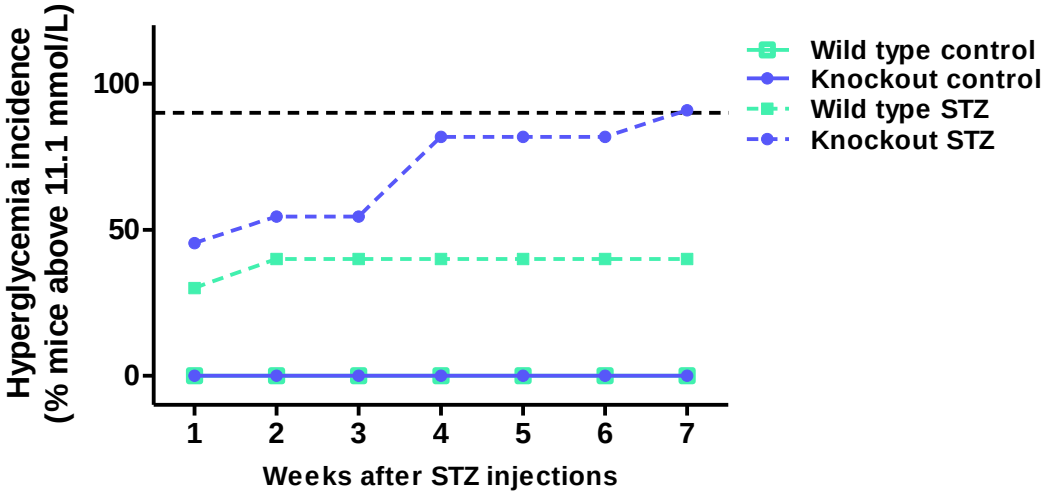

Figure 3.2.2 **Hyperglycemia incidence in male mice.** Blood glucose was measured weekly and values are expressed as the percentage animals displaying glycemic values ≥11.1 mM per group (n=10). The dotted line indicates the 90% hyperglycemia incidence cut-off (criterion 3).

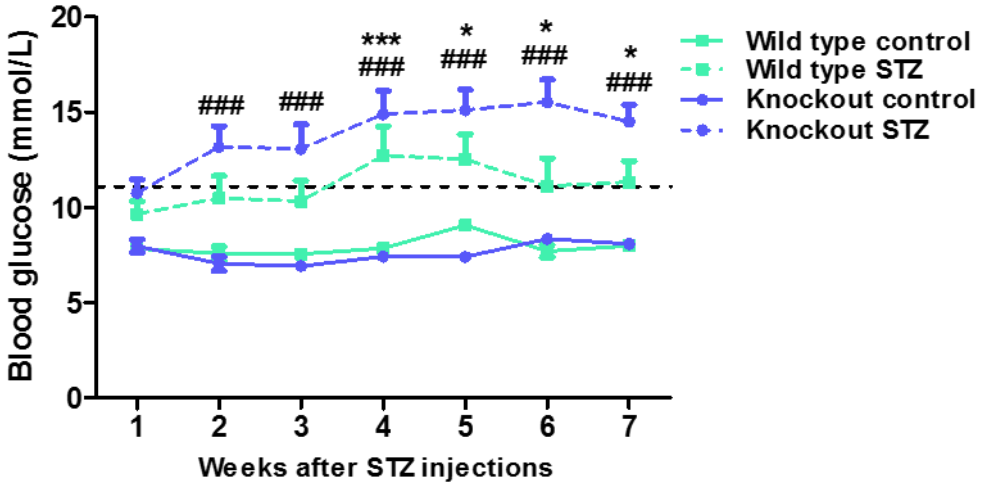

Figure 3.2.3 **Development of hyperglycemia – temporal analysis.** Blood glucose levels were weekly assessed and values expressed as mean ± SEM, n=10. *p<0.05, ***p<0.001 WT control vs. WT STZ; ###p<0.001 TKTL1-KO control vs. TKTL1-KO STZ. The dotted line indicates the 11.1 mmol/L cut-off value (criterion 2).

3.3 Body weights of male and female mice largely unaffected by STZ treatment

Body weights were measured weekly as a general indication of animal welfare (Foltz, 1999; Ullman-Culleré and Foltz, 1999). Within the male groups, TKTL1-KO STZ-injected mice displayed moderately lowered body weights compared to the WT control group (*p=0.04) (refer Figure 3.3.1 A). No other changes were noted within the groups (refer Figure 3.3.1).

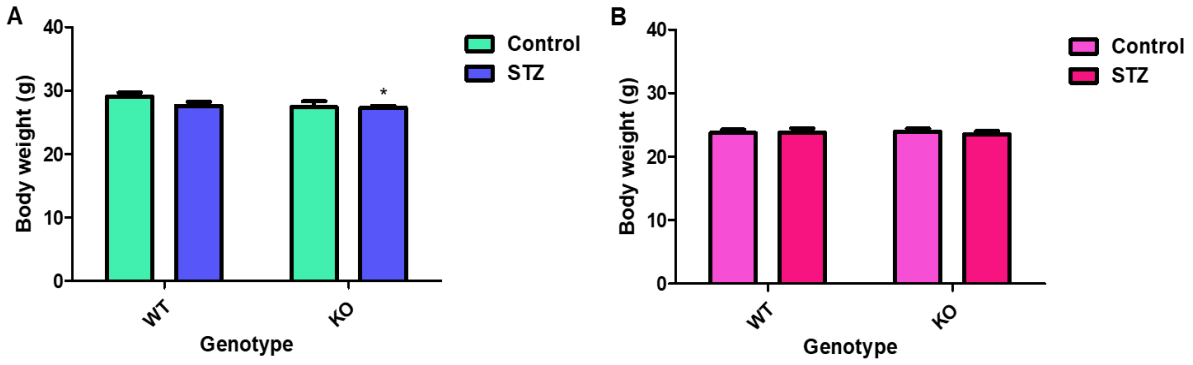

Figure 3.3.1 **Body weights of male (A) and female (B) mice were largely unchanged**. Data presented as mean ± SEM. *p<0.05 vs. WT control, n=10 (males) and n=5 (females).

3.4 Assessment of organ weights in relation to body weight

Following the assessment of blood glucose and body weight, we next evaluated specific organ weights (heart, liver, pancreas, kidney, gastrocnemius muscle and mammary fat pads (females). Organ weights are expressed as a percentage of body weight (refer Table 3.4).

In the male mice, relative organ weight alterations were restricted to the TKTL1-KO mice, with the STZ-treated group displaying the most changes. The male TKTL1-KO STZ-treated group displayed larger relative liver weights compared to controls (p<0.001). An increase was also noted in the relative kidney weights of both TKTL1-KO groups. Gastrocnemii of the TKTL1-KO STZ-treated group was lower than that of the WT control group (p<0.01). The inguinal mammary fat pads of the female TKTL1-KO STZ-treated group displayed lowered relative weight compared to the TKTL1-KO control group.

Table 3.4 **Organ weights as a percentage of body weight.**

Gender	Genotype	Treatment	Heart	Liver	Pancreas	Kidneys	Gastrocnemii	Inguinal fat pad
Male	WT	Control	0.482 ± 0.01	4.885 ±0.07	0.508 ± 0.04	1.216 ± 0.01	1.145 ± 0.01	n/a
		STZ	0.443 ± 0.03	5.168 ±0.27	0.600 ± 0.03	1.189 ± 0.02	1.107 ± 0.02	n/a
	TKTL1-KO	Control	0.523 ± 0.02	4.734 ±0.15	0.606 ± 0.05	1.423 ± 0.05***	1.043 ± 0.05	n/a
		STZ	0.490 ± 0.03	5.8184 ±0.17***, ###	0.590 ± 0.03	1.327 ± 0.03*, #,$$	1.043 ± 0.02**	n/a
Female	WT	Control	0.522 ± 0.03	5.026 ± 0.22	0.594 ±0.10	1.197 ± 0.08	0.953 ± 0.03	0.278 ± 0.06
		STZ	0.456 ± 0.04	4.909 ± 0.36	0.625 ±0.05	1.222 ± 0.04	0.965 ± 0.02	0.335 ± 0.05
	TKTL1-KO	Control	0.519 ± 0.04	4.892 ± 0.18	0.694 ±0.04	1.257 ± 0.06	0.884 ± 0.07	0.538 ± 0.07*
		STZ	0.542 ± 0.03	4.761 ± 0.10	0.538 ±0.08	1.281 ± 0.04	0.960 ± 0.04	0.266 ± 0.09##

Organ weights expressed as percentage of body weight ± SEM. *p<0.05 vs. WT control, #p<0.05 vs. TKTL1-KO control, **p<0.01 vs. WT control, $$p<0.01 vs. WT STZ, ***p<0.001 vs. WT control, ###p<0.001 vs. TKTL1-KO control, n=10 (males), n= 5 (females).

3.5 Analysis of the PPP

Next we aimed to analyze the PPP in depth and employed a commercially available kit to assess G6PD activity, the initial rate-limiting enzyme of the PPP's oxidative branch (Pandolfi *et al*., 1995). We subsequently tested the concentrations of NADPH and $NADP^+$, a by-product of the G6PD reaction, with a commercially available kit. Due to some technical difficulties, only the NADPHt (NADPH + $NADP^+$) could be quantified. Next, we employed a published method for the quantification of transketolase activity (Diaz-Moralli *et al*., 2011). Here total transketolase activity was measured as there is no assay specifically for TKTL1 activity *per se*, the flux controlling enzyme of the non-oxidative branch of the PPP and the main focus of this project (Berthon *et al*., 1992; Schenk *et al*., 1998).

3.5.1 G6PD activity

G6PD activity was measured in both heart and liver samples (refer Figures 3.5.1.1 and 3.5.1.3). No significant alterations in G6PD activity were observed in the heart of any of the experimental groups. Animals that were sensitive to the hyperglycemia-inducing effects of STZ (responders) had higher mean G6PD activity when analyzed separately, however, this was still not significantly different when compared to controls (Figure 3.5.1.1 B). We further aimed to investigate whether a correlation existed between G6PD activity and blood glucose levels. Here we found no significant correlation exists for heart samples (Figure 3.5.1.2). The liver G6PD activity was also not significantly changed in any of the groups (Figure 3.5.1.3 A), while separate analysis of WT responders and non-responders yielded similar results (Figure 3.5.1.3 B and C). Interestingly, there was a significant, moderate negative correlation between liver G6PD activity and blood glucose levels ($r=-0.37$, $p=0.03$; Figure 3.5.1.4).

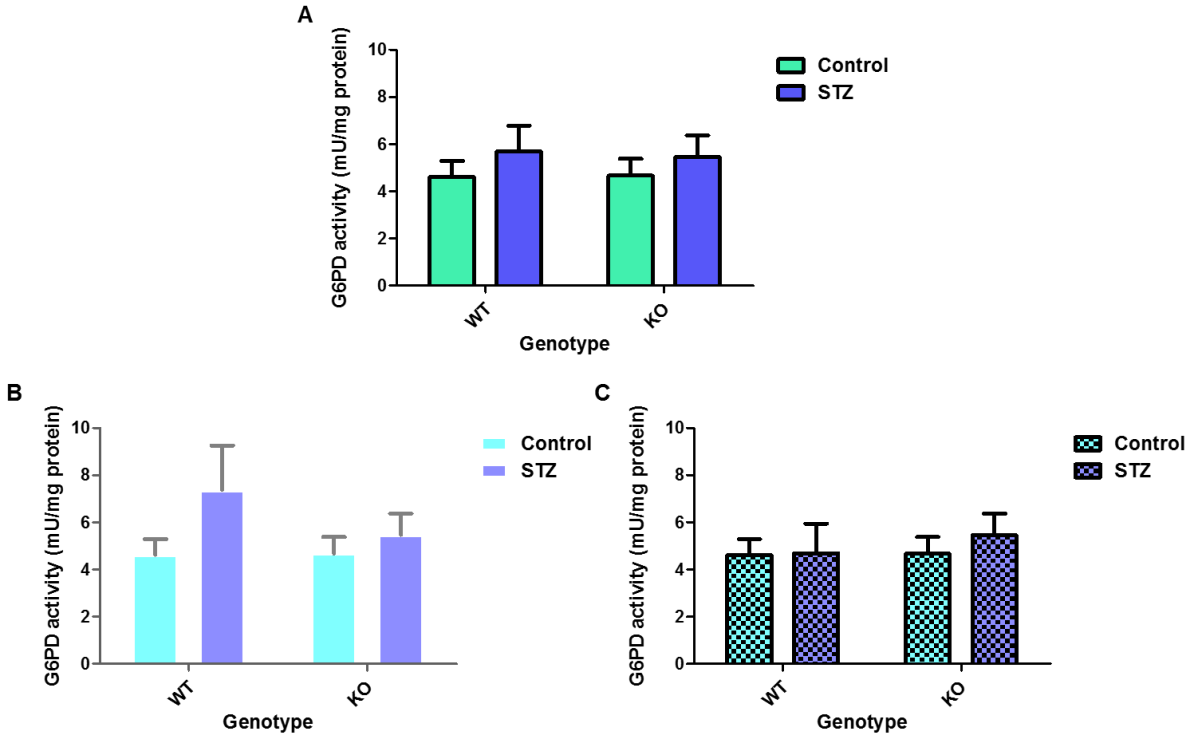

Figure 3.5.1.1 **G6PD activity in the heart: A (combined data), B (WT STZ responders), C (WT STZ non-responders).** Data presented as mean ± SEM, n=8. WT STZ responders n=3 (B), WT STZ non-responders n=5, (C).

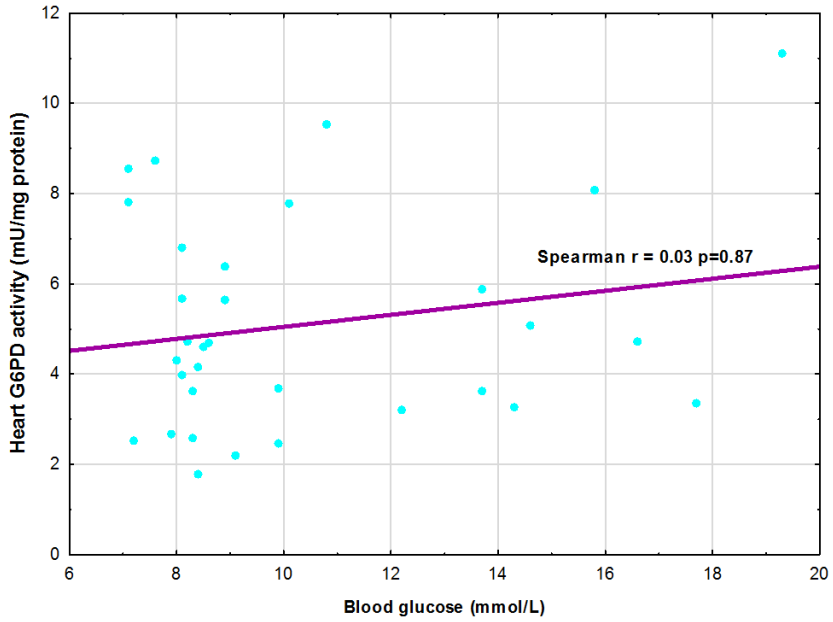

Figure 3.5.1.2 **No significant correlation between G6PD activity in the heart and blood glucose concentrations.** Spearman's correlation coefficient r = 0.03, p=0.87.

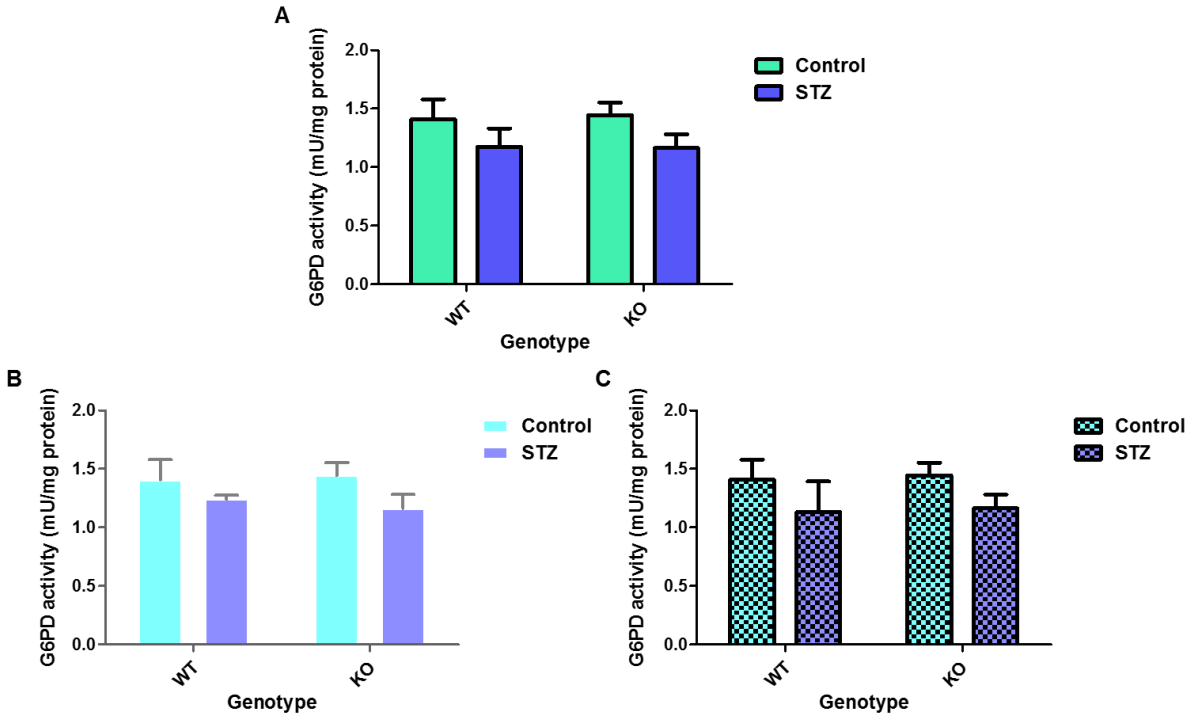

Figure 3.5.1.3 **G6PD activity in the liver: A (combined data), B (WT STZ responders), C (WT STZ non-responders).** Data presented as mean ± SEM, n=8. WT STZ responders n=3 (B), WT STZ non-responders n=5, (C).

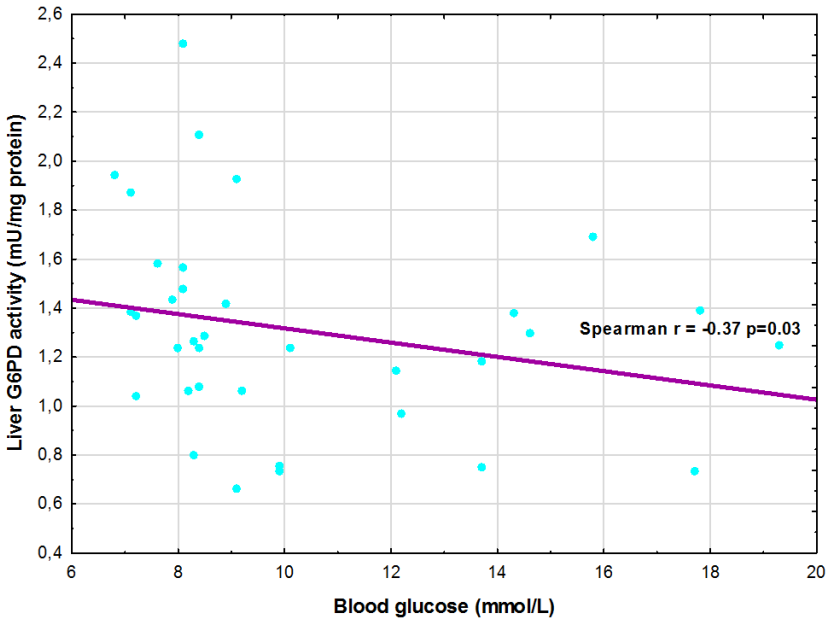

Figure 3.5.1.4 **Significant, moderate negative correlation of G6PD activity in the liver with increasing blood glucose concentrations.** Spearman's correlation coefficient r = -0.37, p=0.03.

3.5.2 NADPt concentration

As mentioned in the Methods, we encountered technical difficulties with this assay due to fat droplet formation (in the boiling step) which interfered with the absorbance readings. Therefore only the NADPt reading was obtainable (refer Figure 3.5.2). No significant differences were found for NADPt levels for the heart groups (Figure 3.5.2.1). Separation of WT-STZ responders and non-responders had no effect. NADPt levels also did not show any correlation with blood glucose levels (Figure 3.5.2.2). Liver NADPt levels were also not significantly different between groups (Figure 3.5.2.3). One of the TKTL1-KO control data points were highly elevated compared to the other values within this group. No correlation exists between NADPt levels and blood glucose concentration (Figure 3.5.2.4).

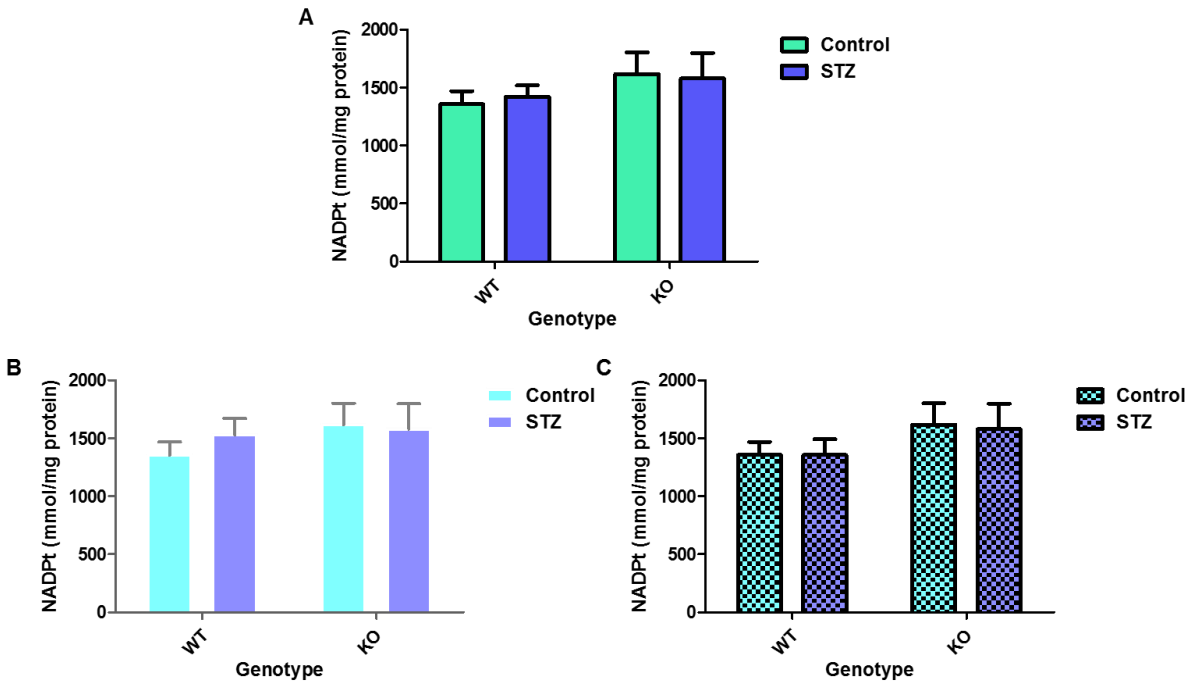

Figure 3.5.2.1 **NADPt$^{(NADPH+NADP+)}$ in the heart: A (combined data), B (WT STZ responders), C (WT STZ non-responders).** Data presented as mean ± SEM, n=8. WT STZ responders n=3 (B), WT STZ non-responders n=5, (C).

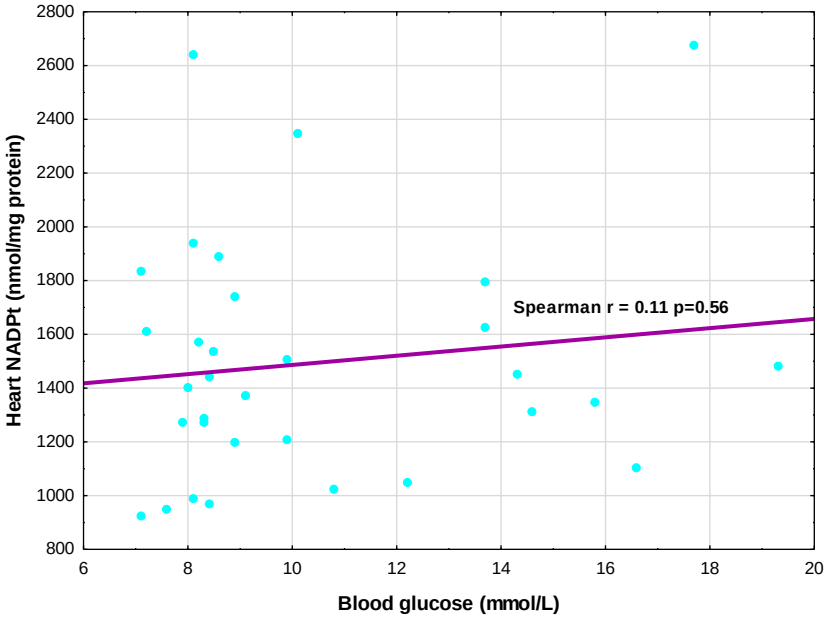

Figure 3.5.2.2 **Lack of correlation between NADPt (NADPH+NADP+) levels and blood glucose concentrations in the heart.** Spearman's correlation coefficient r = 0.11, p=0.56.

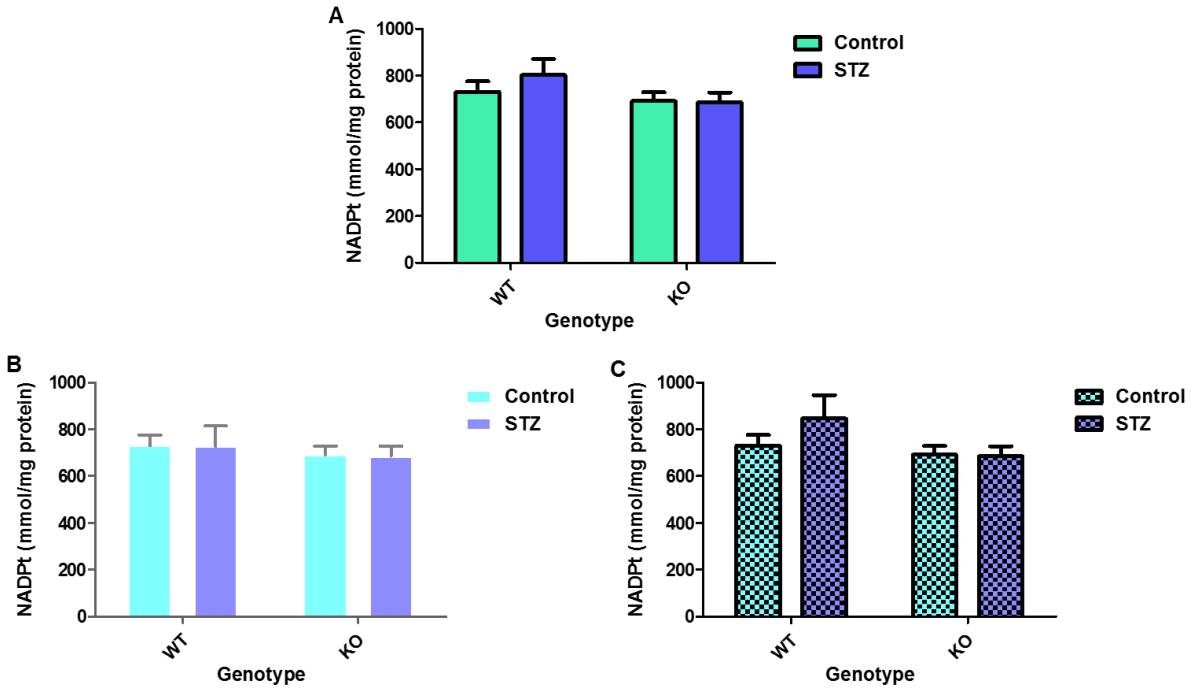

Figure 3.5.2.3 **NADPt (NADPH+NADP+) in the liver: A (all data), B (responders), C (non-responders).** Data presented as mean ± SEM, n=8. WT STZ responders n=3 (B), WT STZ non-responders n=5, (C).

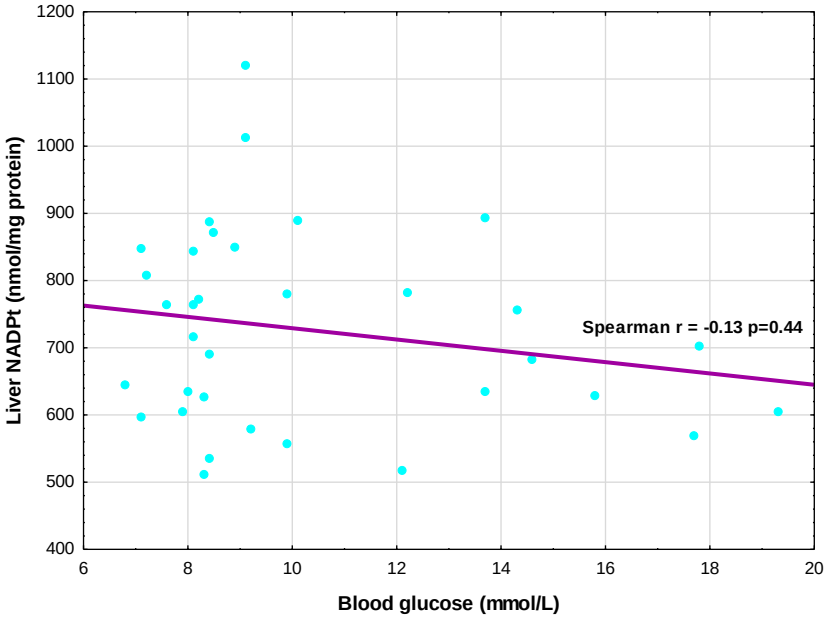

Figure 3.5.2.4 **No correlation between NADPt $^{(NADPH+NADP+)}$ levels in the liver and blood glucose concentrations.** Spearman's correlation coefficient r = -0.13, p=0.44.

3.5.3 Transketolase activity

Total transketolase activity was measured in heart and liver samples using an in-house assay modified from Diaz-Moralli and colleagues (2011). In the heart, both TKTL1-KO groups displayed ~50% diminished transketolase activity compared to the WT control ($p<0.001$) (Figure 3.5.3.1). The heart transketolase activity in the WT STZ group was ~68% of that in the WT control group ($p<0.05$). Of note, responders and non-responders each had similar effects on transketolase activity (Figure 3.5.3.1 B and C). Liver transketolase activity presented negative values, indicating technical difficulties. No significant differences in liver transketolase activity were observed between any of the groups. Furthermore, there was no correlation between heart transketolase activity and blood glucose levels (Figure 3.5.3.2).

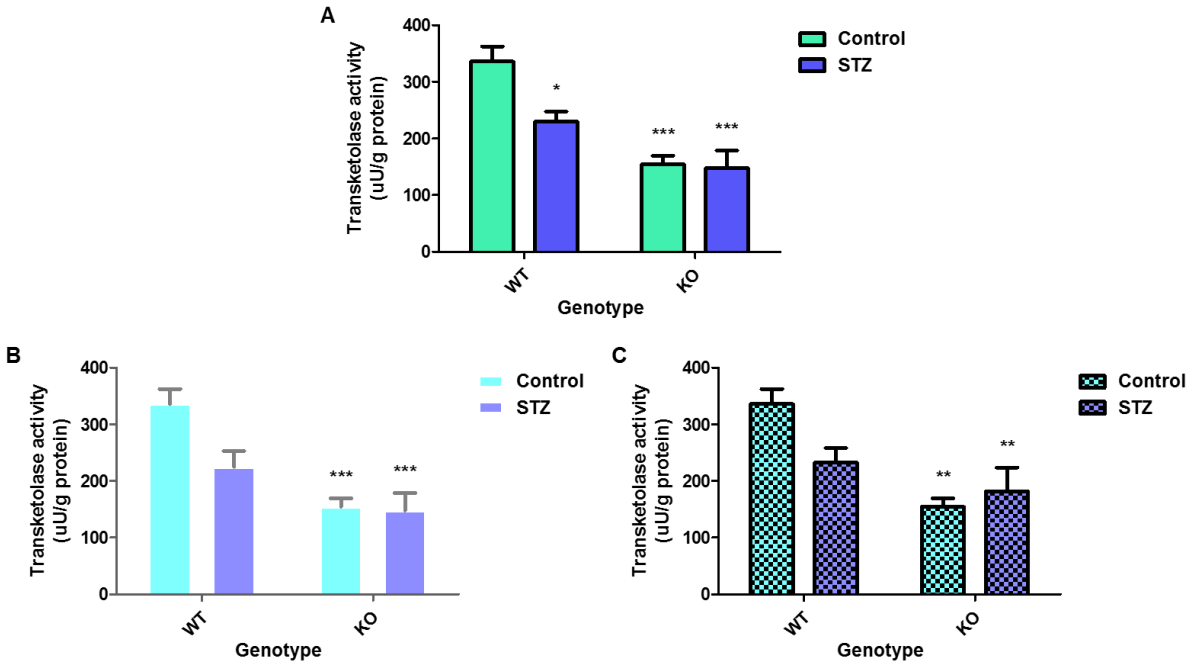

Figure 3.5.3.1 **Total transketolase activity in the heart: A (combined data), B (WT STZ responders), C (WT STZ non-responders).** Data presented as mean ± SEM, n=8. WT STZ responders n=3 (B), WT STZ non-responders n=5, (C). *p<0.05 vs. WT control, **p<0.01 vs. WT control, ***p<0.001 vs. WT control.

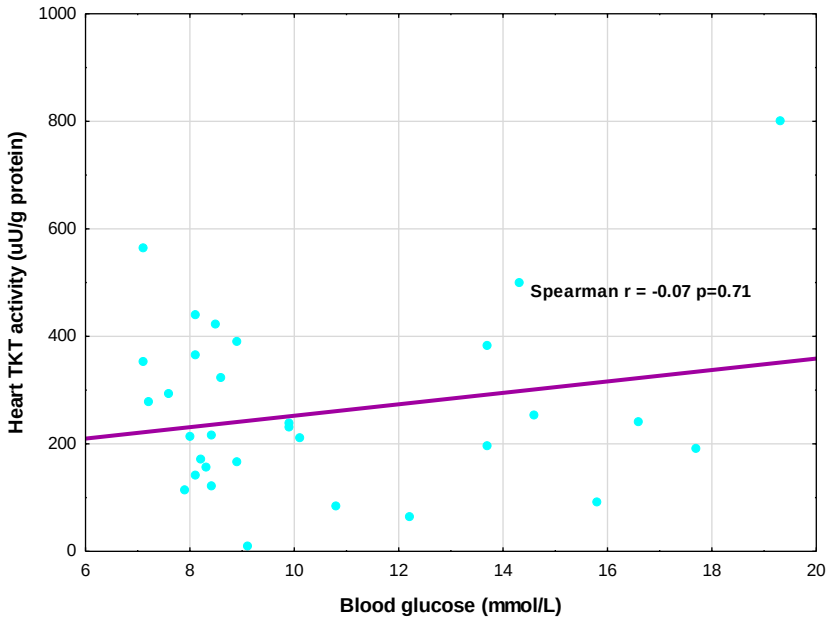

Figure 3.5.3.2 **Lack of correlation between total transketolase activity in the heart and blood glucose concentrations.** Spearman's correlation coefficient r = -0.07, p=0.71.

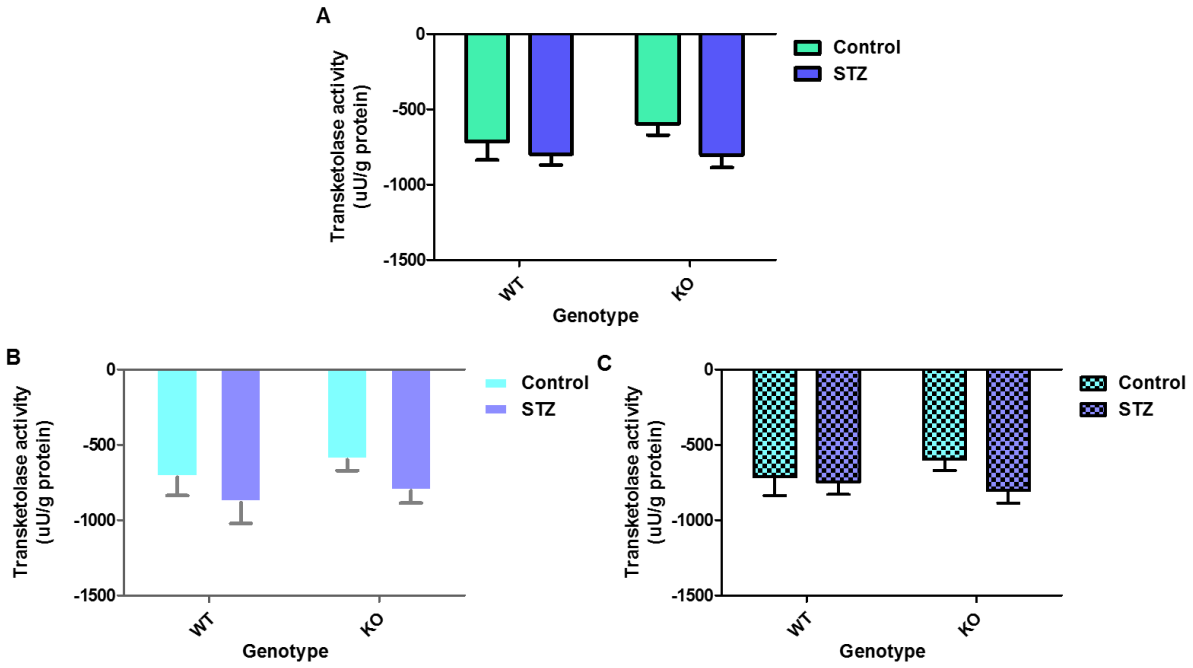

Figure 3.5.3.3 **Total transketolase activity in the liver: A (combined data), B (WT STZ responders), C (WT STZ non-responders).** Data presented as mean ± SEM, n=8. WT STZ responders n=3 (B), WT STZ non-responders n=5, (C).

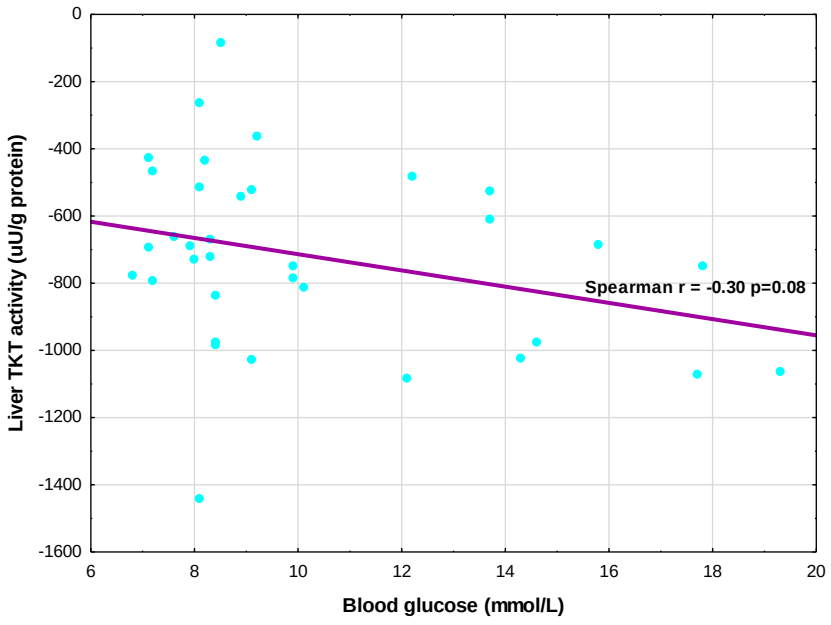

Figure 3.5.3.4 **Non-significant, moderately negative correlation between total transketolase activity in the liver and blood glucose concentrations.** Spearman's correlation coefficient r = -0.30, p=0.08.

3.6 Evaluation of oxidative status

One of the main aims of this study was to evaluate the putative role of TKTL1 in the oxidative status of STZ-induced hyperglycemic mice. As described in Section 2.3, mice were injected with either STZ (40 mg/kg, i.p.) or citrate buffer for five consecutive days after which blood glucose levels were periodically monitored until hyperglycemia was established. Tissues were then collected for analyses. Here we sought to evaluate the oxidative status of blood, heart and liver samples by assessing indicators of oxidative stress and damage as well as an evaluation of anti-oxidant mechanisms.

3.6.1 NOX activity

We started by assessing NOX activity as it is one of the major ROS producing systems in many cell types. Here we employed an in-house luminescence assay protocol adapted from previous work (Abid *et al*. 2007). No significant differences in NOX activity were noted between any of the groups in either the heart (Figure 3.6.1.1) or the liver (Figure 3.6.1.3). However, this could be due to the immense variability within the groups, especially in the heart samples. Notably, NOX activity of the liver greatly exceeds (~10X) that of the heart. NOX activity was also not correlated with blood glucose (Figures 3.6.1.2 and 3.6.1.4).

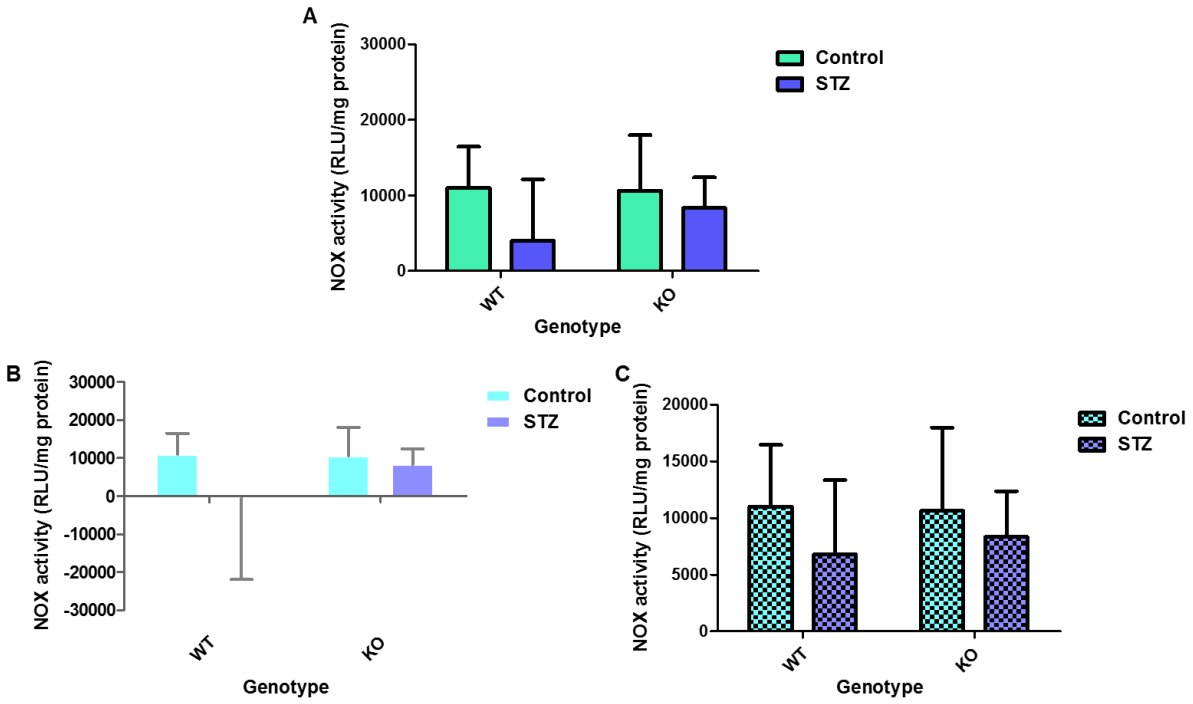

Figure 3.6.1.1 **NOX activity in the heart: A (all data), B (responders), C (non-responders).** Data presented as mean ± SEM, n=8. WT STZ responders n=3 (B), WT STZ non-responders n=5, (C).

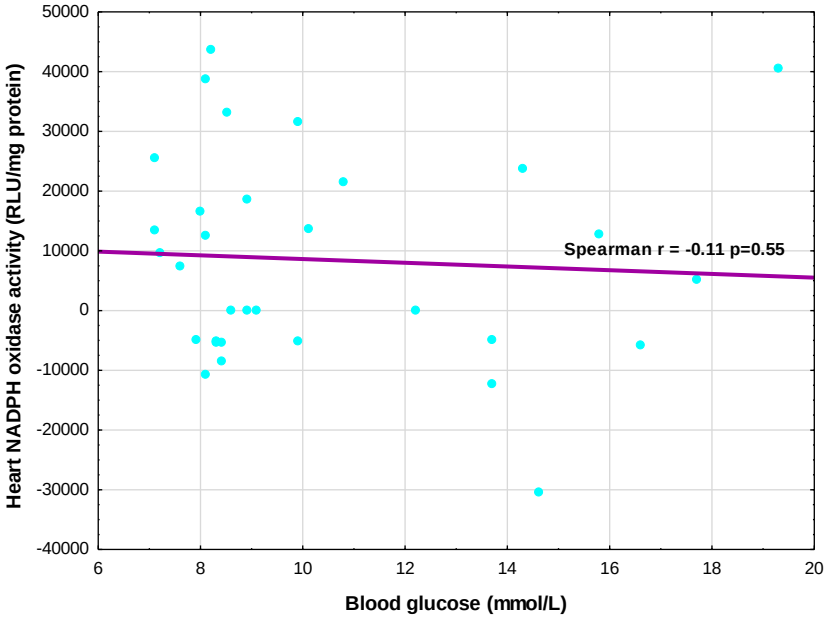

Figure 3.6.1.2 **No correlation between NADPH oxidase activity in the heart and blood glucose concentrations.** Spearman's correlation coefficient r = -0.11, p=0.55.

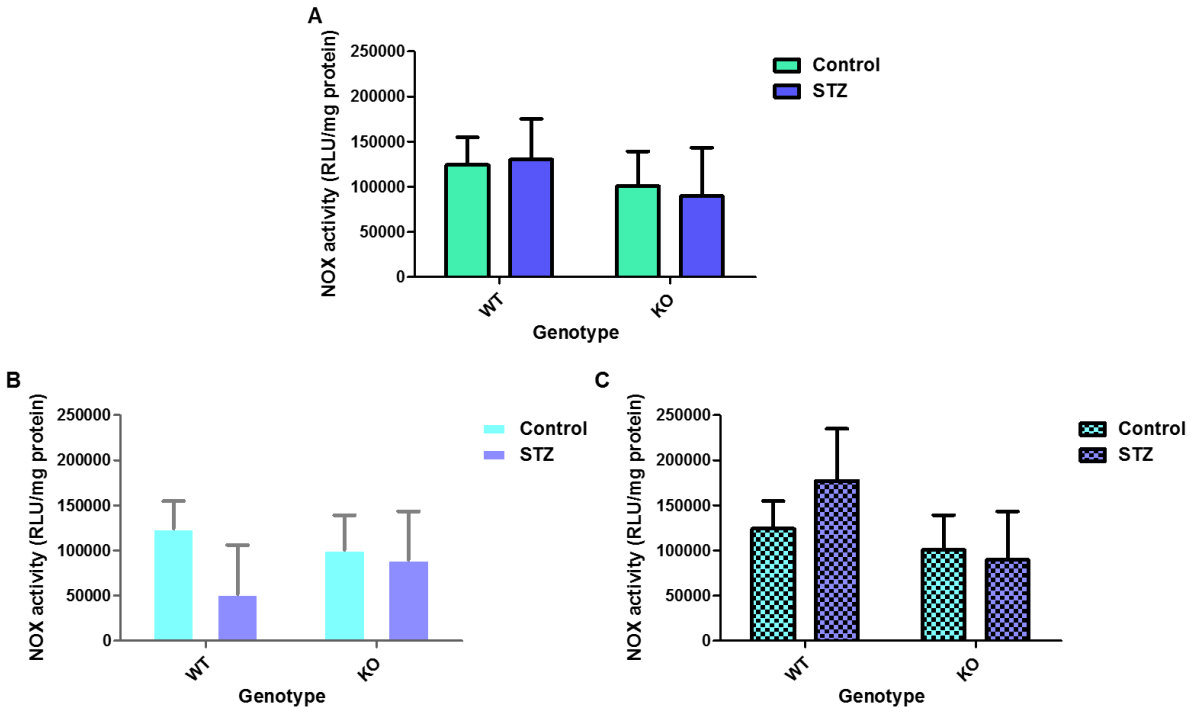

Figure 3.6.1.3 **NOX activity in the liver: A (combined data), B (WT STZ responders), C (WT STZ non-responders).** Data presented as mean ± SEM, n=8. WT STZ responders n=3 (B), WT STZ non-responders n=5, (C).

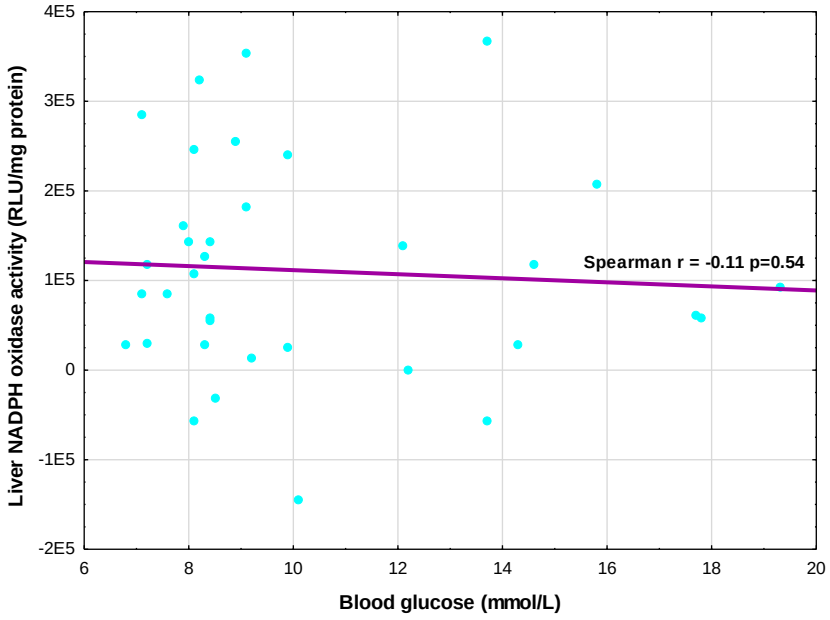

Figure 3.6.1.4 **No correlation between NADPH oxidase activity in the liver and blood glucose concentrations.** Spearman's correlation coefficient r = -0.11, p=0.54.

3.6.2 Quantification of CDs

We next analyzed markers of oxidative damage in circulation, as well as in heart and liver tissues. CD concentration (an early indicator of lipid peroxidation) was not significantly altered in the blood (Figure 3.6.2.1), heart (Figure 3.6.2.3), or liver (Figure 3.6.2.5) of any of the groups. This was despite a ~21% and ~37% decrease in blood and liver, respectively, of WT STZ-treated animals. Separation of responders and non-responders did not alter this result. Furthermore, there were no correlations between CDs and blood glucose levels in any of the tested samples (Figure 3.6.2.2, Figure 3.6.2.4, and Figure 3.6.2.6). However, when analyzing WT and TKTL1-KO samples separately, we observed a strong negative and significant correlation between CDs in the liver and blood glucose levels of WT mice (Spearman correlation coefficient r=-0.47, p= 0.05, data not shown, refer Appendix B for statistical table). This was not observed in the TKTL1-KO animals.

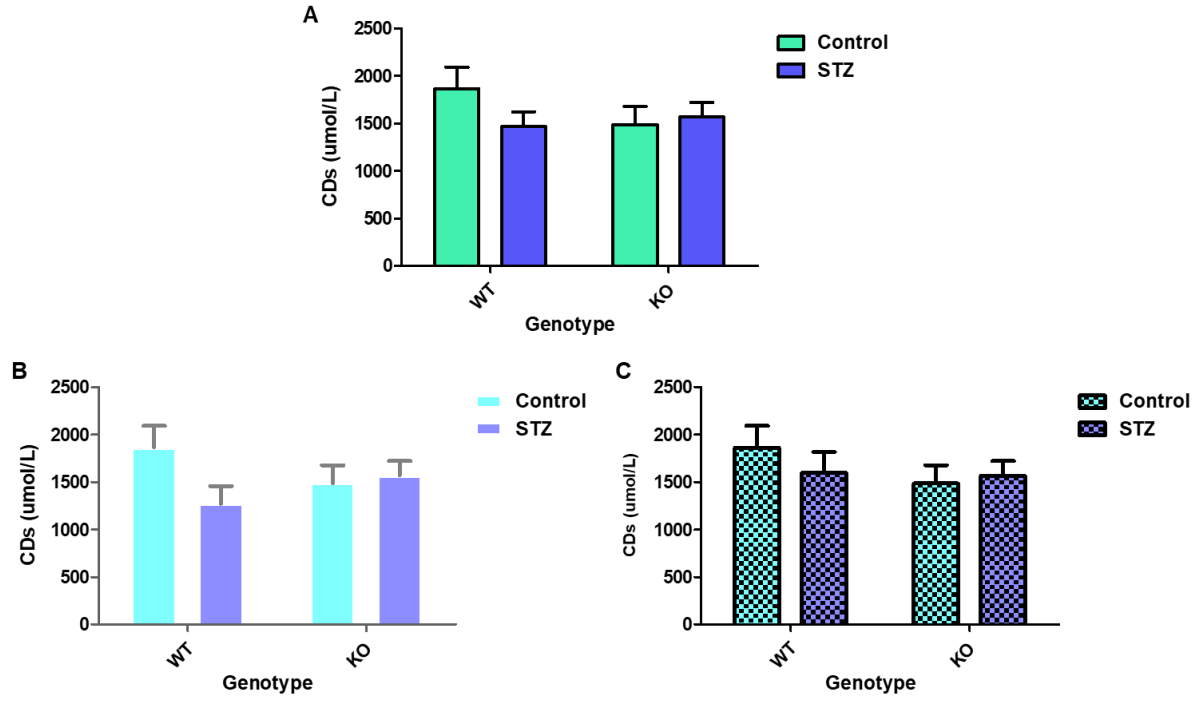

Figure 3.6.2.1 **CDs in circulation: A (combined data), B (WT STZ responders), C (WT STZ non-responders).** Data presented as mean ± SEM, n=8. WT STZ responders n=3 (B), WT STZ non-responders n=5, (C).

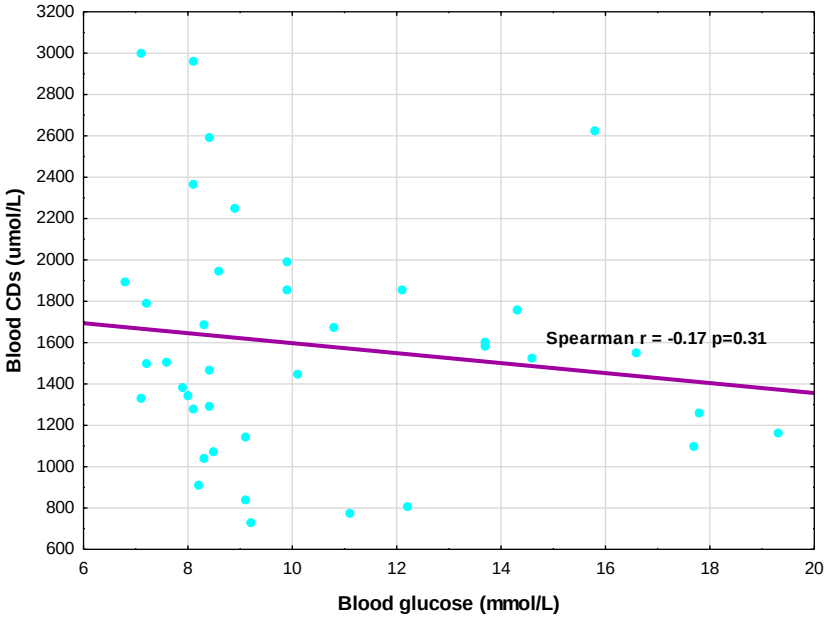

Figure 3.6.2.2 **No correlation between CDs in the blood and blood glucose concentrations.** Spearman's correlation coefficient r = -0.17, p=0.31.

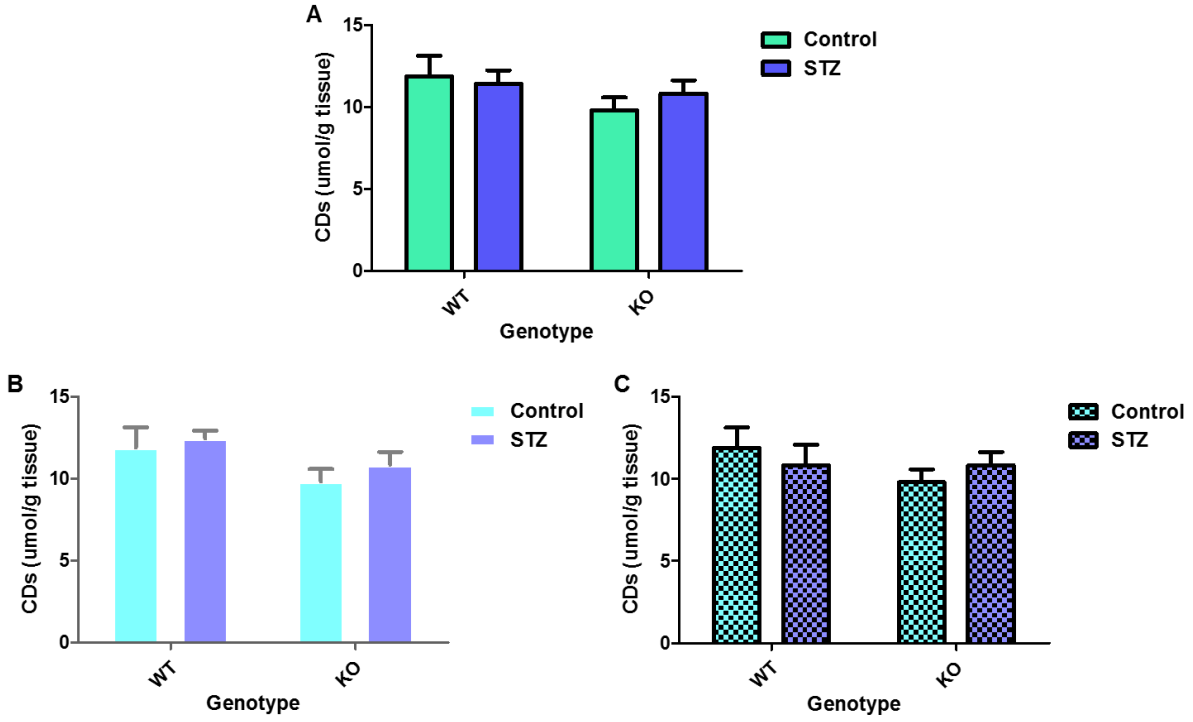

Figure 3.6.2.3 **CDs in the heart: A (combined data), B (WT STZ responders), C (WT STZ non-responders).** Data presented as mean ± SEM, n=8. WT STZ responders n=3 (B), WT STZ non-responders n=5, (C).

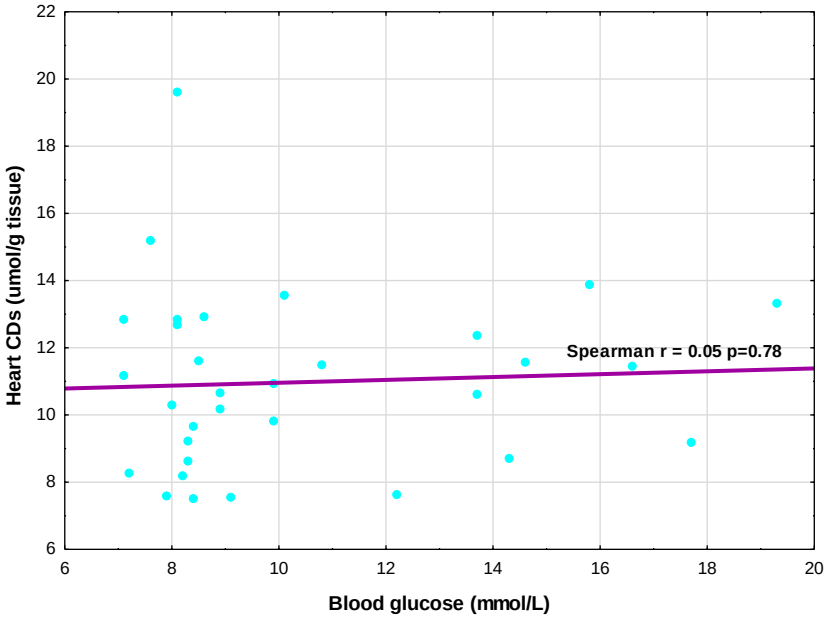

Figure 3.6.2.4 **No correlation between CDs in heart tissue and blood glucose concentrations.** Spearman's correlation coefficient r = 0.05, p=0.78.

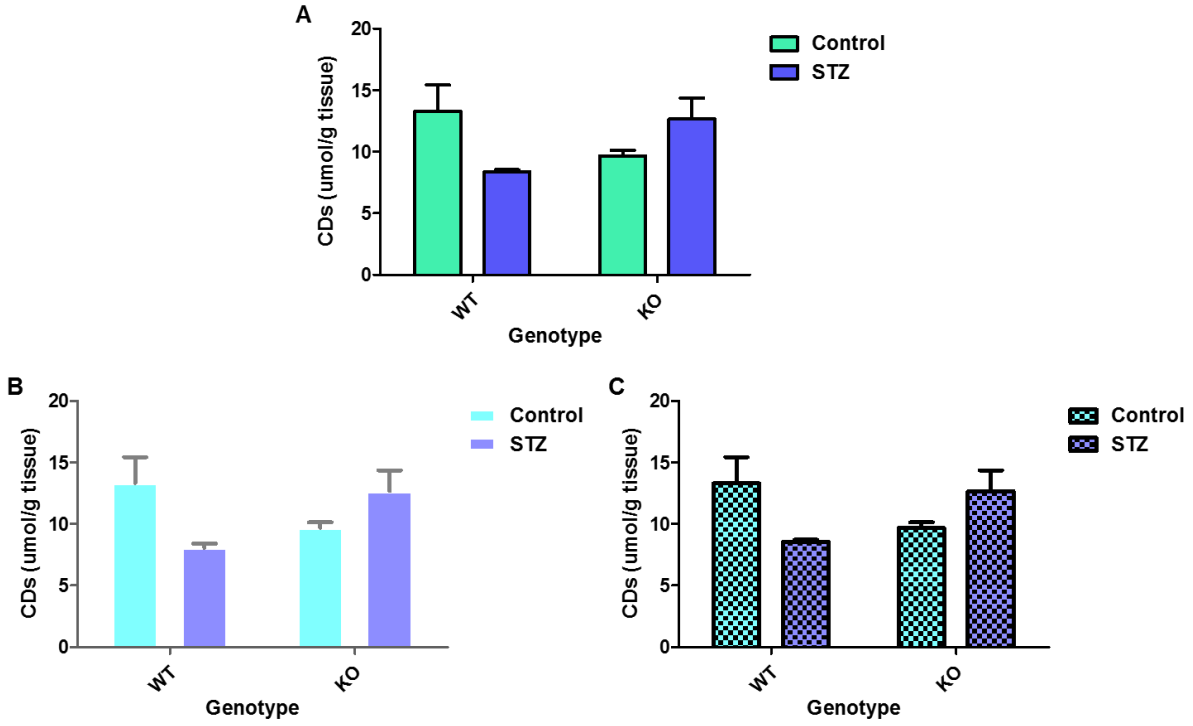

Figure 3.6.2.5 **CDs in the liver: A (combined data), B (WT STZ responders), C (WT STZ non-responders).** Data presented as mean ± SEM, n=8. WT STZ responders n=3 (B), WT STZ non-responders n=5, (C).

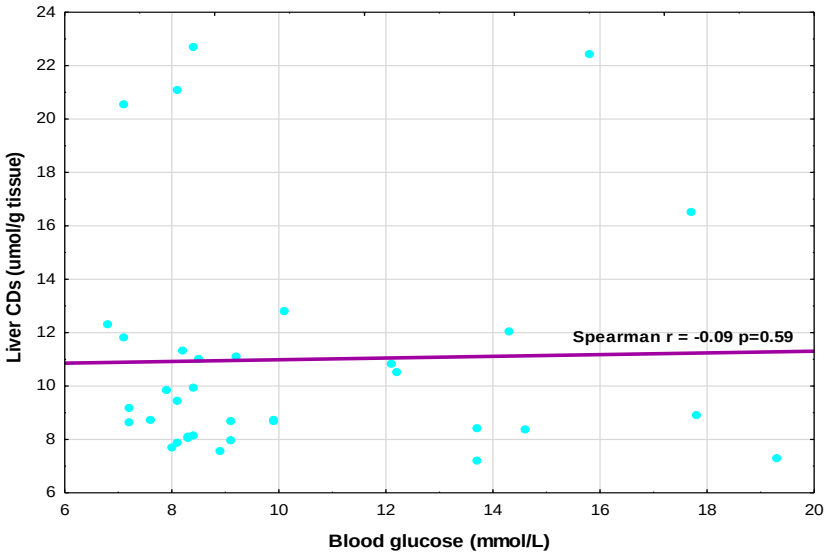

Figure 3.6.2.6 **No correlation between CDs in liver tissue and blood glucose concentrations.** Spearman's correlation coefficient r = -0.09, p=0.59.

3.6.3 Quantification of TBARS in blood, heart, and liver samples

We next assessed TBARS, a marker of lipid peroxidation. No significant differences were detected in TBARS concentration in circulation (Figure 3.6.3.1), heart (Figure 3.6.3.3), or liver (Figure 3.6.3.5).

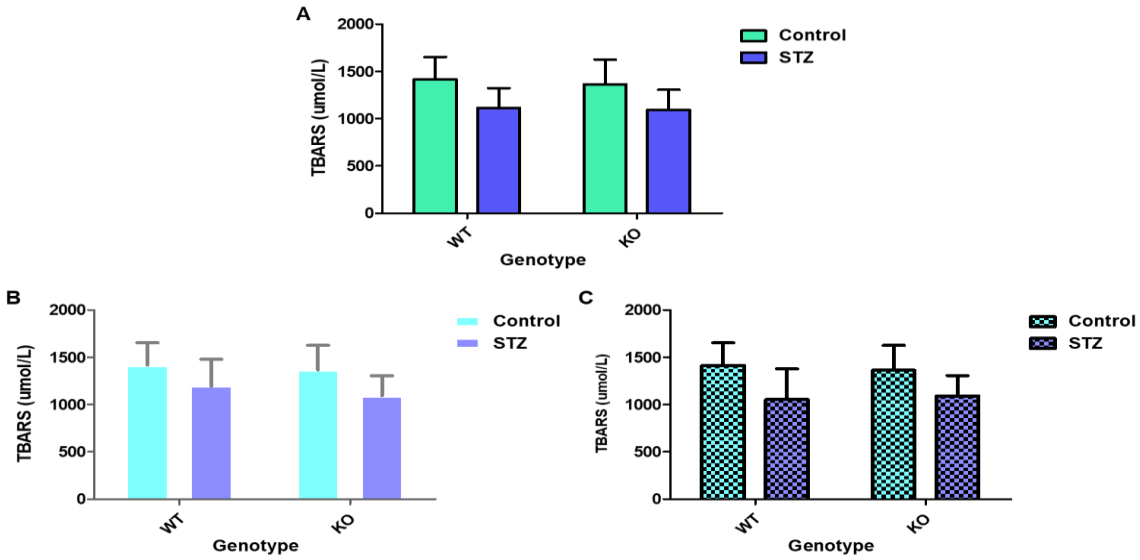

Figure 3.6.3.1 **TBARS in circulation: A (combined data), B (WT STZ responders), C (WT STZ non-responders).** Data presented as mean ± SEM, n=8. WT STZ responders n=3 (B), WT STZ non-responders n=5, (C).

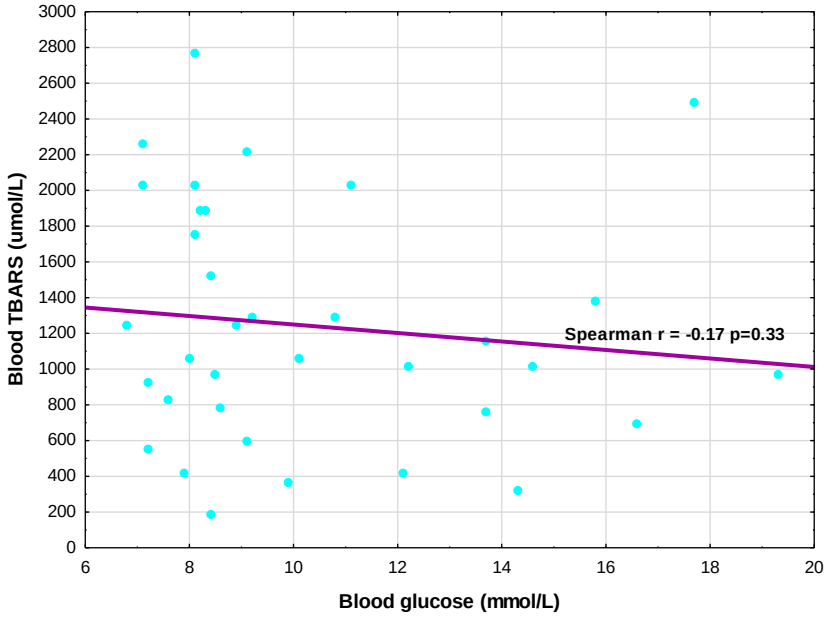

Figure 3.6.3.2 **No correlation between TBARS in blood and blood glucose concentrations.** Spearman's correlation coefficient r = -0.17, p=0.33.

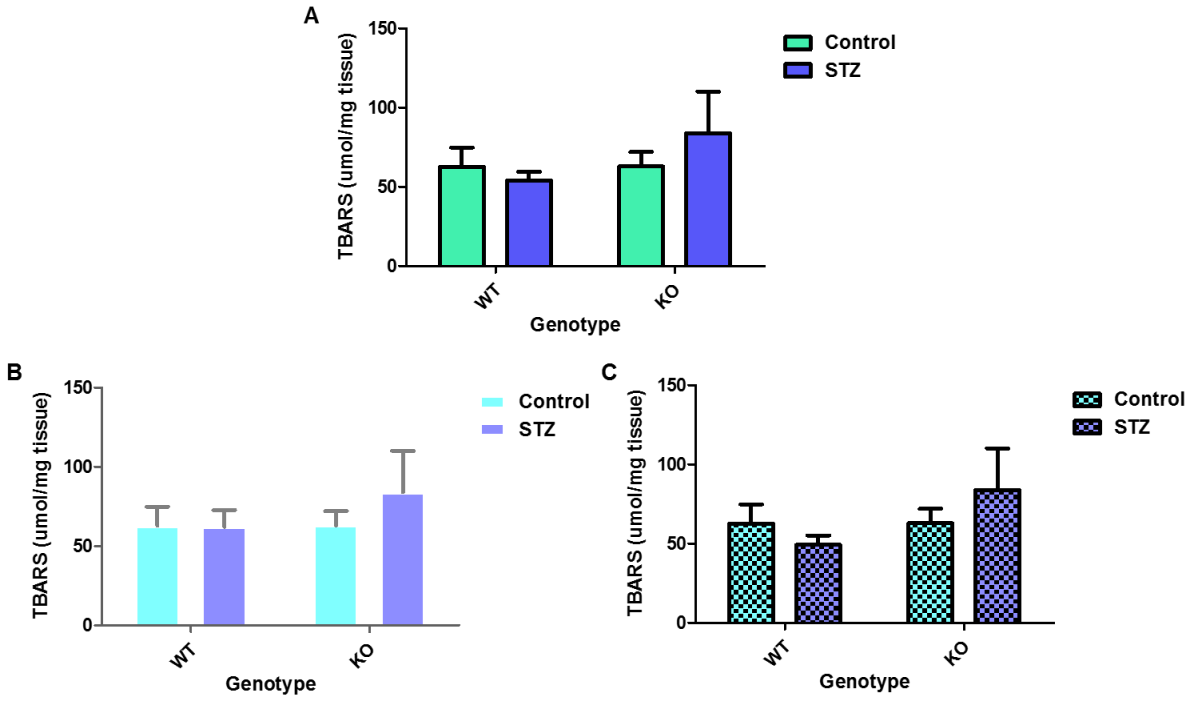

Figure 3.6.3.3 **TBARS in the heart: A (combined data), B (WT STZ responders), C (WT STZ non-responders).** Data presented as mean ± SEM, n=8. WT STZ responders n=3 (B), WT STZ non-responders n=5, (C).

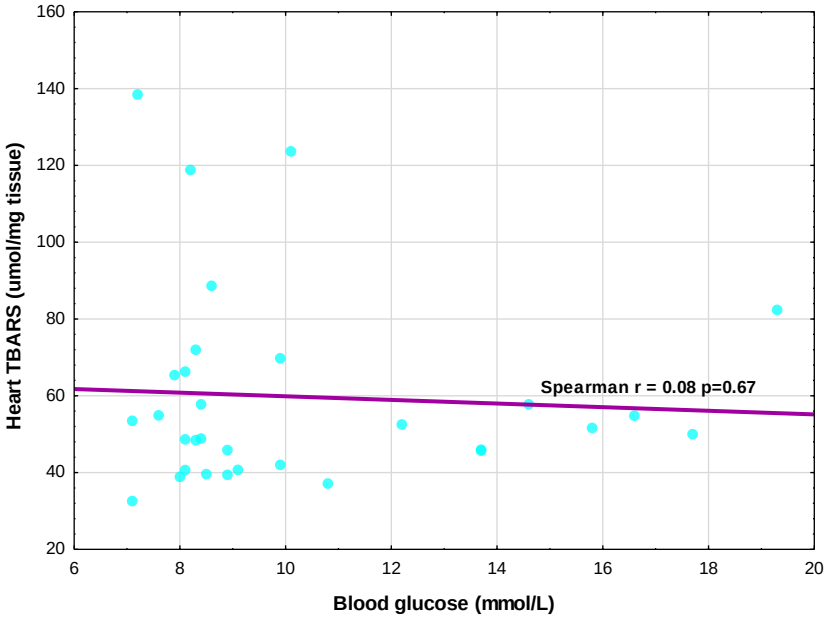

Figure 3.6.3.4 **No correlation between TBARS in heart tissue and blood glucose concentrations.** Spearman's correlation coefficient r = 0.08, p=0.67.

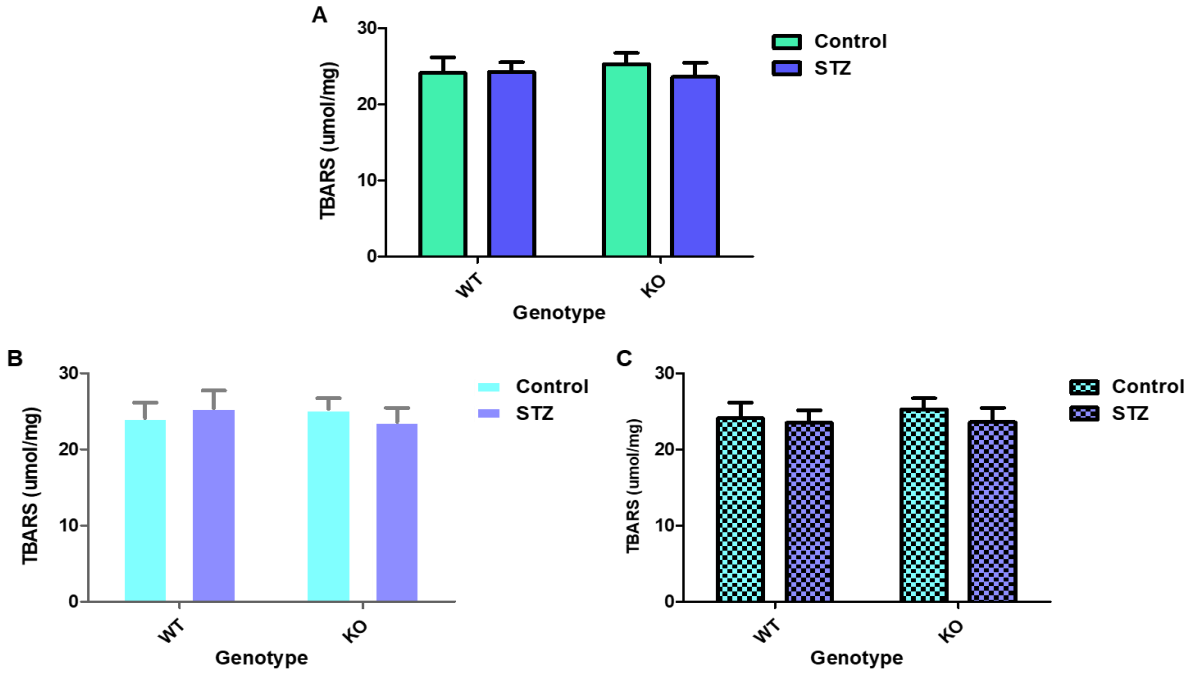

Figure 3.6.3.5 **TBARS in the liver: A (combined data), B (WT STZ responders), C (WT STZ non-responders).** Data presented as mean ± SEM, n=8. WT STZ responders n=3 (B), WT STZ non-responders n=5, (C).

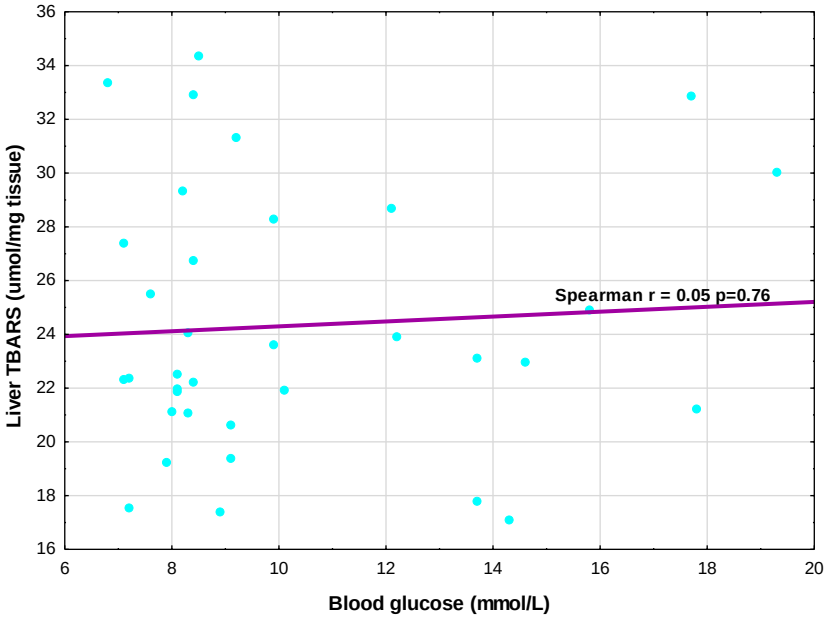

Figure 3.6.3.6 **No correlation between TBARS in liver tissue and blood glucose concentrations.** Spearman's correlation coefficient r = 0.05, p=0.76.

3.6.4 SOD activity in heart and liver samples

We next proceeded to assess the status of anti-oxidant capacity in our model. SOD activity in both the heart (Figure 3.6.4.1) and liver (Figure 3.6.4.3) were unchanged. There were also no correlation between SOD activity and blood glucose levels for either of the tissues (Figures 3.6.4.2 and 3.6.4.4).

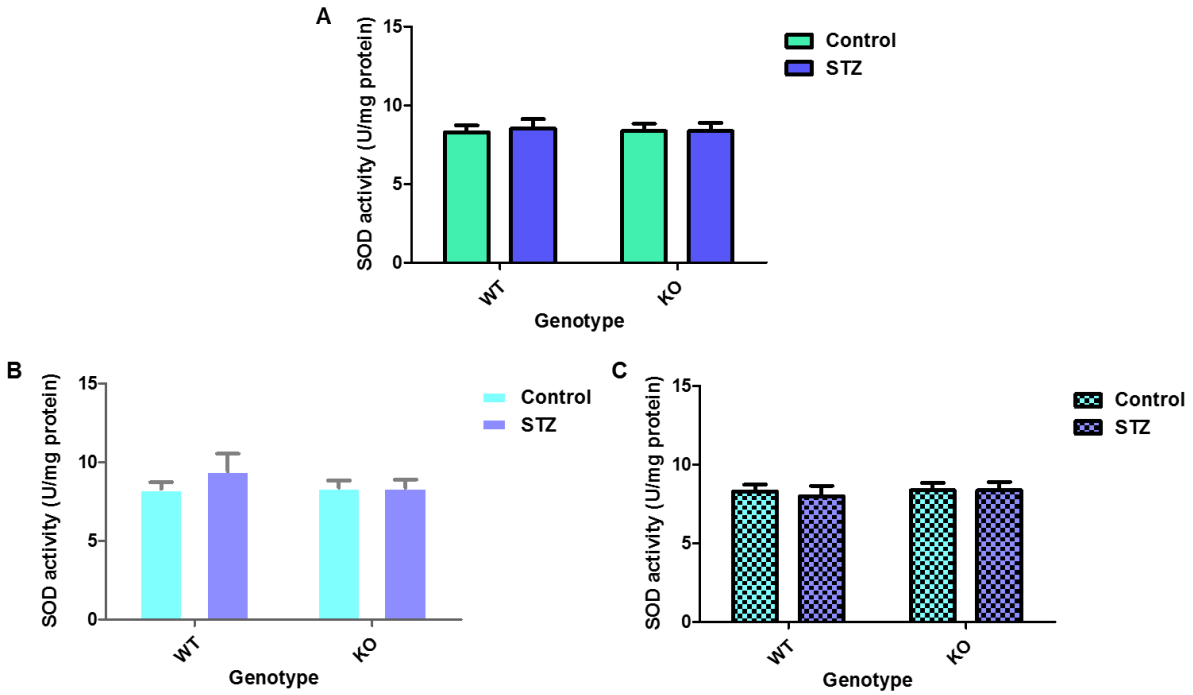

Figure 3.6.4.1 **SOD activity in the heart: A (combined data), B (WT STZ responders), C (WT STZ non-responders).** Data presented as mean ± SEM, n=8. WT STZ responders n=3 (B), WT STZ non-responders n=5, (C).

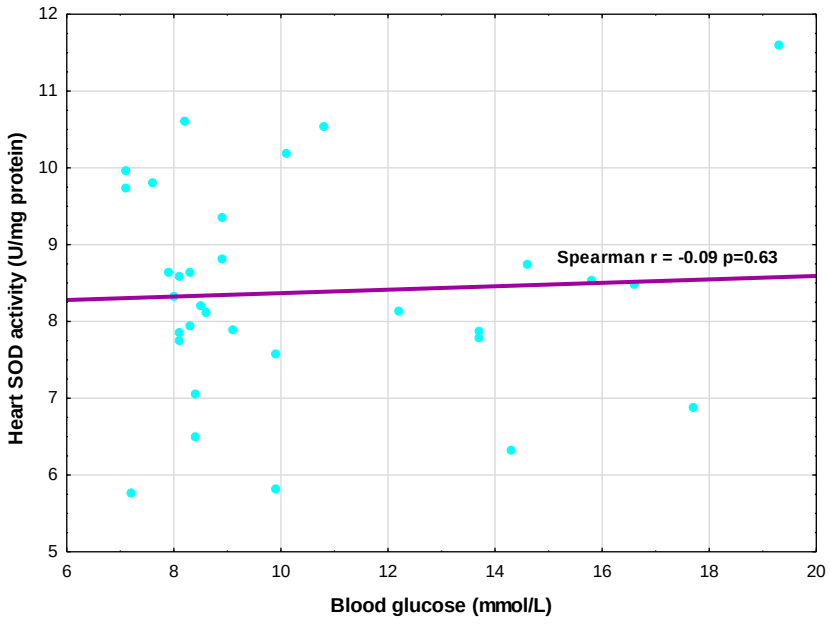

Figure 3.6.4.2 **No correlation between SOD activity in the heart tissue and blood glucose concentrations.** Spearman's correlation coefficient r = -0.09, p=0.63.

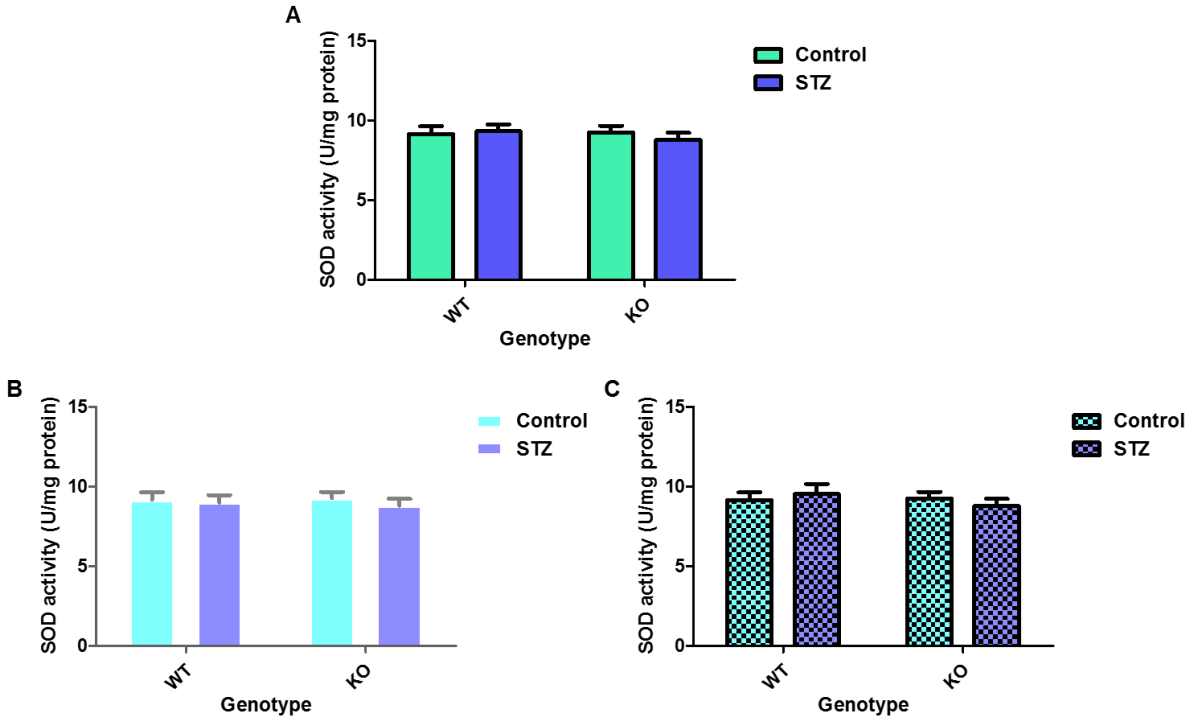

Figure 3.6.4.3 **SOD activity in the liver: A (combined data), B (WT STZ responders), C (WT STZ non-responders).** Data presented as mean ± SEM, n=8. WT STZ responders n=3 (B), WT STZ non-responders n=5, (C).

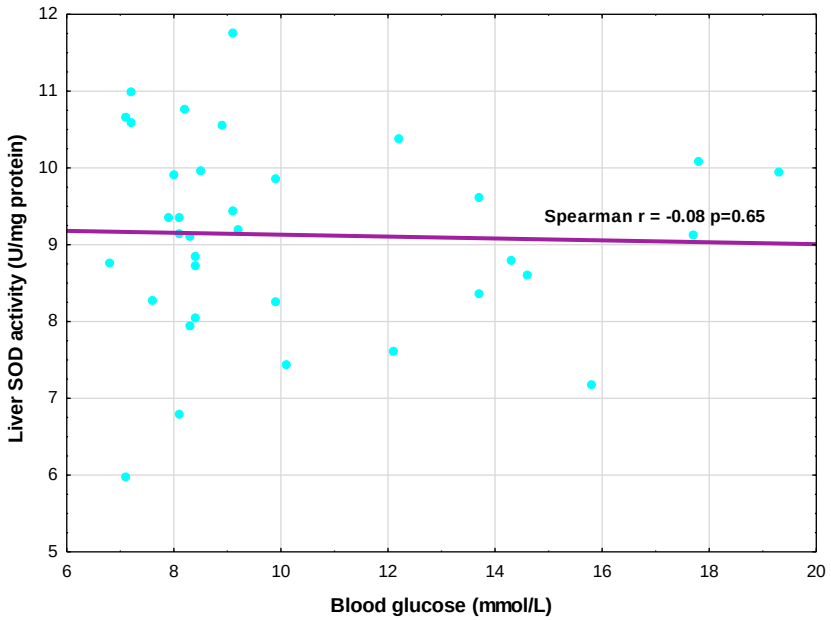

Figure 3.6.4.4 **No correlation of SOD activity in the liver tissue with blood glucose concentrations.** Spearman's correlation coefficient r = -0.08, p=0.65.

3.6.5 Catalase activity in heart and liver samples

No significant differences in catalase activity were detected in the heart in any of the groups (Figure 3.6.5.1), while this also did not correlate with blood glucose levels (Figure 3.6.5.2). Streptozotocin-treated TKTL1-KO mice displayed increased catalase activity in the liver ($p<0.05$ vs. WT control, $p<0.05$ vs. TKTL1-KO control, Figure 3.6.5.3). Furthermore, liver catalase activity showed a significant, moderate positive correlation with blood glucose when all study animals (WT and TKTL1-KO) were considered ($r=0.39$, $p=0.02$, Figure 3.6.5.4). This relationship was lost in the WT group alone. However, TKTL1-KO livers showed a strong positive correlation ($r=0.53$, $p=0.02$, data not shown, refer Appendix B for statistical table).

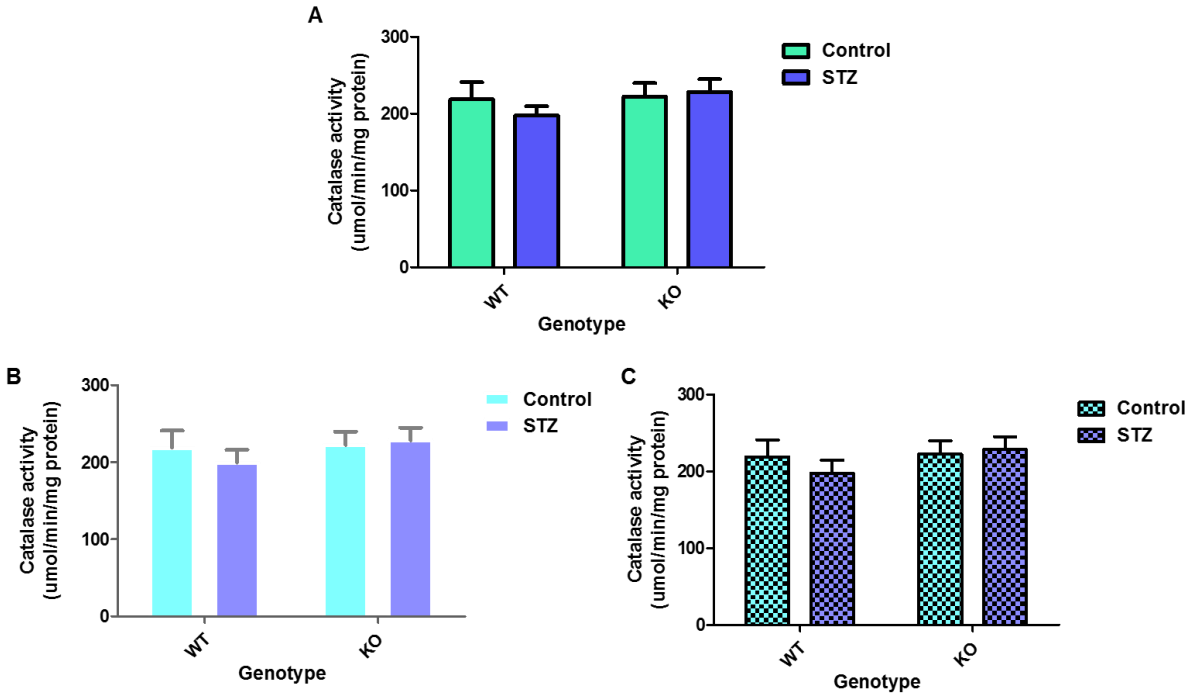

Figure 3.6.5.1 **Catalase activity of the heart: A (combined data), B (WT STZ responders), C (WT STZ non-responders).** Data presented as mean ± SEM, n=8. WT STZ responders n=3 (B), WT STZ non-responders n=5, (C).

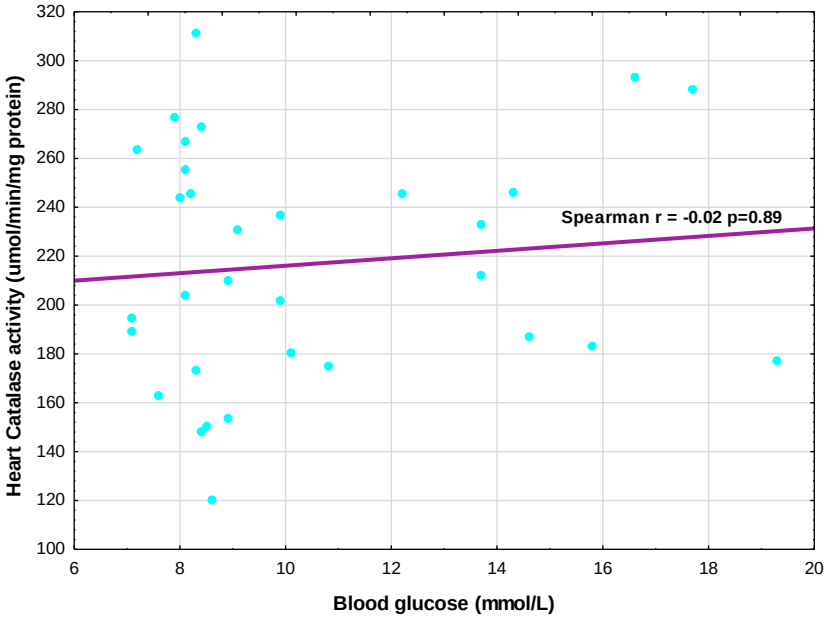

Figure 3.6.5.2 **No correlation of catalase activity in the heart tissue with blood glucose concentrations.** Spearman's correlation coefficient r = -0.02, p=0.89.

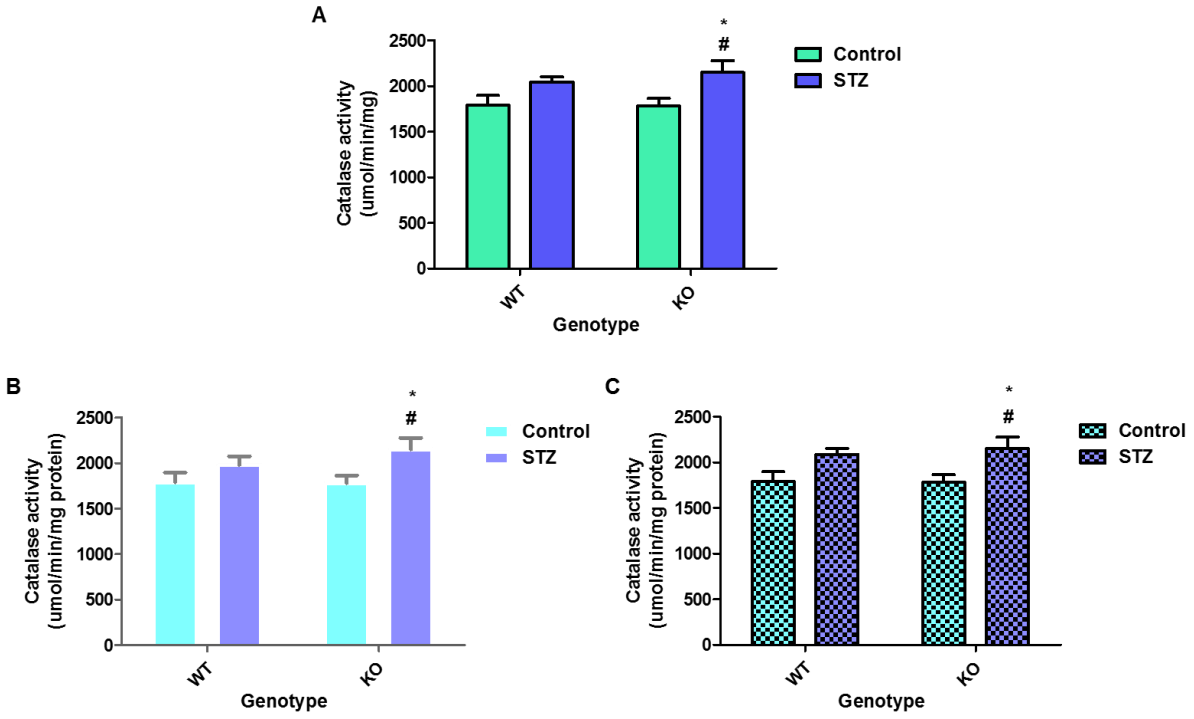

Figure 3.6.5.3 **Catalase activity of the liver: A (combined data), B (WT STZ responders), C (WT STZ non-responders).** Data presented as mean ± SEM, n=8. WT STZ responders n=3 (B), WT STZ non-responders n=5, (C).*p<0.05 vs. WT control, #p<0.05 vs. TKTL1-KO control.

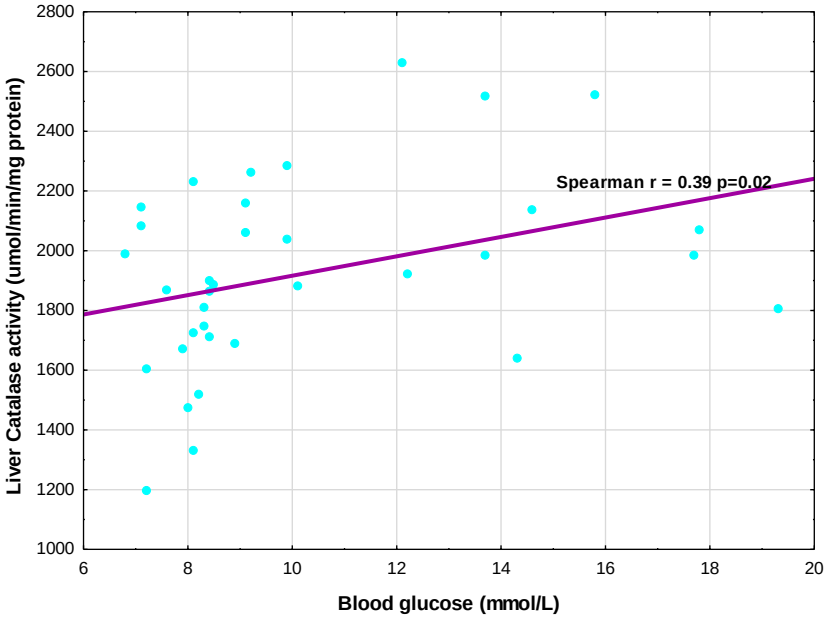

Figure 3.6.5.4 **Positive correlation between hepatic catalase activity and blood glucose concentrations.** Spearman's correlation coefficient r = 0.39, p=0.02.

3.6.6 FRAP measurements in blood, heart and liver samples

We measured FRAP as an indicator of single electron transfer anti-oxidants. No significant differences were noted in the blood (Figure 3.6.6.1) and heart (Figure 3.6.6.2). FRAP concentrations were, however, significantly decreased in STZ-treated TKTL1-KO liver tissue ($p<0.05$ vs. TKTL1-KO control, Figure 3.6.6.3). Furthermore, liver FRAP showed a strong negative correlation with blood glucose levels when assessing all data points ($r=0.45$, $p<0.01$, Figure 3.6.6.6). WT animals did not display this correlation. However, TKTL1-KO animals showed a strong correlation ($r=-0.54$, $p=0.02$, data not shown, refer Appendix B for statistical table).

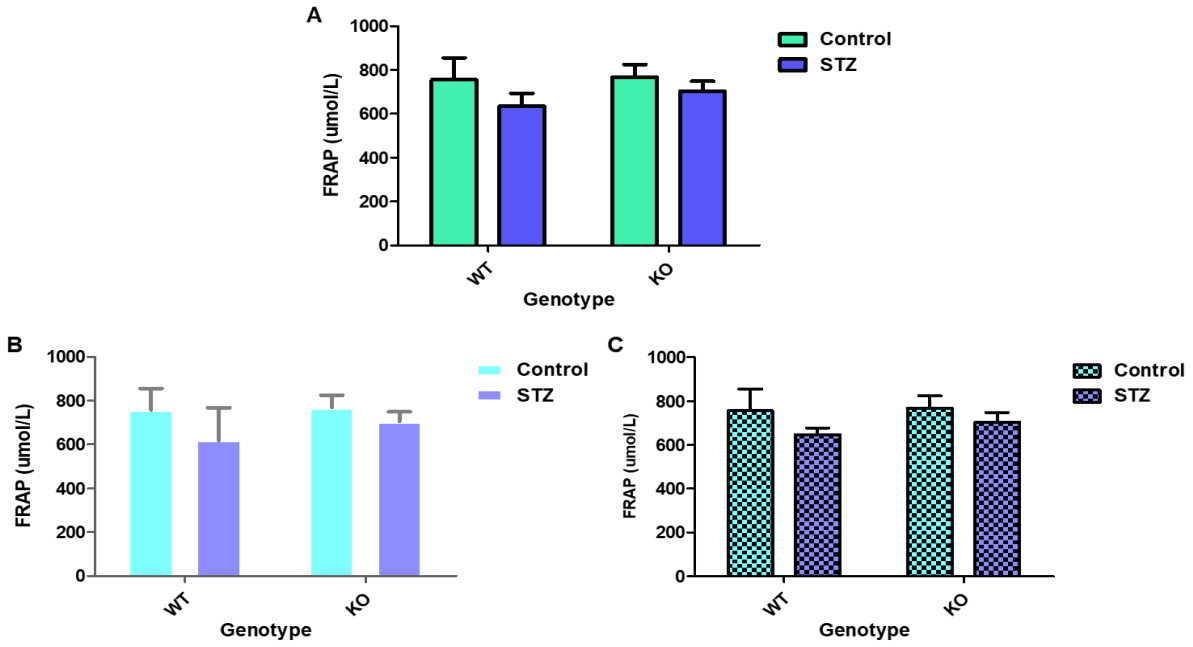

Figure 3.6.6.1 **FRAP in circulation: A (combined data), B (WT STZ responders), C (WT STZ non-responders).** Data presented as mean ± SEM, n=10. WT STZ responders n=4 (B), WT STZ non-responders n=6, (C).

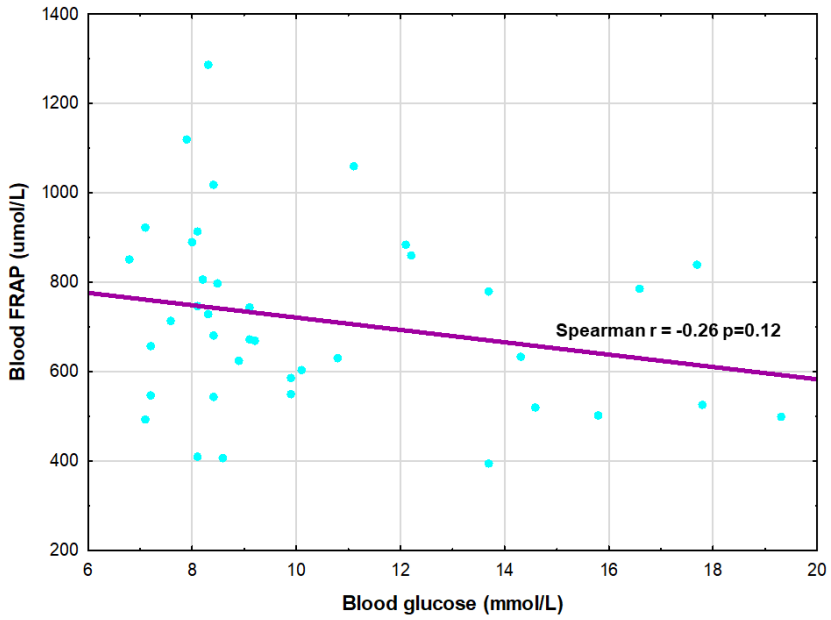

Figure 3.6.6.2 **Non-significant negative correlation between systemic FRAP levels and blood glucose concentrations.** Spearman's correlation coefficient r = -0.26, p=0.12.

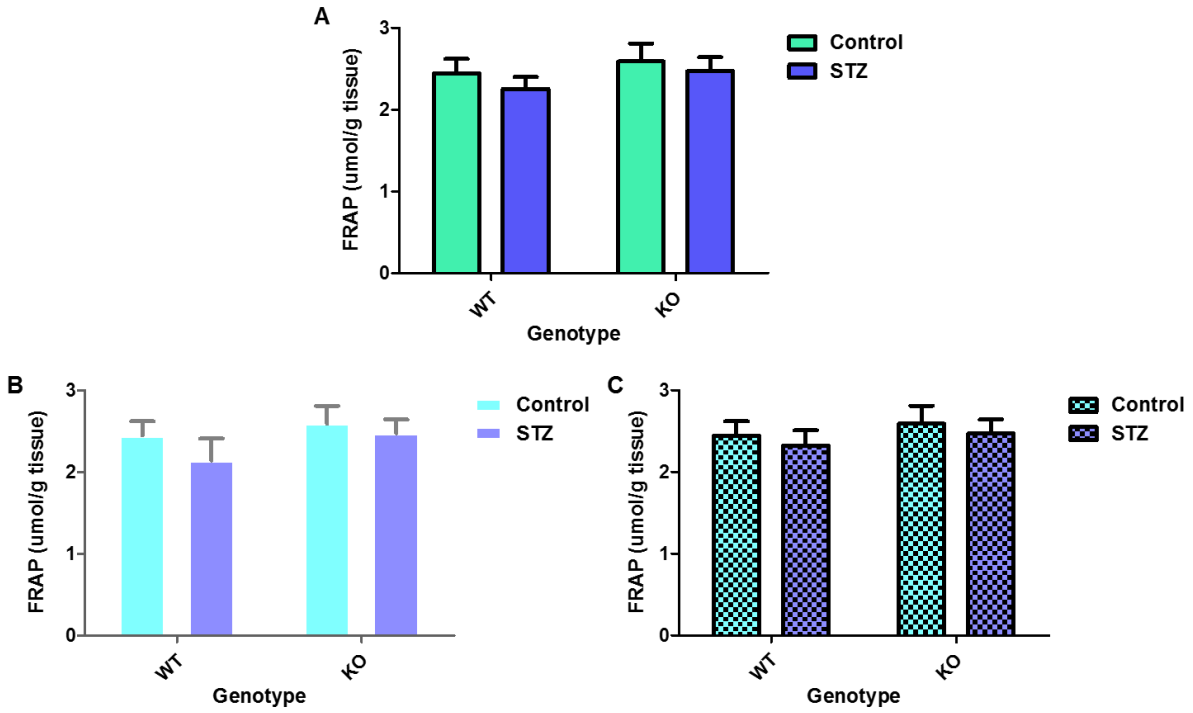

Figure 3.6.6.3 **FRAP in the heart: A (combined data), B (WT STZ responders), C (WT STZ non-responders).** Data presented as mean ± SEM, n=8. WT STZ responders n=3 (B), WT STZ non-responders n=5, (C).

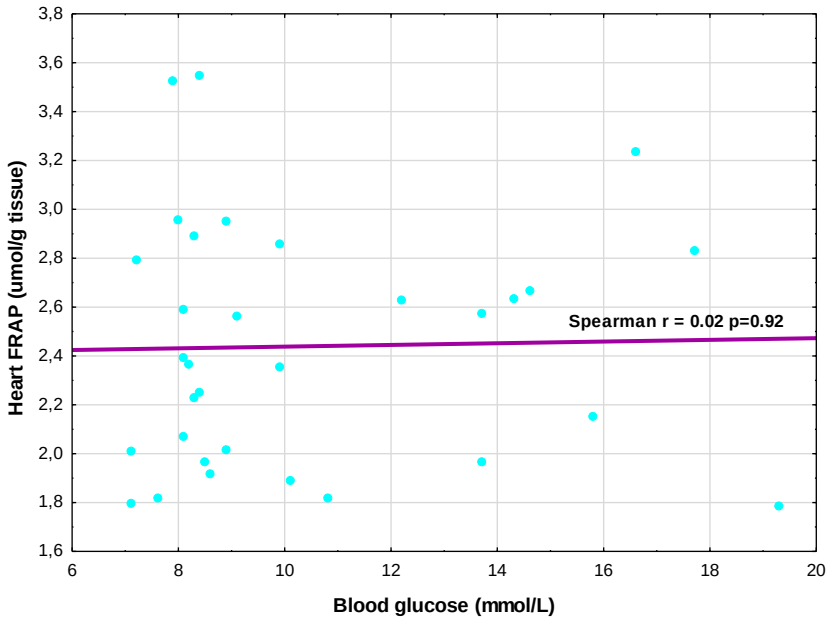

Figure 3.6.6.4 **No correlation between FRAP in the heart tissue and blood glucose concentrations.** Spearman's correlation coefficient r = 0.02, p=0.92.

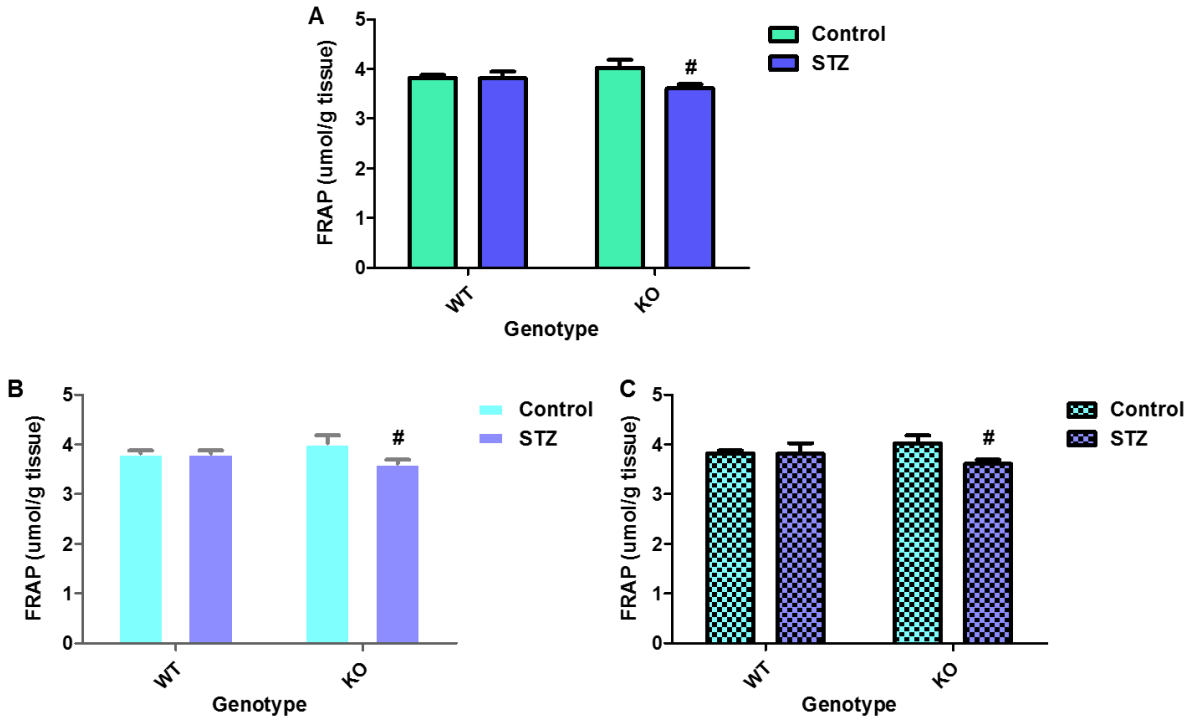

Figure 3.6.6.5 **FRAP in the liver: A (combined data), B (WT STZ responders), C (WT STZ non-responders).** Data presented as mean ± SEM, n=8. WT STZ responders n=3 (B), WT STZ non-responders n=5, (C). #p<0.05 vs. TKTL1-KO control.

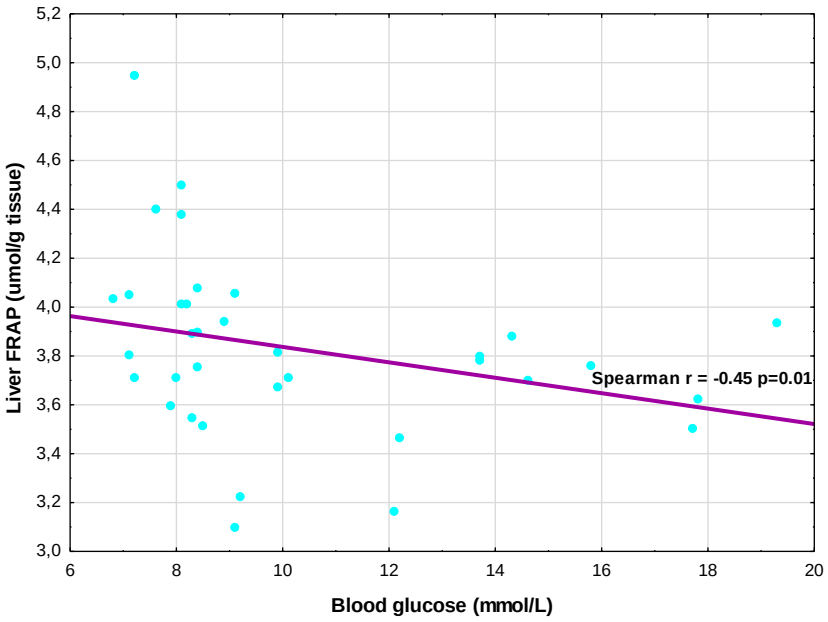

Figure 3.6.6.6 **Significant negative correlation between hepatic FRAP levels and blood glucose concentrations.** Spearman's correlation coefficient r = -0.45, p=0.01.

3.6.7 ORAC quantification in heart and liver samples

ORAC is an indicator of total anti-oxidant capacity and is measured in Trolox (anti-oxidant) equivalents. However, it was not significantly altered in circulation (Figure 3.6.7.1) or in the heart (Figure 3.6.7.2). ORAC of the TKTL1-KO control group was significantly higher in the liver versus the WT control ($p<0.01$) (Figure 3.6.7.3).

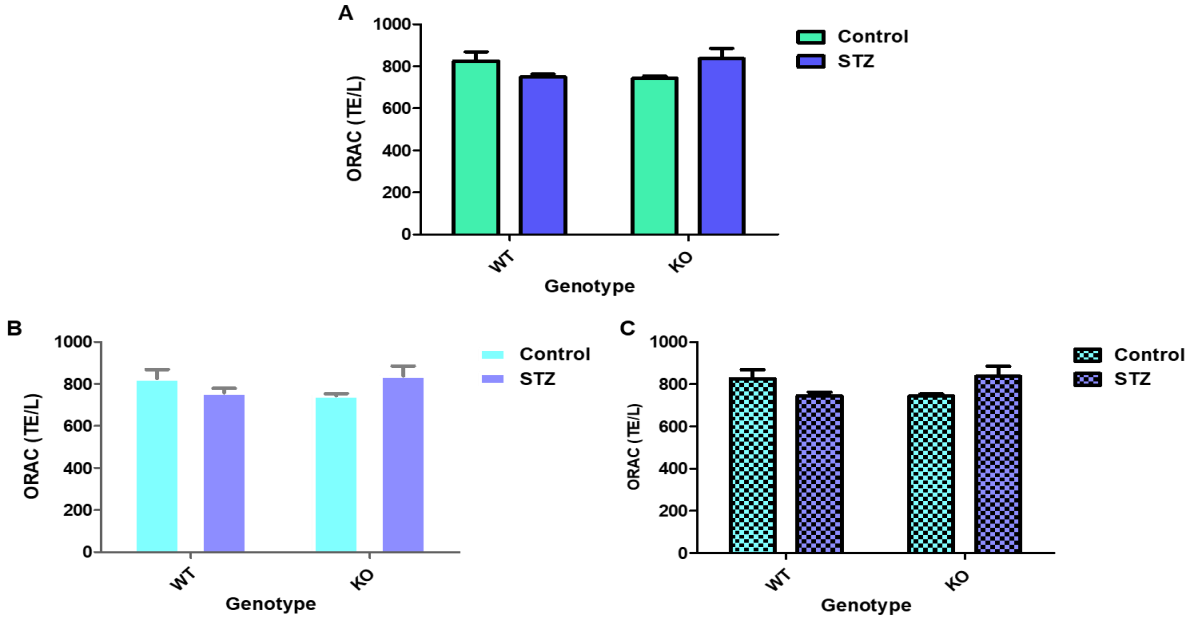

Figure 3.6.7.1 **ORAC in circulation: A (combined data), B (WT STZ responders), C (WT STZ non-responders).** Data presented as mean ± SEM, n=10. WT STZ responders n=4 (B), WT STZ non-responders n=6, (C).

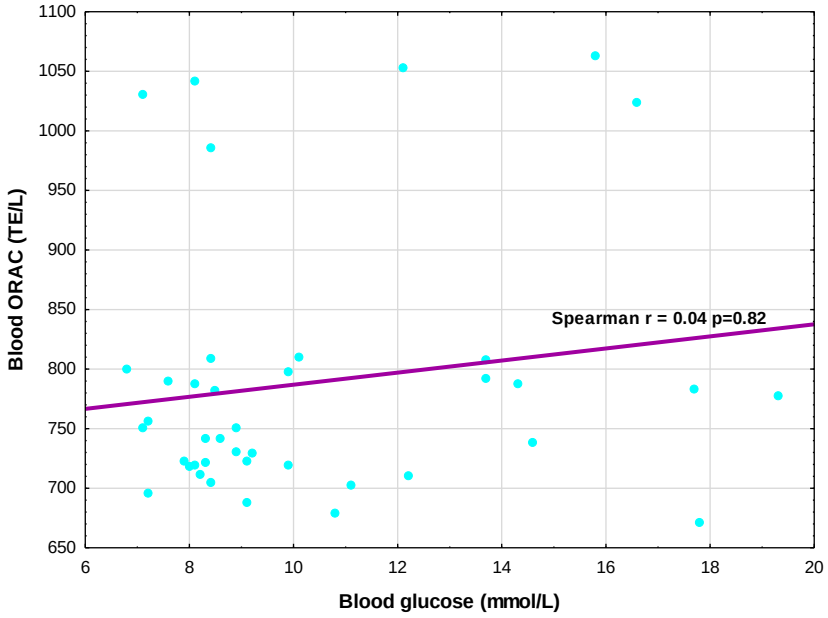

Figure 3.6.7.2 **No correlation between systemic ORAC and blood glucose concentrations.** Spearman's correlation coefficient r = 0.04, p=0.82.

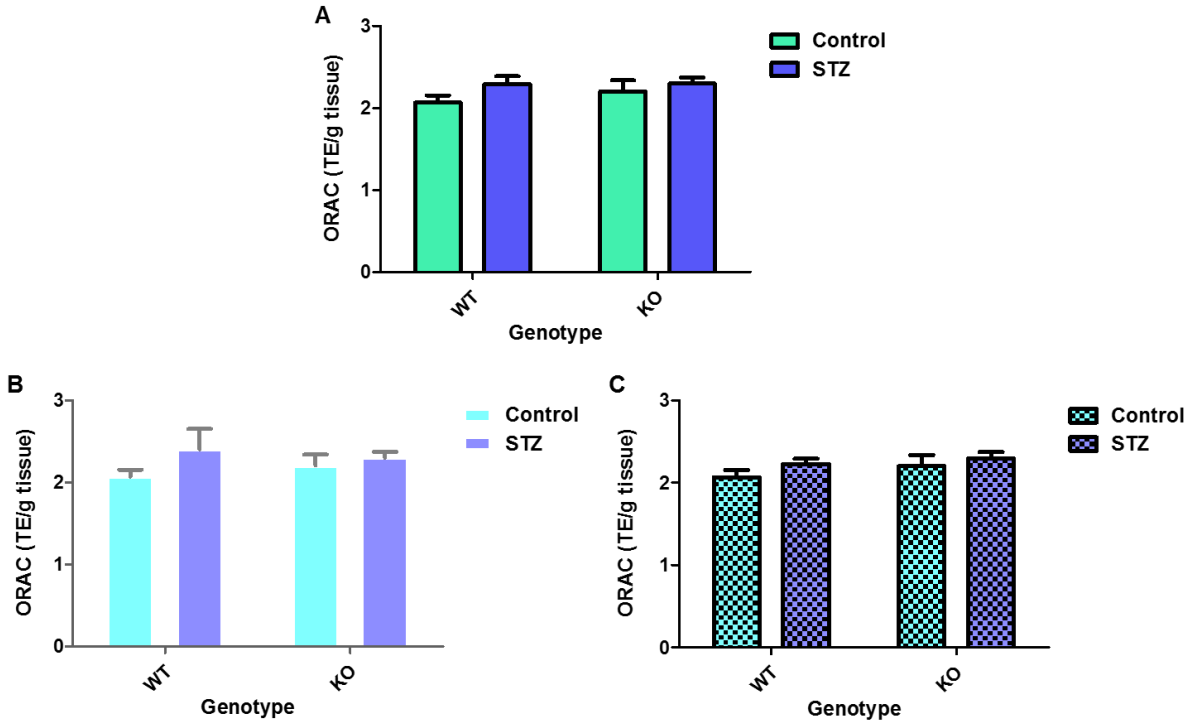

Figure 3.6.7.3 **ORAC in the heart: A (combined data), B (WT STZ responders), C (WT STZ non-responders).** Data presented as mean ± SEM, n=8. WT STZ responders n=3 (B), WT STZ non-responders n=5, (C).

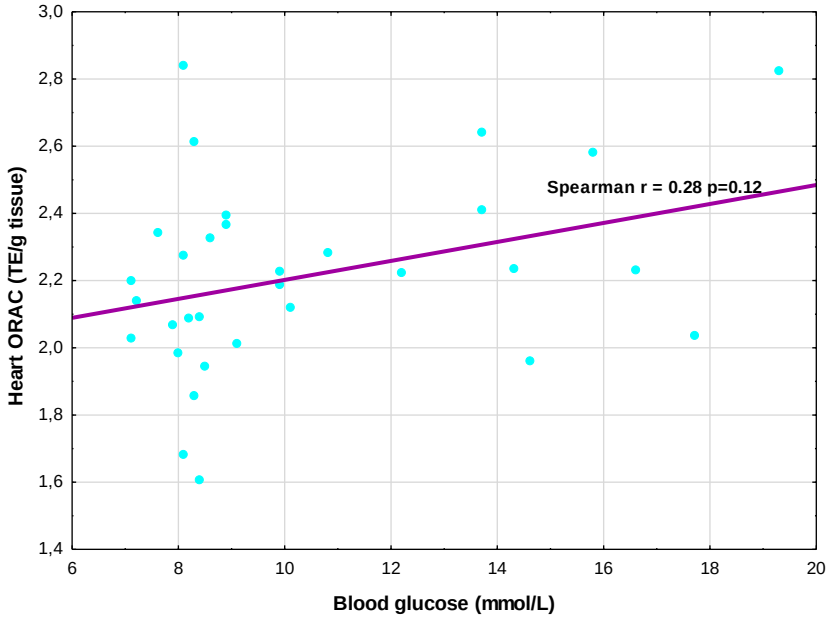

Figure 3.6.7.4 **Non-significant positive correlation between cardiac ORAC and blood glucose concentrations.** Spearman's correlation coefficient r = 0.28, p=0.12.

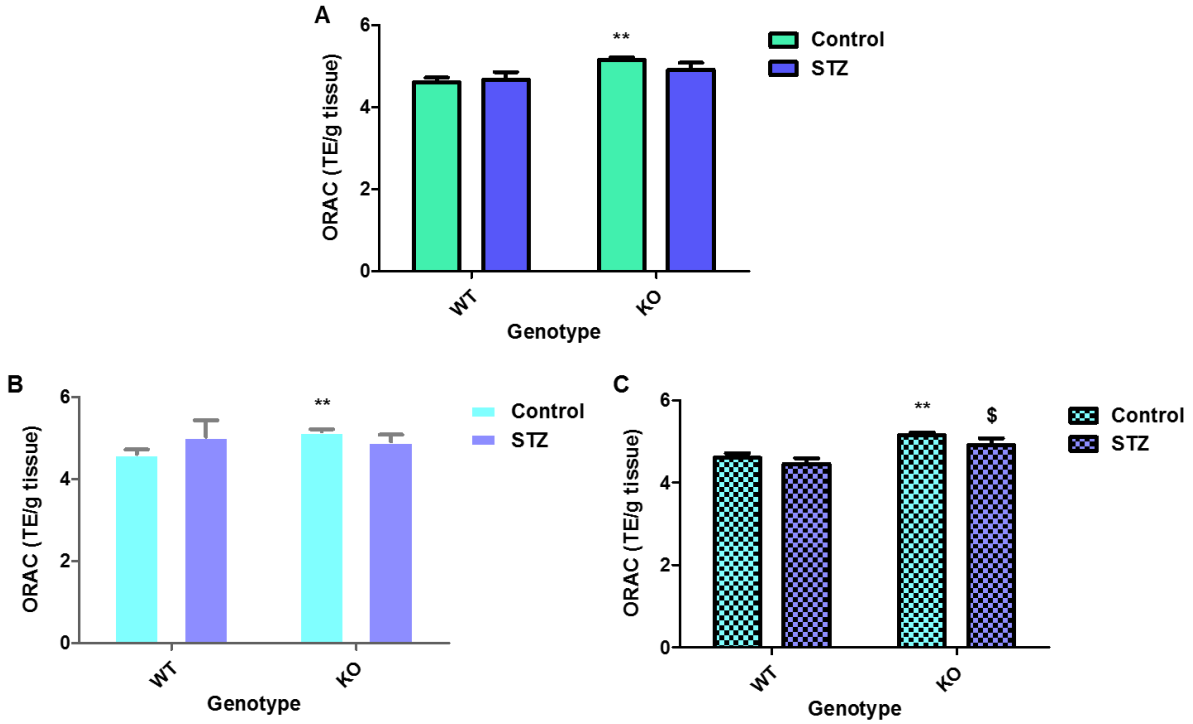

Figure 3.6.7.5 **ORAC in the liver: A (combined data), B (WT STZ responders), C (WT STZ non-responders).** Data presented as mean ± SEM, n=8. WT STZ responders n=3 (B), WT STZ non-responders n=5, (C). **p<0.01 vs. WT control, $p<0.05 vs. WT STZ.

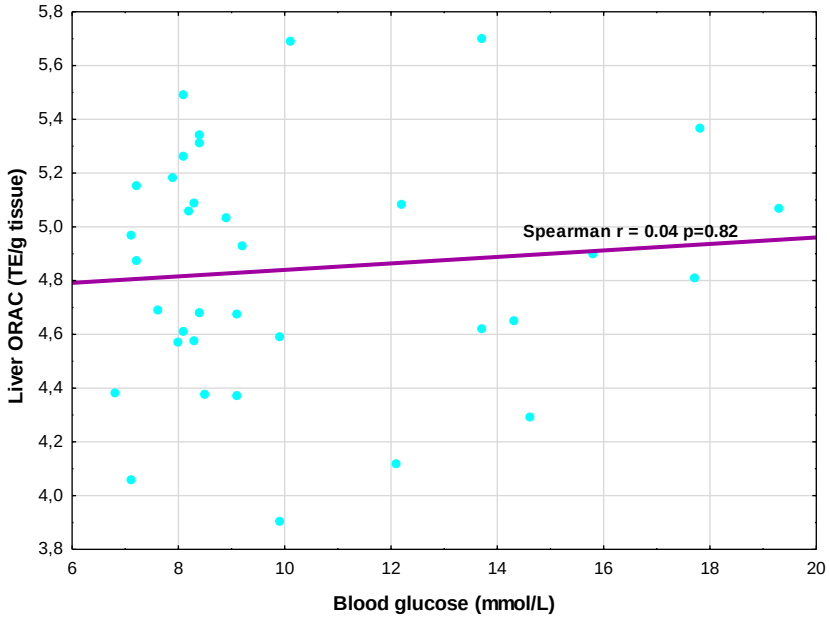

Figure 3.6.7.6 **No correlation between hepatic ORAC and blood glucose concentrations.** Spearman's correlation coefficient r = 0.04, p=0.82.

3.6.8 The glutathione system

The glutathione replenishment system is an important contributor to anti-oxidant capacity. We evaluated glutathione in its reduced (GSH) and oxidized (GSSG) forms, and also the ratio (GSH:GSSG). GSH was not significantly altered in the blood, heart, or liver. The GSH:GSSG ratio of hepatic tissue was decreased in the TKTL1-KO STZ group ($p<0.05$ vs. TKTL1-KO control, Figure 3.6.8.13). The liver GSH:GSSG ratio was also negatively correlated with blood glucose levels ($r=-0.36$, $p=0.03$, Figure 3.6.8.1).

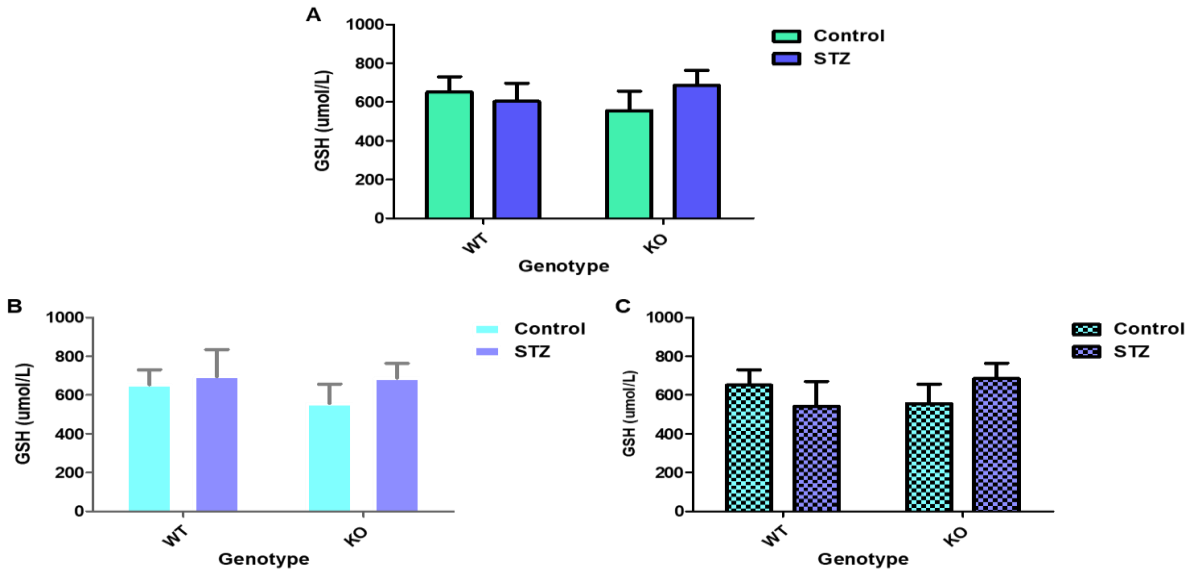

Figure 3.6.8.1 **GSH in circulation: A (combined data), B (WT STZ responders), C (WT STZ non-responders).** Data presented as mean ± SEM, n=10. WT STZ responders n=4 (B), WT STZ non-responders n=6, (C).

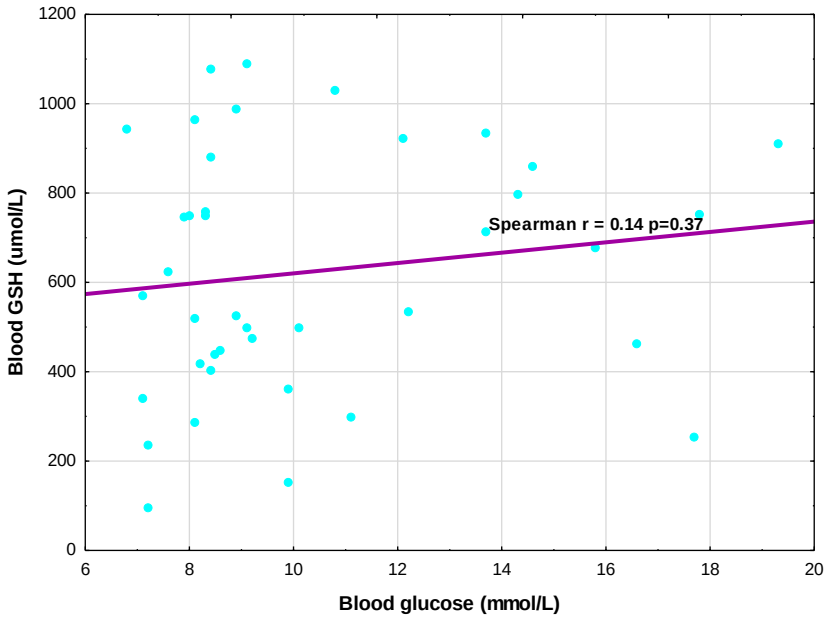

Figure 3.6.8.2 **No correlation between GSH in the blood and blood glucose concentrations.** Spearman's correlation coefficient r = 0.14, p=0.37.

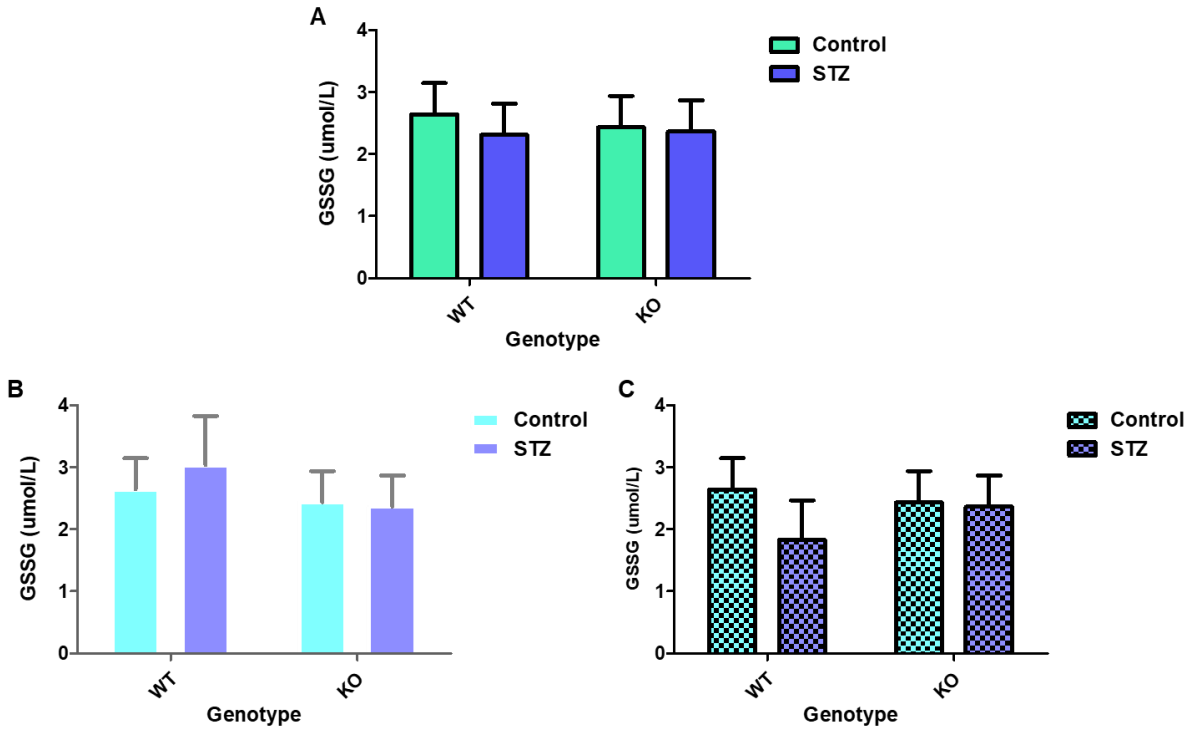

Figure 3.6.8.3 **GSSG in circulation: A (combined data), B (WT STZ responders), C (WT STZ non-responders).** Data presented as mean ± SEM, n=10. WT STZ responders n=4 (B), WT STZ non-responders n=6, (C).

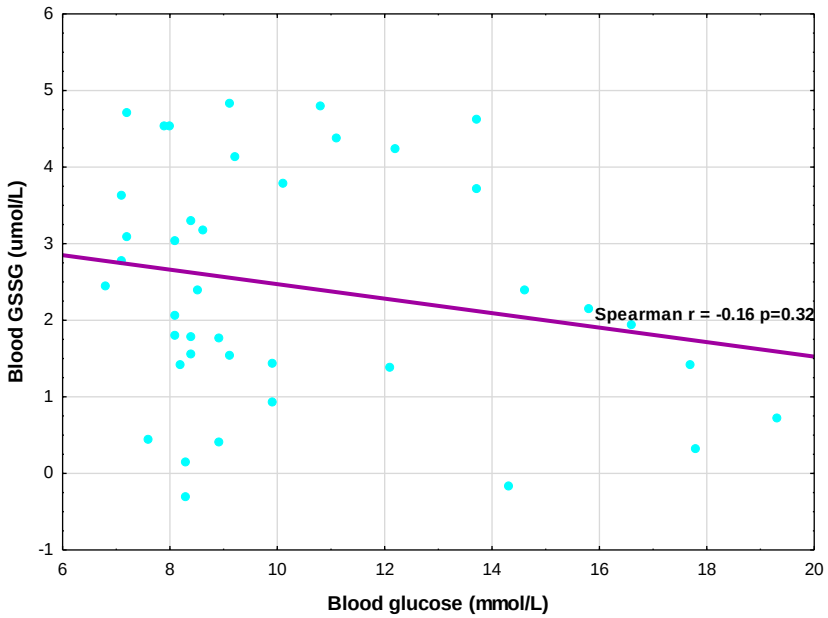

Figure 3.6.8.4 **No correlation between GSSG in the blood and blood glucose concentrations.** Spearman's correlation coefficient r = -0.16, p=0.32.

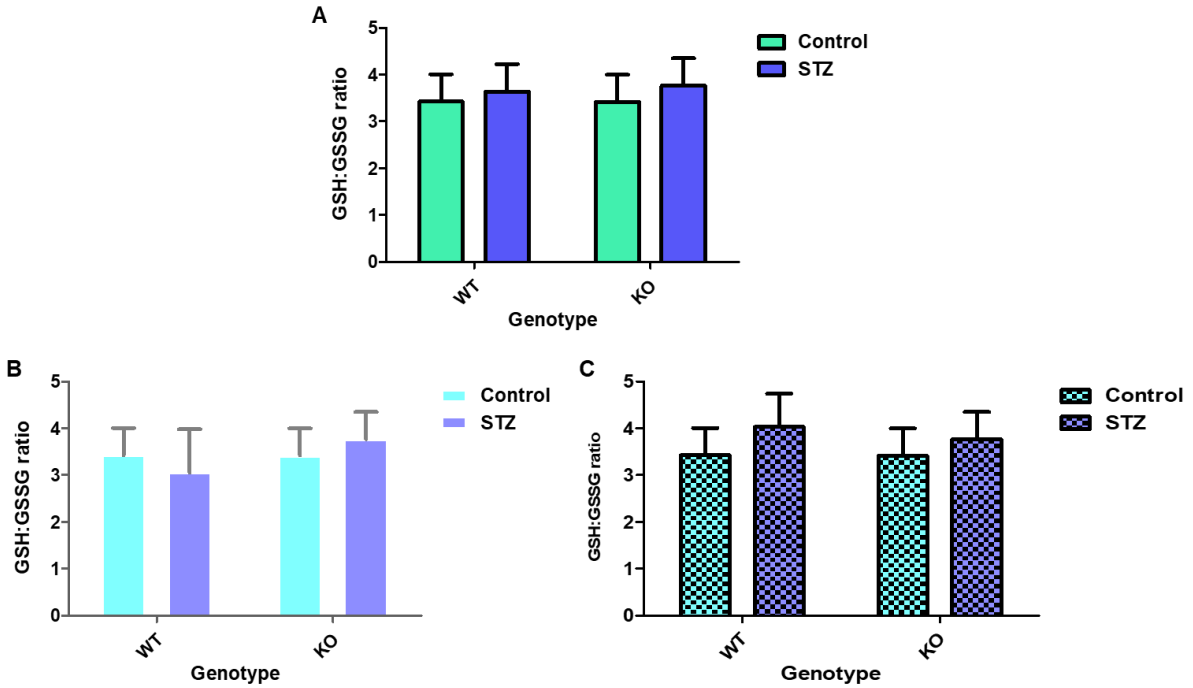

Figure 3.6.8.5 **GSH:GSSG in circulation: A (combined data), B (WT STZ responders), C (WT STZ non-responders).** Data presented as mean ± SEM, n=10. WT STZ responders n=4 (B), WT STZ non-responders n=6, (C).

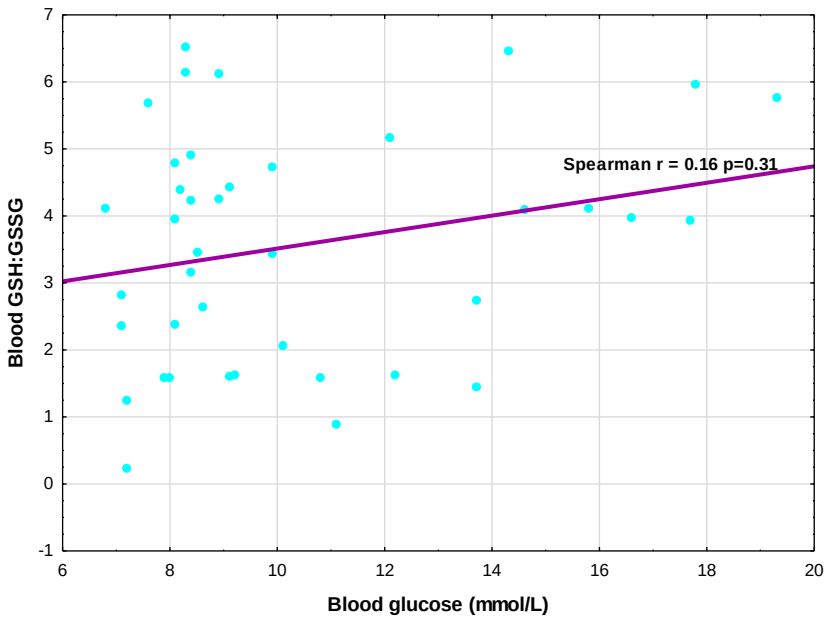

Figure 3.6.8.6 **No correlation between the blood GSH:GSSG and blood glucose concentrations.** Spearman's correlation coefficient r = 0.16, p=0.31.

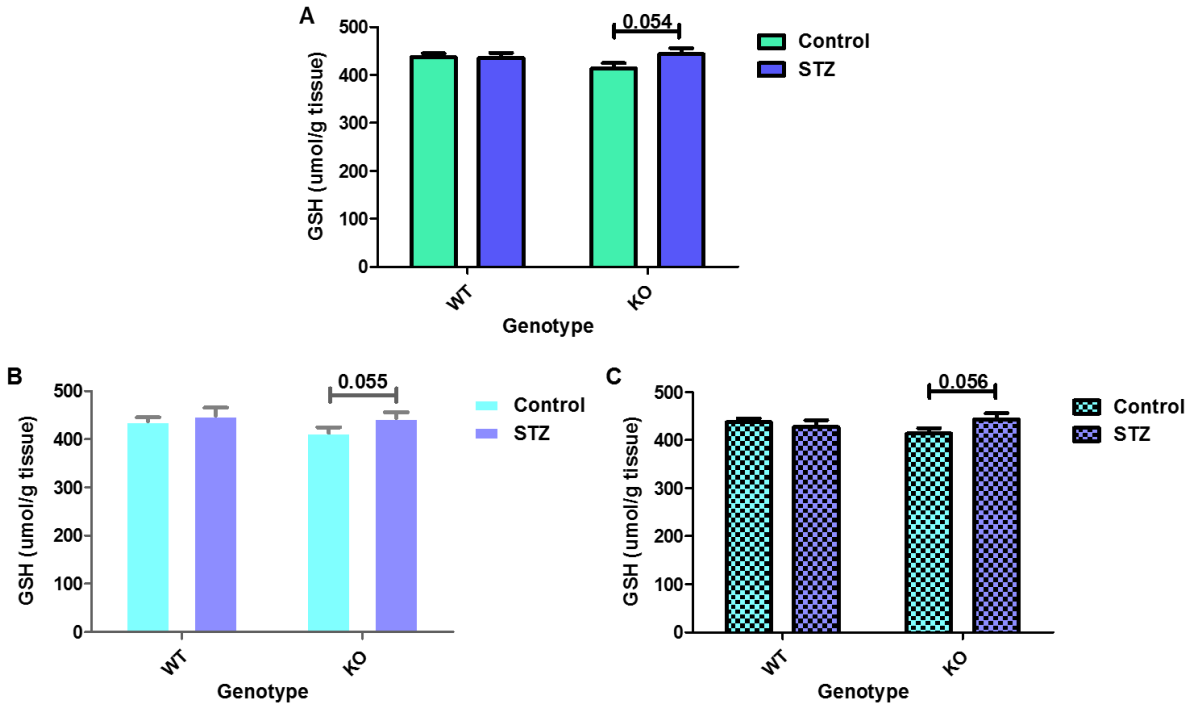

Figure 3.6.8.7 **GSH in the heart: A (combined data), B (WT STZ responders), C (WT STZ non-responders).** Data presented as mean ± SEM, n=8. WT STZ responders n=3 (B), WT STZ non-responders n=5, (C).

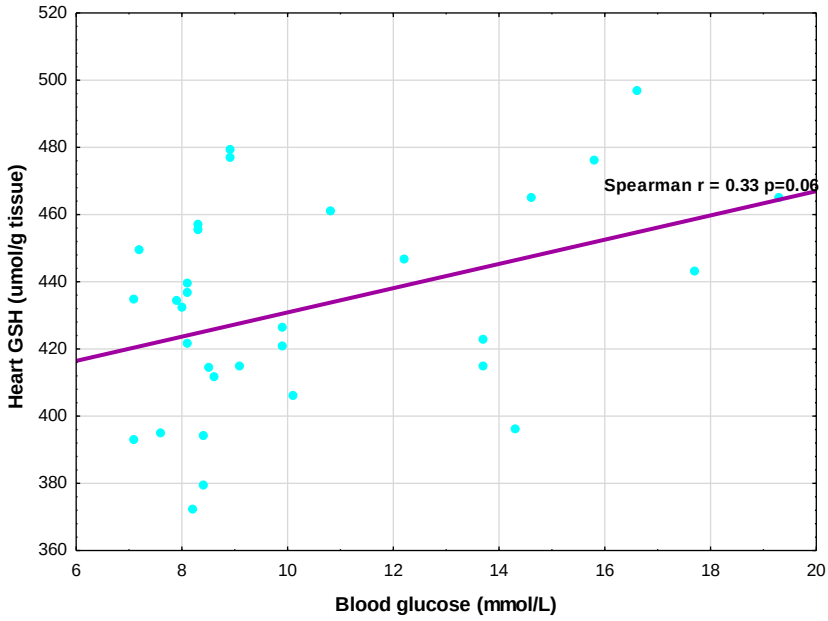

Figure 3.6.8.8 **Non-significant positive correlation between GSH in heart tissue and blood glucose concentrations.** Spearman's correlation coefficient r = 0.33, p=0.06.

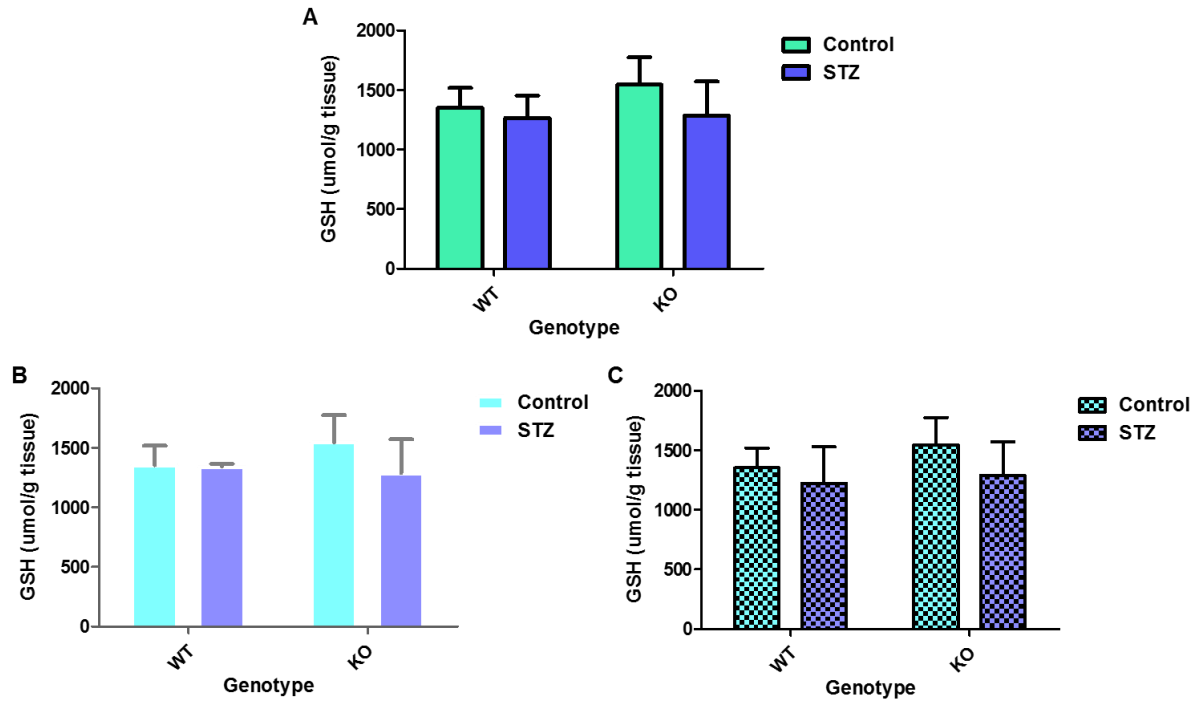

Figure 3.6.8.9 **GSH in the liver: A (combined data), B (WT STZ responders), C (WT STZ non-responders).** Data presented as mean ± SEM, n=8. WT STZ responders n=3 (B), WT STZ non-responders n=5, (C).

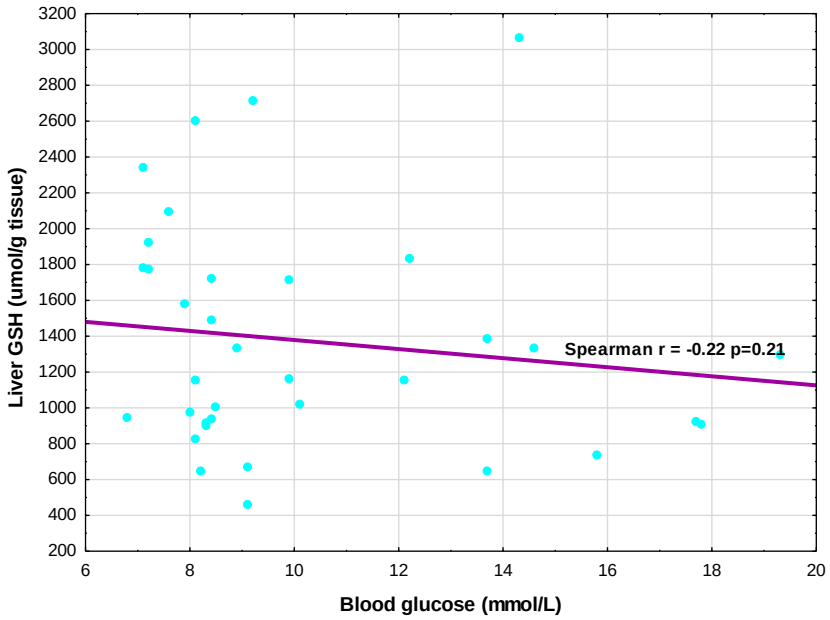

Figure 3.6.8.10 **No correlation between GSH in liver tissue and blood glucose concentrations.** Spearman's correlation coefficient r = -0.22, p=0.21.

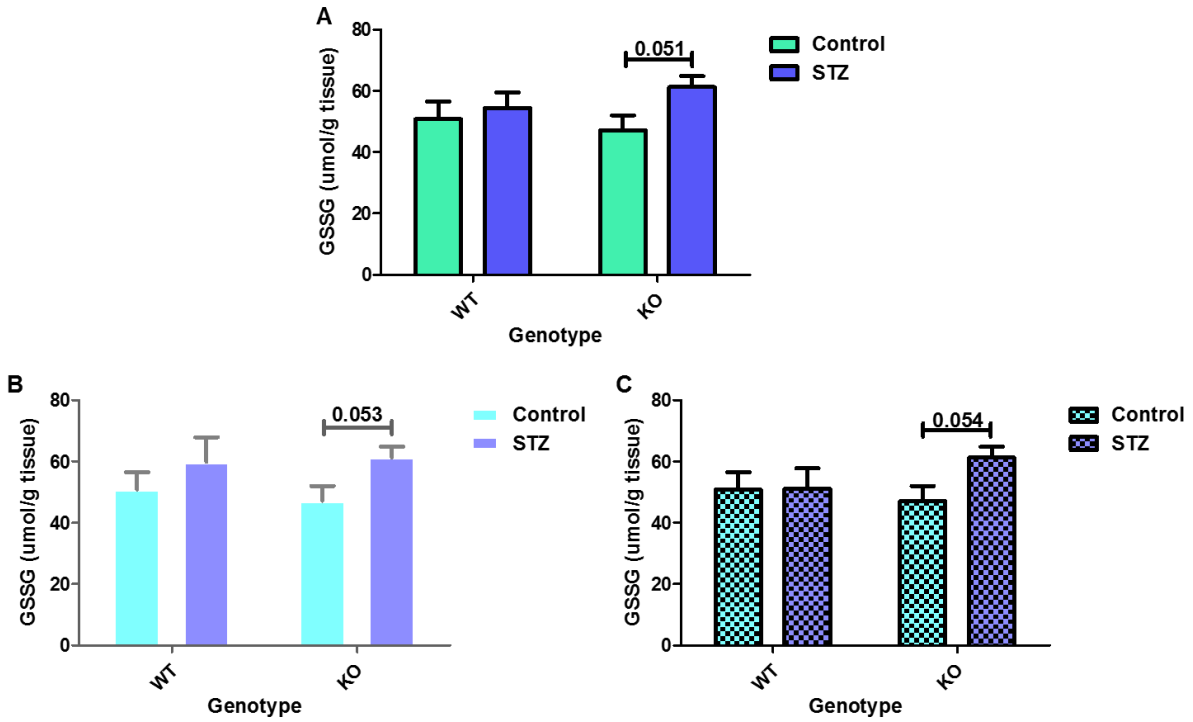

Figure 3.6.8.11 **GSSG in the liver: A (combined data), B (WT STZ responders), C (WT STZ non-responders).** Data presented as mean ± SEM, n=8. WT STZ responders n=3 (B), WT STZ non-responders n=5, (C).

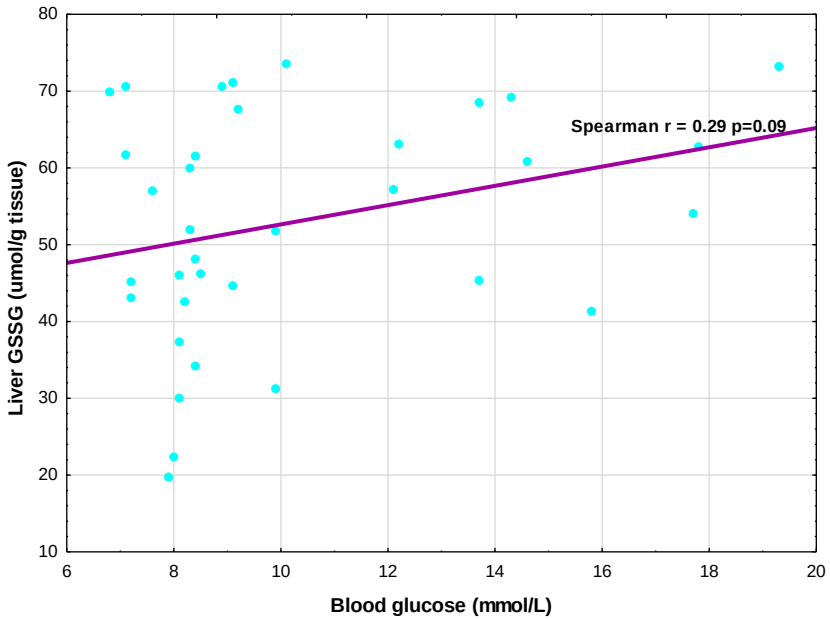

Figure 3.6.8.12 **Non-significant positive correlation between GSSG in liver tissue and blood glucose concentrations.** Spearman's correlation coefficient r = 0.29, p=0.09.

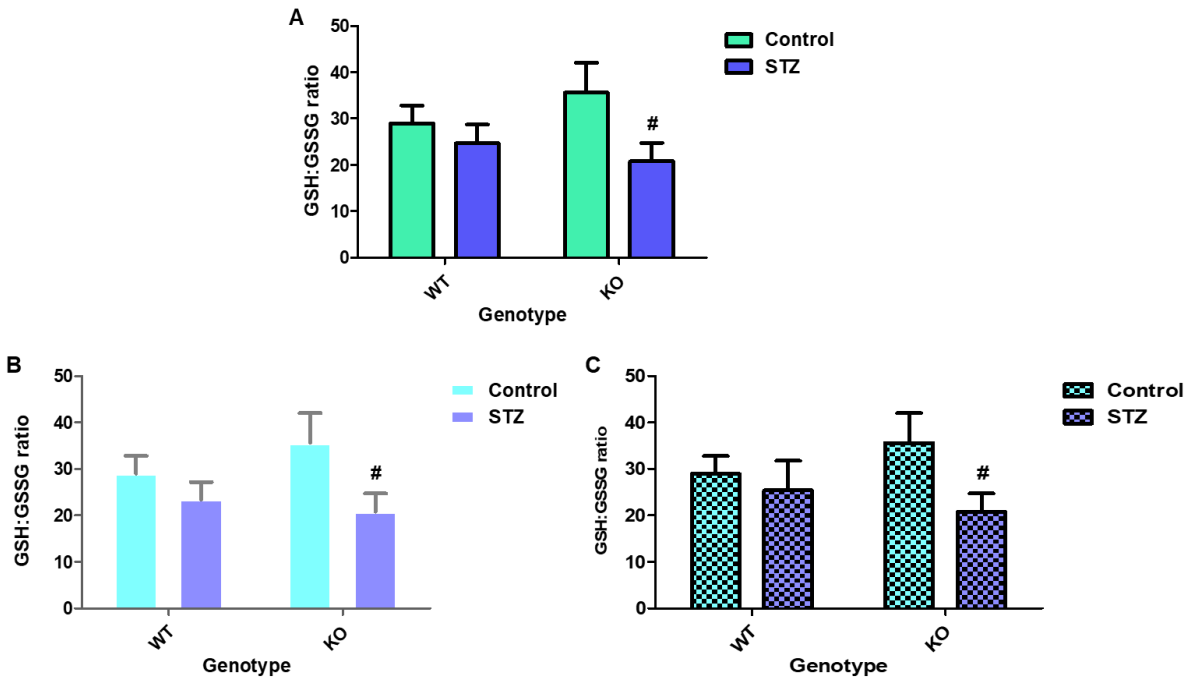

Figure 3.6.8.13 **GSH:GSSG in the liver: A (combined data), B (WT STZ responders), C (WT STZ non-responders).** Data presented as mean ± SEM, n=8. WT STZ responders n=3 (B), WT STZ non-responders n=5, (C). #p<0.05 vs TKTL1-KO control.

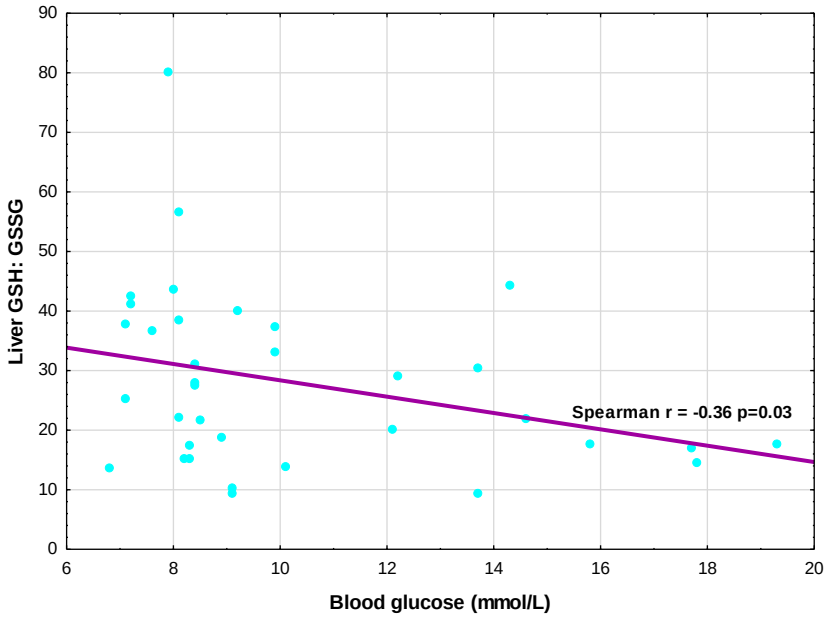

Figure 3.6.8.14 **Significant negative correlation between GSH:GSSG in liver tissue and blood glucose concentrations.** Spearman's correlation coefficient r = -0.36, p=0.03.

3.7 H&E staining of heart and liver sections

Subsequent to the evaluation of oxidative stress, we aimed to acquire ultrastructural data of heart and liver samples by H&E staining. Heart sections did not show discernable differences between groups (Figure 3.7.1). In liver tissue (Figure 3.7.2), STZ treated groups showed clear deposits most likely to be glycogen or lipid deposits that seemed to be more pronounced in the TKTL1-KO STZ group (Figure 3.7.2E).

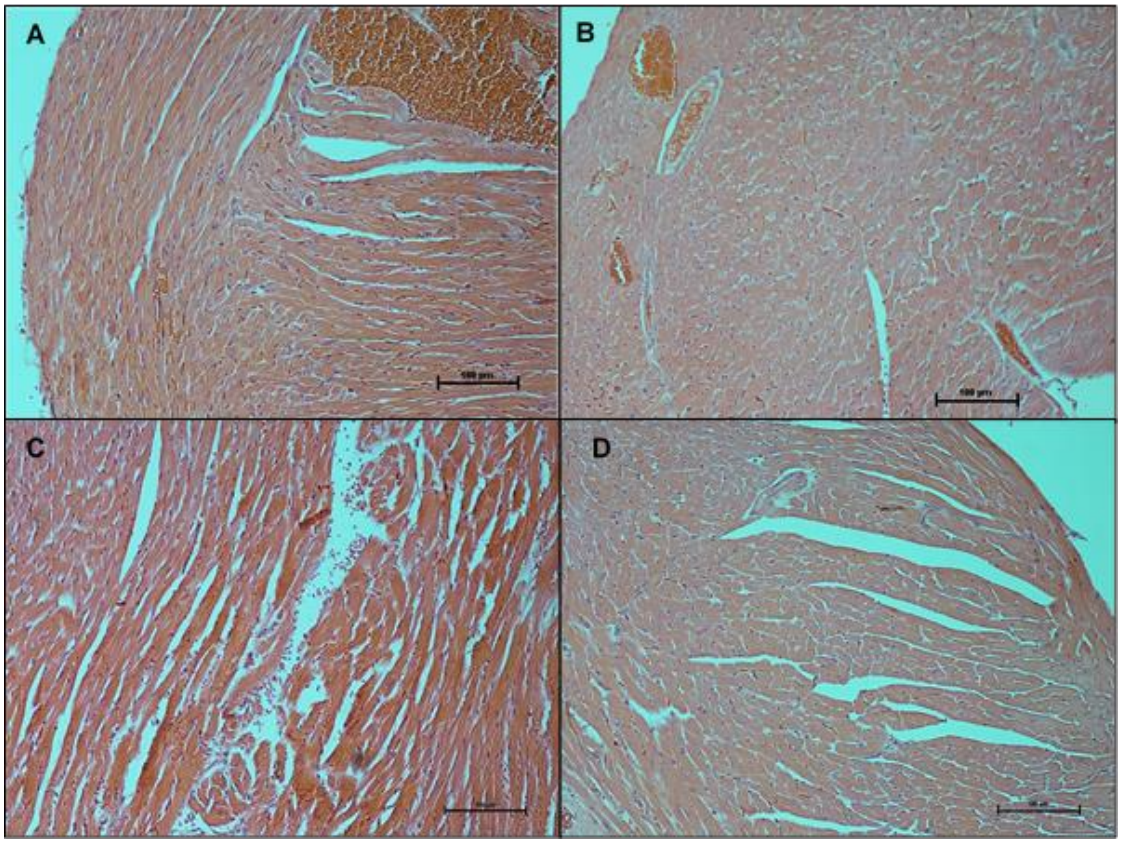

Figure 3.7.1 **H&E stain of heart tissue 20X magnification (n=2)**. None of the groups displayed notable ultrastructural differences. Scale bar denotes 100 µm. **A**: WT control, **B**: WT STZ, **C**: TKTL1-KO Control, **D**: TKTL1-KO STZ.

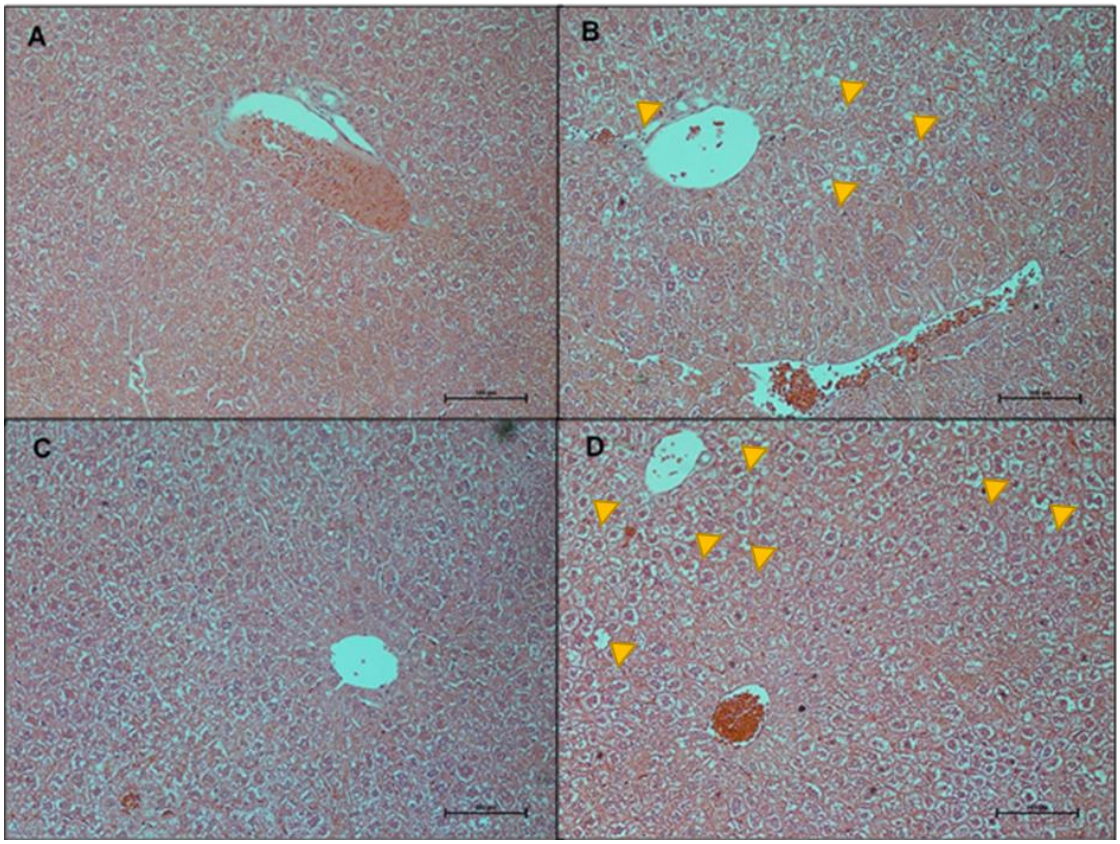

Figure 3.7.2 **H&E stain of liver tissue 20X magnification (n=4)**. Both STZ groups (**B**&**D**) displayed what looked like lipid or glycogen deposits (indicated by yellow arrows). This supports the data from liver weight analysis that indicated increased liver weights in groups treated with STZ especially the TKTL1-KO STZ (**D**) group. Scale bar denotes 100 µm. **A**: WT control, **B**: WT STZ, **C**: TKTL1-KO Control, **D**: TKTL1-KO STZ.

3.8 Sirius red staining of heart and liver sections

We also subjected heart and liver sections to Sirius red staining to discern whether oxidative perturbations possibly manifested in fibrosis. Due to a low number of hearts available for histological processing (Figure 3.7.1), we were unable to quantify the images. However, the two TKTL1-KO groups displayed relatively larger regions of fibrosis (indicated by yellow arrows). Fibrosis in liver samples was quantified as described by Hadi and colleagues (2011) using whole section images (Figure 3.7.2). Tissue processing imperfections, such as folding of sections, were excluded to limit bias. Both STZ groups displayed a reduced amount of fibrotic regions compared to the control groups (fibrotic regions indicated by yellow arrows). Initially, this was thought to be due to increased blood vessels present in the control groups. However, at 20X magnification (Figure 3.7.3) it was clear that fibrous regions were present in areas not localized to blood vessel regions.

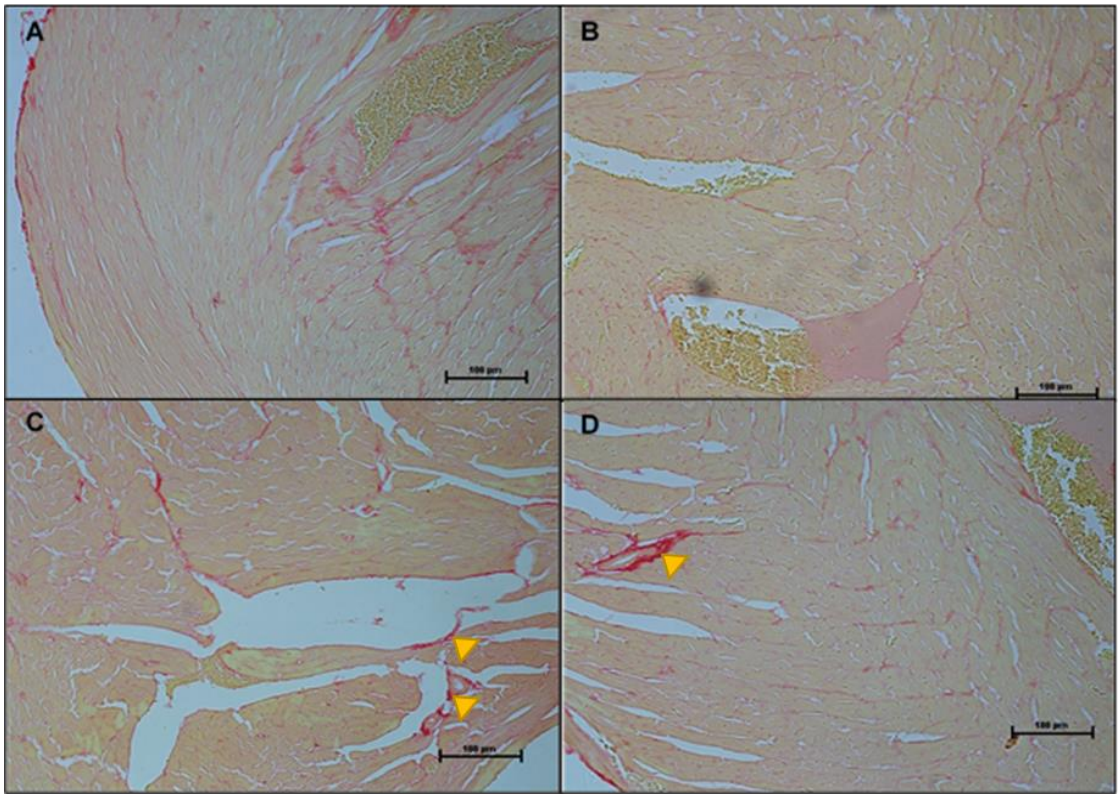

Figure 3.8.1 **Sirius red stain of heart tissue 20X magnification (n=2)**. Scale bar denotes 100 µm, yellow arrows indicate fibrotic regions. **A**: WT control, **B**: WT STZ, **C**: TKTL1-KO Control, **D**: TKTL1-KO STZ.

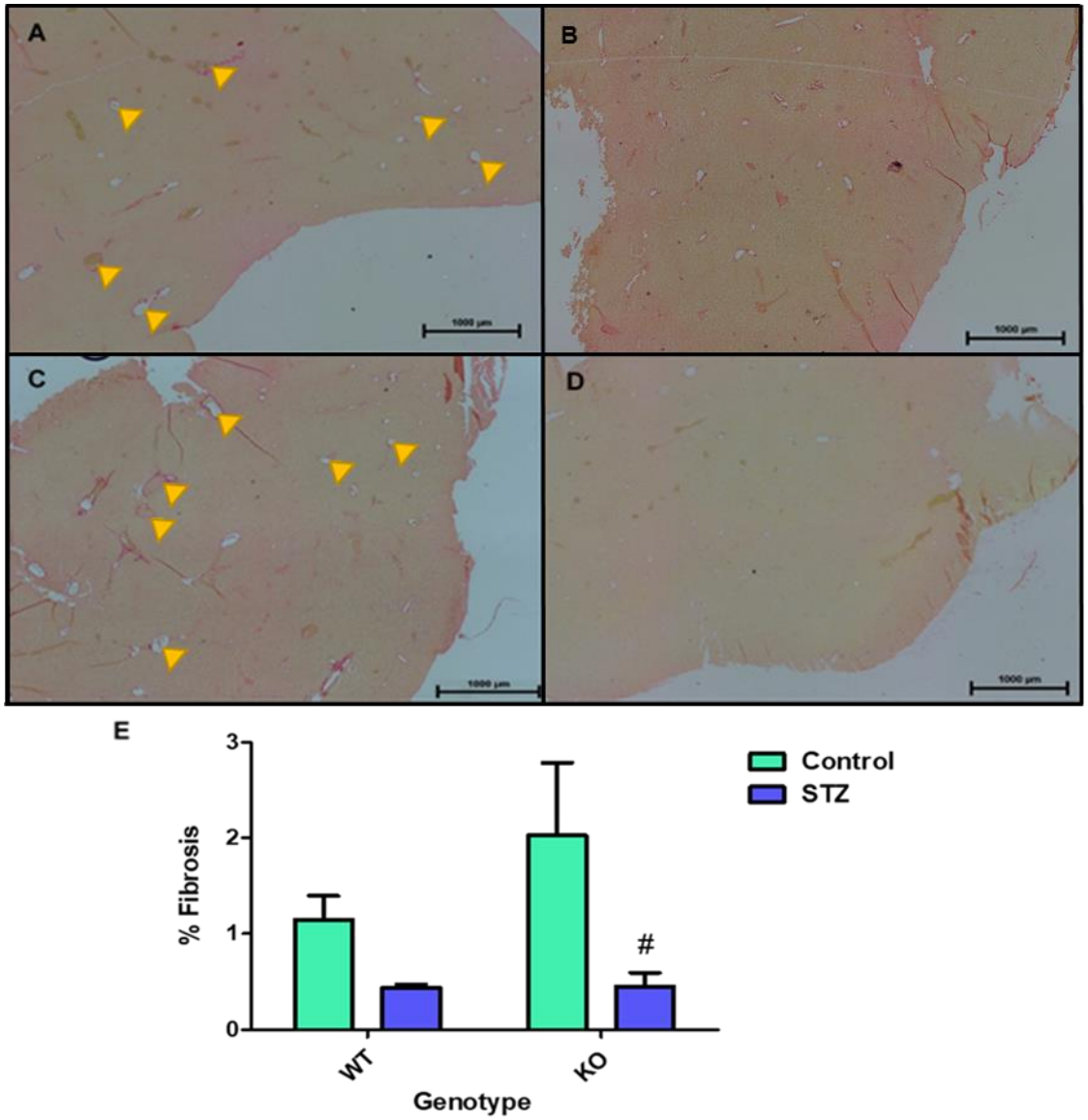

Figure 3.8.2 **Sirius red stain of liver tissue.** (**A**-**E**) Shows Sirius red stain of liver tissue at 4X magnification (n=4). The fibrosis present in both control group is higher than that of the STZ groups with the TKTL1-KO control group displaying a significantly higher presence of fibrosis compared to both the WT and KO control, $p<0.05$. It is worth noting that the control groups display more blood vessels surrounded by connective tissue that is not present to such an extent in the STZ group. Data presented as mean ± SEM, #$p<0.05$ vs. TKTL1-KO control. Scale bar denotes 100 µm, yellow arrows indicate fibrotic regions. **A**: WT control, **B**: WT STZ, **C**: TKTL1-KO Control, **D**: TKTL1-KO STZ.

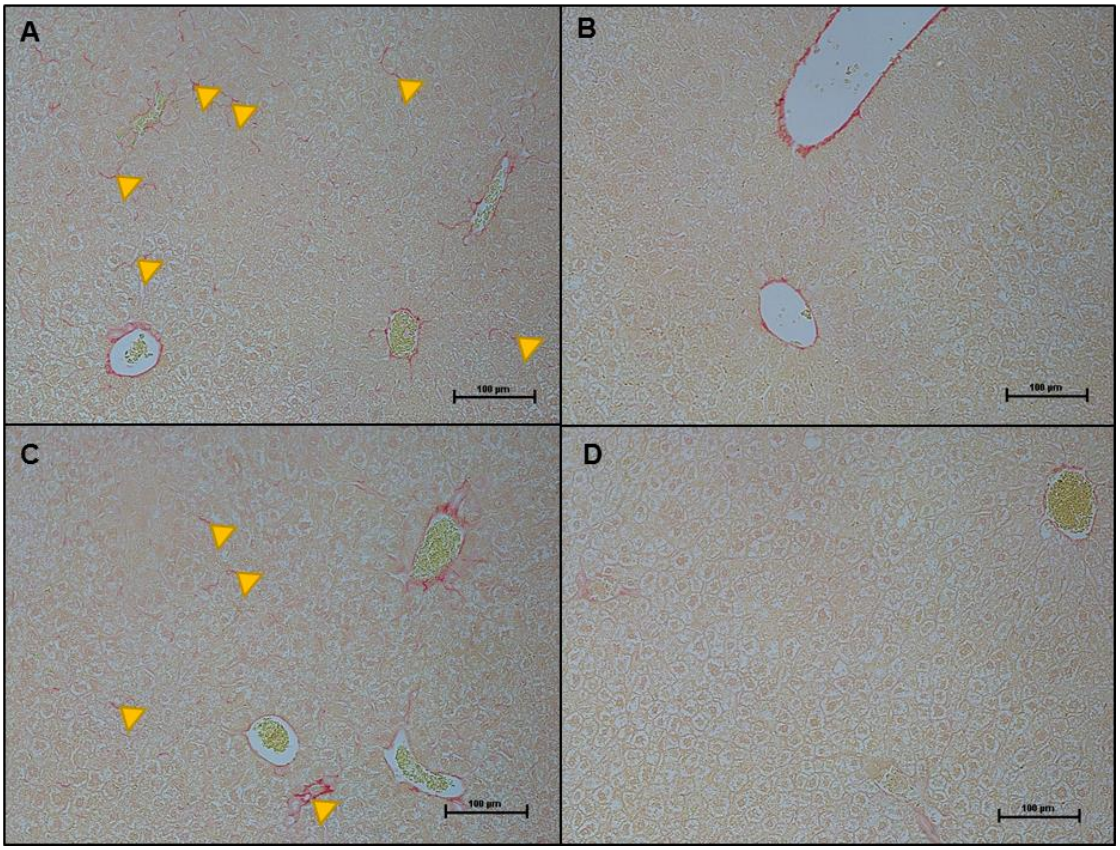

Figure 3.8.3 **Sirius red stain of liver tissue 20X magnification (n=4).** Upon closer inspection of the Sirius red stains of the liver tissue, the control groups display signs of fibrosis that are not limited to only the blood vessel region (indicated by yellow arrows). This is not observed in either of the STZ treated groups. **A**: WT control, **B**: WT STZ, **C**: TKTL1-KO Control, **D**: TKTL1-KO STZ.

3.9 Semi-quantitative protein analysis with Western Blotting

We further aimed to assess apoptosis in heart and liver tissues by evaluating caspase-3 cleavage. Both TKTL1-KO groups exhibited significantly higher levels of cleaved caspase 3 (cCas-3) (17 kDa) in the heart. Although total caspase 3 could not be quantified, we can infer that more apoptosis was present in the TKTL1-KO groups of the heart. No significant differences in cCas-3 were observed in the liver of any of the groups. STZ treated groups displayed a slight and insignificant increase in cCas-3 3 compared to their respective controls.

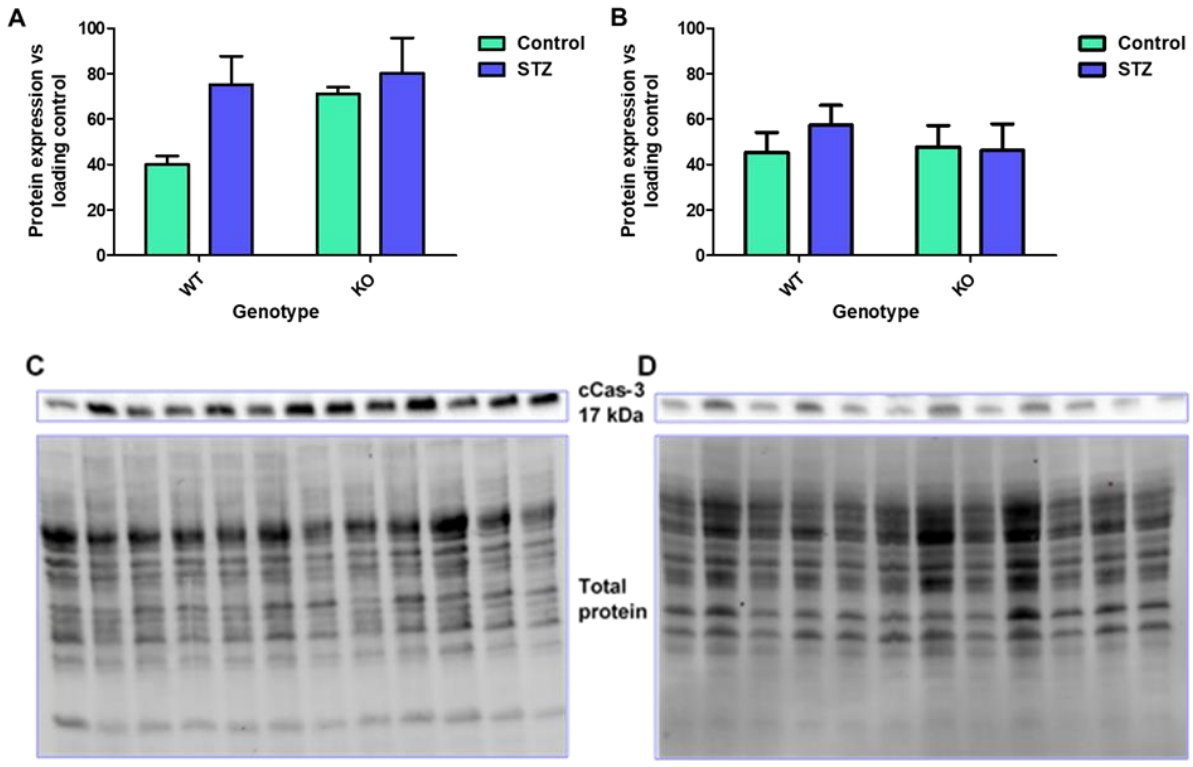

Figure 3.9.1 **Western blot analysis of cleaved Caspase 3 (cCas-3) in the heart (A&C) and liver (B&D).** Data presented as mean ± SEM.

Chapter 4: Discussion

Diabetes is a growing, global concern that has reached a prevalence far beyond the projected statistics. Hyperglycemia is a common denominator of T1DM and T2DM and results in excessive flux through pathways that can elicit damaging outcomes, e.g. oxidative damage and inflammation. This can result in functional consequences at organ level and threaten overall well-being and health. The PPP offers an alternate "safer" route for excess metabolic fuels while also replenishing antioxidant defenses, thus potentially offering value as a novel therapeutic target. As a result, the current study focused on this pathway (and particularly TKTL1) as there are currently no studies – as far as we are aware – focusing on TKTL1 as a therapeutic target for cardio-metabolic diseases. In light of this, the current study evaluated whether TKTL1 can alleviate hyperglycemia-mediated oxidative stress in hepatic and cardiac tissues isolated from STZ-treated mice.

The main findings of this study are: i) TKTL1 knock-out sensitized mice to the development of STZ-induced hyperglycemia; ii) TKTL1-KO mice treated with STZ displayed enlarged livers and kidneys while gastrocnemii weight was reduced; iii) the PPP appear to possess distinct functional roles in the heart and the liver under hyperglycemic conditions, iv) TKTL1 contributed significantly towards total TKT activity in cardiac tissue; and v) while measures of oxidative damage remained relatively unchanged, antioxidant defenses (catalase activity, FRAP levels and the GSH:GSSG ratio) displayed some adaptations in the liver of STZ-treated KO animals.

The protocol of multiple low dose of STZ injection was chosen as it causes inflammation of pancreatic β-cells and insulin deficiency, thereby leading to hyperglycemia and subsequent oxidative damage, both of which were of interest to this study (Furman, 2015). Female mice are known to be resistant towards STZ treatment as confirmed by this study (Friesen *et al*., 2004; Furman, 2015). This may be a result of upregulated antioxidant defenses that protect against STZ insults and/or due to the protective effect of estrogen that prevents inflammation

and also increases insulin sensitivity (Friesen *et al*., 2004; Manrique *et al*., 2012; Shen *et al*., 2014). As female mice did not develop hyperglycemia, we excluded them from subsequent experiments and instead focused on males.

The incidence of hyperglycemia in STZ-treated WT and TKTL1-KO groups were 40% and 90%, respectively. Previous studies utilizing the multiple low-dose STZ injection protocol on C57BL/6 mice reported mixed results regarding the hyperglycemia onset. For example, Hässler and colleagues (2008) found that only 25% of C57BL/6 mice developed hyperglycemia (21 days after injections) whereas Fukudome and colleagues (2008) noted that ~80% of the same strain developed hyperglycemia in a similar period. The protocol selected for this study projected that hyperglycemia would be detectible in ~50% of mice three weeks after injections (Furman, 2015). However, this did not materialize with more than 60% of mice unresponsive by the end of week 4. For this study, a second set of injections was not possible as the risk of mortality in the STZ-treated TKTL1-KO group (presenting with hyperglycemia) was too high. Thus we propose that our STZ model represents an experimental system of moderate hyperglycemia and we expected that associated changes (liver, heart) would therefore not be as pronounced as originally predicted. In support, the STZ treatment protocol was not harsh enough to induce significant damage to macromolecules, i.e. lipid peroxidation, while expression of a downstream marker for apoptosis (caspase 3) was also not significantly different compared to the various controls. However, it can also be interpreted that alterations observed in our model would represent relatively early changes triggered in response to the stimulus and therefore still provide value in terms of deciphering the role of TKTL1 within this context.

The most striking finding of this study is the robust difference between the WT and TKTL1-KO's response to STZ treatment, with the latter developing hyperglycemia at a faster rate and to a greater extent. Thus it supports our premise that TKTL1 offers therapeutic value within the context of diabetes as its lack is linked to hyperglycemia. However, it also raises an unexpected rhetorical question, i.e. how exactly does TKTL1 regulate systemic glucose

levels? We are unable to provide a firm answer at present to this intriguing question but here put forward several proposals, focusing mainly on changes in the liver.

The oxidative stress data generally showed no changes in NOX activity and the lipids remained relatively protected from oxidative damage (CDs and TBARS). It may be useful to investigate other sources of ROS production (e.g. mitochondrial-derived) and assess additional markers of oxidative damage (e.g. protein carbonylation). Our laboratory previously found that different ROS sources (mitochondrial and NOX) may be triggered in response to experimental hyperglycemia and there may be a complex interplay between these processes (Joseph *et al*. 2014; Mapanga *et al*. 2012, 2014). The elevated ROS levels observed in these studies were accompanied by decreased antioxidant system activity and induction of lipid peroxidation and protein carbonylation. By contrast to the current study, glucose levels reported there were considerably higher in *in vitro, ex vivo and in vivo* experimental conditions. For example, Mapanga *et al*. (2012) showed that single high dose STZ injections in rats resulted in mean blood glucose levels exceeding 25 mmol/L compared to ~14.5 mmol/L in our study (in WT responders and KO mice). The severity of hyperglycemia may be an important consideration and, as mentioned above, higher blood glucose levels (and greater hyperglycemia incidence in the WT group), could have translated into more pronounced oxidative stress. Despite this the STZ treatment seemed to elicit mild changes in the liver antioxidant systems of the TKTL1-KO mice. Here we observed increased catalase activity, a decreased GSH:GSSG ratio and lower FRAP levels. These markers also correlated significantly with blood glucose levels. Together these data suggest that the hepatic antioxidant capacity may be de-sensitized, even under the relatively “mild” hyperglycemic conditions in our model. We argue that the fact that this only occurred in the KO group points toward a role for TKTL1 in the maintenance of antioxidant systems. The small alterations in hepatic antioxidant capacity could in turn induce dysregulation of glucose metabolic processes in the liver.

Alternatively, TKTL1 may play a direct inhibitory role in the gluconeogenesis and/or glycogen breakdown pathways to thereby contribute to increased blood glucose levels observed. Although the findings of this study are generally in agreement with this proposal, further studies are required to ascertain which proposal is indeed the correct one.

It is also possible that TKTL1 lack may influence the insulin secretion pathway in pancreatic β–cells, leading to a lower secretion of insulin and hence increased glucose levels. We did unfortunately not assess systemic insulin levels for this project, but such data would be invaluable to help unravel the TKTL1 mystery. Increased oxidative stress in such cells (due to TKTL1 lack) may lead to DNA damage, and AGE formation to uncouple glucose sensing from insulin secretion (reviewed in Cerf, 2013, reviewed in Cichoż-Lach and Michalak, 2014). STZ is a glucose and GlcNAc analog that exerts its cytotoxic effects mainly on pancreatic β-cells (Junod *et al*., 1967). The reason for this specificity is due to GLUT-2 availability on β-cell membranes which provides a shuttle for STZ into such cells (Schnedl *et al*., 1994; Wang and Gleichmann, 1998). Subsequently, the alkylnitroso moiety of STZ directly and indirectly (via generation of ROS and RNS) causes DNA damage which activates PARP to repair the strand breaks (Figure 4.1) (Szabó and Dawson, 1998). According to the suicide theory of PARP activation described by Szabó and Dawson, its activation leads to the depletion of NAD^+ which causes a decrease in glycolysis, TCA cycling, and PPP flux due to insufficient NAD^+ conversion to $NADP^+$. Moreover, PARP has also been link to the recruitment of thymus (T)-cells and monocytes and resultant inflammation and oxidative stress (reviewed in Ba and Garg, 2011). In support, the only previous study that employed the TKTL1-KO mice (in an experimental model of colitis) found that they were more prone to the development of inflammation compared to WT mice (Bentz *et al.*, 2011). Here the colon of TKTL1-KO mice exposed to the colitis-inducing agent presented with a higher histological score (an indication of disease severity) than the WT group receiving the same treatment. Hence we propose that TKTL1 acts as a contributor to TKT activity to promote PPP flux that replenishes antioxidant capacity (Figure 4.1). Moreover, TKTL1 may delay and/or partially prevent the infiltration of

immune cells and subsequent inflammation by augmenting the pancreatic β-cell's antioxidant defense system. These proposals also require further investigation.

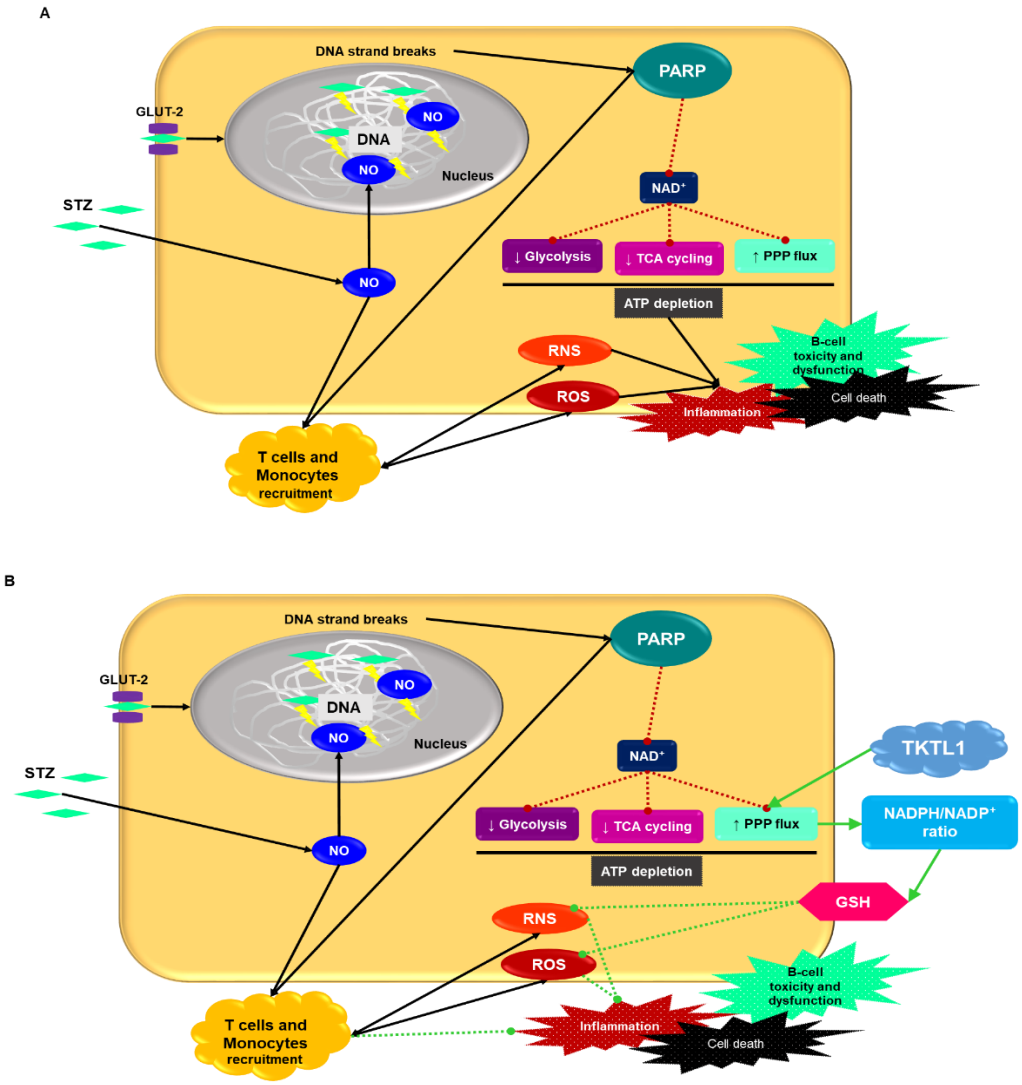

Figure 4.1 **TKTL1 offers protection against STZ. A) STZ mechanism of action in TKTL1-KO mice:** STZ enters pancreatic β-cells via GLUT-2 where the alkylnitroso moiety alkylates DNA thereby causing damage. STZ can also induce the formation of reactive species such as NO and $ONOO^-$ which can cause further damage to DNA and other macromolecules. PARP is activated to restore DNA strand breaks and as a result NAD^+ is depleted causing a decrease in glycolysis, TCA cycling and PPP flux eventually leading to an exhaustion of ATP stores. PARP can also lead to the recruitment and infiltration of immune cells which contribute to accumulating reactive species. The combination of ROS and RNS build-up and inflammatory environment together with ATP depletion can lead to β-cell toxicity and dysfunction as well as cell death most likely via necrosis. Thus, β-cell mass decreases and insulin production and secretion ceases leading to chronic hyperglycemia. **B) STZ mechanism of action in WT mice:** WT mice possess the TKTL1 gene which contributes to TKT activity and can therefore alter PPP flux. By increasing PPP flux, more NADPH is produced which can replenish glutathione antioxidant capacity thereby neutralizing some of the harmful ROS and RNS that accumulate within the cell and surrounding environment and thus, decrease the inflammatory response. Red dotted line indicates decrease with harmful consequences, green arrows indicates increase with positive outcomes, green dotted line indicates decrease with positive outcomes.

The PPP data suggest distinct functional roles in the heart and liver. For hepatic tissues we found that G6PD activity (rate-limiting enzyme of PPP oxidative branch) negatively correlated with blood glucose levels whereas the heart did not display any correlation. This suggests that the heart may be less susceptible to hyperglycemic oxidative damage compared to the liver, as G6PD activity in cardiac tissue was intact. If indeed the case, it may offer an explanation for our oxidative stress data where the hepatic tissues were more responsive to STZ-induced hyperglycemia. NADPH levels would be expected to follow the same trend as G6PD activity, but as only NAPDt levels (NADPH + $NADP^+$) could be measured (technical difficulties - refer Materials and methods section) this remains to be determined. An additional consideration is the presence of GLUT-2 in hepatocytes which provide a point of entry for STZ and could provide another explanation for the oxidative data obtained in this study (Mueckler, 1994).

Evaluation of the non-oxidative branch of the PPP produced a similar pattern. Perplexingly, the assay that was performed on hepatic tissue showed negative values which at first glance appear nonsensical. However, the assay quantifies relative NADH levels as a measure of transketolase activity as NADH is consumed in a downstream reaction. Therefore, if other reactions that produce NADH occur simultaneously, it may result in the negative values here obtained. It is crucial here to bear in mind that overall metabolic functioning and negative values obtained could be due to organ-specific metabolism. The liver is a dominant player in metabolism and is responsible for a great fraction of glucose disposal. Under postprandial conditions, excess glucose enters hepatocytes either to be stored as glycogen or to enter lipid biosynthesis (reviewed in Rui, 2014). Glucose that is stored as fatty acids proceed via glycolysis and the TCA cycle, both of which produces NADH. Thus if NADH is produced more rapidly than it is consumed through the reaction downstream of the TKT catalyzed reaction, then negative values will be obtained.

From the TKT activity assay performed on cardiac tissue, it is evident that TKTL1 may contribute to a significant portion of total TKT activity – at least in the heart. Interestingly, this seems to be the case irrespective of hyperglycemia, as both the STZ-responders and non-

responders showed a relatively similar decrease in TKT activity in WT mice. For both TKTL1-KO groups a ~50% activity was observed indicating that STZ resulted in no further effects on TKT activity. In addition, there was no difference in TKT activity in the responder and non-responder STZ-treated WT mouse groups. Together this suggests that the inhibitory effect of STZ on TKT activity may not be due to hyperglycemia *per se*. This is in contrast to other data where decreased transketolase activity occurred as a direct result of hyperglycemia (Mapanga *et al*., 2014) and also by others that utilized the same STZ-treatment protocol (Katare *et al*., 2013). A possible explanation for these data may be that in our study the mechanism of STZ action impacted negatively on TKT activity as it is able to downregulate the PPP (Figure 4.1). Importantly, these data indicate that TKTL1 may contribute significantly to total transketolase activity in the heart.

The TKT data are complex and other interpretations should also be considered. Our findings (lower WT TKT activity with hyperglycemia) are in agreement with previous studies (Saito *et al*., 1987) and thus strengthen overall data here generated. The significant decrease in TKT activity in STZ KO mice versus STZ WT mice should also be considered. One possibility is that this means that TKTL1 contributes to overall TKT activity (to a significant extent) and that it may actually be upregulated under pre-diabetic and diabetic conditions to counteract the overall decrease in TKT activity observed. This is in agreement with previous data generated in the Essop laboratory that found increased TKTL1 gene expression in pre-diabetic and diabetic individuals. Moreover, STZ treatment did not further decrease TKT activity in the KO mice as would be expected. It is not entirely clear why this is the case and this requires further investigations. We speculate that there may be some compensatory mechanisms at play that prevented lower TKT activity as expected. It is possible that there may be a threshold value to ensure a minimal degree of intracellular TKT activity, and that at this point compensatory mechanisms are triggered to sustain its function. Such mechanisms remain unclear at this time, but it is possible that other isoforms such as TKTL2 may be upregulated in this instance. However, this notion requires further investigations.

Limitations and future studies

The TKT activity assay was based on a published in-house assay and was technically challenging and very expensive to set up in our laboratory. Thus the liver TKT activity data did not reveal optimal results as expected and requires further optimization. An additional limitation was the nature of the TKTL1 antibody used as there is currently a lack of commercially available TKTL1 antibodies that can generate reproducible data.

For future studies, we recommend that the STZ injection protocol be amended in order to achieve a greater degree of hyperglycemia. We now propose to use a single high dose protocol that should elicit significant effects. In addition, studies should be planned to generate a T2DM phenotype in WT and KO mice and to assess the role of TKTL1 within this context. Here feeding mice a high-fat and high carbohydrate diet should ensure increased weight gain and the onset of insulin resistance and diabetes. It is also our aim to design new antibodies (in-house) for TKTL1 that should allow for improved detection (and reproducibility) of this crucial protein. Finally, it is crucial to investigate in more detail the various mechanisms that contribute to overall TKT activity as this not well understood at present.

In summary, the current study shows that TKTL1 may play distinct roles in the liver and heart. Our data reveal that it plays an anti-oxidant role in the liver to protect against hyperglycemia and to maintain overall glucose homeostasis. Here we speculate that TKTL1 lack results in residual oxidative stress that may result in downstream effects impacting on hepatic insulin signaling, gluconeogenesis and glycogen breakdown (Figure 4.2). Thus our study demonstrates novel insights into TKTL1 function and shows that it remains a feasible therapeutic target for the treatment of diabetes. However, as with any good research study it has unearthed several new questions and leads that require extensive investigation to help unravel the mysteries of TKTL1.

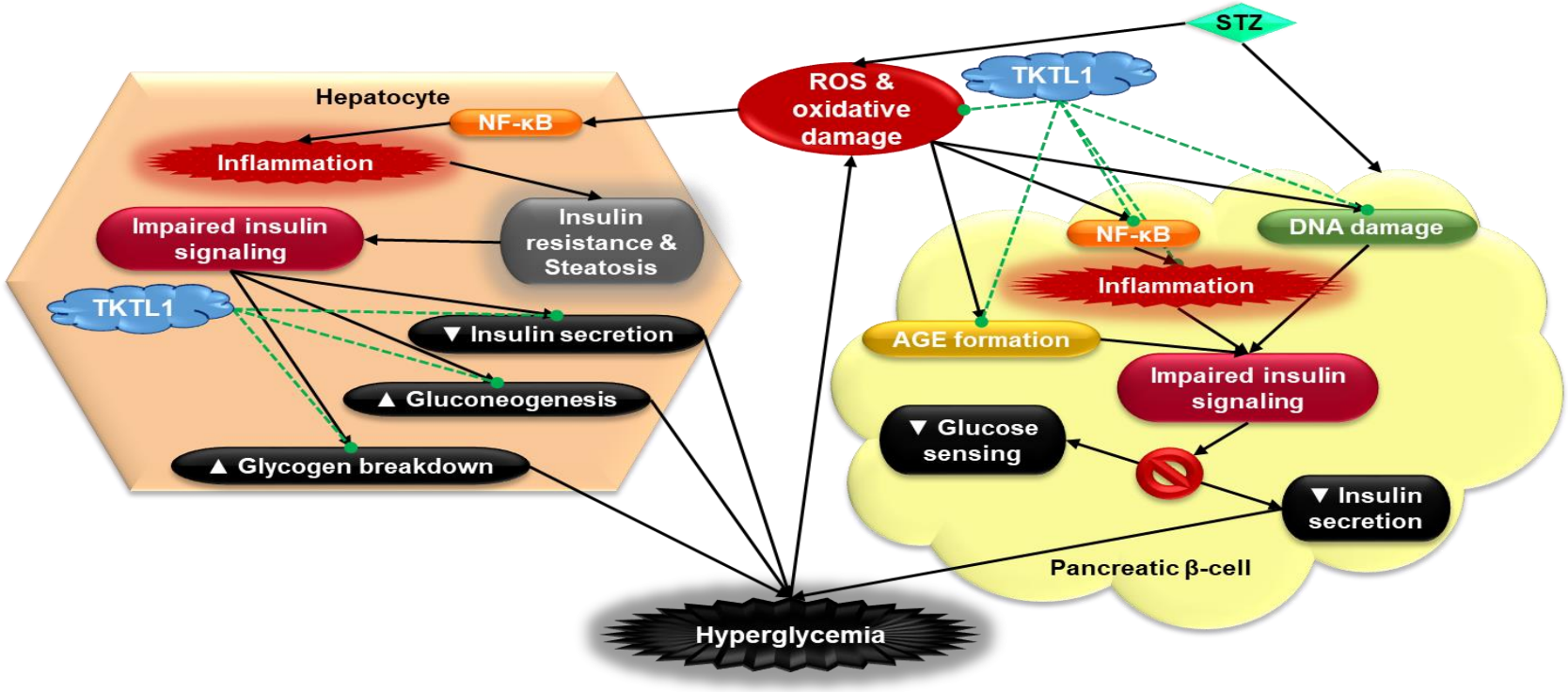

Figure 4.2 **Proposed regulatory role for TKTL1 in glucose metabolism. Pancreatic β-cells:** STZ mainly targets pancreatic β-cells where it elicits various damaging mechanisms that can lead to impaired insulin signaling and disengagement between glucose sensing and insulin secretion. This eventually results in a relative insulin deficiency and hyperglycemia. We propose that the anti-ROS and possible anti-inflammatory effect of TKTL1 enables it to alleviate some of these processes thereby at least partially preventing hyperglycemia. **Hepatocytes:** STZ-induced NF-κB activation and subsequent inflammation can lead to insulin resistance and steatosis which impairs insulin signaling. In hepatocytes this can lead to decreased insulin secretion as well as an increase in glycogen breakdown and gluconeogenesis all of which contribute to hyperglycemia. Here we propose that TKTL1 is able to minimize the damage of this dysregulation either via its anti-ROS function or a yet to be determined mechanism unique to this enzyme. Green dotted line indicates where TKTL1 may have an inhibitory role.

References

Abedinia M, Layfield R, Jones SM, Nixon PF, and Mattick JS. (1992). Nucleotide and predicted amino acid sequence of a cDNA clone encoding part of human transketolase. *Biochemical and Biophysical Research Communications*, 183(3):1159-1166.

Abid MR, Spokes KC, Shih SC, and Aird WC. (2007). NADPH oxidase activity selectively modulates vascular endothelial growth factor signaling pathways. *The Journal of Biological Chemistry*, 282:35373-85.

Ahn WS, Crown SB, and Antoniewicz MR. (2016). Evidence for transketolase-like TKTL1 flux in CHO cells based on parallel labeling experiments and 13C-metabolic flux analysis. *Metabolic Engineering*, 37:72-78.

Ahopelto K, Böckelman C, Hagström J, Koskensalo S, and Haglund C. (2016). Transketolase-like protein 1 expression predicts poor prognosis in colorectal cancer Kaisa. *Cancer Biology & Therapy*, 17(4):163-168.

Ba X and Garg NJ. (2011). Signaling mechanism of poly(ADP-ribose) polymerase-1 (PARP-1) in inflammatory diseases. *The American Journal of Pathology*, 178(3):946-955.

Babaei-Jadidi R, Karachalias N, Ahmed N, Battah S, and Thornalley PJ. (2003). Prevention of incipient diabetic nephropathy by high-dose thiamine and benfotiamine. *Diabetes*, 52(8):2110-2120.

Bailey SL, Ayles H, Beyers N, Godfrey-Faussett P, Muyoyeta M, du Toit E, Yudkin JS, and Floyd S. (2016). Diabetes mellitus in Zambia and the Western Cape province of South Africa : Prevalence, risk factors, diagnosis and management. *Diabetes Research and Clinical Practice*, 118:1-11.

Baines CP. (2009). The molecular composition of the mitochondrial permeability transition pore. *Journal of Molecular and Cellular Cardiology*, 46(6):850-857.

Balakumar P, Chakkarwar VA, and Singh M. (2009). Ameliorative effect of combination of benfotiamine and fenofibrate in diabetes-induced vascular endothelial dysfunction and nephropathy in the rat. *Molecular and Cellular Biochemistry*, 320:149-162.

Balteau M, Tajeddine N, de Meester C, Ginion A, des Rosiers C, Brady NR, Sommereyns C, Horman S, Vanoverschelde JL, Gailly P, Hue L, Bertrand L, and Beauloye C. (2011). NADPH oxidase activation by hyperglycaemia in cardiomyocytes is independent of glucose metabolism but requires SGLT1. *Cardiovascular Research*, 92:237-246.

Basu A, Caumo A, Gelisio A, Alzaid A, Cobelli C, and Rizza RA. (1997). Impaired 'basal' glucose effectiveness in NIDDM: contribution of defects in glucose disappearance and production measured using an optimized minimal model independent protocol. *Diabetes*, 46:421-432.

Baumgard LH, Hausman GJ, and Sanz Fernandez MV. (2016). Insulin: pancreatic secretion and adipocyte regulation. *Domestic Animal Endocrinology*, 54:76-84.

Baynes JW and Thorpe SR. (1999). Role of oxidative stress in diabetic complications: a new perspective on an old paradigm. *Diabetes*, 48:1-9.

Bentz S, Pesch T, Wolfram L, de Valliere C, Leucht K, Fried M, Coy JF, Hausmann M, and Rogler G. (2011). Lack of transketolase-like (TKTL) 1 aggravates murine experimental colitis. *American Journal of Physiolology: Gastrointestinal and Liver Physiology*, 300(4): G598–G607.

Bergman RN, Phillips LS, and Cobelli C. (1981). Physiologic evaluation of factors controlling glucose tolerance in man: Measurement of insulin sensitivity and, β-cell glucose sensitivity from the response to intravenous glucose. *The Journal of clinical investigation*, 68(6):1456-1467.

Berlett BS and Stadtman ER. (1997). Protein oxidation in aging, disease, and oxidative stress. *The Journal of Biological Chemistry*, 272:20313-20316.

Berridge MJ, Bootman MD, and Roderick HL. (2003). Calcium signalling: Dynamics, homeostasis and remodelling. *Nature Reviews Molecular Cell Biology*, 4(7):517-529.

Berridge MJ, Lipp P, and Bootman MD. (2000). The versatility and universality of calcium signalling. *Nature Reviews Molecular Cell Biology*, 1:11-21.

Berthon H, Kuchel P, and Nixon P. (1992). High control coefficient of transketolase in the nonoxidative pentose phosphate pathway of human erythrocytes: NMR, antibody, and computer simulation studies. *Biochemistry*, 31(1981):12792-12798

Bonner-Weir S, Deery D, and Weir GC. (1989). Compensatory growth of pancreatic beta-cells in adult rats after short-term glucose infusion. *Diabetes*, 38(1):49-53.

Bos JL. (1989). Ras oncogenes in human cancer: a review. *Cancer Research*, 49(17):4682-4689.

Brownlee M. (2005). The pathobiology of diabetic complications. *Diabetes*, 54(6):1615-1625.

Burrai GP, Tanca A, Cubedddu T, Abbondio M, Polinas M, Addis MF, and Antuofermo E. (2017). A first immunohistochemistry study of transketolase and transketolase-like 1 expression in canine hyperplastic and neoplastic mammary lesions. *Biomed Central: Veterinary Research*, 13:38-46.

Butler PC and Rizza RA. (1991). Contribution to postprandial hyperglycemia and effect on initial splanchnic glucose clearance of hepatic glucose cycling in glucose-intolerant or NIDDM patients. *Diabetes*, 40(1):73-81.

Cerf ME. (2013). Beta cell dysfunction and insulin resistance. *Frontiers in Endocrinology*, 4:1-12.

Ceriello A and Motz E. (2004). Is oxidative stress the pathogenic mechanism underlying insulin resistance, diabetes, and cardiovascular disease? The common soil hypothesis revisited. Arteriosclerosis, thrombosis, and vascular biology, 24(5):816-823.

Ceriello A, Quagliaro L, D'Amico M, Di Filippo C, Martella R, Nappo F, Berrino L, Rossi F, and Giugliano D. (2002). Acute hyperglycemia induces nitrotyrosine formation and apoptosis in perfused heart from rat. *Diabetes*, 51:1076-1082.

Ceylan-Isik, AF, Wu S, Li Q, Li S_Y, and Ren J. (2006). High-dose benfotiamine rescues cardiomyocyte contractile dysfunction in streptozotocin-induced diabetes mellitus. *Journal of Applied Physiology*, 100(1):150-156.

Chao Y-K, Peng T-L, Chuang W-Y, Yeh C-J, Li Y-L, Lu Y-C, and Chen A-J. (2016) Transketolase serves a poor prognosticator in esophageal cancer by promoting cell invasion via epithelial-mesenchymal transition. *Journal of Cancer*, 7(13):1804-1811.

Chen H, Yue J-X, Yang S-H, Ding H, Zhao R-W, and Wang S. (2009). Overexpression of transketolase-like gene 1 is associated with cell proliferation in uterine cervix cancer. *Journal of Experimental Clinical Cancer Research*, 28:43-51.

Chen L, Alam T, Johnson JH, Hughes S, Newgard CB, and Unger RH. (1990). Regulation of β-cell glucose transporter gene expression. *Proceedings of the National Academy of Sciences of the United States of America*, 87(11):4088-4092.

Cichoż-Lach H and Michalak A. (2014). Oxidative stress as a crucial factor in liver diseases. *World Journal of Gastroenterology*, 20(25):8082-8091.

Circu ML and Aw TY. (2010). Reactive oxygen species, cellular redox systems and apoptosis. *Free Radical Biology and Medicine*, 48(6):749-762.

Clark MG and Williams JF. (1971). The transketolase exchange reaction in vitro. *Biochemistry Journal*, 125:381-384.

Cosentino F, Hishikawa K, Katusic ZS, and Lüscher TF. (1997). High glucose increases nitric oxide synthase expression and superoxide anion generation in human aortic endothelial cells. *Circulation*, 96:25-28.

Coy JF, Dressler D, Wilde J, and Schubert P. (2005). Mutations in the transketolase-like gene TKTL1: clinical implications for neurodegenerative diseases, diabetes and cancer. *Clinical Laboratory*, 51:257-273.

Coy JF, Dübel S, Kioschis P, Thomas K, Micklem G, Delius H, and Poustka A. (1996). Molecular cloning of tissue-specific transcripts of a transketolase- related gene: implications for the evolution of new vertebrate genes. *Genomics*, 32:309-316.

Deng C, Yang J, Scott J, Hanash S, and Richardson BC. (1998). Role of the ras-MAPK signaling pathway in the DNA methyltransferase response to DNA hypomethylation. *The Journal of Biological Chemistry*, 379(7-9):1113-1120.

Desco M-C, Asensi M, Márquez R, Martínez-Valls J, Vento M, Pallardó FV, Sastre J, and Viña J. (2002). Xanthine oxidase is involved in free radical production in type 1 diabetes: protection by allopurinol. *Diabetes*, 51:1118-1124.

Dey A and Swaminathan K. (2010). Hyperglycemia-induced mitochondrial alterations in liver. *Life Sciences*, 87(7=8):197-214.

Dias AS, Porawski M, Alonso M, Marroni N, Collado PS, and González-Gallego J. (2005). Quercetin decreases oxidative stress, NF-kappaB activation, and iNOS overexpression

in liver of streptozotocin-induced diabetic rats. The *Journal of Nutrition*, 135(10):2299-2304.

Diaz-Moralli S, Aguilar E, Marin S, Coy JF, Dewerchin M, Antoniewicz MR, Meca-Cortés O, Notebaert L, Ghesquière B, Eelen G, Thomson TM, Carmeliet P, and Cascante M. (2016). A key role for transketolase-like 1 in tumor metabolic reprogramming. *Oncotarget*, 7(32):51875-51897.

Diaz-Moralli S, Tarrado-Castellarnau M, Alenda C, Castells A, and Cascante M. (2011). Transketolase-like 1 expression is modulated during colorectal cancer progression and metastasis formation. PLoS One, 6(9):e25323.

Dinneen SF. (1997). The postprandial state: mechanisms of glucose intolerance. *Diabetic medicine a journal of the British Diabetic Association*, 14(3):19-24.

Du X, Edelstein D, and Brownlee M. (2008). Oral benfotiamine plus alpha-lipoic acid normalises complication-causing complication-causing pathways in type 1 diabetes. *Diabetologia*; 51:1930-1932.

Du X, Matsumura T, Edelstein D, Rossetti L, Zsengellér Z, Szabó C, and Brownlee M. (2003). Inhibition of GAPDH activity by poly(ADP-ribose) polymerase activates three major pathways of hyperglycemic damage in endothelial cells. *Journal of Clinical Investigation*, 112(7):1049-1057.

Du XL, Edelstein D, Rossetti L, Fantus IG, Goldberg H, Ziyadeh F, Wu J, and Brownlee M. (2000). Hyperglycemia-induced mitochondrial superoxide overproduction activates the hexosamine pathway and induces plasminogen activator inhibitor-1 expression by increasing Sp1 glycosylation. *Proceedings of the National Academy of Sciences*, 97: 12222-12226.

Ebeling P, Koistinen H, and Koivisto V. (1998). Insulin-independent glucose transport regulates insulin sensitivity. *The Federation of the European Biochemical Societies letters*, 436(3):301-303.

Efendić S, Wajngot A, and Vranić M. (1985). Increased activity of the glucose cycle in the liver: early characteristic of type 2 diabetes. *Proceedings of the National Academy of Sciences of the United States of America*, 82(9):2965-2969.

Földi M, Stickeler E, Bau L, Kretz O, Watermann D, Gitsch G, Kayser G, zur Hausen A, and Coy JF. (2007). Transketolase protein TKTL1 overexpression: A potential biomarker and therapeutic target in breast cancer. *Oncology Reports*, 17:841-845.

Forbes JM, Thorpe SR, Thallas-Bonke V, Pete J, Thomas MC, Deemer ER, Bassal S, El-Osta A, Long DM, Panagiotopoulos S, Jerums G, Osicka TM, and Cooper ME. (2005). Modulation of soluble receptor for advanced glycation end products by angiotensin-converting enzyme-1 inhibition in diabetic nephropathy. J*ournal of the American Society of Nephrology*, 16: 2363-2372.

Friesen NTE, Büchau AS, Schott-Ohly P, Lgssair A, and Gleichmann H. (2004). Generation of hydrogen peroxide and failure of antioxidative responses in pancreatic islets of male C57BL/6 mice are associated with diabetes induced by multiple low doses of streptozotocin. *Diabetologia*, 47:676-685.

Fritz P, Coy JF, Mürdter TE, Ott G, Alscher MD, and Friedel G. TKTL-1 expression in lung cancer. *Pathology Research and Practice*, 208(4):245-249.

Fukudome D, Matsuda M, Kawasaki T, Ago Y, and Matsuda T. (2008). The radical scavenger edaravone counteracts diabetes in multiple low-dose streptozotocin-treated mice. *European Journal of Pharmacology*, 583(1):164-169.

Furman BL. (2015). Streptozotocin-Induced Diabetic Models in Mice and Rats. *Current protocols in pharmacology*, 70: 5.47.1-5.47.20

Furuta E, Okuda H, Kobayashi A, and Watabe K. (2010). Metabolic genes in cancer: Their roles in tumor progression and clinical implications. *Biochimica et Biophysica Acta - Reviews on Cancer*, 1805(2):141-152.

Gadau S, Emanueli C, Van Linthout S, Graiani G, Todaro M, Meloni M, Campesi I, Invernici G, Spillmann F, Ward K, and Madeddu P. (2006). Benfotiamine accelerates the healing of ischaemic diabetic limbs in mice through protein kinase B/Akt-mediated potentiation of angiogenesis and inhibition of apoptosis. *Diabetologia*, 49(2):405-420.

Garson K-L, Mapanga RF, Milne R, and Essop, MF. (2014). The effects of benfotiamine in attenuating hyperglycemia-induced cardiac pathology. *Journal of African Association of Physiological Sciences*, 2(1):5-13.

Giacco F and Brownlee M. (2010) Oxidative stress and diabetic complications. *Circulation Research*, 107:1058-70.

Gibson GE, Sheu KFR, Baker AC, Carlson KC, Harding B, Perrino P, and Blass JP. (1988). Reduced activities of thiamine-dependent enzymes in brains and peripheral tissues of Alzheimer's patients. *Archives of Neurology*, 45(8):836-840.

Gillespie, KM. (2006). Type 1 diabetes: pathogenesis and prevention. *CMAJ : Canadian Medical Association 175*(2), 165-70.

González RG, Aguayo J, Cheng H-M, and Chylack LT. (1984). Direct measurement of polyol pathway activity in the ocular lens. *Diabetes*, 33:196-199.

Gumaa KA, MacLeod RM, and McLean P. (1969). The pentose phosphate pathway of glucose metabolism. Influence of a growth-hormone-secreting pituitary tumour on the oxidative and non-oxidative reactions of the cycle in liver. *The Biochemical Journal*, 113(1):215-220.

Hadi AM, Mouchaers KTB, Schalij I, Grunberg K, Meijer GA, Vonk-Noordegraaf A, van der Laarse WJ, and Beliën JAM. (2011). Rapid quantification of myocardial fibrosis: a new macro-based automated analysis. *Cellular Oncology*, 34(4): 343-354.

Hämäläinen H, Rönnemaa T, Halonen JP, and Toikka T. (1999). Factors predicting lower extremity amputations in patients with type 1 or type 2 diabetes mellitus: a population-based 7-year follow-up study. *Journal of Internal Medicine*, 246(1):97-103.

Hammes HP, Du X, Edelstein D, Taguchi T, Matsumura T, Ju Q, Lin J, Bierhaus A, Nawroth P, Hannak D, Neumaie M, Bergfeld R, Giardino I, and Brownlee M. (2003). Benfotiamine blocks three major pathways of hyperglycemic damage and prevents experimental diabetic retinopathy. *Nature Medicine*, 9:294-299.

Hardiville S and Hart GW. (2014). Nutrient regulation of signaling, transcription, and cell physiology by *O*-GlcNAcylation. *Cell Metabolism*, 20(2):208-213.

Hässler S, Peltonen L, Sandler S, and Winqvist O. (2008). Aire deficiency causes increased susceptibility to streptozotocin-induced murine type 1 diabetes. *Scandinavian Journal of Immunology*, 67(6):569-580.

Henriksen EJ and Dokken BB. (2006). Role of glycogen synthase kinase-3 in insulin resistance and type 2 diabetes. *Current Drug Targets*, 7(11):1435-1441.

Horecker, B. L. (1964). In *Comprehensive Biochemistry*, vol. 15, p. 48. Ed. by Florkin, M. & Stotz, E. H. Amsterdam: Elsevier Publishing Co.

Hu L-H, Yang J-H, Zhang D-T, Zhang S, Wang L, Cai P-C, Zheng J-F, and Huang J-S. (2007). The TKTL1 gene influences total transketolase activity and cell proliferation in human colon cancer LoVo cells. *Anti-Cancer Drugs*, 18(4):427-433.

Inoguchi T, Li P, Umeda F, Yu HY, Kakimoto M, Imamura M, Aoki T, Etoh T, Hashimoto T, Naruse M, Sano H, Utsumi H, and Nawata H. (2000). High glucose level and free fatty acid stimulate reactive oxygen species production through protein kinase c–dependent activation of NAD(P)H oxidase in cultured vascular cells. *Diabetes*, 49:1939-1945.

Jagdale AD, Backar LN, More TA, Joglekar MM and Arvindekar AU. (2016). Strong inhibition of the polyol pathway diverts glucose flux to protein glycation leading to rapid establishment of secondary complications in diabetes mellitus. *Journal of Diabetes and Its Complications*, 30:398-405.

Jang YY, Song JH, Shin YK, Han ES, and Lee CS. (2000). Protective effect of boldine on oxidative mitochondrial damage in streptozotocin-induced diabetic mice. Pharmacological Research: *The Official Journal of the Italian Pharmacological Society*, 42(4):361–371.

Jayachandran A, Lo P-H, Chueh AC, Prithviraj P, Molania R, Davalos-Salas M, Anaka M, Walkiewicz M, Cebon J, and Behren A. (2016). Transketolase-like 1 ectopic expression is associated with DNA hypomethylation and induces the Warburg effect in melanoma cells. *Biomed Central: Cancer*, 16:134-148.

Johnson JH, Ogawa A, Chen L, Orci L, Newgard CB, and Alam T. (1990). Underexpression of beta cell high Km glucose transporters in noninsulin-dependent diabetes. *Science*, 205(4980):546-549.

Joseph D and Essop MF. (2014). The effects of thiamine treatment on pre-diabetic versus overt diabetic rat hearts : Role of non-oxidative glucose pathways. *International Journal of Cardiology*, 176(3):1371-1373.

Joseph D, Kimar C, Symington B, Milne R, and Essop, MF. (2014). The detrimental effects of acute hyperglycemia on myocardial glucose uptake. *Life Sciences*, 105:31-42.

Joseph D. (2014). Hyperglycemia-mediated onset of myocardial insulin resistance - unraveling molecular mechanisms and identifying therapeutic targets. Dissertation presented for the degree of Doctor of Philosophy.

Jouvion G, Abadie J, Bach JM, Roux F, Miclard J, Deschamps JY, Guigand L, and Wyers, M. (2006). Lymphocytic insulitis in a juvenile dog with diabetes mellitus. *Endocrine Pathology*, *17*(3), 283-90.

Junod A, Lambert AE, Orci L, Pictet R, Gonet AE, and Renold AE. (1967). Studies of the diabetogenic action of streptozotocin. *Experimental Biology and Medicine*, 126(1):201-205.

Kämmerer U, Gires O, Pfetzer N, Wiegering A, Klement RJ, and Otto C. (2015). TKTL1 expression in human malign and benign cell lines. *Biomed Central: cancer*, 15:2-17.

Katare R, Caporali A, Emanueli C, and Madeddu P. (2010). Benfotiamine improves functional recovery of the infarcted heart via activation of pro-survival G6PD/Akt signaling pathway and modulation of neurohormonal response. *Journal of Molecular and Cellular Cardiology*, 49(4):625-638.

Katare R, Oikawa A, Cesselli D, Beltrami AP, Avolio E, Muthukrishnan D, Munasinghe PE, Angelini G, Emanueli C, and Madeddu P. (2013). Boosting the pentose phosphate pathway restores cardiac progenitor cell availability in diabetes. *Cardiovascular Research*, 97(1):55-65.

Kawamura N, Ookawara T, Suzuki K, Konishi K, Mino M and Taniguchi N. (1992). Increased glycated Cu,Zn-superoxide dismutase levels in erythrocytes of patients with insulin-dependent diabetis mellitus. *The Journal of Clinical Endocrinology & Metabolism*, 74: 1352-1354.

Kayama Y, Raaz U, Jagger A, Adam M, Schellinger IN, Sakamoto M, Suzuki H, Toyama K, Spin JM, and Tsao PS. (2015). Diabetic cardiovascular disease induced by oxidative stress. *International Journal of Molecular Sciences*, 16(10):25234-25263.

Kikuchi A and Takamura T. (2017). Where does liver fat go? A possible molecular link between fatty liver and diabetes. *Journal of Diabetes Investigation*, 8(2):152-154.

Knowler WC, Pettitt DJ, Saad MF, and Bennett PH. (1990).Diabetes mellitus in the Pima Indians: incidence, risk factors and pathogenesis. *Diabetes/Metabolism Research and Reviews,* 6:1-27.

Kochetov GA and Solovjeva ON. (2014). Structure and functioning mechanism of transketolase. *Biochimica et Biophysica Acta*, 1844(9):1608-1618.

Kohrenhagen N, Voelker HU, Schmidt M, Kapp M, Krockenberger M, Frambach T, Dietl J, and Kammerer U. (2008). Expression of transketolase-like 1 (TKTL1) and p-Akt correlates with the progression of cervical neoplasia. *Journal of Obstetrics and Gynaecology Research*, 34(3):293-300.

Koya D and King GL. (1998). Protein kinase C activation and the development of diabetic complications. *Diabetes*, 47(6):859-866.

Krockenberger M, Honig A, Rieger L, Coy JF, Sutterlin M, Kapp M, Horn E, Dietl J, and Kammerer U. (2007). Transketolase-like 1 expression correlates with subtypes of ovarian cancer and the presence of distant metastases. *International Journal of Gynecological Cancer*, 17(1):101-106.

Kumar B, Kowluru A, and Kowluru RA. (2015). Lipotoxicity augments glucotoxicity-induced mitochondrial damage in the development of diabetic retinopathy. *Investigative Ophthalmology & Visual Science*, 56(5):2985-2992.

Kumar D. (2017). Regulation of glycolysis in head and neck squamous cell carcinoma. *Postdoctoral Journal*, 51):14-28.

Kurowski JR, Nedkoff L, Schoen DE, Knuiman M, Norman PE, and Briffa TG. (2015). Temporal trends in initial and recurrent lower extremity amputations in people with and without diabetes in Western Australia from 2000 to 2010. *Diabetes Research and Clinical Practice*, 108(2):280-287.

Langbein S, Zerilli M, zur Hausen A, Staiger W, Rensch-Boschert K, Lukan N, Popa J, Ternullo MP, Steidler A, Weiss C, Grobholz R, Willeke F, Alken P, Stassi G, Schubert P, and Coy JF. (2006). Expression of transketolase TKTL1 predicts colon and urothelial cancer patient survival: Warburg effect reinterpreted. *British Journal of Cancer*, 94:578-585.

Lazar M, Golden P, Furman M, and Lieberman TW. Resistance of the rabbit to Streptozotocin. *The Lancet*, 292(7574):919.

Leahy JL. (2005). Pathogenesis of type 2 diabetes mellitus. *Archives of Medical Research*, 36(3):197-209.

Leigh D, McBurney A, and McIlwain H. (1981). Erythrocyte transketolase activity in the Wernicke-Korsakoff syndrome. *The British Journal of Psychiatry*, 139:153-156.

Leroux J-P, Marchand J-C, Hong Tuan Ha R, and Cartier P. (1975). The influence of insulin on glucose permeability and metabolism of human granulocytes. *European Journal of Biochemistry*, 58(2):367-373.

Li J, Zhu S-C, Li S-G, Zhao Y, Xu J-R, and Song C-Y. (2015). TKTL1 promotes cell proliferation and metastasis in esophageal squamous cell carcinoma. *Biomedicine et Pharmacotherapy*, 74:71-76.

Liberti MV and Locasale JW. (2016). The Warburg effect: how does it benefit cancer cells? *Trends in Biochemical Sciences*, 41(3):211-218.

Lillioja S, Mott DM, Spraul M, Ferraro R, and Foley JE. (1993). Insulin resistance and insulin secretory dysfunction as precursors of non-insulin dependent diabetes mellitus. Prospective studies in PIMA Indians. *New England Journal of Medicine*, 329:1988-1992.

Linqvist Y, Schneider G, Ermler U, and Sundström M. (1992). Three-dimensional structure of transketolase, a thiamine diphosphate dependent enzyme, at 2.5 A resolution. *European Molecular Biology Organization Journal*, 11(7):2373-2379.

Lukivskaya O, Patsenker E, and Buko VU. (2007). Protective effect of ursodeoxycholic acid on liver mitochondrial function in rats with alloxan-induced diabetes: link with oxidative stress. *Life Sciences*, 80(26):2397-2402.

Magnusson I, Rothman DL, Katz LD, Shulman RG, and Shulman GI. (1992). Increased rate of gluconeogenesis in type II diabetes mellitus. A 13C nuclear magnetic resonance study. *Journal of Clinical Investigation*, 90(4):1323-1327.

Manrique C, Lastra G, Habibi J, Mugerfeld I, Garro M, and Sowers JR. (2012). Loss of estrogen receptor α signaling leads to insulin resistance and obesity in young and adult female mice. *Cardiorenal Medicine*, 2:200-210.

Mapanga RF and Essop MF. (2016). Damaging effects of hyperglycemia on cardiovascular function: spotlight on glucose metabolic pathways. *American journal of physiology: Heart and circulatory physiology*, 310:153-173.

Mapanga RF, Rajamani U, Dlamini N, Zungu-Edmondson M, Kelly-Laubscher R, Shafiullah M, Wahab A, Hasan MY, Fahim MA, Rondeau P, Bourdon E, and Essop MF. (2012) Oleanolic acid: a novel cardioprotective agent that blunts hyperglycemia-induced contractile dysfunction. *PLoS ONE* 7(10): e47322

Mapanga RF, Joseph D, Symington B, Garson K-L, Kimar C, Kelly-Laubscher R, and Essop MF. (2014). Detrimental effects of acute hyperglycaemia on the rat heart. *Acta Physiologica*, 210:546-564.

Marayama H, Hisatomi A, Orci L, Grodsky GM, and Unger RH. (1984). Insulin within islets is a physiologic glucagon release inhibitor. *The Journal of Clinical Investigation*, 74:2296-2299.

Martin BC, Warram JH, Krolewski AS, Bergman RN, Soeldner JS, and Kahn CR. (1992). Role of glucose and insulin resistance in development of type 2 diabetes mellitus: results of a 25-year follow-up study. *The Lancet*, 340(8825):925-929.

Maslova AO, Meshalkina LE, and Kochetov GA. (2012). Computer modeling of transketolase-like protein, TKTL1, a marker of certain tumor tissues. *Biochemistry (Moscow)*, 77(3):296-299.

Matteucci E and Giampietro O. (2000). Oxidative stress in families of type 1 diabetic patients. *Diabetes Care*, 23(8):1182-1186.

Mayer A, von Wallbrunn A, and Vaupel P. (2010). Glucose metabolism of malignant cells is not regulated by transketolase-like (TKTL)-1. I*nternational journal of oncology*, 37:265-271.

Mayes, P. (1993). The pentose phosphate pathway & other pathways of hexose metabolism. In Harper's Biochemistry. Murray R, Granner D, Mayes P, and Rodwell V, editors. Appleton & Lange, Norwalk, CT. 201-211.

McCandless D, Schenker S, and Cook M. (1968). Encephalopathy of thiamine deficieny: studies of intracerebral mechanisms. *Journal of Clinical Investigation*, 47(10):2268-2280.

Meloche HP. (1961). Enzymatic utilization of glucose by a basidiomycete. *Journal of bacteriology*, 83:766-774.

Meshalkina LE, Drutsa VL, Koroleva ON, Solovjeva ON, and Kochetov GA. (2013). Is transketolase-like protein, TKTL1, transketolase? *Biochimica et Biophysica Acta - Molecular Basis of Disease*, 1832(3):387-390.

Mueckler M. (1994). Facilitative glucose transporters. *European Journal of Biochemistry*, 219:713-725.

Mitschke L, Parthier C, Schröder-Tittmann K, Coy J, Lüdtke S, and Tittmann K. (2010). The crystal structure of human transketolase and new insights into its mode of action. *The Journal of Biological Chemistry*, 285(41):31559-149955.

Mooradian AD. (2016). Targeting select cellular stress pathways to prevent hyperglycemia-related complications: shifting the paradigm. *Drugs*, 76(11):1081-1091.

Morgan PE, Dean RT, and Davies MJ. (2002). Inhibition of glyceraldehyde- 3-phosphate dehydrogenase by peptide and protein peroxides generated by singlet oxygen attack, *European Journal of Biochemistry*, 269:1916-1925.

Morrison AD, Clements RS Jr, Travis SB, Oski F and Winegrad AI. (1970).Glucose utilization by the polyol pathway in human erythrocytes. *Biochemical and Biophysical Research Communications*, 40:199-205.

Muller YA, Lindqvist Y, Furey W, Schulz GE, and Jordan F. (1993). A thiamine diphosphate binding fold revealed by comparison of the crystal structures of transketolase, pyruvate oxidase and pyruvate decarboxylase. *Structure* (1):95-103.

Münzel T, Camici GG, Maack C, Bonetti NR, Fuster V, and Kovacic JC. (2017). Impact of oxidative stress on the heart and vasculature (part 2 of a 3-part series). *Journal of the American College of Cardiology*, 70(2):212-229.

Murray, CJL and Lopez, AD. (2013). Measuring the global burden of disease. *New England Journal of Medicine*, 369(5):448-457.

Natalizio A, Ruggiero D, Lecomte M, Lagarde M, and Wiernsperger N. (2001). Glycosphingolipid changes induced by advanced glycation end-products. *Biochemical and Biophysiological Research Communications*, 281:78-83.

Newton A. (2003). Regulation of the ABC kinases by phosphorylation: protein kinase C as a paradigm. *Biochemical Journal*, 370:361-371.

Nikkola M, Lindqvist Y, and Schneider G. (1994). Refined structure of transketolase from Saccharomyces cerevisiae at 2.0 A resolution. *Journal of Molecular Biology*, 238:387-404.

Nolan CJ, Damm P, and Prentki M. (2011). Type 2 diabetes across generations: From pathophysiology to prevention and management. *The Lancet*, 378: 169-181.

Novello F, Gumaa P, and McLean P. (1969). The pentose phosphate pathway of glucose metabolism. Hormonal and dietary control of the oxidative and non-oxidative reactions of the cycle in liver. *The Biochemical Journal*, 111(5):713-725.

Olszewska M, Wiatrow J, Bober J, Stachowska E, Golembiewska E, Jakubowska K, Stańczyk-Dunaj M, and Pietrzak-Nowacka M. (2012). Oxidative stress modulates the organization of erythrocyte membrane cytoskeleton. *Postepy Higieny: Medycyny Doswiadczalnej*, 66:534-542.

Page E and McCallister LP. (1973). Quantitative electron microscopic description of heart muscle cells. Application to normal, hypertrophied and thyroxin-stimulated hearts. *The American Journal of Cardiology*, 31(2):172-181.

Pandolfi PP, Sanati F, Rivi R, Mason P, Grosveld F, and Luzzatto L. (1995). Targeted disruption of the housekeeping gene encoding glucose 6-phosphate dehydrogenase (G6PD): G6PD is dispensable for pentose synthesis but essential for defense against oxidative stress. *The EMBO Journal*, 14(21):5209-5215.

Patra KC and Hay N. (2014). The pentose phosphate pathway and cancer. *Trends in Biochemical Sciences*, 39(8):347-354.

Petersen KF and Shulman GI. (2006). Etiology of insulin resistance. *The American Journal of Medicine*, 119(5A):10-16.

Phillip M, Schwaab J, Dietz CT, Hanfstein B, Kalmanti L, Munjal U, Mossner M, Nowak D, Seifarth W, Hofmann WK, Hochhaus A, Müller MC, and Erben P. (2014). Expression of transketolase-like gene 1 (TKTL1) depends on disease phase in patients with chronic myeloid leukaemia (CML). *Journal of Cancer Research and Clinical Oncology*, 140(3):411-417.

Pick A, Clark C, Kubstrup C, Levisetti M, Pugh W, and Bonner-Weir S. (1998). Role of apoptosis in failure of beta-cell mass compensation for insulin resistance and beta-cell defects in the male Zucker diabetic fatty rat. *Diabetes*, 47(3):358-364.

Pircher A, Treps L, Bodrug N, and Carmeliet P. (2016). Endothelial cell metabolism: A novel player in atherosclerosis? Basic principles and therapeutic opportunities. *Atherosclerosis*, 253:247-257.

Piro S, Anello M, Di Pietro C, Lizzio MN, Patan G, Rabuazzo AM, Vigneri R, Purrello M, and Purrello F. (2002). Chronic exposure to free fatty acids or high glucose induces apoptosis in rat pancreatic islets: Possible role of oxidative stress. *Metabolism*, 51(10):1340-1347.

Polonsky KS, Sturis J, and Bell GI. (1996). Seminars in Medicine of the Beth Israel Hospital, Boston. Non-insulin-dependent diabetes mellitus – a genetically programmed failure of the beta cell to compensate for insulin resistance. *New England Journal of Medicine*, 334: 777–783.

Raïs B, Comin B, Puigjaner J, Brandes JL, Creppy E, Saboureau D, Ennamany R, Boros EL and Casante M. (1999). Oxythiamine and dehydroepiandrosterone induce a G1 phase cycle arrest in Ehrlich's tumor cells through inhibition of the pentose cycle. *The Federation of the European Biochemical Societies Letters*, 456(1):113-18.

Rajapakse AG, Ming X-F, Carvas JM, and Yang Z. (2008). The hexosamine biosynthesis inhibitor azaserine prevents endothelial inflammation and dysfunction under hyperglycemic condition through anti-oxidant effects. *American journal of physiology: Heart and circulatory physiology*, 296:815-822.

Riganti C, Gazzano E, Polimeni M, Aldrieri E, and Ghigo D. (2012). The pentose phosphate pathway: An anti-oxidant defense and a crossroad in tumor cell fate. *Free Radical Biology and Medicine*, 53:421-436.

Rui L. (2014). Energy metabolism in the liver. *Comprehensive Physiology*, 4(1):177-197.

Saito N, Kimura M, Kuchiba A, and Itokawa Y. (1987). Blood thiamine levels in outpatients with diabetes mellitus. *Journal of nutrional science and vitaminology*, 33(6):421-430.

Sako Y and Grill VE. (1990). A 48-hour lipid infusion in the rat time-dependently inhibits glucose- induced insulin secretion and B cell oxidation through a process likely coupled to fatty acid oxidation. *Endocrinology*, 127:1580-1589.

Sano H, Kane S, Sano E, Mîinea CP, Asara JM, Lane WS, Garner CW, and Lienhard GE. (2003). Insulin-stimulated phosphorylation of a Rab GTPase-activating protein regulates GLUT4 translocation. *Journal of Biological Chemistry*, 278:14599-14602.

Santos CXC, Anilkumar N, Zhang M, Brewer AC, and Shah AM. (2011). Redox signalling in cardiac myocytes. *Free Radical Biology & Medicine*, 50:777-793.

Satoh M, Fujimoto S, Haruna Y, Arakawa S, Horike H, Komai N, Sasaki T, Tsujioka K, Makino H, and Kashihara N. (2005). NAD(P)H oxidase and uncoupled nitric oxide synthase are major sources of glomerular superoxide in rats with experimental diabetic nephropathy. *American Journal of Physiology: Renal Physiology*, 288: 1144-1152.

Schaffer SW, Jong CJ, and Mozaffari M. (2012). Role of oxidative stress in diabetes-mediated vascular dysfunction: Unifying hypothesis of diabetes revisited. *Vascular Pharmacology*, 57:139-149.

Scheen AJ. (2004). Pathophysiology of type 2 diabetes. *Acta clinica Belgica*, 58(6):335-41.

Schenk G, Duggleby RG, and Nixon PF. (1998). Heterologous expression of human transketolase. *The international journal of biochemistry & cell biology*, 30(3):369-378.

Schmid U, Stopper H, Heidland A, and Schupp N. (2008). Benfotiamine exhibits direct antioxidative capacity and prevents induction of DNA damage in vitro. *Diabetes/Metabolism Research and Reviews*, 24:371-377.

Schmidt AM, Hori O, Brett J, Yan SD, Wautier JL and Stern D. (1994). Cellular receptors for advanced glycation end products. Implications for induction of oxidant stress and cellular dysfunction in the pathogenesis of vascular lesions. *Arteriosclerosis, Thrombosis, and Vascular Biology*, 14:1521-1528.

Schnedl WJ, Ferber S, Johnson JH, and Newgard CB. (1994). STZ Transport and Cytotoxicity. Specific enhancement in GLUT2-expressing cells. *Diabetes*, 43:1326-1333.

Schneider S, Lüdtke S, Schröder-Tittmann, Wechsler C, Meyer D, and Tittmann K. (2012). A Δ38 deletion variant of human transketolase as a model of Transketolase-like protein 1 exhibits no enzymatic activity. *PLoS ONE*, 7(10):1-9.

Schwaab J, Horisberger K, Ströbel P, Bohn B, Gencer D, Kähler G, Kienle P, Post S, Wenz F, Hofmann W-K, Hofheinz R-D, and Erben P. (2011). Expression of transketolase like

gene 1 (TKTL1) predicts disease-free survival in patients with locally advanced rectal cancer receiving neoadjuvant chemoradiotherapy. *Biomed Central: Cancer*, 11(1):363-371.

Seino Y, Nanjo K, Tajima N, Kadowaki T, Kashiwagi A, Araki E, Ito C, Inagaki N, Iwamoto Y, Kasuga M, Hanafusa T, Haneda M, and Ueki K. (2010). Report of the committee on the classification and diagnostic criteria of diabetes mellitus. *Journal of Diabetes Investigation*, 1(5):212-228.

Seltzer HS, Allen EW, Herron AL, and Brennan MT. (1967). Insulin secretion in response to glycemic stimulus: relation of delayed initial release to carbohydrate intolerance in mild diabetes mellitus. *Journal of Clinical Investigations*, 46(3):323-335.

Semilia M, Hennenlotter J, Pavone C, Bischoff T, Kühs U, Gakis G, Bedke J, Stenzl A, Schwetner C, and Todenhöfer. (2015). Expression patterns and prognostic role of transketolase-like 1 in muscle-invasive bladder cancer. *World Journal of Urology*, 33(10):1403-1409.

Serpillon S, Floyd BC, Gupte RS, George S, Kozicky M, Neito V, Recchia F, Stanley W, Wolin MS, and Gupte SA. (2009). Superoxide production by NAD(P)H oxidase and mitochondria is increased in genetically obese and hyperglycemic rat heart and aorta before the development of cardiac dysfunction. The role of glucose-6-phosphate dehydrogenase-derived NADPH. *American Journal of Physiology-Heart and Circulatory Physiology*, 297:153-162.

Shakeel M. (2015). Recent advances in understanding the role of oxidative stress in diabetic neuropathy. *Diabetes & Metabolic Syndrome: Clinical Research & Reviews*, 9:373-378.

Shen M, Kumar SP, and Shi H. (2014). Estradiol regulates insulin signaling and inflammation in adipose tissue. *Hormone Molecular Biology and Clinical Investigation*, 17(1):99-107.

Sheu K-FR, Clarke DD, and Kim Y-T. (1988). Studies of transketolase abnormality in Alzheimer's disease. *Archives of Neurology*, 45(8):841-845.

Shimabukuro M, Zhou Y-T, Levi M, and Unger RH. (1998). Fatty-acid-induced beta-cell apoptosis: a link between obesity and diabetes. *Proceedings of the National Academy of Sciences,* 95(5):2498-2503.

Shisana O, Labadarios D, Rehle T, Simbayi L, Zuma K, Dhansay A, Reddy P, Parker W, Hoosain E, Naidoo P, Hongoro C, Mchiza Z, Steyn NP, Dwane N, Makoae M, Maluleke T, Ramlagan S, Zungu N, Evans MG, Jacobs L, Faber M, and SANHANES-1 Team. (2013). South African National Health and Nutrition Examination Survey (SANHANES-1). Cape Town: *HSRC Press*

Shoeb M and Ramana KV. (2012). Anti-inflammatory effects of benfotiamine are mediated through the regulation of the arachidonic acid pathway in macrophages. *Free Radical Biology and Medicine*, 52:182-190.

Singh PP, Mahadi F, Roy A, and Sharma P. (2009). Reactive oxygen species, reactive nitrogen species and anti-oxidants in etiopathogenesis of diabetes mellitus type-2. *Indian Journal of Clinical Biochemistry*, 24(4):324-342.

Singleton JR, Smith AG, Russel JW, and Feldman EL. (2003). Microvascular complications of impaired glucose tolerance. *Diabetes*, 52(12):2867-2873.

Srivastava LM and Hübscher G. (1966). Glucose metabolism in the mucosa of the small intestine. Enzymes of the pentose phosphate pathway. *The Biochemical journal*, 101(1):48-55.

Stammers AN, Susser SE, Hamm NC, Hlynsky MW, Kimber DE, Kehler DS, and Duhamel TA. (2015). The regulation of sarco(endo)plasmic reticulum calcium-ATPases (SERCA). *Canadian Journal of Physiology and Pharmacology*, 93(10):843-854.

Statistics South Africa. (2013). *Use of health facilities and levels of selected health conditions in South Africa: Findings from the General Household Survey*, 2011.

Statistics South Africa. (2017). *Mortality and causes of death in South Africa, 2015: Findings from death notification*. Statistical release P0309.3:1-127.

Stirban A, Negrean M, Stratmann B, Gawlowski T, Horstmann T, Götting C, Kleesiek K, Mueller-Roesel M, Koschinsky T, Uribarri J, Vlassara H, and Tschoepe D. (2006). Benfotiamine prevents macro- and microvascular endothelial dysfunction and oxidative stress following a meal rich in advanced glycation end products in individuals with type 2 diabetes. *Diabetes Care*, 29(9):2064-2071.

Stratton IM. (2000). Association of glycaemia with macrovascular and microvascular complications of type 2 diabetes (UKPDS 35): prospective observational study. *British Medical Journal*, 321(7258):405-412.

Strömme JH and Eldjarn L. (1962). The role of the pentose phosphate pathway in the reduction of methaemoglobin in human erythrocytes. *The Biochemical Journal*, 84:406-410.

Sun W, Liu Y, Glazer CA, Shao C, Bhan S, Demokan S, Shao M, Rudek MA, Ha PK, and Califano JA. (2010). TKTL1 is activated by promoter hypomethylation and contributes to head and neck squamous cell carcinoma carcinogenesis through increased aerobic glycolysis and HIF1α stabilization. *Human Cancer Biology*, 16(3):857- 866.

Suzuki YJ. (2011). Cell signalling pathways for the regulation of GATA4 transcription factor: Implications for cell growth and apoptosis. *Cell Signalling*, 23(7):1094-1099.

Syed I, Kyathanahalli CN, Jayaram B, Govind S, Rhodes CJ, Kowluru RA, and Kowluru A. (2011). Increased phagocyte-like NADPH oxidase and ROS generation in type 2 diabetic ZDF rat and human islets. Role of Rac1–JNK1/2 signaling pathway in mitochondrial dysregulation in the diabetic islet. *Diabetes*, 60(11):2843-2852.

Szabó C and Dawson VL. (1998). Role of poly(ADP-ribose) synthetase in inflammation and ischaemia–reperfusion. *Trends in Pharmacological Sciences*, 19:287-298.

Szeinberg A and Marks PA. (1961). Substances stimulating glucose catabolism by the oxidative reactions of the pentose phosphate pathway in human erythrocytes. *The Journal of Clinical Investigation*, 40:914-924.

Szkudelski T. (2001). The mechanism of alloxan and streptozotocin action in B cells of the rat pancreas. *Physiology Research*, 50(6):536-546.

Thornalley PJ, Jahan I, and Ng R. (2001). Suppression of the accumulation of triosephosphates and increased formation of methylglyoxal in human red blood cells during hyperglycaemia by thiamine in vitro. *Journal of Biochemistry*, 129(4):543-549.

Traviesa DC. (1974). Magnesium deficiency: a possible cause of thiamine refractoriness in Wernicke-Korsakoff encephalopathy. *Journal of Neurology, Neurosurgery & Psychiatry*, 37(8):959-962.

Unger RH and Orci L. (1981). Glucagon and the α cell –physiology and pathophysiology – (first of two parts). *New England Journal of Medicine*, 304:1518-1524.

Unger RH. (1991). Diabetic hyperglycaemia: Link to impaired glucose transport in pancreatic β cells. *Science*, 251(4998):1200-1205.

Upadhyay M, Samal J, Kandpal M, Vir Singh O, and Vivekanandan P. (2013). The Warburg effect: Insights from the past decade. *Pharmacology & Therapeutics*, 137:318-330.

Wang JJ-L, Martin PR, and Singleton CK. (1997). A transketolase assembly defect in a Wernicke-Korsakoff syndrome patient. *Alcoholism Clinical & Experimental Research*, 21(4):576-580.

Wang Z and Gleichmann H. (1998). GLUT2 in pancreatic islets. Crucial target molecule in diabetes induced with multiple low doses of streptozotocin mice. *Diabetes*, 47(1):50-56.

Wautier J-L, Wautier M-P, Schmidt A-M, Anderson GM, Hori O, Zonkounan C, Capron L, Chappey O, Yan S-D, Brett J, Guillausseau P-J, and Stern D. (1994). Advanced glycation end products (AGEs) on the surface of diabetic erythrocytes bind to the vessel wall via a specific receptor inducing oxidant stress in the vasculature: a link between surface-associated AGEs and diabetic complications. *Proceedings of the National Academy of Sciences,* 91:7742-7746.

WHO Consultation, WHO. (1999). *Definition, diagnosis and classification of diabetes mellitus and its complications*. *Geneva, Switzerland: World Health Organization* (Vol. 31).

WHO. *Global report on diabetes. Geneva: World Health Organization*. (2016).

WHO. *The World Health Report 2006*: Working together for health. (2006).

WHO: *The top 10 causes of death*. (2017). [Accessed 20 May 2017 at: http://www.who.int/mediacentre/factsheets/fs310/en/]

Wild S, Roglic G, Green A, Sicree R, and King H. (2004). Global Prevalence of Diabetes: Estimates for the year 2000 and projection for 2030. *Diabetes Care*, 27(5):1047–1053.

Wu KK and Haun Y. (2008). Streptozotocin-induced diabetic models in mice and rats. *Current Protocols in Pharmacology*, 5.47.1-5.47.14.

Wu S and Ren J. (2006). Benfotiamine alleviates diabetes-induced cerebral oxidative damage independent of advanced glycation end-product, tissue factor and TNF-α. *Neuroscience Letters*, 394(2):158-162.

Xu X, zur Hausen A, Coy JF, and Löchelt M. (2009). Transketolase-like protein 1 (TKTL1) is required for rap and full viability of human tumor cells. *International Journal of Cancer*, 124(6):1330-1337.

Xu Z-P, Wawrousek EF, and Piatigorsky J. (2002). Transketolase haploinsufficiency reduces adipose tissue and female fertility in mice. *Molecular and Cellular Biology*, 22(17):6142-6147.

Yim MB, Yim HS, Lee C, Kang SO, and Chock PB. (2001). Protein glycation: creation of catalytic sites for free radical generation. *Annals of the New York Academy of Sciences*, 928:48-53.

Zhang M, Kho AY, Anilkumar N, Chibber R, Pagano PJ, Shah AM, and Cave AC. (2006). Glycated proteins stimulate reactive oxygen species production in cardiac myocytes involvement of Nox2 (gp91phox)-containing NADPH oxidase. *Circulation*, 113(9):1235-1243.

Zhang P-Y. (2014). Cardiovascular disease in diabetes. *European review for medical and pharmacological sciences*, 18(15):2205-2214.

Zhang S, Yang J-H, Guo C-K, and Cai P-C. (2007). Gene silencing of TKTL1 by RNAi inhibits cell proliferation in human hepatoma cells. *Cancer Letters*, 253(1):108-114.

Zhao J and Zhong C-J. (2009). A review on research progress of transketolase. *Neuroscience Bulletin*, 25(2):94-99.

Zhou YP and Grill VE. (1994). Long-term exposure of rat pancreatic islets to fatty acids inhibits glucose-induced insulin secretion and biosynthesis through a glucose fatty acid cycle. *Journal of Clinical Investigation*, 93:870-876.

Appendices

Appendix A: **Ethics # SU-ACUD16-00052**

UNIVERSITEIT·STELLENBOSCH·UNIVERSITY
jou kennisvennoot • your knowledge partner

Approved with Stipulations

Date: 31-Oct-2016

PI Name: Joseph, Danzil DE

Protocol #: SU-ACUD16-00052

Title: The regulation of TKTL1 with Type 1 and Type 2 diabetes: investigating some of the functional physiological effects

Dear Danzil Joseph, the Response to Modifications submission was reviewed on by Research Ethics Committee: Animal Care and Use via committee review procedures and was approved on condition that the following stipulations are adhered to:

1. The applicant is reminded that proof of SAVC authorisation under Section 21 of the Veterinary and para-veterinary professions act of no. 19 of 1982, must be submitted to the REC.

Applicants are reminded that they are expected to comply with accepted standards for the use of animals in research and teaching as reflected in the South African National Standards 10386: 2008. The SANS 10386: 2008 document is available on the Division for Research Developments website www.sun.ac.za/research.

As provided for in the Veterinary and Para-Veterinary Professions Act, 1982. It is the principal investigator's responsibility to ensure that all study participants are registered with or have been authorised by the South African Veterinary Council (SAVC) to perform the procedures on animals, or will be performing the procedures under the direct and continuous supervision of a SAVC-registered veterinary professional or SAVC-registered para-veterinary professional, who are acting within the scope of practice for their profession.

Please remember to use your protocol number, SU-ACUD16-00052 on any documents or correspondence with the REC: ACU concerning your research protocol.

Any event not consistent with routine expected outcomes that results in any unexpected animal welfare issue (death, disease, or prolonged distress) or human health risks (zoonotic disease or exposure, injuries) must be reported to the committee, by creating an Adverse Event submission within the system.

If you have any questions or need further help, please contact the REC: ACU secretariat at or .

Sincerely,

Winston Beukes

REC: ACU Secretariat

Research Ethics Committee: Animal Care and Use

Appendix B: **Table with correlations between blood glucose levels and experimental values.**

Variable 1	Variable 2	Spearman r	p-value	Subgroup
Blood glucose (mmol/L)	Heart G6PD activity (mU/mg protein)	0,03	0,87	N/A
Blood glucose (mmol/L)	Liver G6PD activity (mU/mg protein)	-0,37	0,03	N/A
Blood glucose (mmol/L)	Heart NADPt (nmol/mg protein)	0,11	0,56	N/A
Blood glucose (mmol/L)	Liver NADPt (nmol/mg protein)	-0,13	0,44	N/A
Blood glucose (mmol/L)	Heart TKT activity (uU/g protein)	-0,07	0,71	N/A
Blood glucose (mmol/L)	Liver TKT activity (uU/g protein)	-0,30	0,08	N/A
Blood glucose (mmol/L)	Heart SOD activity (U/mg protein)	-0,09	0,63	N/A
Blood glucose (mmol/L)	Liver SOD activity (U/mg protein)	-0,08	0,65	N/A
Blood glucose (mmol/L)	Heart Catalase activity (umol/min/mg protein)	-0,02	0,89	N/A
Blood glucose (mmol/L)	Liver Catalase activity (umol/min/mg protein)	0,39	0,02	N/A
Blood glucose (mmol/L)	Heart NADPH oxidase activity (RLU/mg protein)	-0,11	0,55	N/A
Blood glucose (mmol/L)	Liver NADPH oxidase activity (RLU/mg protein)	-0,11	0,54	N/A
Blood glucose (mmol/L)	Blood CDs (umol/L)	-0,17	0,31	N/A
Blood glucose (mmol/L)	Heart CDs (umol/g tissue)	0,05	0,78	N/A
Blood glucose (mmol/L)	Liver CDs (umol/g tissue)	-0,09	0,59	N/A
Blood glucose (mmol/L)	Blood TBARS (umol/L)	-0,17	0,33	N/A

Variable 1	Variable 2	Spearman r	p-value	Subgroup
Blood glucose (mmol/L)	Heart TBARS (umol/mg tissue)	0,08	0,67	N/A
Blood glucose (mmol/L)	Liver TBARS (umol/mg tissue)	0,05	0,76	N/A
Blood glucose (mmol/L)	Blood FRAP (umol/L)	-0,26	0,12	N/A
Blood glucose (mmol/L)	Heart FRAP (umol/g tissue)	0,02	0,92	N/A
Blood glucose (mmol/L)	Liver FRAP (umol/g tissue)	-0,45	<0.01	N/A
Blood glucose (mmol/L)	Blood ORAC (TE/L)	0,04	0,82	N/A
Blood glucose (mmol/L)	Heart ORAC (TE/g tissue)	0,28	0,12	N/A
Blood glucose (mmol/L)	Liver ORAC (TE/g tissue)	0,04	0,82	N/A
Blood glucose (mmol/L)	Blood GSH (umol/L)	0,14	0,37	N/A
Blood glucose (mmol/L)	Heart GSH (umol/g tissue)	0,33	0,06	N/A
Blood glucose (mmol/L)	Liver GSH (umol/g tissue)	-0,22	0,21	N/A
Blood glucose (mmol/L)	Blood GSSG (umol/L)	-0,16	0,32	N/A
Blood glucose (mmol/L)	Liver GSSG (umol/g tissue)	0,29	0,09	N/A
Blood glucose (mmol/L)	Blood GSH: GSSG	0,16	0,31	N/A
Blood glucose (mmol/L)	Liver GSH: GSSG	-0,36	0,03	N/A
Blood glucose (mmol/L)	Blood GSSG (umol/L)(BoxCox)	-0,16	0,32	N/A
Blood glucose (mmol/L)	Blood GSH: GSSG(BoxCox)	0,16	0,31	N/A
Blood glucose (mmol/L)	Heart G6PD activity (mU/mg protein)	-0,07	0,80	KO

Variable 1	Variable 2	Spearman r	p-value	Subgroup
Blood glucose (mmol/L)	Liver G6PD activity (mU/mg protein)	-0,40	0,10	KO
Blood glucose (mmol/L)	Heart NADPt (nmol/mg protein)	-0,13	0,63	KO
Blood glucose (mmol/L)	Liver NADPt (nmol/mg protein)	-0,35	0,15	KO
Blood glucose (mmol/L)	Heart TKT activity (uU/g protein)	-0,06	0,81	KO
Blood glucose (mmol/L)	Liver TKT activity (uU/g protein)	-0,42	0,08	KO
Blood glucose (mmol/L)	Heart SOD activity (U/mg protein)	-0,37	0,16	KO
Blood glucose (mmol/L)	Liver SOD activity (U/mg protein)	-0,25	0,32	KO
Blood glucose (mmol/L)	Heart Catalase activity (umol/min/mg protein)	0,21	0,43	KO
Blood glucose (mmol/L)	Liver Catalase activity (umol/min/mg protein)	0,53	0,02	KO
Blood glucose (mmol/L)	Heart NADPH oxidase activity (RLU/mg protein)	-0,14	0,60	KO
Blood glucose (mmol/L)	Liver NADPH oxidase activity (RLU/mg protein)	-0,04	0,86	KO
Blood glucose (mmol/L)	Blood CDs (umol/L)	-0,04	0,86	KO
Blood glucose (mmol/L)	Heart CDs (umol/g tissue)	0,13	0,62	KO
Blood glucose (mmol/L)	Liver CDs (umol/g tissue)	0,29	0,25	KO
Blood glucose (mmol/L)	Blood TBARS (umol/L)	-0,14	0,58	KO
Blood glucose (mmol/L)	Heart TBARS (umol/mg tissue)	0,02	0,93	KO
Blood glucose (mmol/L)	Liver TBARS (umol/mg tissue)	0,04	0,86	KO
Blood glucose (mmol/L)	Blood FRAP (umol/L)	-0,32	0,17	KO

Variable 1	Variable 2	Spearman r	p-value	Subgroup
Blood glucose (mmol/L)	Heart FRAP (umol/g tissue)	0,22	0,42	KO
Blood glucose (mmol/L)	Liver FRAP (umol/g tissue)	-0,54	0,02	KO
Blood glucose (mmol/L)	Blood ORAC (TE/L)	0,20	0,40	KO
Blood glucose (mmol/L)	Heart ORAC (TE/g tissue)	0,16	0,54	KO
Blood glucose (mmol/L)	Liver ORAC (TE/g tissue)	-0,25	0,31	KO
Blood glucose (mmol/L)	Blood GSH (umol/L)	0,21	0,38	KO
Blood glucose (mmol/L)	Heart GSH (umol/g tissue)	0,47	0,07	KO
Blood glucose (mmol/L)	Liver GSH (umol/g tissue)	-0,25	0,32	KO
Blood glucose (mmol/L)	Blood GSSG (umol/L)	-0,25	0,29	KO
Blood glucose (mmol/L)	Liver GSSG (umol/g tissue)	0,32	0,20	KO
Blood glucose (mmol/L)	Blood GSH: GSSG	0,30	0,20	KO
Blood glucose (mmol/L)	Liver GSH: GSSG	-0,44	0,07	KO
Blood glucose (mmol/L)	Blood GSSG (umol/L)(BoxCox)	-0,25	0,29	KO
Blood glucose (mmol/L)	Blood GSH: GSSG(BoxCox)	0,30	0,20	KO
Blood glucose (mmol/L)	Heart G6PD activity (mU/mg protein)	0,06	0,83	WT
Blood glucose (mmol/L)	Liver G6PD activity (mU/mg protein)	-0,35	0,17	WT
Blood glucose (mmol/L)	Heart NADPt (nmol/mg protein)	0,32	0,22	WT
Blood glucose (mmol/L)	Liver NADPt (nmol/mg protein)	0,20	0,44	WT

Variable 1	Variable 2	Spearman r	p-value	Subgroup
Blood glucose (mmol/L)	Heart TKT activity (uU/g protein)	-0,10	0,71	WT
Blood glucose (mmol/L)	Liver TKT activity (uU/g protein)	-0,27	0,30	WT
Blood glucose (mmol/L)	Heart SOD activity (U/mg protein)	-0,04	0,90	WT
Blood glucose (mmol/L)	Liver SOD activity (U/mg protein)	0,12	0,64	WT
Blood glucose (mmol/L)	Heart Catalase activity (umol/min/mg protein)	-0,20	0,45	WT
Blood glucose (mmol/L)	Liver Catalase activity (umol/min/mg protein)	0,25	0,34	WT
Blood glucose (mmol/L)	Heart NADPH oxidase activity (RLU/mg protein)	-0,17	0,53	WT
Blood glucose (mmol/L)	Liver NADPH oxidase activity (RLU/mg protein)	0,05	0,84	WT
Blood glucose (mmol/L)	Blood CDs (umol/L)	-0,28	0,25	WT
Blood glucose (mmol/L)	Heart CDs (umol/g tissue)	-0,03	0,91	WT
Blood glucose (mmol/L)	Liver CDs (umol/g tissue)	-0,47	0,05	WT
Blood glucose (mmol/L)	Blood TBARS (umol/L)	-0,27	0,30	WT
Blood glucose (mmol/L)	Heart TBARS (umol/mg tissue)	-0,00	1,00	WT
Blood glucose (mmol/L)	Liver TBARS (umol/mg tissue)	0,05	0,85	WT
Blood glucose (mmol/L)	Blood FRAP (umol/L)	-0,28	0,24	WT
Blood glucose (mmol/L)	Heart FRAP (umol/g tissue)	-0,12	0,65	WT
Blood glucose (mmol/L)	Liver FRAP (umol/g tissue)	-0,27	0,30	WT
Blood glucose (mmol/L)	Blood ORAC (TE/L)	-0,21	0,37	WT

Variable 1	Variable 2	Spearman r	p-value	Subgroup
Blood glucose (mmol/L)	Heart ORAC (TE/g tissue)	0,36	0,17	WT
Blood glucose (mmol/L)	Liver ORAC (TE/g tissue)	0,07	0,78	WT
Blood glucose (mmol/L)	Blood GSH (umol/L)	-0,03	0,90	WT
Blood glucose (mmol/L)	Heart GSH (umol/g tissue)	0,17	0,52	WT
Blood glucose (mmol/L)	Liver GSH (umol/g tissue)	-0,12	0,65	WT
Blood glucose (mmol/L)	Blood GSSG (umol/L)	-0,13	0,59	WT
Blood glucose (mmol/L)	Liver GSSG (umol/g tissue)	0,12	0,65	WT
Blood glucose (mmol/L)	Blood GSH: GSSG	0,08	0,73	WT
Blood glucose (mmol/L)	Liver GSH: GSSG	-0,32	0,21	WT
Blood glucose (mmol/L)	Blood GSSG (umol/L)(BoxCox)	-0,13	0,59	WT
Blood glucose (mmol/L)	Blood GSH: GSSG(BoxCox)	0,08	0,73	WT